frontiers | Research Topics

The function of secretory factors in immune disorders

Edited by
Yanbo Wang, Tao Liu, Yujing Zhang and Benjamin Tsang

Published in
Frontiers in Immunology

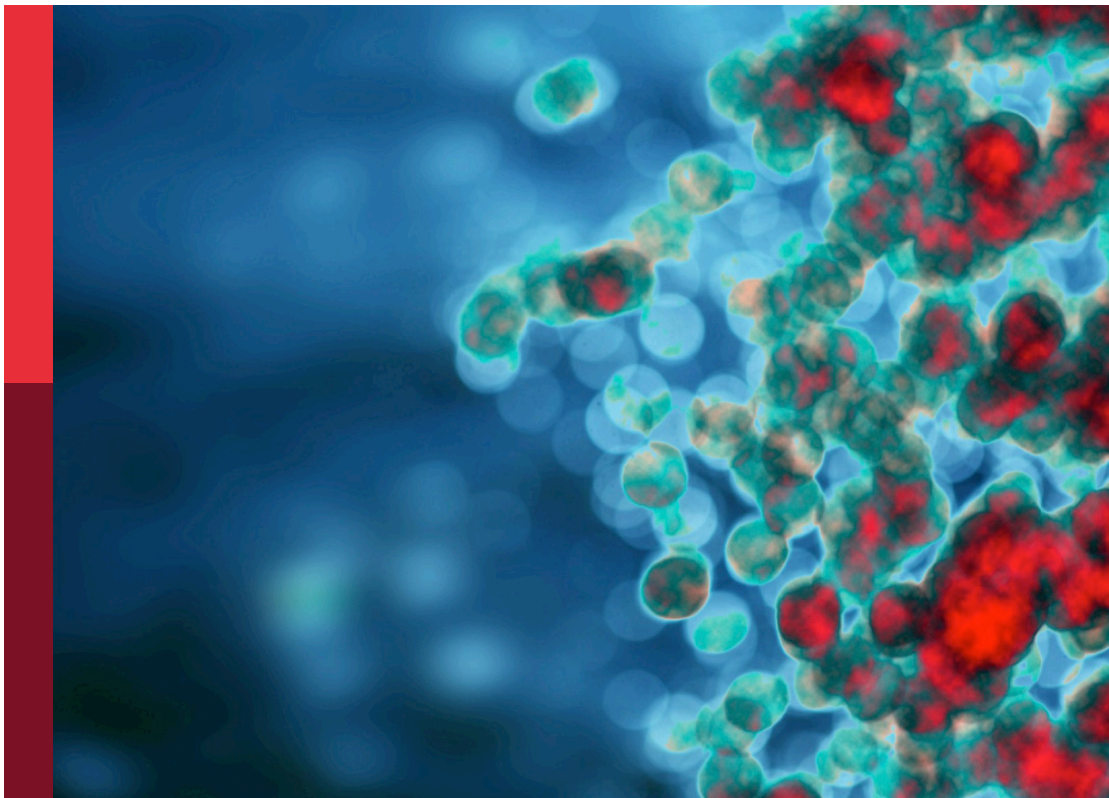

ISSN 1664-8714
ISBN 978-2-8325-3375-8
DOI 10.3389/978-2-8325-3375-8

About Frontiers

Frontiers is more than just an open access publisher of scholarly articles: it is a pioneering approach to the world of academia, radically improving the way scholarly research is managed. The grand vision of Frontiers is a world where all people have an equal opportunity to seek, share and generate knowledge. Frontiers provides immediate and permanent online open access to all its publications, but this alone is not enough to realize our grand goals.

Frontiers journal series

The Frontiers journal series is a multi-tier and interdisciplinary set of open-access, online journals, promising a paradigm shift from the current review, selection and dissemination processes in academic publishing. All Frontiers journals are driven by researchers for researchers; therefore, they constitute a service to the scholarly community. At the same time, the *Frontiers journal series* operates on a revolutionary invention, the tiered publishing system, initially addressing specific communities of scholars, and gradually climbing up to broader public understanding, thus serving the interests of the lay society, too.

Dedication to quality

Each Frontiers article is a landmark of the highest quality, thanks to genuinely collaborative interactions between authors and review editors, who include some of the world's best academicians. Research must be certified by peers before entering a stream of knowledge that may eventually reach the public - and shape society; therefore, Frontiers only applies the most rigorous and unbiased reviews. Frontiers revolutionizes research publishing by freely delivering the most outstanding research, evaluated with no bias from both the academic and social point of view. By applying the most advanced information technologies, Frontiers is catapulting scholarly publishing into a new generation.

What are Frontiers Research Topics?

Frontiers Research Topics are very popular trademarks of the *Frontiers journals series*: they are collections of at least ten articles, all centered on a particular subject. With their unique mix of varied contributions from Original Research to Review Articles, Frontiers Research Topics unify the most influential researchers, the latest key findings and historical advances in a hot research area.

Find out more on how to host your own Frontiers Research Topic or contribute to one as an author by contacting the Frontiers editorial office: frontiersin.org/about/contact

The function of secretory factors in immune disorders

Topic editors

Yanbo Wang — Nanjing University, China

Tao Liu — Brigham and Women's Hospital, Harvard Medical School, United States

Yujing Zhang — Nanjing University, China

Benjamin Tsang — Ottawa Hospital Research Institute (OHRI), Canada

Citation

Wang, Y., Liu, T., Zhang, Y., Tsang, B., eds. (2023). *The function of secretory factors in immune disorders*. Lausanne: Frontiers Media SA.

doi: 10.3389/978-2-8325-3375-8

Table of contents

frontiers | Frontiers in Immunology

TYPE Mini Review
PUBLISHED 08 September 2022
DOI 10.3389/fimmu.2022.1006081

OPEN ACCESS

EDITED BY
Yujing Zhang,
Nanjing University, China

REVIEWED BY
Zhen Huang,
Nanjing University, China

*CORRESPONDENCE
Fang Yan
fang.yan@vumc.org

SPECIALTY SECTION
This article was submitted to Cytokines and Soluble Mediators in Immunity, a section of the journal Frontiers in Immunology

RECEIVED 28 July 2022
ACCEPTED 23 August 2022
PUBLISHED 08 September 2022

CITATION
Kaur H, Ali SA and Yan F (2022) Interactions between the gut microbiota-derived functional factors and intestinal epithelial cells – implication in the microbiota-host mutualism. *Front. Immunol.* 13:1006081. doi: 10.3389/fimmu.2022.1006081

Interactions between the gut microbiota-derived functional factors and intestinal epithelial cells – implication in the microbiota-host mutualism

Harpreet Kaur[1], Syed Azmal Ali[2] and Fang Yan[1,3]*

[1]Department of Pediatrics, Vanderbilt University Medical Center, Nashville, TN, United States, [2]German Cancer Research Center, Division of Proteomics of Stem Cell and Cancer, Heidelberg, Germany, [3]Department of Cell and Developmental Biology, Vanderbilt University, Nashville, TN, United States

Mutual interactions between the gut microbiota and the host play essential roles in maintaining human health and providing a nutrient-rich environment for the gut microbial community. Intestinal epithelial cells (IECs) provide the frontline responses to the gut microbiota for maintaining intestinal homeostasis. Emerging evidence points to commensal bacterium-derived components as functional factors for the action of commensal bacteria, including protecting intestinal integrity and mitigating susceptibility of intestinal inflammation. Furthermore, IECs have been found to communicate with the gut commensal bacteria to shape the composition and function of the microbial community. This review will discuss the current understanding of the beneficial effects of functional factors secreted by commensal bacteria on IECs, with focus on soluble proteins, metabolites, and surface layer components, and highlight the impact of IECs on the commensal microbial profile. This knowledge provides a proof-of-concept model for understanding of mechanisms underlying the microbiota-host mutualism.

KEYWORDS

extracellular vesicle, intestinal inflammation, intestinal epithelial cell, metabolite, probiotics, secretory product, commensal microbiota, mutualism

Introduction

The human microbial community comprises more than one trillion microorganisms, including bacteria, fungus, viruses, and protozoa, which makes the number of the microbial cells almost equal to the total number of cells in human body (1, 2). The taxonomic composition of the human microbiota exhibits high interpersonal differences; however, microbial genes and metabolic modules share similar functions (3, 4). In the

gastrointestinal tract of healthy adults, *Firmicutes*, *Bacteroidetes*, *Proteobacteria*, *Actinobacteria*, and *Verrucomicrobia* are the main commensal microbial phyla (5), with *Firmicutes* and *Bacteroidetes* accounting as the majority of phyla (6). In contrast to the relative abundance of commensal microbiota, the normal human gut also contains pathobiota with potential pathogenic behavior (7). Symbiotic relationships between commensal bacteria and the host are established through a variety of ways that are mutually beneficial. The commensal bacteria provide nutrients to host *via* digesting dietary components that can be used as energy sources (8), prevent the colonization of pathogenic bacteria by competitive inhibition of pathogen binding to host cells and secretion of antimicrobial compounds (9), and affect many aspects of host metabolism and physiological processes that lead to direct influence on modulating protective immune responses (10), maintaining intestinal epithelial homeostasis (11) and mediating the gut–brain axis for the function of the nervous system (12). In turn, the gut microbiota as the most diverse and populous microbial assemblage (13) is influenced by the host factors through several means. In addition to the nutritional support from the host, the composition of the intestinal microbiome is shaped and structured by the genotype of the host and factors associated with lifestyle, environmental exposure, and diseases (1). Further, increasing evidence reveals that host-derived factors participate in regulating bacterial adaptation, growth, and function (14).

The health-promoting impact of the mutualistic relationships between the gut microbiota and the host supports the therapeutic potential of the microbiota-targeting approach such as probiotics and prebiotics. Probiotics, which are beneficial commensal bacteria to host health, have shown promising outcomes in human, animal, and *in vitro* studies (15, 16). The most widely used probiotics, *Lactobacillus* and *Bifidobacterium*, have shown the high survival properties in the gastrointestinal acidic environment (17, 18). Likewise, prebiotics is non-digestible dietary ingredients that promote the survival of beneficial probiotic species (19). However, current understanding is insufficient to exploit the clinical efficacy of probiotics (20, 21). In addition to wide variations in probiotic strain selection and dosing in probiotic clinical trials, uncertain clinical outcomes result from lack of precision in host variables, including the health condition, gut microbiome profile, and diet (15), which may limit probiotic bioavailability and biopharmacology in the gastrointestinal tract. Therefore, probiotic bacteria-derived functional factors with effectiveness for promoting health are in high demand.

The first driver of the gut microbiota and host interactions occurs at the monolayer of intestinal epithelial cells (IECs). IECs contain different cell types with unique functions: enterocytes for absorption of nutrients, transport water and waste products; goblet cells for production of mucus, enteroendocrine cells for hormone secretion; Paneth cells for secretion of antimicrobial peptides (AMPs), and microfold (M) cells involved in antigen capture and presentation to immune cells (22). IECs also contribute to host immunity by secreting cytokines and chemokines (23, 24). Most importantly, IECs serve as the front line for the host to interact with the intestinal luminal factors such as the gut microbiota and their secretory products and metabolites. The mucosal barrier formed by tight junctional complexes within IECs (25) and the layer of mucus protects the host against pathogen and toxic substance invasion (26). Notably, commensal bacteria stimulate several beneficial cellular responses in IECs for intestinal development, mucosal barrier, and intestinal homeostasis (23).

Mechanisms underlying the regulatory effects of commensal bacterium-derived factors on the host and the impact of components in the gut luminal environment supported by the host on shaping the composition and function of commensal bacteria are beginning to be understood. This review will highlight updated information on the mutualistic relationships between IECs and commensal bacteria, with the focus on commensal bacterium-derived functional factors. Knowledge to elucidate the mutualism-led health-promoting outcomes can pave a new avenue for developing microbiota-targeting therapies.

Commensal bacterium-derived factors promote intestinal epithelial homeostasis

Microbe-derived factors refer to a complex of secreted micro- and macromolecules such as products (proteins, enzymes, organic acids, and bacteriocins), metabolites (short-chain fatty acids, SCFAs), and bacterial fractions (muropeptides, teichoic acids, endo- and exopolysaccharides, and surface-layer proteins), which are naturally generated by live bacteria or made in fermentation process (27). Notably, factors produced by commensal bacteria are recognized by IECs and can induce beneficial signaling in IECs, resulting in maintaining intestinal homeostasis. IECs serve as the initial interface with the gut microbiota and a first line of defense against harmful microbes and contribute to translating commensal microbiota-elicited signals into specific cellular responses, thus can operate as the functional connection of commensal bacterial activity and hemostasis in the host (17). The beneficial effects of the interactions between commensal bacteria and epithelial cells occur not only in the gut but also in other parts of the human body. Studies have shown that commensal bacteria protect the skin against local pathogen infection (28). The importance of the interactions between commensal bacteria and IECs is reflected by the genetic evidence that the impaired recognition of commensal bacteria is associated with development of intestinal inflammatory diseases, such as many inflammatory bowel disease (IBD) susceptibility genes have been found to be

involved in regulating host–microbial interactions (29, 30). Therefore, to prevent uncontrolled inflammatory responses, new strategies focused on restoring the normal balance of the intestinal ecosystem are under development (31).

A secretory protein – p40

p40, which was originally isolated from the culture supernatant of *Lactobacillus rhamnosus* GG (LGG) (32), is the first recognized biologically active component of a Gram-positive commensal and probiotic bacterium, *L. rhamnosus GG* (LGG), for benefiting intestinal functional maturation and protecting IECs against inflammatory insults. Genes encoding proteins of the p40 cluster are mainly present in species related to the *L. casei, L. paracasei, L. zeae and L. rhamnosus* taxonomic group. In fact, p40 has been detected in culture supernatants of several strains of *Lactobacillus* (33–35). p40 homolog genes are also present in some species of the families Enterococcaceae and Streptococcaceae (36). C-terminal domain of p40 contains a histidine-dependent amidohydrolase/peptidase (CHAP) domain with cell wall hydrolase activity (33). Interestingly, p40 has been found to bind lipoteichoic acid (LTA) on the external surface of extracellular vesicles (EVs) released by *Lactobacillus casei BL23* (37), suggesting a manner for secretion of p40 by bacteria. It is unknown that whether there is free form of p40 section.

Studies have revealed that p40 exerts immediate and long-lasting effects on IECs (Figure 1) through two distinct mechanisms and these two functions are independent. The immediately effect of p40 is through transactivation of epidermal growth factor receptor (EGFR) and its downstream target, Akt, in IECs. In addition to direct ligand binding to EGFR for its activation, EGFR can be transactivated by other pathways that stimulate A Disintegrin and Metalloproteinase (ADAM)17-triggered releasing transmembrane EGFR ligands for binding to EGFR (38). Studies found that p40 up-regulated ADAM17 catalytic activity to stimulate membrane-bound heparin binding (HB)-EGF release in human and mouse intestinal epithelial cell lines and in mice (32). The biological consequences of EGFR transactivation by p40 have been unraveled, including inhibition of proinflammatory cytokine-induced apoptosis, preserving tight junctions in IECs (39, 40), and promoting mucin production by goblet cells (41). Furthermore, transactivation of EGFR by p40 not only stimulates protective roles on IECs but also induces innate immunity: p40 upregulates gene expression and protein production of proliferation inducing ligand (APRIL) gene expression in IECs, which is a cytokine involved in B cell class switching to IgA^+ cells, thereby increasing IgA^+ plasma cells and IgA production (42). EGFR activation contributes to multiple protective cellular effects in colitis (43). Strong evidence indicates that p40 transactivation of EGFR in IECs contributes to ameliorating colitis in mice (44).

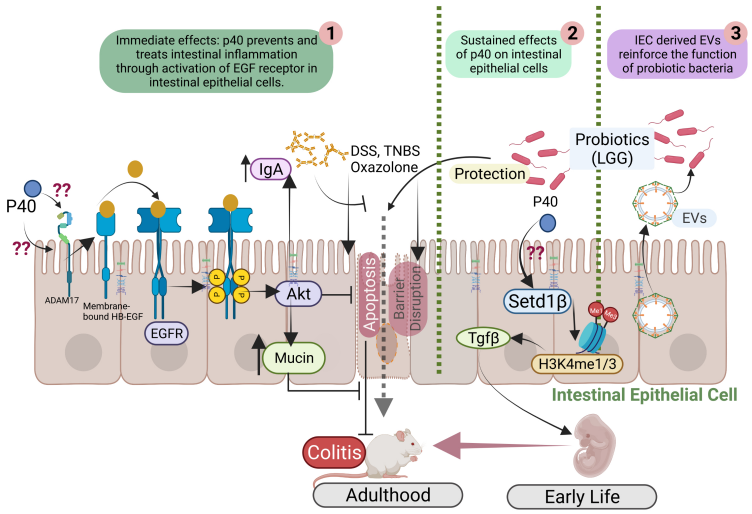

FIGURE 1
Mutual interactions between commensal bacteria and IECs. p40 is a functional factor secreted from the gut commensal bacteria. p40 has immediate effects on transactivation of EGF receptor (EGFR) and its downstream target, Akt, leading to protective responses in IECs for preventing and treating colitis (1). p40 also exerts sustained effects on IECs through upregulation of Setd1β expression and histone 3 (H3) methylation on lysine residue (H3K4me1/3) to stimulate TGFβ gene expression and protein production by IECs, thus p40 supplementation in early life prevents colitis in adulthood (2). IEC-released extracellular vehicles (EVs) communicate with commensal bacteria and promote the function of commensal bacteria (3).

Furthermore, EGFR signaling is required for postnatal growth (45). p40 significantly enhanced functional maturation of the intestine, including intestinal epithelial cell proliferation, differentiation, and tight junction formation, and IgA production in early life in wild-type mice, which is mediated by transactivation of EGFR in IECs (46). These results define a mechanism of p40 regulated immediate effect on protection of intestinal epithelium through induction of ADAM17-mediated EGFR ligand release, leading to transactivation of EGFR in IECs.

Colonization of the gut microbiota in a critical window in early life enables life-long health outcomes in humans and animals (47). It has been reported that p40 supplementation in early life stimulated long-lasting effects on TGF-β production by IECs. Two outcomes of this effects have been reported: promoting induction of differentiation of regulatory T cells (Tregs) in the lamina propria of the small intestine and the colon and protecting of epithelial barrier and inhibiting proinflammatory cytokine production in IECs. One ultimate result by early p40 supplementation is to prevent colitis in adulthood (44, 46).

The long-lasting effects of p40 has been related to its epigenetic modification of IECs. Epigenetic reprogramming refers to global remodeling of epigenetic marks *via* which the host identifies the microbial signal to convert them into the long-term specific cellular signal. In the IECs and immune cells, epigenetic modification permits the gut microbiota to regulate gene expression and cellular responses (48). The COMPASS complex contains methyltransferase and adaptors to activate target gene expression by catalyzing mono- and tri-methylation of histone 3 lysine 4 residue (H3K4me1/3) at enhancer and promoter sites (49). Setd1β, a methyltransferase in COMPASS complex, has a specific function in the assembly and regulation of H3K4 mono-, di and trimethylation. p40 has been found to upregulate *Setd1β* gene expression and protein production, which mediate programming the TGFβ locus into a transcriptionally permissive chromatin state and promoting TGFβ production in IECs. Interestingly, p40 supplementation in early life, but in adulthood, could induce sustained H3K4me1/3 in IECs toward TGFβ production (44). These results establish a novel mechanism involved life-long effects on maintain homeostasis by supplementation with commensal bacterium-derived factor in early life.

Metabolites - short-chain fatty acids and indole

The gut bacteria can metabolite a compound of phytochemicals in dietary fiber-enriched meals into SCFAs, including acetate, butyrate, and propionate. In particularly, butyrate is rapidly absorbed from the intestinal lumen and is the preferred source of energy for colonic epithelial cells (50). Regulation of epithelial barrier by SCFAs has been reported through several mechanisms. Reinforcing the epithelial barrier and enhancing wound healing through promoting the expression of the actin-binding protein synaptopodin (SYNPO) has been identified as a role of a SCFA, butyrate (51). Butyrate decreases gut permeability by enhancing tight junction protein claudin-2 upregulated expression *via* an interleukin 10 receptor subunit alpha (IL-10RA)-dependent mechanism (52). SCFA produced by the symbiotic bacteria, *Akkermansia muciniphila*, *Clostridium butyricum*, and *Faecalibacterium prausnitzii* produce SCFAs in the intestinal tract function as inhibitors of histone deacetylases (HDACs) by upregulating histone acetyltransferases activity, while possessing anti-inflammatory and epithelial barrier maintenance effects in various animal models (53). As proven, the epigenetic effect of SCFAs as inhibitors of HDACs is mostly butyrate>propionate>acetate, which results in increased levels of histone acetylation, decondensation, and relaxing of chromatin (54). *In vitro* studies have shown that SCFAs have the potential to be the intestinal protection barrier by inhibiting the enzyme Histone Deacetylase (HDAC), which has preventative effects on DNA transcription, regulates gene expression, and increases the expression of MUC2, MUC1, MUC3, and MUC4 (55). Furthermore, both butyrate and propionate upregulated MUC2 transcript expression in LS174T cells. Analysis of the MUC2 promoter indicated that an active butyrate-responsive region comprising an AP1 (c-Fos/c-Jun) cis-element is necessary for the activation of MUC2 by acetylation and methylation of histones (56). Another study has shown that SCFAs strengthen the epithelial cell tight junctions, resulting in a robust and healthy intestinal barrier. Butyrate maintains and enhances the transepithelial electrical resistance (TEER) in Caco-2 cells that is mediated by AMP activated protein kinase (AMPK) (57).

SCFAs such as butyrate and propionate play significant roles in immunity through regulation of IECs and immune cells, such as T cells, macrophages, and dendritic cells. A report showed that SCFAs and a high-fiber diet were able to induce vitamin A metabolism in epithelial cells and $CD103^+$ DCs and this was associated with enhanced Foxp3 expression in T cells (58). DCs have been found to play a significant role in the initiation of IgA production in the gut in response to SCFAs. Metabolite-sensing mammalian G protein-coupled receptor (GPR43) in DCs mediated the acetate induction of intestinal IgA response to microbiota, in that GPR43 knock out mice showed lower IgA production and decreased numbers of IgA+ B cells in the intestines (59).

In addition to normal IECs, SCFA plays roles in inhibition of colorectal cancer cell growth. Major anti-proliferative activity of SCFAs is associated with butyrate, acetate, and propionate (with acetate and propionate requiring higher concentrations to be as effective as butyrate). These SCFA compounds can promote apoptosis responses in colon cancer cells by influencing mitochondrial permeability potential, producing reactive oxygen species (ROS), and activating caspase-3 (27).

Indole and its derivatives are derived from the metabolism of tryptophan by the gut bacteria containing tryptophanase such as

Lactobacillus reuteri and Clostridium sporogenes. The absorption of indole and its derivatives (Indole 3-propionic acid (IPA), indole-3-ethanol (IEA), and indole-3-acetaldehyde (IAAld) through the intestinal epithelium is due to the ability to freely diffuse through lipid membranes (60). Indole and its derivatives support intestinal immune homeostasis through activating aryl hydrocarbon receptor (AhR) to protect the intestinal tight junctional barrier. The activation of the AhR pathway in IECs is vital for protecting the stem cell niched and maintaining intestinal barrier integrity (61). The pregnane X receptor (PXR) is a physiologic regulator associated with gut permeability (62). IPA has been found as a ligand for epithelial PXR, and the administration of IPA can up-regulate tight junction protein-coding mRNAs and enhance the expression of claudins and occludins (63). Recent studies have showed that IEA, IPA, and IAAld contribute to maintaining the integrity of the intestinal tight junctional barrier in an AhR-dependent manner and alleviating dextran sodium sulfate (DSS)-induced colitis in mice (64). Indole and its derivatives enhance IL-10 expression through aryl hydrogen receptors (AhR) activation and promote IL-10 signaling which is linked with barrier function. Indole-3-aldehyde (IAld) increases epithelial cells proliferation and upregulates the differentiation of goblet cells, intestinal barrier integrity and downregulates the systemic inflammation caused by aging in geriatric mice. This effect increases the expression of the cytokine IL-10 *via* AhR but does not depend on the type I interferon or IL-22 signaling (65). The activation of AhRs leads to lL-22 transcription, which can further increase the expression of antimicrobial peptides and improve colonization resistance against *Candida albicans* in the gastrointestinal tract (66).

Overall, these studies support the feasibility of commensal bacterial metabolites as a strategy to promote mucosal barrier and intestinal homeostasis. Empirical modulation of the microbiota using probiotics can increase SCFAs and indole-producing bacteria for the maintenance of epithelial barrier integrity in inflammatory models (67). Thus, supplementation with specific probiotics for beneficial metabolites formation could provide new avenues to manage disease activity.

Surface layer components - surface layer protein, exopolysaccharide, peptidoglycan, and lipoteichoic acid

Bacterial surface layers contain ubiquitous proteins structures that are abundant in Gram negative and Gram-positive bacteria. In Gram-positive bacteria, the S-layer lattice is generally composed of a single protein and is attached to peptidoglycan-bound secondary cell-wall polymer by non-covalent interactions (68). As the outermost structure of the cell, the surface layer lattice is generally considered to be the first bacterial components that have a direct interaction with host cells. The effects of cell surface molecules are diverse and have been shown to play roles in many bacterial functionalities, such as adhesion to the host cells, strengthening of the gut barrier integrity, pathogen exclusion, stimulation of the host mucosal system to improve mucus production, and secretion of defense molecules such as β defensins (69).

Surface layer protein A (SPA-A) derived from *Lactobacillus acidophilus* NCK2187 binds to the C-type lectin SIGNR3 and initiates regulatory signals, leading to maintenance of healthy gastrointestinal microbiota, protecting gut mucosal barrier function, and prevention of colitis (70). Recent study revealed that SLP of *Lactobacillus acidophilus* NCFM strain led to a reduction in myeloperoxidase activity and TNF-α expression whereas significantly increased the IL-10 levels. The administration of these surface proteins significantly reversed the histopathological damages induced by the colitogens and improved the overall histological score in TNBS colitis mice model (71). Results from *in vitro* studies indicated that purified SLPs from *L. plantarum* exert a protective effect on Caco-2 cells infected with EPEC by increasing their transepithelial resistance (TEER) and down-regulating their permeability (72). Further, *L. acidophilus* contains three different SLPs, SLP-A, SLP-B, and SLP-X, which interact with pattern recognition receptors (PRRs) in IECs and modulate the immune response. *L. acidophilus* SLPs decrease interleukin (IL-8) secretion in Caco-2 cells stimulated by *S. typhimurium* (73).

Exopolysaccharide (EPS) are metabolic by-product of microorganisms (74). EPS consists of homopolysaccharides (HoPS) or heteropolysaccharides (HePS), depending on the main chain composition and mechanisms of synthesis. The most HePS-producing bacteria are *Lactobacillus, Lactococcus*, *Streptococcus* and *Enterococcus* strains frequently isolated from fermented dairy products and the human gastrointestinal tract (GIT), whereas most HoPS are produced by *Lactobacillus, Leuconostoc, Pediococcus, Streptococcus*, and Weissella strains present in animal GIT, vegetables and fermented beverages (75). EPS-1 contributes to maintaining the intestinal barrier integrity against the disruption by lipopolysaccharide (LPS) in Caco-2 monolayer mediated by enhancing. the expression of tight junction. On the transcriptional level, LPS-decreased expression of several tight junction genes was inhibited by *S. thermophilus*-derived HePS *in vivo* (76). Further, the role of EPS in epithelial adhesion of commensal bacteria makes EPS of particular interest for preventing adhesion of pathogenic bacteria. It has been demonstrated that EPS produced by *Lactobacillus paracasei subsp. Paracasei* BGSJ2 plays an essential role in the prevention of adhesion of *E. coli* to Caco-2 cells (77). Further, the immunoregulatory effects of EPS on IECs are supported by the fact that EPS activates C-type lectin receptors on IECs to elicit an immunological response. Upon stimulation by EPS, IECs secrete several cytokines and chemokines, including interleukins, TNF, growth factors, and beta-defensins (78). Therefore, IECs play an essential role in the recruitment of dendritic cells, which are responsible for controlling both innate and acquired immunological responses (79). In addition, EPS has shown to mitigate experimental colitis, improving mucosal barrier function,

and modulating gut microbiota composition (80–82). Moreover, recent studies have suggested that applying EPS from lactic acid bacteria to the skin enhances skin health and proven to be aid in gastrointestinal wound healing in different *in-vitro* and *in-vivo* studies (83, 84). It would be advantageous to consider EPS as a feasible prebiotic choice for therapeutic purposes due to its two feathers: EPS is indigestibility to the host cells, thus, arriving in the colon intact and consumed by specific gut microbiota in the colon (85).

Peptidoglycan (PGN) is a large polymeric molecule present in the Gram positive and Gram-negative bacterial cell wall. The basic overall structure of PGN is conserved between different organisms, but there are backbone and crosslinking modifications that increase the variability among the bacterial species. PGN in probiotic bacteria undergo variety of modifications in the sugar structure including deacetylation, O-acetylation, and N-glycosylation, which create the differences in sugar structure leading to the alteration in the properties of the cell wall (86). There are different receptors to detect the peptidoglycan or its fragments, for example, the innate immune system can detect PGN through peptidoglycan recognition proteins (PGLYRPs) (87), which are mostly expressed in eosinophils and neutrophils and could potentially act on inflammation (88). In the intestinal lumen, PGN-contained cell wall fragments can be released from commensal bacteria after digestion by Paneth cell-derived lysozyme. It has been suggested that PGN can be absorbed by crypt-based immature intestinal epithelial cells and in transported over the intestinal epithelium (89). Functional analysis has shown that PGN secreted by *Lactobacillus* and *Bifidobacterium* enhanced the expression of tight junction proteins, including claudins, occludin, and ZO-1 and improved the integrity of the gut barrier *via* Toll-like receptors 2 signaling (90, 91).

Lipoteichoic acid (LTA) is one of the major cell wall components of Gram-positive bacteria that can be considered the pivotal components for immunomodulating effects (92). In addition to its immunoregulatory effects, such as LTA from *L. casei* YIT9029 and *L. fermentum* YIT0159 cause TNF-α production in macrophages through TLR2 receptors (93), LTA from *Lactobacillus plantarum* confers anti-inflammatory responses in porcine intestinal epithelial cell line, IPEC-J2 (94).

This evidence supports the note that commensal bacterial surface components act through evolutionary-optimized mechanism that targets IECs to benefit intestinal homeostasis.

IECs modulate the composition and function of the gut microbiota

The microbiota-host interactions result in a mutually advantageous setting that provides a nutrient-rich environment favorable to microbiota development and survival. It is well-known that microbiota composition is mostly influenced by host genetics and environmental factors, such as diet, nutrient availability, immunological responses, and disease states (95, 96). A recent study has demonstrated the contribution of IECs to shape the composition of the gut microbiota. The lack of MHC class II in IECs resulted in the decrease in microbial-bound IgA, regulatory T cells, and immune repertoire selection, which is associated with the increase in interindividual microbiota variation and altered proportions of two taxa in the ileum. This evidence suggests that MHC class II in IECs regulates the microbiota composition (97). Paneth cells in the intestinal epithelium are the primary source of lysozyme that directly encounters commensal bacteria. It has been reported that luminal lysozyme abundance determines the composition of mucolytic microbiota in the gut and regulates mucosal inflammatory responses (98). These findings reveal the specific molecules in IECs that are involved in shaping the gut microbial community.

Regarding the impact of IECs on the function of the gut microbiota, a study has revealed that a cellular structure, extracellular vesicles (EVs) released by IECs mediate trans-kingdom interactions and regulation of the function of the gut microbial community. EVs are the membrane-bound vesicles secreted through multivesicular bodies and are comprised of complex cargos including lipids, proteins, and nucleic acids. EVs are important messengers for the intercellular communication among mammalian cells (99). The first action of IEC-released EVs on the gut microbes was discovered to inhibit growth of pathogens (100, 101). Recent studies have unraveled novel effects of EVs released by IECs on promoting the function of commensals (Figure 1). As a commensal bacterial model, protein cargos in IEC-released EVs were found to be transferred to LGG, suggesting that EVs can serve as a communication approach between LGG and IECs. Further, IEC-released EVs stimulate production of functional factor by LGG (102). Remarkably, HSP90 in EVs has been shown to contribute the increase the function of LGG (102). HSP90 is highly conserved from bacteria to mammals and displays functional overlaps in protein folding, enabling the stability and transportation of client proteins (103, 104). Client proteins of HSPs in *Lactobacilli* regulate growth, metabolism, transport functions, and protein synthesis under normal and stress conditions (105). Therefore, this finding provides knowledge for mechanistic understanding of the impact of the host on the functional aspects of the gut microbiota.

Discussion

There are several challenges in the research area of the gut microbiota-derived functional factors. Elucidating the potential of commensal bacterium-derived functional factors in treatment and prevention of diseases, such inflammatory bowel disease (IBD), including ulcerative colitis (UC) and Crohn's disease (CD) has high clinical relevance. IBD is caused by inappropriate immune

responses to the intestinal microbiota in genetically susceptible individuals, leading to autoimmune damage of the intestinal barrier and chronic inflammation (106). IBD is associated with an increased risk of development of colorectal cancer (CRC). Dysbiosis serves as a risk factor or/and a consequence of inflammation and inflammation-associated carcinogenesis. Studies showed that qualitative and quantitative alteration in gut microbiota is highly associated with the abnormal immune responses and thus influence the course and development of IBD (107, 108). Moreover, the concentration of butyrate in IBD is considerably lower than in healthy controls, indicating that the dysbiosis has likely produced metabolic changes (109). Although there is evidence to show that specific intestinal microbes are associated with CRC development and progression, the mechanisms through which the abnormal microbial community mediates CRC development remains unclear. *Enterotoxigenic Bacteroides fragilis* (ETBF) can raise levels of chemokine L20 and prostaglandin E2 in intestinal epidermal cells; prostaglandin E2 plays a vital role in proliferation and enhances the secretion of IL-17 and related factors secreted by Th17 cells, leading to the development of inflammation-related CRC (110). Further, microbial products are sensed by Toll-like receptors, which trigger MyD88-mediated production of IL-23 proinflammatory cytokine which activates IL-17a, IL-6, and IL-22 release and thus promotes CRC development (111, 112). Dysbiosis related to CRC aids its progression *via* different pathways, such as driving inflammatory response, inducing DNA damage, stimulating cell and causes microbial homeostasis in specific microbiota. The imbalance of the gut microbial profile promotes functions associated with cancer such as uncontrolled cell proliferation and the loss of apoptosis. Moreover, differences in the species of gut microflora during tumorigenesis can be used as a biomarker and diagnostic tool for CRC (113).

Recent advances defining the protective effects of commensal bacterium-derived functional factors raise the theoretical possibility for alleviating the epithelial damage by commensal bacterium-derived functional as adjunct therapies for current IBD treatments that are focused on functional failure inhibition of proinflammatory responses.

The efficacy of probiotics in clinical applications is poorly understood (20, 21). Probiotics exert beneficial effects through multiple mechanisms and modalities (114–117). Approaches to enhance the action of probiotics, including increasing production of functional factors, will broaden the therapeutic applications of probiotics. Ongoing work towards comprehensively understanding of the host impact on the microbiota will likely open new avenues towards developing approaches for increasing the efficacy of probiotics for clinical application and generating next-generation probiotics.

Author contributions

HK, SA, and FY wrote and revised the manuscript. All authors contributed to the article and approved the submitted version.

Funding

This work was supported by National Institutes of Health (NIH) grant R01DK081134-12 (FY) and the Crohn's & Colitis Foundation Senior Research Award (FY).

Conflict of interest

The authors declare that the research was conducted in the absence of any commercial or financial relationships that could be construed as a potential conflict of interest.

Publisher's note

References

1. Qin Y, Havulinna AS, Liu Y, Jousilahti P, Ritchie SC, Tokolyi A, et al. Combined effects of host genetics and diet on human gut microbiota and incident disease in a single population cohort. *Nat Genet* (2022) 54(2):134–42. doi: 10.1038/s41588-021-00991-z

2. Sender R, Fuchs S, Milo R. Revised estimates for the number of human and bacteria cells in the body. *PloS Biol* (2016) 14(8):1002533. doi: 10.1371/journal.pbio.1002533

3. Human Microbiome Project Consortium, Huttenhower C, Gevers D, Knight R, Abubucker S, Badger JH, et al. Structure, function and diversity of the healthy human microbiome. *Nature* (2012) 486(7402):207–14. doi: 10.1038/nature11234

4. Lloyd-Price J, Abu-Ali G, Huttenhower C. The healthy human microbiome. *Genome Med* (2016) 8(1):1–1. doi: 10.1186/s13073-016-0307

5. Magne F, Gotteland M, Gauthier L, Zazueta A, Pesoa S, Navarrete P, et al. The firmicutes/bacteroidetes ratio: a relevant marker of gut dysbiosis in obese patients? *Nutrients* (2020) 12(5):1474. doi: 10.3390/nu12051474

6. Cholewińska P, Wołoszyńska M, Michalak M, Czyż K, Rant W, Smoliński J, et al. Influence of selected factors on the firmicutes, bacteroidetes phyla and the lactobacillaceae family in the digestive tract of sheep. *Sci Rep* (2021) 11(1):1–8. doi: 10.1038/s41598-021-03207-w

7. Krezalek MA, DeFazio J, Zaborina O, Zaborin A, Alverdy JC. The shift of an intestinal "microbiome" to a "pathobiome" governs the course and outcome of sepsis following surgical injury. *Shock Augusta Ga* (2016) 45(5):475. doi: 10.1097/SHK.0000000000000534

8. Lindsay EC, Metcalfe NB, Llewellyn MS. The potential role of the gut microbiota in shaping host energetics and metabolic rate. *J Anim Ecol* (2020) 89 (11):2415–26. doi: 10.1111/1365-2656.13327

9. Khan I, Bai Y, Zha L, Ullah N, Ullah H, Shah SR, et al. Mechanism of the gut microbiota colonization resistance and enteric pathogen infection. *Front Cell Infect Microbiol* (2021) 11:1273. doi: 10.3389/fcimb.2021.716299

10. Rooks MG, Garrett WS. Gut microbiota, metabolites and host immunity. *Nat Rev Immunol* (2016) 6(6):341–52. doi: 10.1038/nri.2016.42

11. Zheng D, Liwinski T, Elinav E. Interaction between microbiota and immunity in health and disease. *Cell Res* (2020) 30(6):492–506. doi: 10.1038/s41422-020-0332-7

12. Rutsch A, Kantsjö JB, Ronchi F. The gut-brain axis: how microbiota and host inflammasome influence brain physiology and pathology. *Front Immunol* (2020) 11:604179. doi: 10.3389/fimmu.2020.604179

13. Roswall J, Olsson LM, Kovatcheva-Datchary P, Nilsson S, Tremaroli V, Simon MC, et al. Developmental trajectory of the healthy human gut microbiota during the first 5 years of life. *Cell Host Microbe* (2021) 29(5):765–76. doi: 10.1016/j.chom.2021.02.021

14. Guo Y, Kitamoto S, Kamada N. Microbial adaptation to the healthy and inflamed gut environments. *Gut Microbes* (2020) 12(1):1857505. doi: 10.1080/19490976.2020.1857505

15. Suez J, Zmora N, Segal E, Elinav E. The pros, cons, and many unknowns of probiotics. *Nat Med* (2019) 25(5):716–29. doi: 10.1038/s41591-019-0439-x

16. Yan F, Polk DB. Probiotics and probiotic-derived functional factors–mechanistic insights into applications for intestinal homeostasis. *Front Immunol* (2020) 11:1428. doi: 10.3389/fimmu.2020.01428

17. Ali SA, Singh P, Tomar SK, Mohanty AK, Behare P. Proteomics fingerprints of systemic mechanisms of adaptation to bile in *Lactobacillus fermentum*. *J Proteomics* (2020) 213:103600. doi: 10.1016/j.jprot.2019.103600

18. Corcoran BM, Stanton C, Fitzgerald GF, Ross R. Survival of probiotic lactobacilli in acidic environments is enhanced in the presence of metabolizable sugars. *Appl Environ Microbiol* (2005) 71(6):3060–7. doi: 10.1128/AEM.71.6.3060-3067.2005

19. Swanson KS, Gibson GR, Hutkins R, Reimer RA, Reid G, Verbeke K, et al. The international scientific association for probiotics and prebiotics (ISAPP) consensus statement on the definition and scope of synbiotics. *Nat Rev Gastroenterol Hepatol* (2020) 17(11):687–701. doi: 10.1038/s41575-020-0344-2

20. Hill C, Guarner F, Reid G, Gibson GR, Merenstein DJ, Pot B, et al. Expert consensus document: The international scientific association for probiotics and prebiotics consensus statement on the scope and appropriate use of the term probiotic. *Nat Rev Gastroenterol Hepatol* (2014) 11:506–14. doi: 10.1038/nrgastro.2014.66

21. Lichtenstein L, Avni-Biron I, Ben-Bassat O. Probiotics and prebiotics in crohn's disease therapies. *Best Pract Res Clin Gastroenterol* (2016) 30(1):81–8. doi: 10.1016/j.bpg.2016.02.002

22. Von Moltke J, Ji M, Liang HE, Locksley RM. Tuft-cell-derived IL-25 regulates an intestinal ILC2–epithelial response circuit. *Nature* (2016) 529 (7585):221–5. doi: 10.1038/nature16161

23. Ivanov II, Honda K. Intestinal commensal microbes as immune modulators. *Cell Host Microbe* (2012) 12(4):496–508. doi: 10.1016/j.chom.2012.09.009

24. Allaire JM, Crowley SM, Law HT, Chang SY, Ko HJ, Vallance BA. The intestinal epithelium: Central coordinator of mucosal immunity. *Trends Immunol* (2018) 39(9):677–96. doi: 10.1016/j.it.2018.04.002

25. Sun M, He C, Cong Y, Liu Z. Regulatory immune cells in regulation of intestinal inflammatory response to microbiota. *Mucosal Immunol* (2015) 8 (5):969–78. doi: 10.1038/mi.2015.49

26. La Fata G, Weber P, Mohajeri MH. Probiotics and the gut immune system: Indirect regulation. *Probiotics Antimicrob Proteins* (2018) 10(1):11–21. doi: 10.1007/s12602-017-9322-6

27. Parada Venegas D, de la Fuente MK, Landskron G, González MJ, Quera R, Dijkstra G, et al. Short chain fatty acids (SCFAs)-mediated gut epithelial and immune regulation and its relevance for inflammatory bowel diseases. *Front Immunol* (2019) 10:277. doi: 10.3389/fimmu.2019.00277

28. Naik S, Bouladoux N, Wilhelm C, Molloy MJ, Salcedo R, Kastenmuller W, et al. Compartmentalized control of skin immunity by resident commensals. *Science* (2012) 337(6098):1115–9. doi: 10.1126/science.1225152

29. Hayes CL, Dong J, Galipeau HJ, Jury J, McCarville J, Huang X, et al. Commensal microbiota induces colonic barrier structure and functions that contribute to homeostasis. *Sci Rep* (2018) 8(1):1–4. doi: 10.1038/s41598-018-32366-6

30. Loh G, Blaut M. Role of commensal gut bacteria in inflammatory bowel diseases. *Gut Microbes* (2012) 3(6):544–55. doi: 10.4161/gmic.22156

31. Martín R, Miquel S, Ulmer J, Kechaou N, Langella P, Bermúdez-Humarán LG. Role of commensal and probiotic bacteria in human health: a focus on inflammatory bowel disease. *Microb Cell Factories* (2013) 12(1):1–1. doi: 10.1186/1475-2859-12-71

32. Yan F, Cao H, Cover TL, Whitehead R, Washington MK, Polk DB. Soluble proteins produced by probiotic bacteria regulate intestinal epithelial cell survival and growth. *Gastroenterology* (2007) 132(2):562–75. doi: 10.1053/j.gastro.2006.11.022

33. Bauerl C, Perez-Martinez G, Yan F, Polk DB, Monedero V. Functional analysis of the p40 and p75 proteins from *Lactobacillus casei* BL23. *J Mol Microbiol Biotechnol* (2010) 19(4):231–41. doi: 10.1159/000322233

34. Claes IJ, Schoofs G, Regulski K, Courtin P, Chapot-Chartier MP, Rolain T, et al. Genetic and biochemical characterization of the cell wall hydrolase activity of the major secreted protein of *Lactobacillus rhamnosus* GG. *PloS One* (2012) 7(2): e31588. doi: 10.1371/journal.pone.0031588

35. Regulski K, Courtin P, Meyrand M, Claes IJ, Lebeer S, Vanderleyden J, et al. Analysis of the peptidoglycan hydrolase complement of *Lactobacillus casei* and characterization of the major gamma-D-Glutamyl-L-Lysyl-Endopeptidase. *PloS One* (2012) 7(2):e32301. doi: 10.1371/journal.pone.0032301

36. Bauerl C, Abitayeva G, Sosa-Carrillo S, Mencher-Beltran A, Navarro-Lleo N, Coll-Marques JM, et al. P40 and P75 are singular functional muramidases present in the *Lactobacillus casei/paracasei/rhamnosus* taxon. *Front Microbiol* (2019) 10:1420. doi: 10.3389/fmicb.2019.01420

37. Bauerl C, Coll-Marques JM, Tarazona-Gonzalez C, Perez-Martinez G. *Lactobacillus casei* extracellular vesicles stimulate EGFR pathway likely due to the presence of proteins P40 and P75 bound to their surface. *Sci Rep* (2020) 10 (1):19237. doi: 10.1038/s41598-020-75930-9

38. Arribas J, Bech-Serra JJ, Santiago-Josefat B. ADAMs, cell migration and cancer. *Cancer Metastasis Rev* (2006) 25(1):57–68. doi: 10.1007/s10555-006-7889-6

39. Yan F, Liu L, Dempsey PJ, Tsai YH, Raines EW, Wilson CL, et al. A *Lactobacillus rhamnosus* GG-derived soluble protein, p40, stimulates ligand release from intestinal epithelial cells to transactivate epidermal growth factor receptor. *J Biol Chem* (2013) 288(42):30742–51. doi: 10.1074/jbc.M113.492397

40. Yan F, Cao H, Cover TL, Washington MK, Shi Y, Liu L, et al. Colon-specific delivery of a probiotic-derived soluble protein ameliorates intestinal inflammation in mice through an EGFR-dependent mechanism. *J Clin Invest* (2011) 121 (6):2242–53. doi: 10.1172/JCI44031

41. Wang L, Cao H, Liu L, Wang B, Walker WA, Acra SA, et al. Activation of epidermal growth factor receptor mediates mucin production stimulated by p40, a *Lactobacillus rhamnosus* GG-derived protein. *J Biol Chem* (2014) 289(29):20234–44. doi: 10.1074/jbc.M114.553800

42. Wang Y, Liu L, Moore DJ, Shen X, Peek RM, Acra SA, et al. An LGG-derived protein promotes IgA production through upregulation of APRIL expression in intestinal epithelial cells. *Mucosal Immunol* (2017) 10(2):373–84. doi: 10.1038/mi.2016.57

43. Dubé PE, Yan F, Punit S, Girish N, McElroy SJ, Washington MK, et al. Epidermal growth factor receptor inhibits colitis-associated cancer in mice. *J Clin Investig* (2012) 122(8):2780–92. doi: 10.1172/JCI62888

44. Deng Y, McDonald OG, Means AL, Peek RMJr., Washington MK, Acra SA, et al. Exposure to p40 in early life prevents intestinal inflammation in adulthood through inducing a long-lasting epigenetic imprint on TGFβ. *Cell Mol Gastroenterol* (2021) 11(5):1327–45. doi: 10.1016/j.jcmgh.2021.01.004

45. Miettinen PJ, Berger JE, Meneses J, Phung Y, Pedersen RA, Werb Z, et al. Epithelial immaturity and multiorgan failure in mice lacking epidermal growth factor receptor. *Nature* (1995) 376(6538):337–41. doi: 10.1038/376337a0

46. Shen X, Liu L, Peek RM, Acra SA, Moore DJ, Wilson KT, et al. Supplementation of p40, a *Lactobacillus rhamnosus* GG-derived protein, in early life promotes epidermal growth factor receptor-dependent intestinal development and long-term health outcomes. *Mucosal Immunol* (2018) 11(5):1316–28. doi: 10.1038/s41385-018-0034-3

47. Tamburini S, Shen N, Wu HC, Clemente JC. The microbiome in early life: Implications for health outcomes. *Nat Med* (2016) 22(7):713–22. doi: 10.1038/nm.4142

48. Ganal SC, Sanos SL, Kallfass C, Oberle K, Johner C, Kirschning C, et al. Priming of natural killer cells by nonmucosal mononuclear phagocytes requires instructive signals from commensal microbiota. *Immunity* (2012) 37(1):171–86. doi: 10.1016/j.immuni.2012.05.020

49. Shilatifard A. The COMPASS family of histone H3K4 methylases: mechanisms of regulation in development and disease pathogenesis. *Annu Rev Biochem* (2012) 81:65–95. doi: 10.1146/annurev-biochem-051710-134100

50. Salvi PS, Cowles RA. Butyrate and the intestinal epithelium: modulation of proliferation and inflammation in homeostasis and disease. *Cells* (2021) 10 (7):1775. doi: 10.3390/cells10071775

51. Wang RX, Lee JS, Campbell EL, Colgan SP. Microbiota-derived butyrate dynamically regulates intestinal homeostasis through regulation of actin-associated protein synaptopodin. *Proc Natl Acad Sci* (2020) 117(21):11648–57. doi: 10.1073/pnas.1917597117

52. Zheng L, Kelly CJ, Battista KD, Schaefer R, Lanis JM, Alexeev EE, et al. Microbial-derived butyrate promotes epithelial barrier function through IL-10 receptor–dependent repression of claudin-2. *J Immunol* (2017) 199(8):2976–84. doi: 10.4049/jimmunol.1700105

53. Lukovac S, Belzer C, Pellis L, Keijser BJ, de Vos WM, Montijn RC, et al. Differential modulation by akkermansia muciniphila and faecalibacterium prausnitzii of host peripheral lipid metabolism and histone acetylation in mouse gut organoids. *M Bio* (2014) 5(4):e01438–14. doi: 10.1128/mBio.01438-14

54. Bolduc JF, Hany L, Barat C, Ouellet M, Tremblay MJ. Epigenetic metabolite acetate inhibits class I/II histone deacetylases, promotes histone acetylation, and increases HIV-1 integration in CD4+ T cells. *J Virol* (2017) 91(16):e01943–16. doi: 10.1128/JVI.01943-16

55. Hatayama H, Iwashita J, Kuwajima A, Abe T. The short chain fatty acid, butyrate, stimulates MUC2 mucin production in the human colon cancer cell line, LS174T. *Biochem Biophys Res Commun* (2007) 356(3):599–603. doi: 10.1016/j.bbrc.2007.03.025

56. Burger-van Paassen N, Vincent A, Puiman PJ, van der Sluis M, Bouma J, Boehm G, et al. The regulation of intestinal mucin MUC2 expression by short-chain fatty acids: implications for epithelial protection. *Biochem J* (2009) 420 (2):211–9. doi: 10.1042/BJ20082222

57. Peng L, Li ZR, Green RS, Holzman IR, Lin J. Butyrate enhances the intestinal barrier by facilitating tight junction assembly *via* activation of AMP-activated protein kinase in caco-2 cell monolayers. *J Nutr* (2009) 139(9):1619–25. doi: 10.3945/jn.109.104638

58. Luu M, Monning H, Visekruna A. Exploring the molecular mechanisms underlying the protective effects of microbial SCFAs on intestinal tolerance and food allergy. *Front Immunol* (2020) 11:1225. doi: 10.3389/fimmu.2020.01225

59. Wu W, Sun M, Chen F, Cao AT, Liu H, Zhao Y, et al. Microbiota metabolite short-chain fatty acid acetate promotes intestinal IgA response to microbiota which is mediated by GPR43. *Mucosal Immunol* (2017) 10(4):946–56. doi: 10.1038/mi.2016.114

60. Li X, Zhang B, Hu Y, Zhao Y. New insights into gut-bacteria-derived indole and its derivatives in intestinal and liver diseases. *Front Pharmacol* (2021) 12:769501. doi: 10.3389/fphar.2021.769501

61. Metidji A, Omenetti S, Crotta S, Li Y, Nye E, Ross E, et al. The environmental sensor AHR protects from inflammatory damage by maintaining intestinal stem cell homeostasis and barrier integrity. *Immunity* (2018) 49(2):353–62. doi: 10.1016/j.immuni.2018.07.010

62. Ye X, Li H, Anjum K, Zhong X, Miao S, Zheng G, et al. Dual role of indoles derived from intestinal microbiota on human health. *Front Immunol* (2022) 13:903526. doi: 10.3389/fimmu.2022.903526

63. Beaumont M, Neyrinck AM, Olivares M, Rodriguez J, de Rocca Serra A, Roumain M, et al. The gut microbiota metabolite indole alleviates liver inflammation in mice. *FASEB J* (2018) 32(12):6681–93. doi: 10.1096/fj.201800544

64. Scott SA, Fu J, Chang PV. Microbial tryptophan metabolites regulate gut barrier function *via* the aryl hydrocarbon receptor. *Proc Natl Acad Sci* (2020) 117 (32):19376–87. doi: 10.1073/pnas.2000047117

65. Powell DN, Swimm A, Sonowal R, Bretin A, Gewirtz AT, Jones RM, et al. Indoles from the commensal microbiota act *via* the AHR and IL-10 to tune the cellular composition of the colonic epithelium during aging. *Proc Natl Acad Sci* (2020) 117(35):21519–26. doi: 10.1073/pnas.2003004117

66. Ehrlich AM, Henrick B, Pacheco A, Taft D, Xu G, Huda N, et al. Bifidobacterium grown on human milk oligosaccharides produce tryptophan metabolite indole-3-lactic acid that significantly decreases inflammation in intestinal cells *in vitro*. *FASEB J* (2018) 32:359. doi: 10.1096/fasebj.2018.32.1

67. Rose EC, Odle J, Blikslager AT, Ziegler AL. Probiotics, prebiotics and epithelial tight junctions: A promising approach to modulate intestinal barrier function. *Int J Mol Sci* (2021) 22(13):6729. doi: 10.3390/ijms22136729

68. do Carmo FL, Rabah H, De Oliveira Carvalho RD, Gaucher F, Cordeiro BF, da Silva SH, et al. Extractable bacterial surface proteins in probiotic–host interaction. *Front Microbiol* (2018) 9:2018.00645. doi: 10.3389/fmicb.2018.00645

69. Liu Q, Yu Z, Tian F, Zhao J, Zhang H, Zhai Q, et al. Surface components and metabolites of probiotics for regulation of intestinal epithelial barrier. *Microb Cell Factories* (2020) 19(1):1–1. doi: 10.1186/s12934-020-1289-4

70. Lightfoot YL, Selle K, Yang T, Goh YJ, Sahay B, Zadeh M, et al. SIGNR 3-dependent immune regulation by *Lactobacillus acidophilus* surface layer protein a in colitis. *EMBO J* (2015) 34(7):881–95. doi: 10.15252/embj.201490296

71. Chandhni PR, Pradhan D, Sowmya K, Gupta S, Kadyan S, Choudhary R, et al. Ameliorative effect of surface proteins of probiotic lactobacilli in colitis mouse models. *Front Microbiol* (2021) 12:679773. doi: 10.3389/fmicb.2021.679773

72. Li PN, Herrmann J, Tolar BB, Poitevin F, Ramdasi R, Bargar JR, et al. Nutrient transport suggests an evolutionary basis for charged archaeal surface layer proteins. *ISME J* (2018) 12(10):2389–402. doi: 10.1038/s41396-018-0191-0

73. Li P, Yu Q, Ye X, Wang Z, Yang Q. Lactobacillus s-layer protein inhibition of salmonella-induced reorganization of the cytoskeleton and activation of MAPK signalling pathways in caco-2 cells. *Microbiology* (2011) 157(9):2639–46. doi: 10.1099/mic.0.049148-0

74. Angelin J, Kavitha M. Exopolysaccharides from probiotic bacteria and their health potential. *Int J Biol Macromol* (2020) 162:853–65. doi: 10.1016/j.ijbiomac.2020.06.190

75. Werning ML, Hernández-Alcántara AM, Ruiz MJ, Soto LP, Dueñas MT, López P, et al. Biological functions of exopolysaccharides from lactic acid bacteria and their potential benefits for humans and farmed animals. *Foods* (2022) 11 (9):1284. doi: 10.3390/foods11091284

76. Chen Y, Zhang M, Ren F. A role of exopolysaccharide produced by *Streptococcus thermophilus* in the intestinal inflammation and mucosal barrier in caco-2 monolayer and dextran sulphate sodium-induced experimental murine colitis. *Molecules* (2019) 24(3):513. doi: 10.3390/molecules24030513

77. Živković M, Miljković MS, Ruas-Madiedo P, Markelić MB, Veljović K, Tolinački M, et al. EPS-SJ exopolisaccharide produced by the strain *Lactobacillus paracasei* subsp. paracasei BGSJ2-8 is involved in adhesion to epithelial intestinal cells and decrease on e. coli association to caco-2 cells. *Front Microbiol* (2016) 7:286. doi: 10.3389/fmicb.2016.00286

78. Wells JM, Rossi O, Meijerink M, van Baarlen P. Epithelial crosstalk at the microbiota-mucosal interface. *Proc Natl Acad Sci* (2011) 108:4607–14. doi: 10.1073/pnas.1000092107

79. Li Y, Wang W, Yang F, Xu Y, Feng C, Zhao Y. The regulatory roles of neutrophils in adaptive immunity. *Cell Commun Signal* (2019) 17(1):1–1. doi: 10.1186/s12964-019-0471

80. Liu Y, Zheng S, Cui J, Guo T, Zhang J, Li B. Alleviative effects of exopolysaccharide produced by *Lactobacillus helveticus* KLDS1. 8701 on dextran sulfate sodium-induced colitis in mice. *Microorganisms* (2021) 9(10):2086. doi: 10.3390/microorganisms9102086

81. Zhou X, Qi W, Hong T, Xiong T, Gong D, Xie M, et al. Exopolysaccharides from *Lactobacillus plantarum* NCU116 regulate intestinal barrier function *via* STAT3 signaling pathway. *J Agric Food Chem* (2018) 66(37):9719–27. doi: 10.1021/acs.jafc.8b03340

82. Zhou X, Zhang D, Qi W, Hong T, Xiong T, Wu T, et al. Exopolysaccharides from *Lactobacillus plantarum* NCU116 facilitate intestinal homeostasis by modulating intestinal epithelial regeneration and microbiota. *J Agric Food Chem* (2021) 69(28):7863–73. doi: 10.1021/acs.jafc.1c01898

83. Lukic J, Chen V, Strahinic I, Begovic J, Lev-Tov H, Davis SC, et al. Probiotics or pro-healers: the role of beneficial bacteria in tissue repair. *Wound Repair Regeneration* (2017) 25(6):912–22. doi: 10.1111/wrr.12607

84. Zaghloul EH, Ibrahim MI. Production and characterization of exopolysaccharide from newly isolated marine probiotic *Lactiplantibacillus plantarum* EI6 with *in vitro* wound healing activity. *Front Microbiol* (2022) 13:903363. doi: 10.3389/fmicb.2022.903363

85. Oerlemans MM, Akkerman R, Ferrari M, Walvoort MT, de Vos P. Benefits of bacteria-derived exopolysaccharides on gastrointestinal microbiota, immunity and health. *J Funct Foods* (2021) 76:104289. doi: 10.1016/j.jff.2020.104289

86. Wolf AJ, Underhill DM. Peptidoglycan recognition by the innate immune system. *Nat Rev Immunol* (2018) 18(4):243–54. doi: 10.1038/nri.2017.136

87. Kashyap DR, Kuzma M, Kowalczyk DA, Gupta D, Dziarski R. Bactericidal peptidoglycan recognition protein induces oxidative stress in *Escherichia coli* through a block in respiratory chain and increase in central carbon catabolism. *Mol Microbiol* (2017) 105(5):755–76. doi: 10.1111/mmi.13733

88. Dabrowski AN, Shrivastav A, Conrad C, Komma K, Weigel M, Dietert K, et al. Peptidoglycan recognition protein 4 limits bacterial clearance and inflammation in lungs by control of the gut microbiota. *Front Immunol* (2019) 10:2106. doi: 10.3389/fimmu.2019.02106

89. Bu HF, Wang X, Tang Y, Koti V, Tan XD. Toll-like receptor 2-mediated peptidoglycan uptake by immature intestinal epithelial cells from apical side and exosome-associated transcellular transcytosis. *J Cell Physiol* (2010) 222(3):658–68. doi: 10.1002/jcp.21985

90. Sultana R, McBain AJ, O'Neill CA. Strain-dependent augmentation of tight-junction barrier function in human primary epidermal keratinocytes by *Lactobacillus* and *Bifidobacterium* lysates. *Appl Environ Microbiol* (2013) 79 (16):4887–94. doi: 10.1128/AEM.00982-13

91. Yang F, Wang A, Zeng X, Hou C, Liu H, Qiao S. *Lactobacillus reuteri* I5007 modulates tight junction protein expression in IPEC-J2 cells with LPS stimulation and in newborn piglets under normal conditions. *BMC Microbiol* (2015) 15(1):1–1. doi: 10.1186/s12866-015-0372-1

92. Rajagopal M, Walker S. Envelope structures of gram-positive bacteria. *Protein Sugar Export Assembly Gram-positive Bacteria* (2015) 404:1–44. doi: 10.1007/82_2015_5021

93. Jastrzab R, Graczyk D, Siedlecki P. Molecular and cellular mechanisms influenced by postbiotics. *Int J Mol Sci* (2021) 22(24):13475. doi: 10.3390/ijms222413475

94. Kim KW, Kang SS, Woo SJ, Park OJ, Ahn KB, Song KD, et al. Lipoteichoic acid of probiotic *Lactobacillus plantarum* attenuates poly I: C-induced IL-8 production in porcine intestinal epithelial cells. *Front Microbiol* (2017) 8:1827. doi: 10.3389/fmicb.2017.01827

95. Donaldson GP, Lee SM, Mazmanian SK. Gut biogeography of the bacterial microbiota. *Nat Rev Microbiol* (2016) 14(1):20–32. doi: 10.1038/nrmicro3552

96. Spor A, Koren O, Ley R. Unravelling the effects of the environment and host genotype on the gut microbiome. *Nat Rev Microbiol* (2011) 9(4):279–90. doi: 10.1038/nrmicro2540

97. Stephens WZ, Kubinak JL, Ghazaryan A, Bauer KM, Bell R, Buhrke K, et al. Epithelial-myeloid exchange of MHC class II constrains immunity and microbiota composition. *Cell Rep* (2021) 37(5):109916. doi: 10.1016/j.celrep.2021.109916

98. Yu S, Balasubramanian I, Laubitz D, Tong K, Bandyopadhyay S, Lin X, et al. Paneth cell-derived lysozyme defines the composition of mucolytic microbiota and the inflammatory tone of the intestine. *Immunity* (2020) 53(2):398–416. doi: 10.1016/j.immuni.2020.07.010

99. Maas SL, Breakefield XO, Weaver AM. Extracellular vesicles: unique intercellular delivery vehicles. *Trends Cell Biol* (2017) 27(3):172–88. doi: 10.1016/j.tcb.2016.11.003

100. Hu G, Gong AY, Roth AL, Huang BQ, Ward HD, Zhu G, et al. Release of luminal exosomes contributes to TLR4-mediated epithelial antimicrobial defense. *PloS Pathog* (2013) 9(4):e1003261. doi: 10.1371/journal.ppat.1003261

101. Shifrin DAJr., McConnell RE, Nambiar R, Higginbotham JN, Coffey RJ, Tyska MJ. Enterocyte microvillus-derived vesicles detoxify bacterial products and regulate epithelial-microbial interactions. *Curr Biol* (2012) 22(7):627–31. doi: 10.1016/j.cub.2012.02.022

102. Yang L, Higginbotham JN, Liu L, Zhao G, Acra SA, Peek RMJr., et al. Production of a functional factor, p40, by *Lactobacillus rhamnosus* GG is promoted by intestinal epithelial cell-secreted extracellular vesicles. *Infect Immun* (2019) 87(7):00113–19. doi: 10.1128/IAI.00113-19

103. Chen B, Zhong D, Monteiro A. Comparative genomics and evolution of the HSP90 family of genes across all kingdoms of organisms. *BMC Genet* (2006) 7(1):1–9. doi: 10.1186/1471-2164-7-156

104. Johnson JL. Evolution and function of diverse Hsp90 homologs and cochaperone proteins. *Biochim Biophys Acta Mol Cell Res* (2012) 1823(3):607–13. doi: 10.1016/j.bbamcr.2011.09.020

105. Rossi F, Zotta T, Iacumin L, Reale A. Theoretical insight into the heat shock response (HSR) regulation in *Lactobacillus casei* and l. rhamnosus. *J Theor Biol* (2016) 402:21–37. doi: 10.1016/j.jtbi.2016.04.029

106. Xavier RJ, Podolsky DK. Unravelling the pathogenesis of inflammatory bowel disease. *Nature* (2007) 448(7152):427–34. doi: 10.1038/nature06005

107. Hur SJ, Kang SH, Jung HS, Kim SC, Jeon HS, Kim IH, et al. Review of natural products actions on cytokines in inflammatory bowel disease. *Nutr Res Rev* (2012) 32(11):801–16. doi: 10.1016/j.nutres.2012.09.013

108. Rioux KP, Fedorak RN. Probiotics in the treatment of inflammatory bowel disease. *J Clin Gastroenterol* (2006) 40:260–3. doi: 10.1097/00004836-200603000-00019

109. Sultan S, El-Mowafy M, Elgaml A, Ahmed TA, Hassan H, Mottawea W. Metabolic influences of gut microbiota dysbiosis on inflammatory bowel disease. *Front Physiol* (2021) 1489:715506. doi: 10.3389/fphys.2021.715506

110. Wu S, Rhee KJ, Albesiano E, Rabizadeh S, Wu X, Yen HR, et al. A human colonic commensal promotes colon tumorigenesis *via* activation of T helper type 17 T cell responses. *Nat Med* (2009) 15(9):1016–22. doi: 10.1038/nm.2015

111. Housseau F, Wu S, Wick EC, Fan H, Wu X, Llosa NJ, et al. Redundant innate and adaptive sources of IL17 production drive colon TumorigenesisIL17 and microbial-induced colon cancer. *Cancer Res* (2016) 76(8):2115–24. doi: 10.1158/0008-5472.CAN-15-0749

112. Grivennikov SI, Wang K, Mucida D, Stewart CA, Schnabl B, Jauch D, et al. Adenoma-linked barrier defects and microbial products drive IL-23/IL-17-mediated tumour growth. *Nature* (2012) 491(7423):254–8. doi: 10.1038/nature11465

113. Fan X, Jin Y, Chen G, Ma X, Zhang L. Gut microbiota dysbiosis drives the development of colorectal cancer. *Digestion* (2021) 102(4):508–15. doi: 10.1159/000508328

114. Kaur H, Ali SA. Probiotics and gut microbiota: Mechanistic insights into gut immune homeostasis through TLR pathway regulation. *Food Funct* (2022) 13:7423–47. doi: 10.1039/D2FO00911K

115. Gupta T, Kaur H, Kapila S, Kapila R. Potential probiotic *Lacticaseibacillus rhamnosus* MTCC-5897 attenuates escherichia coli induced inflammatory response in intestinal cells. *Arch Microbiol* (2021) 203(9):5703–13. doi: 10.1007/s00203-021-02541-x

116. Gupta T, Kaur H, Kapila S, Kapila R. *Lactobacillus fermentum* (MTCC-5898) alleviates escherichia coli-induced inflammatory responses in intestinal epithelial cells by modulating immune genes and NF-κB signalling. *J Appl Microbiol* (2021) 131(6):3008–17. doi: 10.1111/jam.15153

117. Kaur H, Gupta T, Kapila S, Kapila R. Protective effects of potential probiotic *Lactobacillus rhamnosus* (MTCC-5897) fermented whey on reinforcement of intestinal epithelial barrier function in a colitis-induced murine model. *Food Funct* (2021) 12(13):6102–16. doi: 10.1039/d0fo02641g

frontiers | Frontiers in Immunology

TYPE Original Research
PUBLISHED 13 September 2022
DOI 10.3389/fimmu.2022.995610

OPEN ACCESS

EDITED BY
Yanbo Wang,
Nanjing University, China

REVIEWED BY
Raquel Planas,
University of Barcelona, Spain
Iria Gomez-Tourino,
University of Santiago de Compostela, Spain

*CORRESPONDENCE
Zhiguo Xie
xiezhiguo@csu.edu.cn
Zhiguang Zhou
zhouzhiguang@csu.edu.cn

†These authors have contributed equally to this work

SPECIALTY SECTION
This article was submitted to Cytokines and Soluble Mediators in Immunity, a section of the journal Frontiers in Immunology

RECEIVED 16 July 2022
ACCEPTED 26 August 2022
PUBLISHED 13 September 2022

CITATION
Fan W, Pang H, Shi X, Li J, Wang Y, Luo S, Lin J, Yu H, Xiao Y, Li X, Huang G, Xie Z and Zhou Z (2022) Plasma-derived exosomal mRNA profiles associated with type 1 diabetes mellitus.
Front. Immunol. 13:995610.
doi: 10.3389/fimmu.2022.995610

Plasma-derived exosomal mRNA profiles associated with type 1 diabetes mellitus

Wenqi Fan[1,2†], Haipeng Pang[1,2†], Xiajie Shi[1,2], Jiaqi Li[1,2], Yimeng Wang[1,2], Shuoming Luo[1,2], Jian Lin[1,2], Haibo Yu[1,2], Yang Xiao[1,2], Xia Li[1,2], Gan Huang[1,2], Zhiguo Xie[1,2*] and Zhiguang Zhou[1,2*]

[1]National Clinical Research Center for Metabolic Diseases, Key Laboratory of Diabetes Immunology (Central South University), Ministry of Education, Changsha, China, [2]Department of Metabolism and Endocrinology, The Second Xiangya Hospital of Central South University, Changsha, China

Background: Exosomes carry various types of transcripts, such as messenger RNAs (mRNAs), and play an important role in mediating cell-to-cell communication, thus influencing multiple physiological and pathological processes. However, the role of exosomal mRNAs in T1DM is largely unknown. Here, we aimed to identify the plasma-derived exosomal mRNA expression profiles in T1DM and to explore their potential biological functions in T1DM.

Materials and Methods: Plasma-derived exosomes were isolated from 10 patients with T1DM and 10 age- and sex-matched control subjects by size exclusion chromatography methods. Transmission electron microscopy, nanoparticle tracking analysis, and western blot analysis confirmed the presence of exosomes. The exosomal mRNAs were analyzed using the Illumina HiSeq platform. Six differentially expressed mRNAs (DEMs) were randomly selected to determine the expression level by quantitative real-time PCR (qRT–PCR) in a larger cohort (T1DM subjects N=40; control subjects N=40). The biological functions of DEMs were predicted by Gene Ontology (GO) and Kyoto Encyclopedia of Genes and Genomes (KEGG) analyses. Protein–protein interaction networks were constructed to explore the potential associations among DEMs.

Results: In total, 112 DEMs were identified in T1DM, among which 66 mRNAs were upregulated and 46 mRNAs were downregulated. Four of six candidate exosomal mRNAs were successfully validated by qRT–PCR. Bioinformatics analysis indicated that these mRNAs were most significantly involved in positive regulation by host viral transcription (GO enrichment analysis) and oxidative phosphorylation (KEGG pathway analysis).

Conclusions: Our study reported the plasma-derived exosomal mRNA expression profiles of T1DM for the first time. The identified DEMs might be

associated with the pathogenesis of T1DM, and some DEMs have the potential to serve as biomarkers and therapeutic targets for T1DM.

KEYWORDS

type 1 diabetes mellitus, exosomes, messenger RNAs, biomarker, plasma

Introduction

Type 1 diabetes mellitus (T1DM) is defined as a chronic disease caused by autoimmune attack against pancreatic islet beta-cells (1). At present, most patients with T1DM have to rely on lifelong insulin replacement therapy. It has been indicated that the incidence of T1DM peaks at the ages of 10-14 years, and the estimated number of children and adolescents with T1DM is increasing worldwide (2). In addition, because of long-standing hyperglycemia, diabetes mellitus will induce severe chronic injury and dysfunction in all kinds of tissues and organs, imposing tremendous health and economic burdens on patients. It has been widely accepted that the pathophysiological process of T1DM is induced by environmental factors in individuals who are at high genetic risk (3, 4). However, many aspects of the pathogenic process of T1DM are unknown.

Recently, a small membrane-derived lipid bilayer vesicle, namely, the exosome (30-200 nm in diameter), has been shown to be of great importance in mediating intercellular and interorgan communication (5, 6). The bioactive materials delivered by exosomes, such as DNA, RNA (mRNA, lncRNA, and miRNA) and proteins, can be transferred into recipient cells and can alter their status and function (7, 8). In the context of T1DM, the abnormal interactions between pancreatic beta-cells and immune cells, especially T lymphocytes, represent the main pathogenic mechanism (9). Interestingly, mounting evidence has suggested that exosomes might serve as novel mediators between beta-cells and immune cells. For instance, islet-derived exosomes contain beta-cell autoantigens and can be taken up by dendritic cells, thus leading to cell activation (10). In addition, exosome release by T lymphocytes can induce beta-cell apoptosis *via* certain exosomal miRNA-mediated signaling (11). In addition, given that the content of exosomes can reflect the status of the originating cells, exosomes are viewed as promising diagnostic tools for many diseases. It has been indicated that human islet-derived exosomal RNAs are dysregulated under cytokine stress (12). Our recent study characterized the lncRNA profiles of plasma-derived exosomes from T1DM patients and explored their potential biomarker use (13). In addition, a study measured plasma-derived exosomal miRNA expression profiles and reported a distinct miRNA signature in long-duration T1DM (14), which highlighted the biomarker potential of exosomes in T1DM.

Existing studies have mostly focused on exosomal miRNAs. Here, we report the mRNA expression profiles of plasma-derived exosomes in T1DM for the first time. Our work might provide novel insights into the pathogenesis of T1DM and lay the foundation for the use of exosomal mRNA as a biomarker.

Materials and methods

Study subjects

This study was approved by the institutional ethics review board of the Second Xiangya Hospital of Central South University, and all experiments complied with the ethical principles of the Declaration of Helsinki. The inclusion and exclusion criteria of T1DM patients and control subjects have been described previously (13). In the discovery phase, 10 cases and 10 age- (P=0.732) and sex- (P=0.650) matched controls were recruited (13). We used a larger cohort (T1DM N=40; controls N=40) for the subsequent validation phase. All peripheral blood samples were obtained after full informed consent was received.

Isolation and characterization of exosomes

Peripheral blood samples (5 ml) from participants were collected in EDTA tubes. The plasma was separated and stored at -80°C after centrifugation at 3000×g for 15 min at 4°C. Exosomes were isolated by using size exclusion chromatography with Exosupur® columns (Echobiotech, China) and were characterized by transmission electron microscopy (TEM), nanoparticle tracking analysis (NTA), and western blotting (WB) (performed by EchoBio Technology, Beijing, China). The detailed procedures have been described previously (13). In brief, the filtered plasma was diluted with phosphate-buffered saline and purified by Exosupur® columns. The collected fraction was concentrated by a 100-kDa molecular weight cutoff Amicon® Ultra spin filter (Merck, Germany) to obtain exosomes. Exosomes (10 μL) were placed on a copper

mesh and negatively stained with uranyl acetate solution. Then, the sample was examined by TEM (H7650, Hitachi Ltd, Tokyo, Japan). The size distribution of isolated exosomes was determined by a ZetaView PMX 110 (Particle Metrix, Meerbusch, Germany) and analyzed by NTA software (ZetaView 8.02.28). Finally, the exosomes were subjected to WB analysis using rabbit polyclonal antibodies against TSG101, Alix, CD63 and calnexin. The verification of exosomes was entrusted to the company (Echo Biotech Co., Ltd, Beijing, P. R. China).

RNA extraction and mRNA sequencing

The exosomal RNA was extracted using the miRNeasy Serum/Plasma Advanced Kit (Qiagen, cat. No. 217204). RNA profiles were assessed by using the RNA Nano 6000 Assay Kit of the Agilent Bioanalyzer 2100 System (Agilent Technologies, CA, USA). After library construction and evaluation, sequencing was performed by an Illumina NovaSeq6000 platform (performed by EchoBio Technology, Beijing, China).

mRNA analysis

Raw reads in fastq format were first processed through in-house Perl scripts. In this step, clean reads were obtained by removing reads containing adapters, reads containing poly-N sequences and low-quality reads from the raw data. At the same time, the Q20, Q30, GC content and sequence duplication level of the clean data were calculated. All downstream analyses were based on clean data with high quality. Paired-end clean reads were aligned to the reference genome GRCh38 using HISAT2. Mapped reads were used for the quantification of gene expression levels and differential expression analysis. StringTie was used to explore novel mRNAs and to calculate FPKMs (reads per kilobase per million mapped reads) of coding genes in each sample. Gene FPKMs were computed by summing the FPKMs of transcripts in each gene group. Sequencing data analyses were mainly performed using R v3.5.1. We applied the Mann–Whitney U test to carry out the differential expression analysis with the cutoffs of FPKM > 5, P value < 0.05 and $|\log2(FC)| > 0.584$. Heatmaps, volcano diagrams, and MA plots were generated to visualize the differentially expressed mRNAs (DEMs) using the R packages "pheatmap" and "ggplot2".

Functional enrichment analysis of identified mRNAs

After the completion of mRNA analysis, BLAST software was adopted to compare the new genes with the NR, SwissProt, GO, COG, and KEGG databases to obtain annotation information, and then Gene Ontology (GO) and Kyoto Encyclopedia of Genes and Genomes (KEGG) pathway enrichment analyses were performed by using the topGO R packages and KOBAS software to explore the potential functions of the identified exosomal DEMs (15).

Protein–protein interaction network

The Search Tool for the Retrieval of Interacting Genes (STRING) (v11.5) was used to predict the associations among DEMs. A combined score > 0.4 was considered a statistically significant interaction. A protein-protein interaction (PPI) network was constructed using Cytoscape v3.7.0. Using the CytoHubba plug-in of Cytoscape software, each gene was scored based on the MNC, DMNC, MCC, EPC, and degree algorithms. Based on the scoring results of the five algorithms, the top 8 genes in each algorithm were considered hub genes.

Quantitative real-time PCR analysis

To validate the expression level of DEMs, six mRNAs, namely, ENSG00000158417, ENSG00000185883, ENSG00000198763, ENSG00000198786, ENSG00000198840 and ENSG00000269028, were randomly selected to perform qRT–PCR analysis in an independent cohort including 40 T1DM and 40 control subjects. The detailed information of the participants is summarized in Table 1. All T1DM patients were at a symptomatic stage, characterized by the presence of islet autoantibodies and persistent hyperglycemia. GAPDH was used as an internal reference. Briefly, total RNA was extracted from plasma-derived exosomes and then reverse transcribed into cDNA by using the PrimeScript™ RT reagent Kit (Perfect Real Time) (TAKARA, RR037A). The expression level of candidate mRNAs was measured with the TaqMan® probe using qPCR, and all experiments were performed in triplicate wells. The primers and probes are shown in Table 2. We used an unpaired t test to compare the expression levels of selected mRNAs between the two groups. A P value < 0.05 was considered statistically significant. The results were visualized using the R package.

Results

Characterization of exosomes

To validate the detection of exosomes, we performed TEM, NTA, and WB analysis. As shown in Figures 1A, B, the isolated particles were oval- and cup-shaped and were approximately 121.5 nm in diameter (30 nm to 200 nm), consistent with the

10.3389/fimmu.2022.995610

TABLE 1 Detailed information of T1DM patients and control subjects in the validation phase.

Characteristics	T1DM (n=40)	Control (n=40)	*P* value
Sex (male/female)	17/23	19/21	0.65
Age (years)	27.35 ± 8.68	28.4 ± 5.00	0.51
Duration (months)	25.76 ± 14.37	NA	NA
FPG (mmol/L)	7.79 ± 3.25	4.75 ± 0.40	0.00
HbA1c %	7.55 ± 2.04	5.37 ± 0.23	0.00
TC (mmol/L)	4.26 ± 0.83	4.28 ± 0.46	0.90
HDL (mmol/L)	1.59 ± 0.43	1.31 ± 0.39	0.01
LDL (mmol/L)	2.36 ± 0.70	2.49 ± 0.42	0.34
TG (mmol/L)	0.76 ± 0.30	0.90 ± 0.32	0.08
CREA (μmol/L)	63.07 ± 12.53	66.21 ± 14.75	0.36
Age of onset (years)	25.60 ± 8.13	NA	NA
FCP (pmol/L)	94.40 (39.10-148.40)	NA	NA
2 h-PCP (pmol/L)	157.05 (88.93-466.45)	NA	NA
GADA positivity (%)	90.00	NA	NA
GADA titer (u/ml)	149.25 (27.73-575.88)	NA	NA
IA-2A positivity (%)	55.00	NA	NA
IA-2A titer (u/ml)	17.79 (0-800.52)	NA	NA
ZnT8A positivity (%)	35.00	NA	NA

FPG, fasting plasma glucose; HbA1c, hemoglobin A1c; TC, total cholesterol; LDL, low-density lipoprotein; CREA, creatinine; FCP, fasting C-peptide; PCP, postprandial C-peptide; GADA, glutamic acid decarboxylase antibody; IA-2A, protein tyrosine phosphatase antibody; ZnT8A, zinc transporter 8 antibody; NA, not applicable.

TABLE 2 Primer list.

mRNA	Symbol	Primer Sequence (5'-3')
ENSG00000158417	EIF5B	F-GATGGTGAAGCAGGTGGTAT
		R-CCTTTGCTCGCTCCTCAA
		P-CCTGACTCTGATGTGGCTGCTACTTT
ENSG00000185883	ATP6V0C	F-Forward-CTCATCTTCGCCGAGGTG
		R-CGTTCTGGAATGAGGAGGG
		P-CGAGCCCACCAGCCACAGAA
ENSG00000198763	MT-ND2	F-ACTCAACTTAAACTCCAGCACC
		R-TAGGCGTAGGTAGAAGTAGAGG
		P-ATCTCGCACCTGAAACAAGCTAACA
ENSG00000198786	MT-ND5	F-CCTGTAGCATTGTTCGTTACATG
		R-ATGCTAAGGCGAGGATGAAAC
		P-CAACACAGCAGCCATTCAAGCAATC
ENSG00000198840	MT-ND3	F-CCACAACTCAACGGCTACAT
		R-GTTGTTTGTAGGGCTCATGGT
		P-CGAGTGCGGCTTCGACCCT
ENSG00000269028	MTRNR2L12	F-AGATTTATAGGTAGAGGCGACAAAC
		R-ACGATGGGTGTTGAGCTTG
		P-TGGTGATAGCTGGTTGTCCAAGATAGAATC

F-, forward sequence; R-, reverse sequence; P-, probe sequence.

morphological characteristics of exosomes. With WB analysis, the well-known exosomal marker proteins Alix, Tsg101, and CD63 were detected in isolated fractions, while the negative marker of exosomes, calnexin, was absent (Figure 1C). Thus, exosome samples were well prepared and had good purity.

Plasma-derived exosome mRNA profiling

The analytical process for the sequencing data is summarized in Figure 2. A total of 20 samples, including 10 patients and 10 healthy controls, with 478.89 Gb of clean data were constructed. The clean data of each sample were at least 19.67 Gb. Each sample was compared with the reference genome sequence, and the alignment efficiency ranged from 23.42% to 68.53%. A total of 22,298 mRNAs, including 19,986 known mRNAs and 2312 novel mRNAs, were generated (Table S1). The annotation information of new genes was obtained by using BLAST software (Table S2).

Differentially expressed mRNAs

In this study, plasma-derived exosome samples from 10 patients with T1DM and 10 healthy controls were used for RNA sequencing. A total of 112 mRNAs were differentially expressed (P value < 0.05), of which 66 mRNAs were upregulated and 46 mRNAs were downregulated. We performed hierarchical clustering to sort the identified exosomal DEMs (Figure 3A). A volcano diagram was used to intuitively show the relationship between the P value and the fold change of all transcripts to quickly view the expression level difference and statistical significance of mRNAs between the two groups of samples (Figure 3B). The overall distribution of the expression abundance and fold changes of mRNAs in the two groups is shown through the M-versus-A plot (Figure 3C). In addition, all DEMs sorted by P values are detailed in Table 3. Our results demonstrated that the mRNA expression profiles of plasma-derived exosomes were distinctly different between T1DM patients and controls.

Verification of exosomal mRNA expression by qRT–PCR

To further assess the biomarker potential for T1DM, six exosomal DEMs, including five upregulated DEMs, ENSG00000185883 (ATP6VOC), ENSG00000198763 (MT-ND2), ENSG00000198786 (MT-ND5), ENSG00000198840 (MT-ND3) and ENSG00000269028 (MTRNR2L12), and one

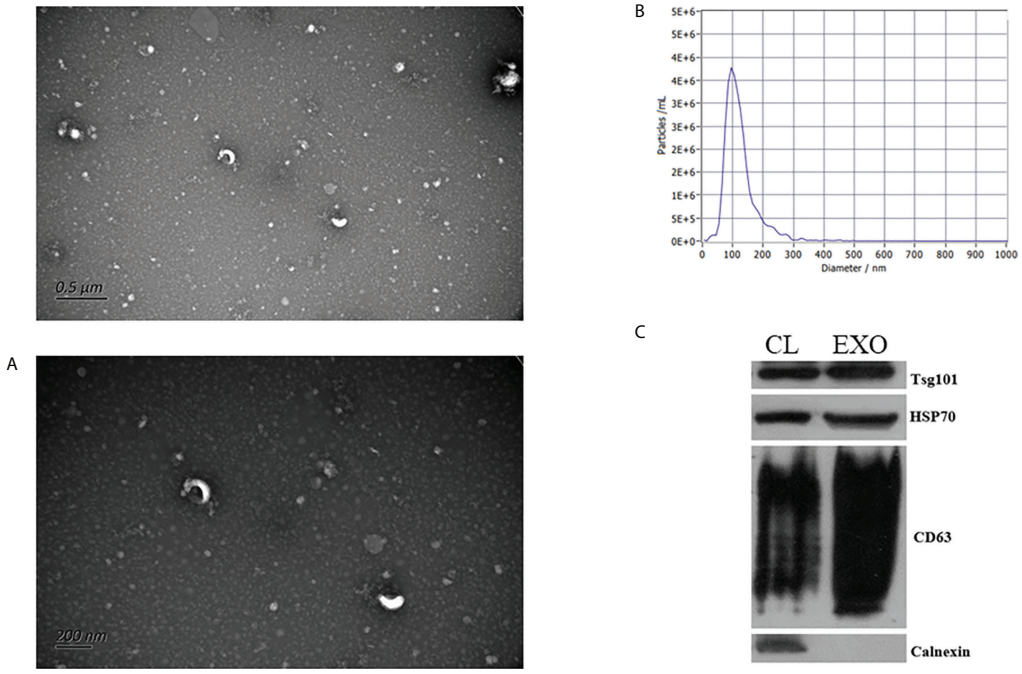

FIGURE 1
Identification of exosomes. Transmission electron microscopy images of exosomes **(A)**. Nanoparticle tracking analysis results **(B)**. Western blot analysis of exosome marker proteins **(C)**.

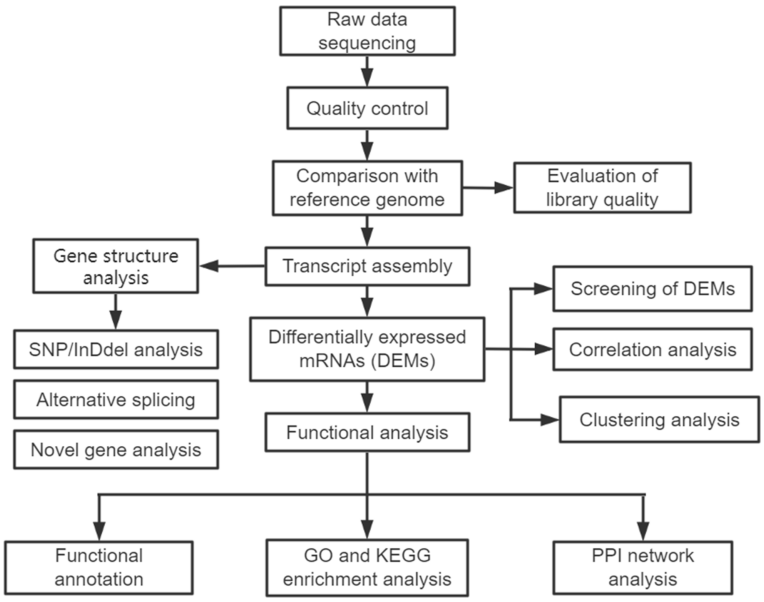

FIGURE 2
The analytical procedure for the sequencing data of exosomal mRNAs.

downregulated DEM, ENSG00000158417 (MTRNR2L12), were selected to validate the sequencing data in an independent cohort. As shown in Figure 4, the qRT–PCR results indicated that four of six candidate mRNAs, namely, ENSG00000198763 (MT-ND2) (P=2.9e-10), ENSG00000198786 (MT-ND5) (P=1.8e-07), ENSG00000198840 (MT-ND3) (P=1.2e-08) and ENSG00000269028 (MTRNR2L12) (P=5.8e-10), were significantly upregulated in T1DM patients compared with control subjects, demonstrating the predictive accuracy of the sequencing data and the biomarker potential of exosomal mRNAs. The remaining two mRNAs, that is, ENSG00000185883 (ATP6VOC) and ENSG00000158417 (MTRNR2L12), failed to reach statistical significance.

Functional analysis of exosomal mRNAs

To explore the potential biological function of 112 DEMs, GO enrichment analysis and KEGG pathway analysis were employed. The GO database is a structured standard biological annotation system and aims to establish a standard vocabulary system of genes and their products. The GO annotation system includes three main branches, namely, biological process, molecular function, and cellular component. We summarized the significantly enriched GO terms of mRNAs with respect to biological process (Table S3), cellular component (Table S4), and molecular function (Table S5) and (Figure 5A). The mRNAs were significantly associated with biological processes, such as positive regulation by host of viral transcription (GO:0043923), axon regeneration (GO:0009154), and cellular senescence (GO:0035026) (Figure 5B). The top 10 GO terms ("positive regulation by host of viral transcription" to "cellular senescence") of biological processes still showed statistical significance after correcting the P value (Table S3). Membrane (GO:0016020), RISC complex (GO:0016442), and condensed nuclear chromosome (GO:0000794) were the most enriched cellular components (Figure 5C). RNA binding (GO:0044822), HMG box domain binding (GO:0071837), and RNA–DNA hybrid ribonuclease activity (GO:0004523) were mostly involved in molecular function (Figure 5D). However, the results of the cellular component and molecular function analyses should be interpreted with caution because the Q-value (corrected P value) indicated that the significance disappeared after multiple hypothesis testing (Tables S4, S5).

As the main public database related to the pathway enrichment analysis, KEGG provides a query of the integrated metabolic pathways, including metabolism of carbohydrates, nucleosides, and amino acids and the biodegradation of organic matter. It not only provides all possible metabolic pathways but also comprehensively annotates the enzymes that catalyze each step of the reaction. In this study, KEGG pathway analysis (Figure 6 and Table S6) suggested that the DEMs between T1DM patients and healthy controls involved in oxidative phosphorylation (ko00190) and Parkinson's disease (ko05012) and other pathways did not reach statistical significance after correcting the P values.

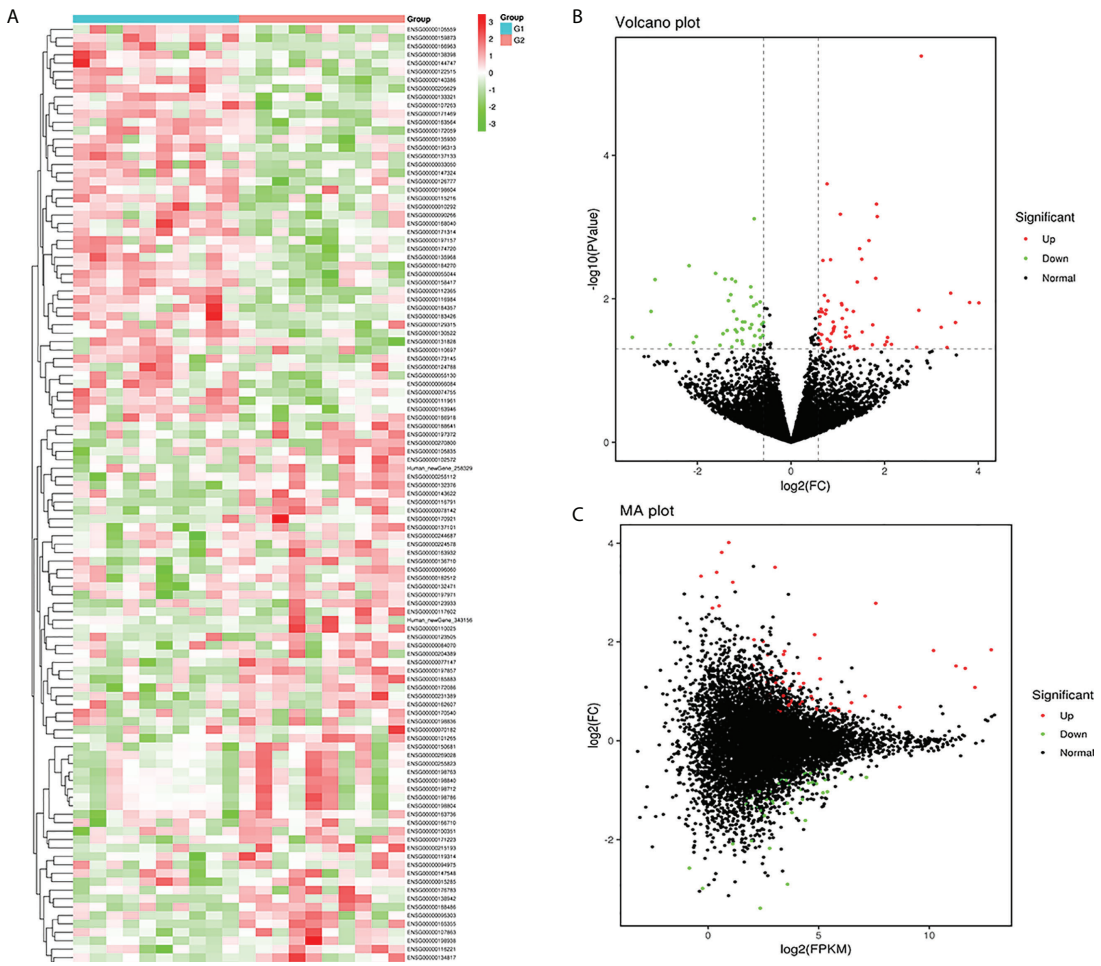

FIGURE 3
Exosomal mRNA profiles of type 1 diabetes mellitus (T1DM). Heatmap **(A)** of the expression levels of the identified differentially expressed mRNAs (DEMs). Red and green represent high and low expression, respectively. G1: control group (N=10); G2: case group (N=10). A volcano diagram **(B)** and M-versus-A **(C)** plot were used to show DEMs in T1DM. The Mann–Whitney U test was used to identify DEMs with cutoffs of FPKM > 5, *P* value < 0.05 and |log2(FC)| > 0.584. Upregulated DEMs (red dots); downregulated DEMs (green dots); nondifferentially expressed mRNAs (black dots).

Establishment of the PPI network

STRING is a database of protein–protein interactions that have been predicted and experimentally verified, including direct physical interactions and indirect functional correlations, in multiple species. Combined with the results of differential expression analysis and the interaction pairs recorded in the database, the PPI network of exosomal DEMs was constructed (Figure 7). In total, 66 nodes and 74 protein interaction pairs were identified in the PPI network. According to the score obtained by five algorithms, 8 hub mRNAs, including MT-ND5, MT-ND2, MT-CO1, MT-ND3, MT-CO2, MT-CO3, NDUFB2, and PTGS1, were identified. Among them, MT-ND5 ranks first in each algorithm and is the core hub gene.

Discussion

Existing studies have emphasized the importance of exosomes in multiple pathological processes (7, 16). Valadi et al. first reported that exosomes contain certain mRNAs and that exosomal mRNAs can be delivered to other cells and translated into proteins in a new location (6). Yokoi et al. reported that MMP1 mRNA-carrying extracellular vesicles from highly metastatic cells can induce apoptosis in mesothelial cells and facilitate the peritoneal dissemination of ovarian cancer (17). In addition, *in vivo* experiments have indicated that exosomes can transfer the mRNA encoding Cre recombinase and can induce Cre-LoxP-mediated recombination in recipient cells (18). These results suggested that exosomes can

TABLE 3 Detailed information on the DEMs.

Gene ID	Symbol	*P* Value	log2FC	Direction of Regulation
ENSG00000198938	MT-CO3	4.14E-06	2.782842	up
ENSG00000185883	ATP6V0C	0.00025	0.770056	up
ENSG00000198840	MT-ND3	0.000478	1.825964	up
ENSG00000101265	RASSF2	0.00066	1.053995	up
ENSG00000198763	MT-ND2	0.000713	1.841181	up
ENSG00000158417	EIF5B	0.000766	-0.78645	down
ENSG00000269028	MTRNR2L12	0.001543	1.665036	up
ENSG00000198712	MT-CO2	0.002004	1.464607	up
ENSG00000198786	MT-ND5	0.002809	1.512536	up
ENSG00000105835	NAMPT	0.002853	0.844394	up
ENSG00000166710	B2M	0.002921	0.681995	up
ENSG00000171469	ZNF561	0.003456	-2.17733	down
ENSG00000130522	JUND	0.004426	-1.61195	down
ENSG00000255823	MTRNR2L8	0.005186	1.810294	up
ENSG00000159873	CCDC117	0.005312	-1.26336	down
ENSG00000140386	SCAPER	0.005329	-1.41142	down
ENSG00000205629	LCMT1	0.0054	-2.90529	down
ENSG00000055044	NOP58	0.005735	-1.18571	down
ENSG00000095303	PTGS1	0.00584	1.416542	up
ENSG00000135968	GCC2	0.006818	-0.86068	down
ENSG00000138942	RNF185	0.00834	3.411566	up
ENSG00000111961	SASH1	0.008765	-1.2861	down
ENSG00000123505	AMD1	0.008967	0.714045	up
ENSG00000138398	PPIG	0.009431	-0.85431	down
ENSG00000129315	CCNT1	0.010629	-1.33722	down
ENSG00000198836	OPA1	0.010736	0.789939	up
ENSG00000198604	BAZ1A	0.011056	-0.66033	down
ENSG00000165355	FBXO33	0.011263	3.816015	up
ENSG00000116791	CRYZ	0.011406	4.014323	up
ENSG00000198804	MT-CO1	0.011611	1.079629	up
ENSG00000184357	H1-5	0.01183	-0.74095	down
ENSG00000172086	KRCC1	0.012191	1.085618	up
ENSG00000144747	TMF1	0.012538	-0.8008	down
ENSG00000231389	HLA-DPA1	0.013866	0.642742	up
ENSG00000197971	MBP	0.014185	1.189494	up
ENSG00000182512	GLRX5	0.014364	0.750828	up
ENSG00000096060	FKBP5	0.014452	0.747055	up
ENSG00000134817	APLNR	0.014467	2.730512	up
ENSG00000186918	ZNF395	0.014881	-1.22411	down
ENSG00000132376	INPP5K	0.014988	1.332368	up
ENSG00000183426	NPIPA1	0.014994	-2.98966	down
ENSG00000132471	WBP2	0.015164	0.595977	up
ENSG00000102572	STK24	0.015314	0.611512	up
ENSG00000147548	NSD3	0.015318	0.671293	up
ENSG00000117602	RCAN3	0.016233	0.735737	up
ENSG00000163946	TASOR	0.017167	-0.67946	down
ENSG00000170540	ARL6IP1	0.017579	0.614128	up
ENSG00000077147	TM9SF3	0.018746	1.095219	up

(Continued)

TABLE 3 Continued

Gene ID	Symbol	*P* Value	log2FC	Direction of Regulation
ENSG00000116984	MTR	0.01916	-1.15852	down
ENSG00000150681	RGS18	0.020987	0.900095	up
ENSG00000090266	NDUFB2	0.020992	-1.03341	down
ENSG00000168040	FADD	0.021014	-0.98522	down
ENSG00000115216	NRBP1	0.021257	-0.58867	down
Human_newGene_343156	Human_newGene_343156	0.021403	3.513743	up
ENSG00000171314	PGAM1	0.022593	-0.62364	down
ENSG00000084070	SMAP2	0.022629	0.616291	up
ENSG00000174720	LARP7	0.022858	-0.84092	down
ENSG00000171223	JUNB	0.023075	1.745297	up
ENSG00000188641	DPYD	0.024545	0.926448	up
ENSG00000197857	ZNF44	0.024939	3.208025	up
ENSG00000123933	MXD4	0.024984	1.183135	up
ENSG00000131828	PDHA1	0.025616	-0.86785	down
ENSG00000010292	NCAPD2	0.025664	-0.87864	down
ENSG00000163736	PPBP	0.025931	0.904892	up
ENSG00000135930	EIF4E2	0.026074	-1.05251	down
ENSG00000162607	USP1	0.026174	0.913166	up
ENSG00000066084	DIP2B	0.026774	-1.02817	down
ENSG00000173145	NOC3L	0.027063	-1.18953	down
ENSG00000126777	KTN1	0.027356	-0.67727	down
ENSG00000122515	ZMIZ2	0.027625	-1.36426	down
ENSG00000124788	ATXN1	0.028118	0.901701	up
ENSG00000147324	MFHAS1	0.028845	-1.15761	down
ENSG00000224578	HNRNPA1P48	0.028899	1.162777	up
ENSG00000119138	KLF9	0.028975	1.519606	up
Human_newGene_258329	Human_newGene_258329	0.030406	0.594307	up
ENSG00000143622	RIT1	0.030444	0.864708	up
ENSG00000163564	PYHIN1	0.030631	-1.4525	down
ENSG00000176783	RUFY1	0.031496	0.654268	up
ENSG00000107263	RAPGEF1	0.032437	-0.5992	down
ENSG00000184270	H2AC21	0.032671	-0.77486	down
ENSG00000244687	UBE2V1	0.033077	1.247281	up
ENSG00000172059	KLF11	0.033546	-2.02393	down
ENSG00000255112	CHMP1B	0.034315	1.172022	up
ENSG00000137133	HINT2	0.03444	-3.39021	down
ENSG00000215193	PEX26	0.034691	2.062326	up
ENSG00000133321	PLAAT4	0.03473	-0.65363	down
ENSG00000163932	PRKCD	0.036475	0.773031	up
ENSG00000015285	WAS	0.037959	0.60375	up
ENSG00000196313	POM121	0.038182	-1.15236	down
ENSG00000074755	ZZEF1	0.038615	-1.04987	down
ENSG00000094975	SUCO	0.039027	0.831962	up
ENSG00000197372	ZNF675	0.039596	2.043903	up
ENSG00000112365	ZBTB24	0.040781	-2.08374	down
ENSG00000100351	GRAP2	0.042412	0.631413	up
ENSG00000033050	ABCF2	0.042467	-1.0362	down
ENSG00000119314	PTBP3	0.043109	0.592799	up

(Continued)

10.3389/fimmu.2022.995610

TABLE 3 Continued

Gene ID	Symbol	*P* Value	log2FC	Direction of Regulation
ENSG00000270800	RPS10-NUDT3	0.043157	2.146459	up
ENSG00000166963	MAP1A	0.043679	-2.57825	down
ENSG00000136710	CCDC115	0.043705	1.737544	up
ENSG00000188486	H2AX	0.043761	2.00797	up
ENSG00000197157	SND1	0.043813	-0.6606	down
ENSG00000105559	PLEKHA4	0.044362	-1.51678	down
ENSG00000055130	CUL1	0.045369	-0.80061	down
ENSG00000107863	ARHGAP21	0.045763	1.343528	up
ENSG00000116221	MRPL37	0.04672	1.264366	up
ENSG00000110697	PITPNM1	0.046935	-1.26335	down
ENSG00000170921	TANC2	0.047316	2.686476	up
ENSG00000110025	SNX15	0.047671	3.333243	up
ENSG00000070182	SPTB	0.048006	0.859222	up
ENSG00000078142	PIK3C3	0.048936	0.677108	up
ENSG00000204389	HSPA1A	0.048937	1.410393	up
ENSG00000137101	CD72	0.049889	1.362187	up

lead to the delivery of functional mRNA and can alter the phenotype of recipient cells. However, research concerning the association between T1DM and exosomal mRNAs is relatively lacking. In this study, we characterized the expression profiles of exosomal mRNAs in the plasma of T1DM patients and further explored the biomarker potential of the identified exosomal mRNAs. In addition, we performed bioinformatic analysis (GO and KEGG) to clarify the biological functions of the identified DEMs.

Here, a total of 112 exosomal DEMs were detected, of which 66 mRNAs were upregulated and 46 mRNAs were downregulated in T1DM patients compared to controls. These results strongly indicated that the expression profiles of plasma-derived exosomal mRNAs in patients with T1DM differ from

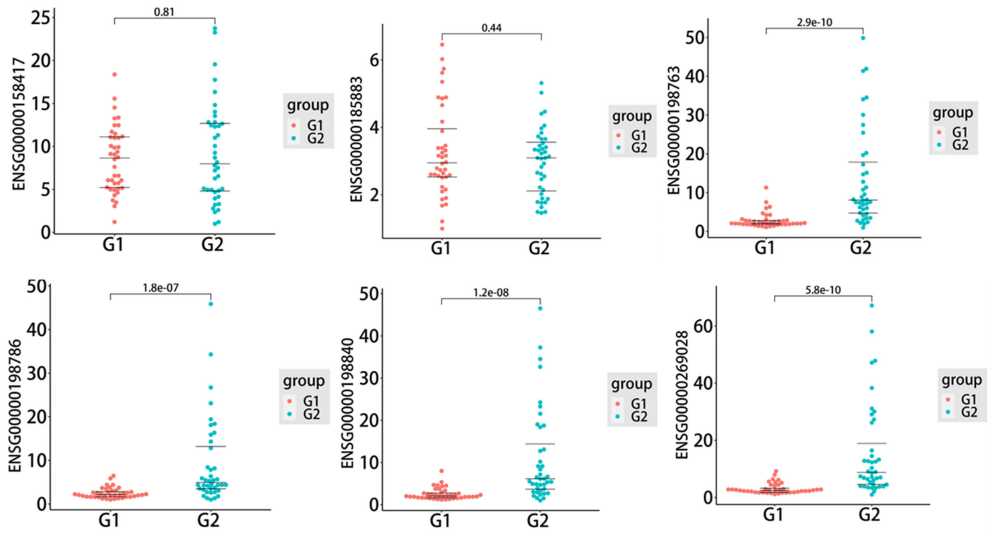

FIGURE 4
The quantitative real-time PCR (qRT–PCR) results of six selected differentially expressed mRNAs (DEMs) in the type 1 diabetes mellitus (T1DM) and control groups (T1DM N=40; controls N=40). Statistically significant differences (*P* value < 0.05) were calculated by unpaired t test. The three lines in each figure represent the median and interquartile spacing. G1: control group; G2: case group.

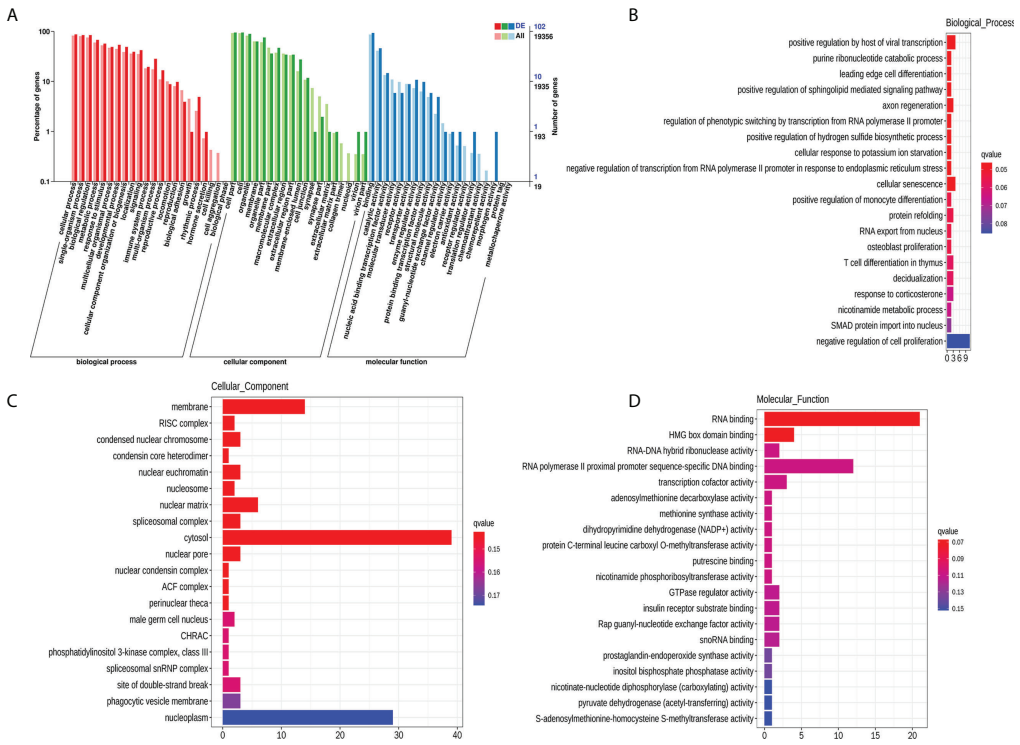

FIGURE 5
GO enrichment analysis of 112 DEMs. GO categories of DEMs **(A)**. Top 20 significantly enriched biological processes **(B)**, cellular components **(C)**, and molecular functions **(D)** of DEMs. The x-axis represents the number of mRNAs.

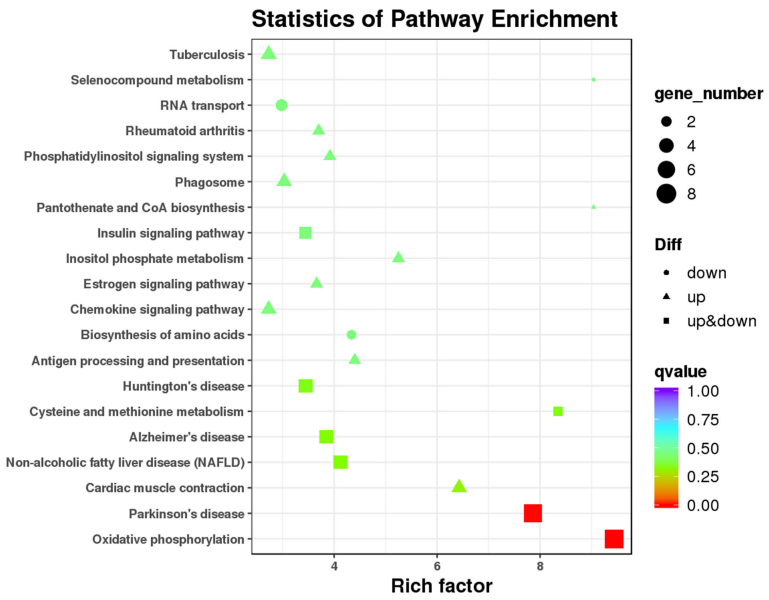

FIGURE 6
Kyoto Encyclopedia of Genes and Genomes (KEGG) pathway analysis of 112 DEMs.

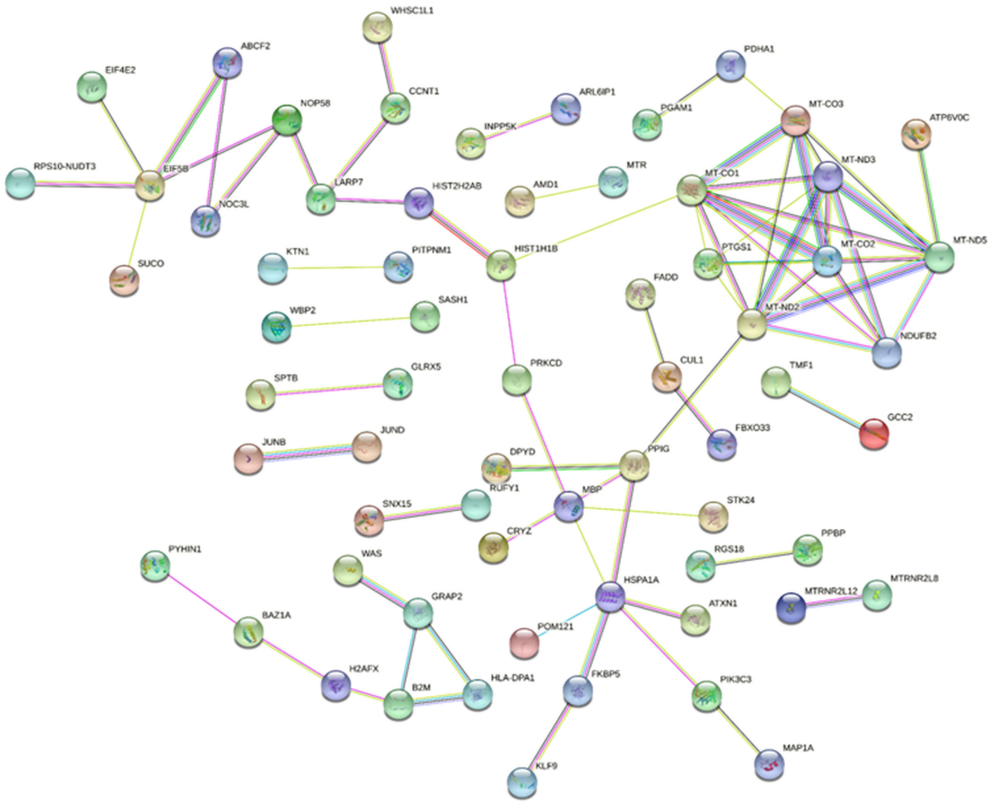

FIGURE 7
The protein–protein interaction network of DEMs. Network nodes represent proteins, and edges represent protein–protein associations.

those in healthy individuals. Next, six candidate mRNAs were selected to verify the sequencing results by qRT–PCR. Four of six mRNAs, namely, ENSG00000198763 (MT-ND2), ENSG00000198786 (MT-ND5), ENSG00000198840 (MT-ND3) and ENSG00000269028 (MTRNR2L12), were indicated to have significant differences between T1DM patients and control subjects and followed the same tendency as the sequencing data. This result highlighted that plasma-derived exosomal mRNAs might serve as novel minimally invasive diagnostic tools for T1DM. However, two of six mRNAs failed to show statistical significance in the qRT–PCR analysis. Therefore, the biomarker use of other DEMs identified by sequencing requires further validation. At present, the lack of a robust biomarker for T1DM prevents the early recognition and intervention that could preserve residual pancreatic beta-cells. Previous studies have strongly suggested the possible biomarker utility of plasma RNA (19, 20). However, there are some alternative advantages with regard to exosomal RNA in disease diagnosis. For instance, exosomal RNAs tend to be more stable in plasma because the lipid bilayer-enclosed structure can protect the RNA cargo from degradation. In addition, the release and contents of exosomes are strictly regulated by physical and pathological conditions, thus reflecting the biological status of the body.

Next, we performed bioinformatic analysis to predict the biological functions of the identified exosomal DEMs. GO enrichment analysis revealed that the most significantly enriched term was positive regulation by host of viral transcription among the biological processes. Previous studies have also indicated that viral infections play an essential role in T1DM development. Data revealed that more T1DM patients were diagnosed during cold months (21, 22), which suggested that viruses play a role in triggering T1DM because viral infections are more common in winter than in summer. Viral respiratory tract infections in early life have also been reported to be associated with islet autoimmunity and beta-cell damage (23, 24). Moreover, some viruses, such as coxsackieviruses, can induce the onset of T1DM in animal models and can be isolated from the pancreas in patients with newly diagnosed T1DM (25–27). In addition to pathogenic effects, some studies have also shown the protective role of viral infection, which is in agreement with the hygiene hypothesis. It has been reported that the inoculation of young nonobese diabetic (NOD) mice, models of spontaneous autoimmune diabetes mellitus, with some

viruses was followed by long-term protection from T1DM (28, 29). However, the underlying mechanisms behind the interactions of viral infections and the onset of T1DM have not been fully elucidated. Our results suggested that exosomal mRNAs might be involved in this process, but the exact functions of the exosomal mRNAs need further investigation. KEGG analysis indicated that the main pathways of the identified DEMs were involved in oxidative phosphorylation and Parkinson's disease. Interestingly, our previous study also indicated that the KEGG pathway analysis regarding exosomal lncRNAs was associated with Parkinson's disease (13). Oxidative phosphorylation (OXPHOS) is a metabolic pathway with low glucose utilization and high ketone production. Generally, immune cells generate energy through OXPHOS or aerobic glycolysis, another metabolic pathway associated with high glucose utilization. However, it has been indicated that aerobic glycolysis is suppressed while OXPHOS is exacerbated in individuals with T1DM (30, 31). The dysregulation of lymphoid metabolism might partially explain why T1DM patients were more susceptible to ketosis than type 2 diabetes mellitus (T2DM) patients (32). More interestingly, it has been indicated that the bacillus Calmette-Guerin (BCG) could lower blood glucose levels by shifting the glucose metabolism of the immune system from overactive OXPHOS to aerobic glycolysis (30, 31). Taken together, the bioinformatic analysis suggested that these identified DEMs were involved in the development of T1DM *via* different pathways. In addition, we constructed a PPI network and identified 8 hub genes (MT-ND5, MT-ND2, MT-CO1, MT-ND3, MT-CO2, MT-CO3, NDUFB2, and PTGS1) among the identified exosomal DEMs. These genes might play an important role in T1DM. For example, a recent study indicated that rare variants within MT-ND5 were associated with fasting insulin (33). In addition, it has been indicated that MT-ND2 could modify resistance against T1DM in NOD mice by modulating beta-cell sensitivity to T-cell effectors (34). However, the exact role of these genes in T1DM in the context of exosomes needs further investigation.

In conclusion, this study identified the characteristics of the plasma-derived exosomal mRNA transcriptome of T1DM for the first time, and the results highlighted the biomarker potential of exosomal mRNA.

Data availability statement

The datasets presented in this study can be found in online repositories. The names of the repository/repositories and accession number(s) can be found below: https://db.cngb.org/search/project/CNP0002574/, CNP0002574.

Ethics statement

The studies involving human participants were reviewed and approved by the institutional ethics review board of the Second Xiangya Hospital of Central South University. The patients/participants provided their written informed consent to participate in this study.

Author contributions

ZZ, ZX, and HP conceived and designed the experiments. WF, HP, JiaqL, YW, SL, JianL, HY, YX, GH, and XL collected samples. WF, HP, and XS performed the experiments and analyzed the data. WF and HP wrote the manuscript. All authors contributed to the article and approved the submitted version.

Funding

This work was supported by the National Key R&D Program of China (grant number 2018YFE0114500), the National Natural Science Foundation of China (grant numbers 82070813 and 81873634), and the Hunan Province Natural Science Foundation of China (grant numbers 2022JJ30858, 2018JJ2573, and 2020JJ2053).

Conflict of interest

The authors declare that the research was conducted in the absence of any commercial or financial relationships that could be construed as a potential conflict of interest.

Publisher's note

Supplementary material

The Supplementary Material for this article can be found online at: https://www.frontiersin.org/articles/10.3389/fimmu.2022.995610/full#supplementary-material

References

1. DiMeglio LA, Evans-Molina C, Oram RA. Type 1 diabetes. *Lancet* (2018) 391 (10138):2449–62. doi: 10.1016/S0140-6736(18)31320-5

2. Patterson CC, Karuranga S, Salpea P, Saeedi P, Dahlquist G, Soltesz G, et al. Worldwide estimates of incidence, prevalence and mortality of type 1 diabetes in children and adolescents: Results from the international diabetes federation diabetes atlas, 9th edition. *Diabetes Res Clin Pract* (2019) 157:107842. doi: 10.1016/j.diabres.2019.107842

3. Pang H, Luo S, Huang G, Xia Y, Xie Z, Zhou Z. Advances in knowledge of candidate genes acting at the beta-cell level in the pathogenesis of T1DM. *Front Endocrinol (Lausanne)* (2020) 11:119. doi: 10.3389/fendo.2020.00119

4. Ilonen J, Lempainen J, Veijola R. The heterogeneous pathogenesis of type 1 diabetes mellitus. *Nat Rev Endocrinol* (2019) 15(11):635–50. doi: 10.1038/s41574-019-0254-y

5. Thery C, Zitvogel L, Amigorena S. Exosomes: Composition, biogenesis and function. *Nat Rev Immunol* (2002) 2(8):569–79. doi: 10.1038/nri855

6. Valadi H, Ekstrom K, Bossios A, Sjostrand M, Lee JJ, Lotvall JO. Exosome-mediated transfer of mRNAs and microRNAs is a novel mechanism of genetic exchange between cells. *Nat Cell Biol* (2007) 9(6):654–9. doi: 10.1038/ncb1596

7. Pang H, Luo S, Xiao Y, Xia Y, Li X, Huang G, et al. Emerging roles of exosomes in T1DM. *Front Immunol* (2020) 11:593348. doi: 10.3389/fimmu.2020.593348

8. Castano C, Novials A, Parrizas M. Exosomes and diabetes. *Diabetes Metab Res Rev* (2019) 35(3):e3107. doi: 10.1002/dmrr.3107

9. Roep BO, Thomaidou S, van Tienhoven R, Zaldumbide A. Type 1 diabetes mellitus as a disease of the beta-cell (do not blame the immune system)? *Nat Rev Endocrinol* (2021) 17(3):150–61. doi: 10.1038/s41574-020-00443-4

10. Cianciaruso C, Phelps EA, Pasquier M, Hamelin R, Demurtas D, Alibashe Ahmed M, et al. Primary human and rat beta-cells release the intracellular autoantigens GAD65, IA-2, and proinsulin in exosomes together with cytokine-induced enhancers of immunity. *Diabetes* (2017) 66(2):460–73. doi: 10.2337/db16-0671

11. Guay C, Kruit JK, Rome S, Menoud V, Mulder NL, Jurdzinski A, et al. Lymphocyte-derived exosomal MicroRNAs promote pancreatic beta cell death and may contribute to type 1 diabetes development. *Cell Metab* (2019) 29(2):348–61 e6. doi: 10.1016/j.cmet.2018.09.011

12. Krishnan P, Syed F, Jiyun Kang N, Mirmira RG, Evans-Molina C. Profiling of RNAs from human islet-derived exosomes in a model of type 1 diabetes. *Int J Mol Sci* (2019) 20(23). doi: 10.3390/ijms20235903

13. Pang H, Fan W, Shi X, Li J, Wang Y, Luo S, et al. Characterization of lncRNA profiles of plasma-derived exosomes from type 1 diabetes mellitus. *Front Endocrinol (Lausanne)* (2022) 13:822221. doi: 10.3389/fendo.2022.822221

14. Garcia-Contreras M, Shah SH, Tamayo A, Robbins PD, Golberg RB, Mendez AJ, et al. Plasma-derived exosome characterization reveals a distinct microRNA signature in long duration type 1 diabetes. *Sci Rep* (2017) 7(1):5998. doi: 10.1038/s41598-017-05787-y

15. Mao X, Cai T, Olyarchuk JG, Wei L. Automated genome annotation and pathway identification using the KEGG orthology (KO) as a controlled vocabulary. *Bioinformatics* (2005) 21(19):3787–93. doi: 10.1093/bioinformatics/bti430

16. Sun Y, Tao Q, Wu X, Zhang L, Liu Q, Wang L. The utility of exosomes in diagnosis and therapy of diabetes mellitus and associated complications. *Front Endocrinol (Lausanne)* (2021) 12:756581. doi: 10.3389/fendo.2021.756581

17. Yokoi A, Yoshioka Y, Yamamoto Y, Ishikawa M, Ikeda SI, Kato T, et al. Malignant extracellular vesicles carrying MMP1 mRNA facilitate peritoneal dissemination in ovarian cancer. *Nat Commun* (2017) 8:14470. doi: 10.1038/ncomms14470

18. Zomer A, Maynard C, Verweij FJ, Kamermans A, Schafer R, Beerling E, et al. *In vivo* imaging reveals extracellular vesicle-mediated phenocopying of metastatic behavior. *Cell* (2015) 161(5):1046–57. doi: 10.1016/j.cell.2015.04.042

19. Assmann TS, Recamonde-Mendoza M, Punales M, Tschiedel B, Canani LH, Crispim D. MicroRNA expression profile in plasma from type 1 diabetic patients: Case-control study and bioinformatic analysis. *Diabetes Res Clin Pract* (2018) 141:35–46. doi: 10.1016/j.diabres.2018.03.044

20. Garavelli S, Bruzzaniti S, Tagliabue E, Di Silvestre D, Prattichizzo F, Mozzillo E, et al. Plasma circulating miR-23~27~24 clusters correlate with the immunometabolic derangement and predict c-peptide loss in children with type 1 diabetes. *Diabetologia* (2020) 63(12):2699–712. doi: 10.1007/s00125-020-052

21. Joner G, Sovik O. Increasing incidence of diabetes mellitus in Norwegian children 0-14 years of age 1973-1982. *Diabetologia* (1989) 32(2):79–83. doi: 10.1007/BF00505178

22. Karvonen M, Jantti V, Muntoni S, Stabilini M, Stabilini L, Muntoni S, et al. Comparison of the seasonal pattern in the clinical onset of IDDM in Finland and Sardinia. *Diabetes Care* (1998) 21(7):1101–9. doi: 10.2337/diacare.21.7.1101

23. Beyerlein A, Donnachie E, Jergens S, Ziegler AG. Infections in early life and development of type 1 diabetes. *JAMA* (2016) 315(17):1899–901. doi: 10.1001/jama.2016.2181

24. Beyerlein A, Wehweck F, Ziegler AG, Pflueger M. Respiratory infections in early life and the development of islet autoimmunity in children at increased type 1 diabetes risk: evidence from the BABYDIET study. *JAMA Pediatr* (2013) 167 (9):800–7. doi: 10.1001/jamapediatrics.2013.158

25. Al-Hello H, Paananen A, Eskelinen M, Ylipaasto P, Hovi T, Salmela K, et al. An enterovirus strain isolated from diabetic child belongs to a genetic subcluster of echovirus 11, but is also neutralised with monotypic antisera to coxsackievirus A9. *J Gen Virol* (2008) 89(Pt 8):1949–59. doi: 10.1099/vir.0.83474-0

26. Dotta F, Censini S, van Halteren AG, Marselli L, Masini M, Dionisi S, et al. Coxsackie B4 virus infection of beta cells and natural killer cell insulitis in recent-onset type 1 diabetic patients. *Proc Natl Acad Sci U.S.A.* (2007) 104(12):5115–20. doi: 10.1073/pnas.0700442104

27. Yoon JW, Austin M, Onodera T, Notkins AL. Isolation of a virus from the pancreas of a child with diabetic ketoacidosis. *N Engl J Med* (1979) 300(21):1173–9. doi: 10.1056/NEJM197905243002102

28. Smith KA, Efstathiou S, Cooke A. Murine gammaherpesvirus-68 infection alters self-antigen presentation and type 1 diabetes onset in NOD mice. *J Immunol* (2007) 179(11):7325–33. doi: 10.4049/jimmunol.179.11.7325

29. Tracy S, Drescher KM, Chapman NM, Kim KS, Carson SD, Pirruccello S, et al. Toward testing the hypothesis that group b coxsackieviruses (CVB) trigger insulin-dependent diabetes: inoculating nonobese diabetic mice with CVB markedly lowers diabetes incidence. *J Virol* (2002) 76(23):12097–111. doi: 10.1128/jvi.76.23.12097-12111.2002

30. Kuhtreiber WM, Faustman DL. BCG Therapy for type 1 diabetes: Restoration of balanced immunity and metabolism. *Trends Endocrinol Metab* (2019) 30(2):80–92. doi: 10.1016/j.tem.2018.11.006

31. Kuhtreiber WM, Tran L, Kim T, Dybala M, Nguyen B, Plager S, et al. Long-term reduction in hyperglycemia in advanced type 1 diabetes: The value of induced aerobic glycolysis with BCG vaccinations. *NPJ Vaccines* (2018) 3:23. doi: 10.1038/s41541-018-0062-8

32. Faustman DL. Benefits of BCG-induced metabolic switch from oxidative phosphorylation to aerobic glycolysis in autoimmune and nervous system diseases. *J Intern Med* (2020) 288(6):641–50. doi: 10.1111/joim.13050

33. Kraja AT, Liu C, Fetterman JL, Graff M, Have CT, Gu C, et al. Associations of mitochondrial and nuclear mitochondrial variants and genes with seven metabolic traits. *Am J Hum Genet* (2019) 104(1):112–38. doi: 10.1016/j.ajhg.2018.12.001

34. Chen J, Gusdon AM, Piganelli J, Leiter EH, Mathews CE. Mt-Nd2(a) modifies resistance against autoimmune type 1 diabetes in NOD mice at the level of the pancreatic beta-cell. *Diabetes* (2011) 60(1):355–9. doi: 10.2337/db10-1241

frontiers | Frontiers in Immunology

TYPE Original Research
PUBLISHED 16 November 2022
DOI 10.3389/fimmu.2022.1058532

OPEN ACCESS

EDITED BY
Yujing Zhang,
Nanjing University, China

REVIEWED BY
Theodore Cory,
University of Tennessee Health Science Center (UTHSC), United States
Dameng Li,
Xuzhou Medical University, China

*CORRESPONDENCE
Qinjie Weng
wengqinjie@zju.edu.cn
Qiaojun He
qiaojunhe@zju.edu.cn
Jiajia Wang
wangjiajia3301@zju.edu.cn

SPECIALTY SECTION
This article was submitted to Cytokines and Soluble Mediators in Immunity, a section of the journal Frontiers in Immunology

RECEIVED 30 September 2022
ACCEPTED 31 October 2022
PUBLISHED 16 November 2022

CITATION
Cai X, Zha H, Yang Z, Du Y, Dai X, Yang B, Wang J, He Q and Weng Q (2022) Genetic dominance of transforming growth factor-β1 polymorphisms in chronic liver disease.
Front. Immunol. 13:1058532.
doi: 10.3389/fimmu.2022.1058532

Genetic dominance of transforming growth factor-β1 polymorphisms in chronic liver disease

Xuanyan Cai[1,2], Huiyan Zha[1,2], Zhaoxu Yang[1,2], Yiwen Du[1,2], Xiaoyang Dai[1,2], Bo Yang[1,2], Jiajia Wang[1,2]*, Qiaojun He[1,2,3]* and Qinjie Weng[1,2,3]*

[1]Center for Drug Safety Evaluation and Research, College of Pharmaceutical Sciences, Zhejiang University, Hangzhou, China, [2]Zhejiang Province Key Laboratory of Anti-Cancer Drug Research, College of Pharmaceutical Sciences, Zhejiang University, Hangzhou, China, [3]The Second Affiliated Hospital, Zhejiang University School of Medicine, Hangzhou, China

Chronic liver disease (CLD) is an extremely common clinical condition accompanied by sustained inflammatory response leading to tissue damage. Transforming growth factor-β1 (TGF-β1) is known as a master immune regulator in CLDs, but the association between TGF-β1 polymorphisms and CLD risk is controversial and inconclusive, and the genetic dominance of CLDs remains unknown. In this study, the relationship between *TGF-β1* polymorphisms and CLD susceptibility is systematically analyzed based on 35 eligible studies. Individuals with the *TGF-β1*-509 allele (TT or CT) or codon 10 allele (Pro/Pro) show an increased risk of CLDs. Subgroup analyses indicate *TGF-β1*-509C/T has a significant correlation with cirrhosis and chronic hepatitis C, codon 10 is associated with chronic hepatitis B occurrence, and codon 25 exhibits a relationship with autoimmune hepatitis risk. Missense mutations in G29E, A105S, D191N, and F321L of *TGF-β1* are the genetic factors of HCC susceptibility. Furthermore, the *TGF-β1* gene expression is significantly elevated in CLD patients, and the *TGF-β1* codon 263 is located close to the region where the TGF-β1 dimerization interacts, indicating the *TGF-β1* codon 263 variant may affect the secretion of TGF-β1 by altering its dimerization. Together, our findings provide new insights into the immune regulator gene *TGF-β1* polymorphisms as susceptibility factors for CLD occurrence and regulators for TGF-β1 expression, which have implications for the regulation of immune factors during CLD development.

KEYWORDS

transforming growth factor-β1, polymorphisms, susceptibility, chronic liver disease, cirrhosis

Introduction

Chronic liver disease (CLD) is a continuous and gradual process caused by multifactorial etiologies including genetic factors. The pathogenesis of CLD is complicated and is related to sustained inflammatory response leading to tissue damage (1, 2). Chronic hepatotoxic injuries, such as hepatitis B virus (HBV) or hepatitis C virus (HCV) infections, autoimmune hepatitis (AIH), non-alcoholic steatohepatitis (NASH) and alcohol abuse, can severely impair liver functions, progressing to cirrhosis, hepatocellular carcinoma (HCC) or even liver failure (1). CLDs represent big challenges to the public health system worldwide, which account for more than 800 million individuals and approximately 2 million deaths per year in the world (1–3). Interestingly, the risk of CLDs varies from one individual to another (4–6), indicating that the host genetic factors might determine the susceptibility of CLDs.

Transforming growth factor-β1 (TGF-β1), a member of the TGF-β super-family, is regarded as a crucial immune regulator in a variety of CLDs (7). In the hepatocarcinogenic process, TGF-β1 functions as an anti-inflammatory cytokine that promotes immune surveillance escape in HCC, leading to cell migration and invasion (8–10). TGF-β also activates SMAD2/3 and cooperates with IL-21 activity to promote naïve $CD4^+$ T cell generation of Th17 cells, contributing to NASH-associated liver inflammation and HCC (11, 12). In the pathogenesis of chronic hepatitis, TGF-β1 leads to prolonged HBV/HCV infections *via* increasing T regulatory lymphocyte activation and recruiting these cells to the infected livers (13–15). During fibrogenesis, TGF-β1 could be secreted by different immune cells, such as hepatic macrophages and regulatory T lymphocytes, and induce hepatic stellate cells to transform into proliferative fibrogenic myofibroblasts, synthesizing and secreting excess collagen (16–18).

Several studies have found that single-nucleotide polymorphisms (SNPs) of *TGF-β1* may play important roles in CLDs. Up to now, *TGF-β1*-509C/T (rs1800469) and *TGF-β1* codon 10 (rs1800470) polymorphisms have been reported to have a potential relationship with the susceptibility of HBV/HCV-induced cirrhosis or HCC (19–25). However, the findings are contradictory and inconclusive. Specifically, one study pointed out that patients with the *TGF-β1*-509 TT genotype were significantly associated with cirrhosis risk (24), while another study concluded that the *TGF-β1*-509C/T polymorphism had a limited role in predicting cirrhosis occurrence (21, 22). Similar controversial results were also found in HCC risk prediction (19, 20, 23, 25). In addition, although *TGF-β1* genetic variation occurs in cirrhosis and HCC, two etiologies of CLDs, whether *TGF-β1* polymorphisms are associated with other types of CLD risk and which polymorphisms are high genetic dominance of CLDs remain unidentified.

A series of studies found that TGF-β1 expression was significantly higher in patients with cirrhosis (26, 27), and upregulated in tumor tissues of HCC (28–30). Clinic studies showed that individuals with *TGF-β1*-509C/T or codon 10 displayed increased plasma concentration of TGF-β1, implying that *TGF-β1* polymorphisms may regulate TGF-β1 expression in CLD patients (21, 31–33). However, how these genetic variants intervene the transcription, translation, or protein 3D structure of TGF-β1 is complicated and mysterious. The investigation between *TGF-β1* genetic variants and TGF-β1 expression will have great implications for the development of CLDs.

Accordingly, we performed a systematic meta-analysis to determine the associations between SNPs of immune regulator gene *TGF-β1* and CLD susceptibility. We assessed the *TGF-β1* polymorphisms in diverse etiologies and identified a strong association of specific *TGF-β1* gene variants with different CLD types. Furthermore, we applied bioinformatic analysis to establish *TGF-β1* expression in CLDs with different etiologies and explore the potential way by which *TGF-β1* polymorphisms affect its expression. Consequently, our findings reveal a previously unidentified role of *TGF-β1* polymorphisms in predicting CLD susceptibility and the underlying mechanisms involved.

Materials and methods

Study selection and identification

The analysis was conducted following the Preferred Reporting Items for Systematic Reviews and Network Meta-Analyses (PRISMA) guidelines (34). We searched English-language publications in Embase, Pubmed, Web of Science, Cochrane Library, and HuGe Navigator from database inception through June 2022 that reported the *TGF-β1* polymorphisms and CLDs in humans. We used various combinations of the search terms to screen for relevant studies: ((TGFB1 OR TGF beta 1 OR Transforming Growth Factor OR TGF-β) AND (single nucleotide polymorphism OR SNP OR genetic variation OR genetic polymorphism OR Polymorphism OR Variant OR Variation OR Mutation OR Genome-wide Association Study OR Genetic Association Study)) AND (Non-Alcoholic Fatty Liver Disease OR Non-Alcoholic Fatty Liver OR Non-Alcoholic Steatohepatitis OR NASH OR NAFLD). Three investigators independently selected the references and reviewed the study abstracts and full text.

The inclusion criteria were as follows: (1) studies evaluating the association between *TGF-β1* polymorphisms and CLD risk, (2) studies including case and control populations, (3) the incidence of *TGF-β1* polymorphisms in case and control groups, and (4) studies with sufficient available data to estimate an odds ratio (OR) with its 95% confidence interval (95% CI). OR is a precise estimate of the

occurrence of a specific event. The involved studies should meet all of the above criteria. Exclude any studies with errors or inconsistent data. All potentially eligible trials were considered regardless of outcomes.

Data extraction and quality assessment

The following information was extracted for each eligible study: the name of the first author, the publication year, the country of origin, ethnicity, genotyping method, sex, disease type, sample sizes of cases and controls, and genotype number in cases and controls. In our study, we used the Newcastle-Ottawa Scale (NOS) to assess the quality (35). The NOS contains the following 3 dimensions: selection, comparability, and exposure, covered by 8 items. The overall score was nine, with higher scores indicating better quality. Studies with a score of 4-6 were deemed intermediate quality, and those with a score > 7 were deemed high quality.

Gene expression, mutation, and transcription factor analysis of TGF-β1

The *TGF-β1* gene expression profiles were downloaded from the Gene Expression Omnibus (GEO) database: GSE202853 (HCC), GSE25097 (Cirrhosis), GSE38941 (CHB), GSE154055 (CHC), GSE159676 (AIH), GSE28619 (Alcohol hepatitis) and GSE48452 (NASH). Expression profiles of these datasets were reanalyzed using R and correlated packages (http://www.r-project.org/). We used cBioPortal (https://www.cbioportal.org/) to investigate the gene mutation of *TGF-β1* in HCC (36). The transcription factors of *TGF-β1* were downloaded from Genecard, Ominer, Promo, and TRRUST databases.

Single-cell RNA sequencing analysis

We reanalyzed the published scRNA-seq data of human liver cirrhosis from GSE136103 (37). The raw reads were aligned to the mm10 (Ensembl 84) reference genomes, utilizing an in-house pipeline of the Cell Ranger v5.0.1 Single-Cell Software Suite from 10X Genomics. Additional analysis was then executed by the "Seurat" (v4.0.0) package for R (v4.0.4) (https://www.r-project.org/). Genes expressed in fewer than three cells in a sample were excluded, as were cells that expressed fewer than 200 genes or mitochondrial gene content > 10% of the total UMI count. In addition, cells were used for further analysis if they passed an expressed gene threshold of 4000 genes. Cluster identification was based on the 50 most significant principal components. Cell type recognition was automatically annotated by the software "SingleR" (v3.15) (38). All uniform manifold approximation and projection (UMAP) visualizations and violin plots were produced using Seurat functions in conjunction with the ggplot2.

Structure modeling of TGF-β1

The crystal structure of residues between 1 and 29 was not solved by experiments, and we modeled it using the GalaxyHomomer method of GalaxyWeb (39, 40). The best model predicted by GalaxyWeb was applied for the following analysis.

Statistical analysis

The Hardy-Weinberg Equilibrium (HWE) is a useful indicator of genotype frequencies within a population and whether they are based on a valid definition of alleles and a randomly mating sample, which was measured in the controls by Pearson's chi-square test ($P < 0.05$ was considered a departure from HWE). Statistical analysis was performed by RevMan 5.3 (Cochrane Community, 2014), which generated a forest plot, pooled ORs, and 95% CIs for each risk factor. We calculated the pooled ORs and 95% CIs to assess the association between *TGF-β1* polymorphisms and the susceptibility to CLDs. The significance of the ORs was determined with the Z-test, which is used to infer the probability of difference with the theory of standard normal distribution, and $P < 0.05$ was considered statistically significant. The heterogeneity assumption was evaluated by the Cochrane I^2 test and Q-statistic (P_{het}) (41). When the $P_{het} > 0.1$ and $I^2 < 50\%$, the fixed-effects (FE) model was adopted to calculate the pooled ORs; otherwise, the random-effects (RE) model was applied. The publication bias was assessed using funnel plots generated by RevMan 5.3. The Begg's test (42) and Egger's test (43) were also used to evaluate publication bias performed by Stata 15 (StataCorp 2017, Dallas, Texas, USA).

Results

Study selection and study characteristics

A total of 2,636 references were identified through Embase, Pubmed, Web of Science, Cochrane Library, and HuGe Navigator, of which 2,479 were excluded for irrelevance and duplication. After reviewing 157 articles, 88 articles did not satisfy the selection criteria, leaving 69 studies for detailed full-text evaluation. Ultimately, 35 studies were judged to meet the inclusion criteria for this meta-analysis (Figure 1).

The eligible 35 studies included 5,225 patients with a variety of CLDs, such as HCC, cirrhosis, chronic hepatitis B (CHB), chronic hepatitis C (CHC), AIH, alcoholic liver disease (ALD), and primary biliary cirrhosis (PBC). These studies were performed in countries around the globe, including China, America, India, Brazil, Spain, Italy, Iran, Mexico, Japan, Pakistan, Turkey, and Egypt, and were mixed-sex, showing the data are comprehensive and extensive. Moreover, we assessed the quality of 35 studies based on the NOS criteria (35). All of these studies exhibited comparatively high quality with a score of more than six (Table 1).

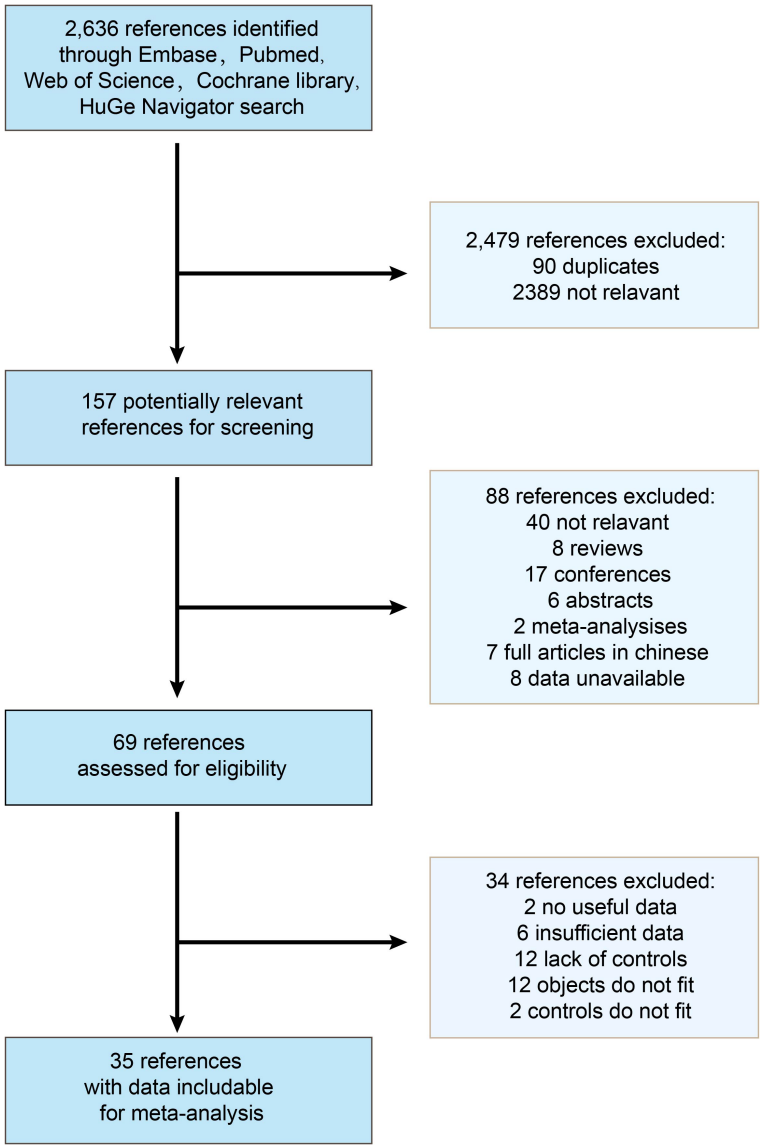

FIGURE 1
Flow chart of the study selection process. 35 studies were determined to be eligible for inclusion in the meta-analysis.

Genotype distributions of *TGF-β1* polymorphisms

Five *TGF-β1* polymorphisms participated in these 35 studies, including *TGF-β1*-509C/T (rs1800469), *TGF-β1* codon 10 (rs1800470), *TGF-β1* codon 25 (rs1800471), *TGF-β1*-800G/A (rs1800468) and *TGF-β1* codon 263 (rs1800472) polymorphisms. The genotypes and allele frequencies of every *TGF-β1* polymorphism distribution in the involved studies were summarized: *TGF-β1*-509C/T (Table 2), *TGF-β1* codon 10 (Table 3), *TGF-β1* codon 25 (Table 4), *TGF-β1*-800G/A (Table S1) and *TGF-β1* codon 263 (Table S2). According to the HWE examination, genotype distributions in controls of the overwhelming majority of studies were in agreement with HWE except for several studies. Thus, studies with HWE less than 0.05 were excluded for further meta-analysis.

Relationship between *TGF-β1* polymorphisms and CLD Risk

The results of CLD risk associated with three SNPs (*TGF-β1*-509C/T, codon 10, and codon 25) under five genetic models were summarized in Table 5. Given that less than three references were available on *TGF-β1*-800G/A and codon 263

10.3389/fimmu.2022.1058532

TABLE 1 The characteristics of included studies.

Reference	Country	Ethnicity	Genotyping method	Sex	Disease	Number		Study quality (NOS)
						Case/n	Control/n	
Suzuki, S. 2003	Japan	Asian	PCR-RFLP	Mixed	CHC	206	101	8
Kikuchi, K. 2007	Japan	Asian	PCR-RFLP	Mixed	PBC	65	71	7
Basturk, B. 2008	Turkey	Caucasian	PCR-SSP	Mixed	CHB	27	60	8
Romani, S. 2011	Iran	Caucasian	PCR-RFLP	Mixed	CHC	164	169	7
Talaat, R. M. 2013	Egypt	Egyptian	SSP-PCR	Mixed	CHB	65	27	9
Hosseini Razavi, A. 2014	Iran	Caucasian	PCR-RFLP	Mixed	CHB	220	220	8
Fabríciosilva-Silva. 2015	Brazil	Mixed-race	TaqMan	Mixed	CHC	245	189	8
Dondeti, M. F. 2017	Egypt	Egyptian	ARMS-PCR	Mixed	CHB	115	119	9
Obada, M. 2017	Egypt	Egyptian	PCR-RFLP	Mixed	CHC	150	100	9
Ghani, M. U. 2019	Pakistan	Asian	PCR-RFLP	Mixed	CHC	96	98	9
					HCC	94	98	
Sánchez-Parada. 2013	Mexico	Mixed-race	TaqMan	Mixed	CHC	38	50	8
Oliver, J. et al., 2005	Spain	Caucasian	PCR-RFLP	Mixed	ALD	165	185	8
Armendáriz-Borunda, J. 2008	Mexico	Mixed-race	PCR-RFLP	Mixed	CHC	13	30	8
					ALD	7	30	
Qi, P. 2009	China	Asian	PCR-RFLP	Mixed	CHB	196	299	8
					HCC	379	299	
Radwan. 2012	Egypt	Egyptian	PCR-RFLP	Mixed	Cirrhosis	152	160	9
					HCC	128	160	
Roy, N. 2012	India	Asian	PCR-RFLP	Male	ALD	169	108	8
Conde, S. R. 2013	Brazil	Mixed-race	PCR-RFLP	Mixed	CHB	53	97	8
Mohy, A. 2014	Egypt	Egyptian	PCR-RFLP	Mixed	Cirrhosis	40	40	9
Saxena. 2014	India	Asian	PCR-RFLP	Mixed	CHB	61	153	8
					Cirrhosis	60	153	
					HCC	59	153	
Bader El Din, N. G. 2017	Egypt	Egyptian	PCR-RFLP	Mixed	CHC	72	50	9
Brito, W. 2020	Brazil	Mixed-race	TaqMan	Mixed	CHC	97	300	7
Nomair. 2021	Egypt	Egyptian	TaqMan	Mixed	Cirrhosis	36	20	8
					HCC	34	20	
Vidigal, P. G. 2002	America	Caucasian	PCR-RFLP	Male	CHC	80	37	9
Zein. 2004	Mixed	Egyptian	PCR-RFLP	Mixed	CHC	24	45	7
		Caucasian	PCR-RFLP	Mixed	CHC	31	36	
Falleti, E. 2008	Italy	Caucasian	PCR-SSP	Mixed	Cirrhosis	188	140	9
Pereira, F. A. 2008	Brazil	Mixed-race	PCR-RFLP	Mixed	CHC	128	94	9
Wang, H. 2008	China	Asian	ARMS-PCR	Mixed	Cirrhosis	118	104	9
Paladino, N. 2010	America		SSOP	Mixed	AIH	178	189	6
Lee, J. J. 2011	Korea	Asian	SSCP	Mixed	Cirrhosis	182	119	7
Shi, H. Z. 2012	China	Asian	PCR-RFLP	Mixed	HCC	72	117	6
Xin, Z. H. 2012	China	Asian	TaqMan	Mixed	HCC	347	881	8
Maria. 2013	Mexico	Mixed-race	TaqMan	Mixed	CHC	38	50	9
Ma, J. 2015	China	Asian	PCR-RFLP	Mixed	CHC	234	375	9
					HCC	159	375	
Eskandari, E. 2017	Iran	Caucasian	ARMS-PCR	Mixed	CHB	196	198	8
Yousefi, A. 2019	Iran	Caucasian	PCR-SSP	Mixed	AIH	44	138	8

PCR, polymerase chain reaction; RFLP, restriction fragment length polymorphism; SSP, sequence-specific primer; ARMS, amplification refractory mutation system; SSOP, sequence-specific oligonucleotide probing; SSCP, single stranded conformational polymorphism; HCC, hepatocellular carcinoma; PBC, primary biliary cirrhosis; CHB, chronic hepatitis B; CHC, chronic hepatitis C; ALD, alcoholic liver disease; AIH, autoimmune hepatitis; NOS, Newcastle-Ottawa Scale.

TABLE 2 The genotype and allele frequencies of *TGF-β1*-509C/T distribution of included studies.

Reference	Disease	Number		Case			Control			*P* for HWE	
		Case/n	Control/n	CC	CT	TT	CC	CT	TT	Case	Control
Bader El Din, N. G. 2017	CHC	72	50	22	32	18	23	23	4	0.358	0.595
Brito, W. 2020	CHC	97	300	17	49	31	90	154	56	0.754	0.488
Conde, S. R. 2013	CHB	53	97	17	19	17	24	39	34	0.039	0.065
Dondeti, M. F. 2017	CHB	115	119	11	85	19	35	75	9	0.000	0.000
Eskandari, E. 2017	CHB	178	154	78	78	22	71	54	29	0.715	0.003
Falleti, E. 2008	Cirrhosis	188	140	50	85	53	57	61	22	0.190	0.404
Ghani, M. U. 2019	CHC	96	98	22	47	27	38	42	18	0.859	0.296
	HCC	94	98	18	47	29	38	42	18	0.893	0.296
Hosseini Razavi, A. 2014	CHB	220	220	50	116	54	65	97	58	0.416	0.082
Kikuchi, K. 2007	PBC	65	71	21	32	12	27	31	13	0.975	0.441
Ma, J. 2015	CHC	234	375	91	101	42	143	161	71	0.137	0.036
	HCC	159	375	50	67	42	143	161	71	0.051	0.036
Mohy, A. 2014	Cirrhosis	40	40	9	21	10	33	4	3	0.749	0.001
Oliver, J. 2005	ALD	165	185	64	78	23	79	85	21	0.921	0.795
Qi, P. 2009	CHB	196	299	31	101	64	50	156	93	0.396	0.257
	HCC	379	299	89	198	92	50	156	93	0.382	0.257
Radwan. 2012	Cirrhosis	152	160	34	74	44	62	68	30	0.785	0.147
	HCC	128	160	24	64	40	62	68	30	0.857	0.147
Roy, N. 2012	ALD	169	108	80	75	14	39	48	21	0.539	0.373
Shi, H. Z. 2012	HCC	72	117	24	40	8	55	53	9	0.152	0.438
Wang, H. 2008	Cirrhosis	118	104	31	53	34	29	50	25	0.272	0.706
Xin, Z. H. 2012	HCC	347	881	82	177	88	212	432	237	0.703	0.583
Saxena. 2014	CHB	61	153	8	37	16	44	94	15	0.067	0.001
	Cirrhosis	60	153	8	48	4	44	94	15	0.000	0.001
	HCC	59	153	9	39	11	44	94	15	0.013	0.001

HCC, hepatocellular carcinoma; PBC, primary biliary cirrhosis; CHB, chronic hepatitis B; CHC, chronic hepatitis C; ALD, alcoholic liver disease; HWE, Hardy–Weinberg Equilibrium; C, Cytosine; T, Thymine.

polymorphisms, a further meta-analysis was not performed for these two variants.

Seventeen studies were involved in determining the association between *TGF-β1*-509C/T polymorphism and CLD risk. The sample number of the cases and control groups were 2,611 and 3,387, respectively. Except for the recessive model (TT vs CC+CT), the other four genetic models showed a significant association of *TGF-β1*-509C/T polymorphism with CLD risk (Figure 2; Table 5). The pooled OR of allele model (T vs C) was 1.25 (95% CI: 1.06-1.48, $p = 0.009$). The pooled OR of homozygote model (TT vs CC) was 1.51 (95% CI: 1.08-2.11, $p = 0.02$). The pooled OR of heterozygote model (CT vs CC) was 1.31 (95% CI: 1.09-1.58, $p = 0.005$). The pooled OR of dominant model (CT+TT vs CC) was 1.38 (95% CI: 1.10-1.73, $p = 0.005$). Taken together, these results showed that *TGF-β1*-509C/T was significantly associated with an increased risk of CLDs.

Thirteen studies were involved in determining the association between *TGF-β1* codon 10 polymorphism and CLD risk. The sample number of the cases and control groups were 2,027 and 1,685, respectively. Three genetic models showed association with susceptibility to CLDs (Figure 3; Table 5), including allele model (Pro vs Leu, OR: 1.12, 95% CI: 1.02-1.23, $p = 0.01$), homozygote model (Pro/Pro vs Leu/Leu, OR: 1.28, 95% CI: 1.06-1.54, $p = 0.01$) and recessive model (Pro/Pro vs Leu/Leu+Leu/Pro, OR: 1.23, 95% CI: 1.05-1.44, $p = 0.009$). Together, our results indicated that patients with the *TGF-β1* codon 10 Pro/Pro genotype would have a higher CLD occurrence.

Nineteen studies were involved in determining the association between *TGF-β1* codon 25 polymorphism and CLD risk. The sample number of the cases and control groups were 1,896 and 1,861, respectively. In our study, *TGF-β1* codon 25 polymorphism had no significant association with the susceptibility to CLDs (Table 5).

Subgroup analysis by etiologies

We conducted a subgroup analysis to assess the effect of etiology on the relationship between *TGF-β1* polymorphisms and CLD risk. As illustrated in Table 6, patients with the *TGF-β1*-509 TT genotype had a significantly higher risk of cirrhosis or CHC, consistent with a

10.3389/fimmu.2022.1058532

TABLE 3 The genotype and allele frequencies of *TGF-β1* codon 10 distribution of included studies.

Reference	Disease	Number		Case			Control			*P* for HWE	
		Case/n	Control/n	Leu/Leu	Leu/Pro	Pro/Pro	Leu/Leu	Leu/Pro	Pro/Pro	Case	Control
Basturk, B. 2008	CHB	27	60	2	20	5	16	31	13	0.009	0.781
Dondeti, M. F. 2017	CHB	115	119	44	70	1	40	70	9	0.000	0.004
Eskandari, E. 2017	CHB	196	198	23	118	55	46	103	49	0.001	0.567
Fabríciosilva-Silva. 2015	CHC	245	189	70	117	58	54	103	32	0.505	0.149
Falleti, E. 2008	Cirrhosis	188	140	51	95	42	49	62	29	0.859	0.257
Lee, J. J. 2011	Cirrhosis	182	119	61	79	42	35	53	31	0.099	0.238
Obada, M. 2017	CHC	150	100	42	78	30	32	47	21	0.567	0.628
Oliver, J. 2005	ALD	165	185	72	68	25	75	77	33	0.186	0.096
Paladino, N. 2010	AIH	178	189	46	65	67	55	95	39	0.001	0.863
Pereira, F. A. 2008	CHC	128	94	26	65	37	24	49	21	0.793	0.672
Romani, S. 2011	CHC	164	169	50	81	33	49	85	35	0.985	0.867
Suzuki, S. 2003	CHC	206	101	56	84	66	28	52	21	0.009	0.727
Talaat, R. M. 2013	CHB	65	27	10	44	11	0	15	12	0.004	0.046
Vidigal, P. G. 2002	CHC	80	37	29	38	13	12	21	4	0.926	0.246
Wang, H. 2008	Cirrhosis	118	104	34	53	31	25	50	29	0.272	0.706
Yousefi, A. 2019	AIH	44	138	6	7	31	27	91	20	0.000	0.000
Zein. 2004	CHC(Caucasian)	31	36	10	4	17	12	3	21	0.000	0.000
	CHC (Egyptian)	24	45	6	3	15	12	11	22	0.001	0.001

CHB, chronic hepatitis B; CHC, chronic hepatitis C; ALD, alcoholic liver disease; AIH, autoimmune hepatitis; HWE, Hardy–Weinberg Equilibrium; Leu, Leucine; Pro, Proline.

TABLE 4 The genotype and allele frequencies of *TGF-β1* codon 25 distribution of included studies.

Reference	Disease	Number		Case			Control			*P* for HWE	
		Case/n	Control/n	Arg/Arg	Arg/Pro	Pro/Pro	Arg/Arg	Arg/Pro	Pro/Pro	Case	Control
Armendáriz. 2008 (ALD)	ALD	7	30	7	0	0	11	13	6	/	0.552
	CHC	13	30	13	0	0	11	13	6	/	0.552
Basturk, B. 2008	CHB	27	60	23	4	0	51	6	3	0.678	0.001
Dondeti, M. F. 2017	CHB	115	119	96	19	0	104	13	2	0.334	0.054
Fabríciosilva-Silva. 2015	CHC	245	189	213	30	2	161	26	2	0.417	0.420
Falleti, E. 2008	Cirrhosis	187	140	156	31	0	127	13	0	0.216	0.565
Hosseini Razavi, A. 2014	CHB	220	220	193	23	4	197	21	2	0.003	0.105
Maria. 2013	CHC	38	50	34	4	0	46	4	0	0.732	0.768
Nomair. 2021	Cirrhosis	36	20	2	32	2	4	14	2	0.000	0.064
	HCC	34	20	10	24	0	4	14	2	0.001	0.064
Obada, M. 2017	CHC	150	100	127	22	1	84	15	1	0.965	0.721
Oliver, J. 2005	ALD	165	185	135	28	2	148	34	3	0.690	0.523
Paladino, N. 2010	AIH	178	189	154	15	9	156	32	1	0.000	0.638
Pereira, F. A. 2008	CHC	128	94	113	14	1	64	29	1	0.451	0.244
Romani, S. 2011	CHC	164	169	145	18	1	151	16	2	0.595	0.052
Sánchez-Parada. 2013	CHC	38	50	34	4	0	46	4	0	0.732	0.768
Vidigal, P. G. 2002	CHC	80	37	68	11	1	34	3	0	0.480	0.797
Yousefi, A. 2019	AIH	43	138	26	7	10	119	17	2	0.000	0.146
Zein. 2004	CHC(Caucasian)	31	36	25	6	0	33	3	0	0.551	0.794
	CHC (Egyptian)	24	45	21	3	0	41	4	0	0.744	0.755

HCC, hepatocellular carcinoma; CHB, chronic hepatitis B; CHC, chronic hepatitis C; ALD, alcoholic liver disease; AIH, autoimmune hepatitis; HWE, Hardy–Weinberg Equilibrium; Arg, Arginine; Pro, Proline.

TABLE 5 Main results of the meta-analysis of *TGF-β1* polymorphisms in CLDs.

SNPs	Gene model	Number of study	OR (95% CI)	*P*	Test for heterogeneity		Analysis model	Publication bias	
					I^2, %	P_{het}		Begg	Egger
-509C/T	T vs C	17	1.25 (1.06, 1.48)	0.009	78	<0.00001	RE	0.2661	0.1428
	TT vs CC	17	1.51 (1.08, 2.11)	0.02	77	<0.00001	RE	0.387	0.1492
	CT vs CC	17	1.31 (1.09, 1.58)	0.005	49	0.01	RE	0.3031	0.2309
	CT+TT vs CC	17	1.38 (1.10, 1.73)	0.005	69	<0.00001	RE	0.2016	0.1632
	TT vs CC+CT	17	1.25 (1.00, 1.57)	0.05	65	0.0001	RE	0.5923	0.1469
Codon 10	Pro vs Leu	13	1.12 (1.02, 1.23)	0.01	18	0.27	FE	1.3307	0.7615
	Pro/Pro vs Leu/Leu	13	1.28 (1.06, 1.54)	0.01	23	0.21	FE	0.9514	0.6462
	Leu/Pro vs Leu/Leu	13	1.05 (0.90, 1.23)	0.54	35	0.1	FE	0.5022	0.1072
	Pro/Pro+Leu/Pro vs Leu/Leu	13	1.11 (0.96, 1.29)	0.15	28	0.17	FE	0.2997	0.1229
	Pro/Pro vs Leu/Leu+Leu/Pro	13	1.23 (1.05, 1.44)	0.009	29	0.15	FE	1.5723	0.3629
Codon 25	Pro vs Arg	19	1.09 (0.78, 1.52)	0.60	69	<0.00001	RE	0.7526	0.1072
	Pro/Pro vs Arg/Arg	14	0.97 (0.38, 2.51)	0.95	55	0.007	RE	1.984	0.0008
	Arg/Pro vs Arg/Arg	19	1.01 (0.73, 1.39)	0.98	55	0.002	RE	0.6488	0.5689
	Pro/Pro+Arg/Pro vs Arg/Arg	19	1.07 (0.76, 1.52)	0.68	64	<0.0001	RE	0.5515	0.2743
	Pro/Pro vs Arg/Arg+Arg/Pro	14	1.00 (0.42, 2.41)	1.00	49	0.02	RE	1.9625	0.0006

SNPs, single-nucleotide polymorphisms; OR, pooled odds ratios; 95% CI, 95% confidence interval; P, P value for Z test. I^2, Cochrane I^2 test; P_{het}, P value for heterogeneity; Begg, Begg's tests; Egger, Egger's tests; RE, random-effects model; FE, fixed-effects model; C, Cytosine; T, Thymine; Leu, Leucine; Arg, Arginine; Pro, Proline; vs, versus.

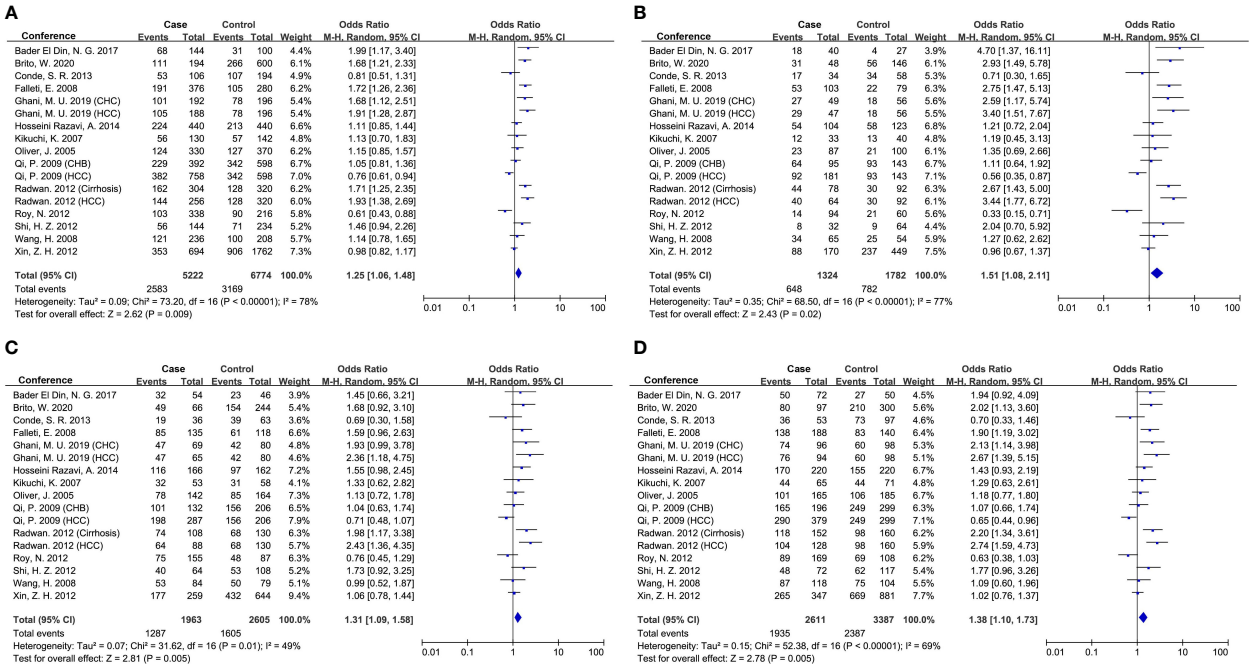

FIGURE 2
Forest plot of OR with 95% CI for associations between *TGF-β1*-509C/T polymorphism and CLD risk. **(A)** allele model, T vs C; **(B)** homozygote model, TT vs CC; **(C)** heterozygote model, CT vs CC; **(D)** dominant model, CT +TT vs CC. OR, pooled odds ratios; 95% CI, 95% confidence interval; T, Thymine; C, Cytosine.

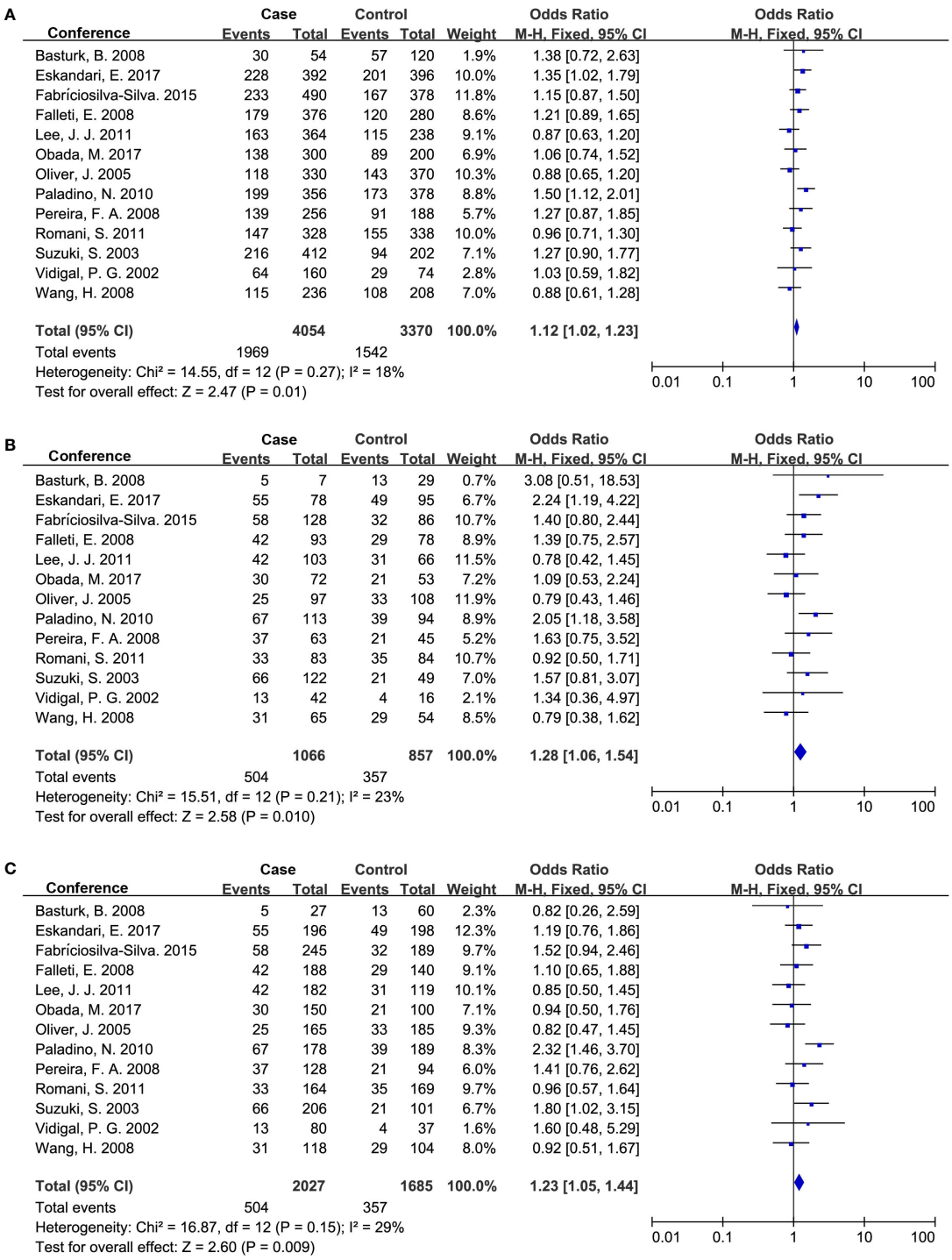

FIGURE 3
Forest plot of OR with 95% CI for associations between *TGF-β1* codon 10 polymorphism. **(A)** dominant model, Pro vs Leu) and CLD risk; **(B)** homozygote model, Pro/Pro vs Leu/Leu; **(C)** recessive model, Pro/Pro vs Leu/Leu+Leu/Pro. OR, pooled odds ratios; 95% CI, 95% confidence interval; Pro, Proline; Leu, Leucine.

previous study (24). Lamentedly, *TGF-β1*-509C/T polymorphism had a limited role in HCC susceptibility. The *TGF-β1* codon 10 polymorphism was significantly associated with CHB risk (Table 7), which was distinct from the current literature that *TGF-β1* codon 10 polymorphism was not associated with the HBV/HCV-induced cirrhosis or HCC (19–21, 24). In addition, we concluded that the *TGF-β1* codon 25 polymorphism had a potential relationship in patients with AIH for the first time (Table 8).

Sensitivity analysis

We performed a leave-one-out sensitivity analysis to ascertain the stability of the meta-analysis by removing a single study at a time under the random-effects model. As shown in Tables S3, S4, the statistical significance of the result was not altered when a single study was omitted, indicating that our results were reliable and stable.

TABLE 6 Subgroups results of the role of *TGF-β1*-509C/T polymorphism in different CLDs.

Gene model	Subgroup	Numberof study	OR (95% CI)	*P*	Test for heterogeneity		Analysis model
					I^2, %	P_{het}	
T vs C	Overall	17	1.25 (1.06, 1.48)	0.009	78	<0.00001	RE
	HCC	5	1.28 (0.90, 1.84)	0.17	88	<0.00001	RE
	Cirrhosis	3	1.54 (1.27, 1.86)	<0.0001	42	0.18	FE
	CHB	3	1.04 (0.87, 1.23)	0.67	0	0.54	FE
	CHC	3	1.73 (1.38, 2.18)	<0.00001	0	0.85	FE
	ALD	2	0.85 (0.46, 1.57)	0.60	85	0.009	RE
	PBC	1	1.13 (0.70, 1.83)	0.62	–	–	–
TT vs CC	Overall	17	1.51 (1.08, 2.11)	0.02	77	<0.00001	RE
	HCC	5	1.57 (0.77, 3.21)	0.22	86	<0.00001	RE
	Cirrhosis	3	2.21 (1.52, 3.21)	<0.0001	35	0.22	FE
	CHB	3	1.07 (0.76, 1.51)	0.7	0	0.56	FE
	CHC	3	3.04 (1.89, 4.88)	<0.00001	0	0.72	FE
	ALD	2	0.67 (0.17, 2.71)	0.58	86	0.007	RE
	PBC	1	1.19 (0.45, 3.13)	0.73	–	–	–
CT vs CC	Overall	17	1.31 (1.09, 1.58)	0.005	49	0.01	RE
	HCC	5	1.42 (0.89, 2.25)	0.14	77	0.02	RE
	Cirrhosis	3	1.53 (1.12, 2.10)	0.008	26	0.26	FE
	CHB	3	1.19 (0.87, 1.63)	0.28	38	0.2	FE
	CHC	3	1.70 (1.15, 2.52)	0.008	0	0.86	FE
	ALD	2	0.96 (0.68, 1.35)	0.8	20	0.26	FE
	PBC	1	1.33 (0.62, 2.82)	0.46	–	–	–
CT+TT vs CC	Overall	17	1.38 (1.10, 1.73)	0.005	69	<0.00001	RE
	HCC	5	1.48 (0.86, 2.53)	0.15	85	<0.0001	RE
	Cirrhosis	3	1.74 (1.30, 2.33)	0.0002	41	0.18	FE
	CHB	3	1.15 (0.85, 1.54)	0.36	29	0.24	FE
	CHC	3	2.04 (1.41, 2.95)	0.0002	0	0.98	FE
	ALD	2	0.87 (0.47, 1.61)	0.66	72	0.06	RE
	PBC	1	1.29 (0.63, 2.61)	0.49	–	–	–
TT vs CC+CT	Overall	17	1.25 (1.00, 1.57)	0.05	65	0.0001	RE
	HCC	5	1.21 (0.80, 1.83)	0.38	73	0.005	RE
	Cirrhosis	3	1.71 (1.24, 2.36)	0.001	0	0.48	FE
	CHB	3	0.98 (0.75, 1.28)	0.87	0	0.81	FE
	CHC	3	2.11 (1.44, 3.11)	0.0001	0	0.51	FE
	ALD	2	0.70 (0.21, 2.30)	0.55	84	0.01	RE
	PBC	1	1.01 (0.42, 2.41)	0.98	–	–	–

HCC, hepatocellular carcinoma; PBC, primary biliary cirrhosis; CHB, chronic hepatitis B; CHC, chronic hepatitis C; ALD, alcoholic liver disease; OR, pooled odds ratios; 95% CI, 95% confidence interval; P, P value for Z test. I^2, Cochrane I^2 test; P_{het}, P value for heterogeneity; RE, random-effects model; FE, fixed-effects model; C, Cytosine; T, Thymine; vs, versus.

TABLE 7 Subgroups results of the role of *TGF-β1* codon 10 polymorphism in different CLDs.

Gene model	Subgroup	Number of study	OR (95% CI)	*P*	Test for heterogeneity		Analysis model
					I^2, %	P_{het}	
Pro vs Leu	Overall	13	1.12 (1.02, 1.23)	0.01	18	0.27	FE
	Cirrhosis	3	0.99 (0.82, 1.20)	0.92	24	0.27	FE
	CHB	2	1.35 (1.05, 1.75)	0.02	0	0.95	FE
	CHC	6	1.12 (0.97, 1.29)	0.12	0	0.84	FE
	AIH	1	1.50 (1.12, 2.01)	0.006	–	–	–
	ALD	1	0.88 (0.65, 1.20)	0.43	–	–	–
Pro/Pro vs Leu/Leu	Overall	13	1.28 (1.06, 1.54)	0.01	23	0.21	FE
	Cirrhosis	3	0.97 (0.67, 1.41)	0.87	6	0.34	FE
	CHB	2	2.33 (1.28, 4.22)	0.005	0	0.75	FE
	CHC	6	1.28 (0.96, 1.70)	0.09	0	0.84	FE
	AIH	1	2.15 (1.18, 3.58)	0.01	–	–	–
	ALD	1	0.79 (0.43, 1.46)	0.45	–	–	–
Leu/Pro vs Leu/Leu	Overall	13	1.05 (0.90, 1.23)	0.54	35	0.1	FE
	Cirrhosis	3	1.04 (0.76, 1.43)	0.81	35	0.21	FE
	CHB	2	2.58 (1.52, 4.37)	0.0004	0	0.34	FE
	CHC	6	0.95 (0.76, 1.20)	0.69	0	0.82	
	AIH	1	0.35 (0.11, 1.12)	0.08	–	–	–
	ALD	1	0.92 (0.58, 1.46)	0.72	–	–	–
Pro/Pro+Leu/Pro vs Leu/Leu	Overall	13	1.11 (0.96, 1.29)	0.15	28	0.17	FE
	Cirrhosis	3	1.02 (0.76, 1.37)	0.91	43	0.17	FE
	CHB	2	2.51 (1.50, 4.18)	0.0004	0	0.41	FE
	CHC	6	1.04 (0.84, 1.30)	0.71	0	0.92	FE
	AIH	1	1.18 (0.74, 1.86)	0.49	–	–	–
	ALD	1	0.88 (0.58, 1.35)	0.56	–	–	–
Pro/Pro vs Leu/Leu+Leu/Pro	Overall	13	1.23 (1.05, 1.44)	0.009	29	0.15	FE
	Cirrhosis	3	0.96 (0.69, 1.31)	0.78	0	0.79	FE
	CHB	2	1.13 (0.74, 1.71)	0.57	0	0.56	FE
	CHC	6	1.32 (1.04, 1.68)	0.02	0	0.54	FE
	AIH	1	2.32 (1.46, 3.70)	0.0004	–	–	–
	ALD	1	0.82 (0.47, 1.45)	0.5	–	–	–

CHB, chronic hepatitis B; CHC, chronic hepatitis C; ALD, alcoholic liver disease; AIH, autoimmune hepatitis; OR, pooled odds ratios; 95% CI, 95% confidence interval; P, P value for Z test. I^2, Cochrane I^2 test; P_{het}, P value for heterogeneity; FE, fixed-effects model; Pro, Proline; Leu, Leucine; vs, versus.

Publication bias

We assessed the publication bias with the Begg's and Egger's test, and used a funnel plot to graphically represent the bias. Our results showed there was no publication bias in studies associated with *TGF-β1*-509C/T and codon 10 (Table 5). Similarly, the funnel plots were approximately symmetric, indicating no evidence of potential publication bias (Figure 4).

TGF-β1 gene expression in human CLDs

Studies have shown that *TGF-β1*-509C/T and codon 10 displayed increased expression and plasma concentration of TGF-β1 (21, 31–33), implying that *TGF-β1* genetic variants could affect TGF-β1 protein expression. Here, the association of *TGF-β1* polymorphisms with the gene expression of TGF-β1 was explored. We firstly evaluated the *TGF-β1* mRNA levels in all sorts of CLD patients based on GEO datasets (Figure 5). Compared to healthy controls, a significantly higher mRNA level of *TGF-β1* was observed in patients with CHB, AIH, NASH and cirrhosis (Figures 5A-D). Nevertheless, there were no significant differences in *TGF-β1* expression between control and patients with CHC, alcohol hepatitis, and HCC (Figures 5E-G). Furthermore, we integrated all data and compared the difference in *TGF-β1* mRNA levels. Results showed that the gene expression of *TGF-β1* was markedly higher in CLD patients compared to healthy controls (Figure 5H).

Among these etiologies of CLDs, the *TGF-β1* mRNA level was the most significantly associated with cirrhosis

10.3389/fimmu.2022.1058532

TABLE 8 Subgroups results of the role of *TGF-β1* codon 25 polymorphism in different CLDs.

Gene model	Subgroup	Number of study	OR (95% CI)	*P*	Test for heterogeneity		Analysis model
					I^2, %	P_{het}	
Pro vs Arg	Overall	19	1.09 (0.78, 1.52)	0.6	69	<0.00001	RE
	HCC	1	0.67 (0.30, 1.48)	0.32	–	–	–
	Cirrhosis	2	1.57 (0.95, 2.59)	0.08	0	0.42	FE
	CHB	2	1.22 (0.80, 1.87)	0.35	0	0.87	FE
	CHC	10	0.91 (0.58, 1.44)	0.68	55	0.02	RE
	AIH	2	2.37 (0.45, 12.35)	0.31	94	<0.0001	RE
	ALD	2	0.28 (0.02, 5.29)	0.40	76	0.04	RE
Pro/Pro vs Arg/Arg	Overall	14	0.97 (0.38, 2.51)	0.95	55	0.007	RE
	HCC	1	0.09 (0.00, 2.17)	0.14	–	–	–
	Cirrhosis	1	2.00 (0.15, 26.73)	0.6	–	–	–
	CHB	2	1.04 (0.28, 3.90)	0.95	38	0.2	FE
	CHC	6	0.44 (0.17, 1.14)	0.09	0	0.77	FE
	AIH	2	14.73 (3.92, 55.37)	<0.0001	0	0.48	FE
	ALD	2	0.38 (0.09, 1.63)	0.19	7	0.3	FE
Arg/Pro vs Arg/Arg	Overall	19	1.01 (0.73, 1.39)	0.98	55	0.002	RE
	HCC	1	0.69 (0.18, 2.60)	0.58	–	–	–
	Cirrhosis	2	2.15 (1.13, 4.10)	0.02	0	0.39	FE
	CHB	2	1.29 (0.80, 2.08)	0.3	0	0.49	FE
	CHC	10	0.92 (0.56, 1.51)	0.73	56	0.01	RE
	AIH	2	0.90 (0.23, 3.47)	0.88	81	0.02	RE
	ALD	2	0.33 (0.02, 4.74)	0.42	70	0.07	RE
Pro/Pro+Arg/Pro vs Arg/Arg	Overall	19	1.07 (0.76, 1.52)	0.68	64	<0.0001	RE
	HCC	1	0.60 (0.16, 2.25)	0.45	–	–	–
	Cirrhosis	2	2.14 (1.12, 4.06)	0.02	0	0.43	FE
	CHB	2	1.26 (0.80, 2.00)	0.32	0	0.78	FE
	CHC	10	0.90 (0.55, 1.50)	0.7	59	0.01	RE
	AIH	2	1.70 (0.32, 9.14)	0.54	92	0.0005	RE
	ALD	2	0.26 (0.01, 5.57)	0.39	77	0.04	RE
Pro/Pro vs Arg/Arg+Arg/Pro	Overall	14	1.00 (0.42, 2.41)	1	49	0.02	RE
	HCC	1	0.11 (0.00, 2.35)	0.16	–	–	–
	Cirrhosis	1	0.53 (0.07, 4.08)	0.54	–	–	–
	CHB	2	1.01 (0.27, 3.77)	0.99	41	0.19	FE
	CHC	6	0.53 (0.20, 1.41)	0.2	0	0.93	FE
	AIH	2	14.69 (3.98, 54.23)	<0.0001	0	0.58	FE
	ALD	2	0.51 (0.11, 2.28)	0.38	0	0.54	FE

HCC, hepatocellular carcinoma; CHB, chronic hepatitis B; CHC, chronic hepatitis C; AIH, autoimmune hepatitis; ALD, alcoholic liver disease; OR, pooled odds ratios; 95% CI, 95% confidence interval; P, P value for Z test. I^2, Cochrane I^2 test; P_{het}, P value for heterogeneity; RE, random-effects model; FE, fixed-effects model; Pro, Proline; Arg, Arginine; vs, versus.

(Figure 5D). We further explored the *TGF-β1* expression patterns in a published scRNA-seq dataset of human liver non-parenchymal cells from patients with cirrhosis and healthy individuals (37). Unsupervised clustering using UMAP uncovered nine cell lineages containing cells from both healthy and cirrhotic livers (Figures 5I, J). *TGF-β1* was mainly expressed in natural killer (NK) cells, macrophages, monocytes, adipocytes and endothelial cells (Figure 5K). Notably, cirrhotic patients had a significantly elevated expression of *TGF-β1* (Figure 5L). Above all, these data further demonstrated a remarkable association between *TGF-β1* gene expression and CLDs.

Transcription analysis of TGF-β1

TGF-β1-509C/T and -800G/A are located in the promoter region at positions -509 and -800, which might result in a transcript shift of *TGF-β1* by affecting the activity of the promoter. Transcription factors bind DNA in a sequence-

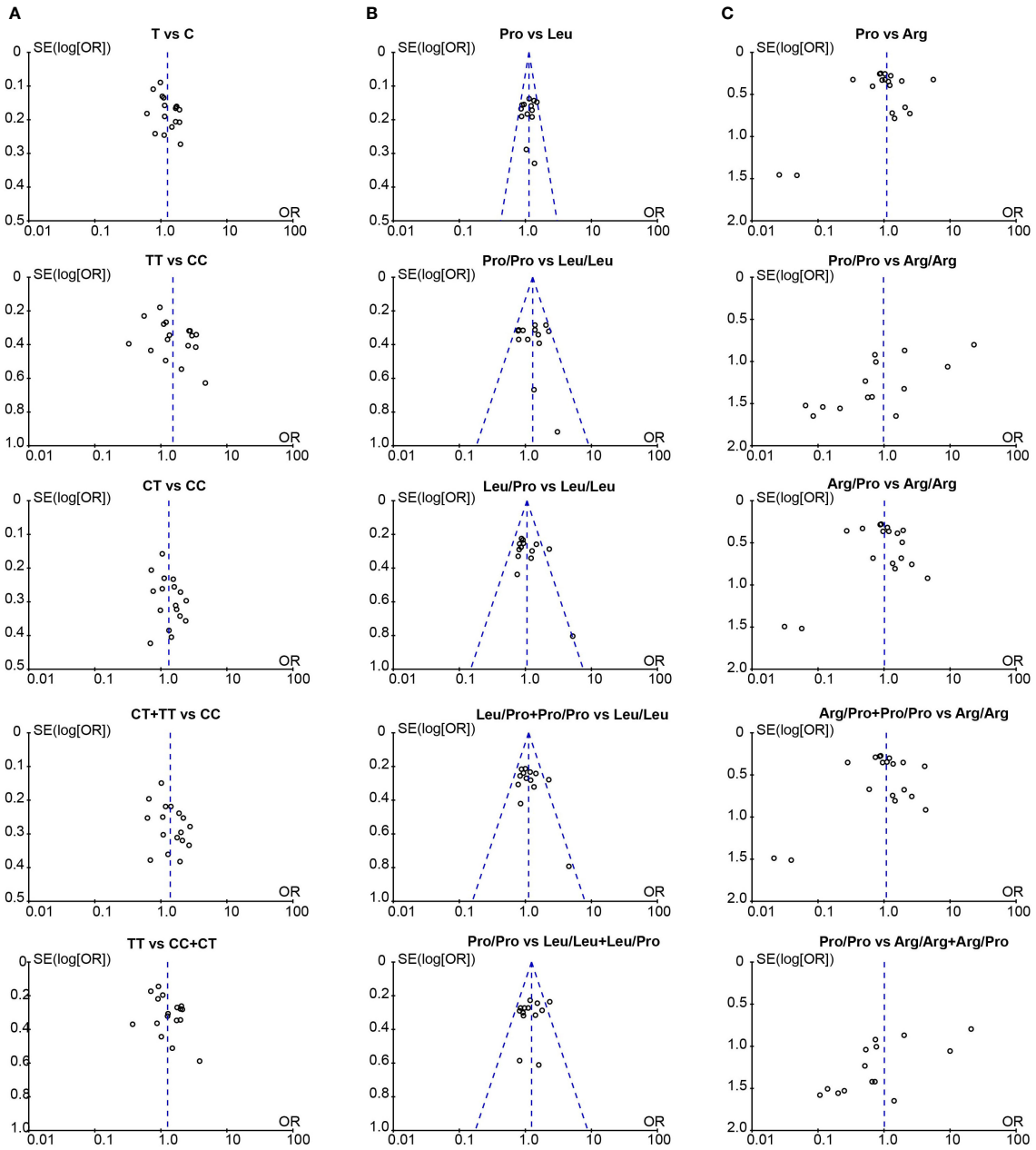

FIGURE 4
The funnel plot for publication bias assessment in the meta-analysis. **(A)** Funnel plot of *TGF-β1*-509C/T polymorphism and CLD risk; **(B)** Funnel plot of *TGF-β1* codon 10 polymorphism and CLD risk; **(C)** Funnel plot of *TGF-β1* codon 25 polymorphism and CLD risk. T, Thymine; C, Cytosine; Pro, Proline; Leu, Leucine; Arg, Arginine.

specific way and play an important role in regulating gene transcription. Thus, we wonder if the *TGF-β1* genetic variants interfere with the DNA binding of its transcription factors. We combined the candidates that were reported in Genecard, Ominer, Promo, and TRRUST databases to identify the most potential transcription factors involved in *TGF-β1* transcription. Based on the overlapping data, we eventually identified three transcription factors, including specific protein-1 (SP-1), upstream stimulatory factor 2 (USF2), and JUN (Figure 5M).

SP-1 is the main nuclear protein involved in the regulation of *TGF-β1* gene activation, which can greatly boost the activity of the *TGF-β1* promoter (44–47). There are 11 conserved sequences of

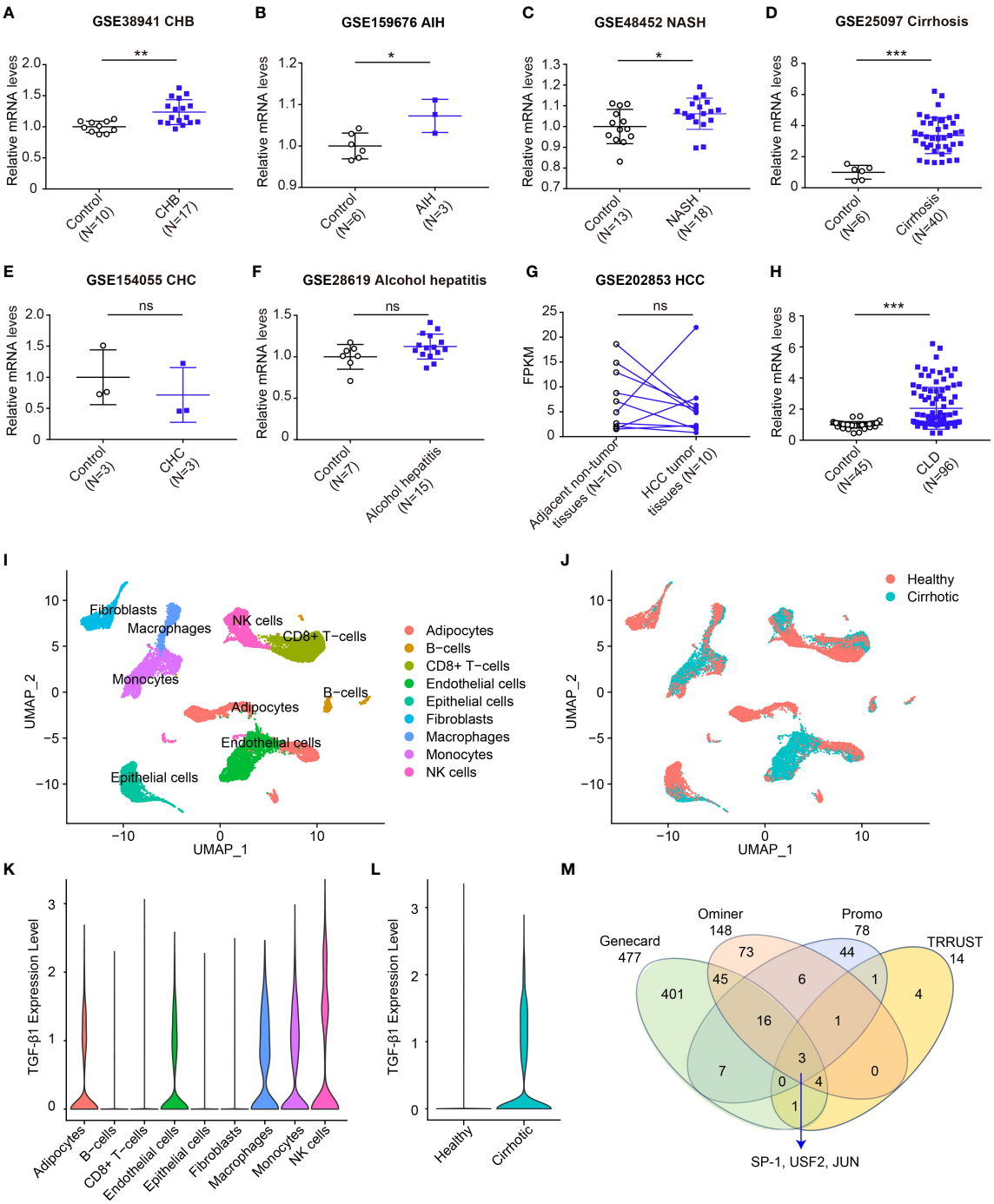

FIGURE 5
Expression of *TGF-β1* mRNA increases in CLDs. **(A-F)** Transcript levels of TGF-β1 in healthy individuals or patients with CHB (**A**, GSE38941), AIH (**B**, GSE159676), NASH (**C**, GSE48452), cirrhosis (**D**, GSE25097), CHC (**E**, GSE154055), and alcohol hepatitis (**F**, GSE28619); **(G)** Transcript levels of *TGF-β1* in adjacent non-tumor or HCC tumor (GSE202853); **(H)** Transcript levels of *TGF-β1* in healthy individuals or patients with CLDs; **(I, J)** UMAP plot showing all liver non-parenchymal cells dependent on the cluster **(I)** and dependent on the origin **(J)**; **(K)** TGF-β1 gene expression in all cell clusters; **(L)** TGF-β1 gene expression in healthy individuals and liver cirrhosis patients; **(M)** The transcription factor analysis of TGF-β1. Data are mean ± SD. **P*<0.05, ***P*<0.01, and ****P*<0.001 vs. Control. ns, not significant. Significance was calculated by two-tailed unpaired Student's *t*-test.

SP-1 binding sites (5'-GGGCGG) in the human *TGF-β1* promoter. According to the present findings, *TGF-β1*-509C/T and -800G/A genetic variants weren't involved in the binding sites of SP-1 in the *TGF-β1* promoter, revealing these two variants may not affect the transcriptional regulation of SP-1 on *TGF-β1* gene.

USF2 belongs to the basic helix-loop-helix leucine zipper family of transcription factors characterized by a highly conserved COOH-terminal domain responsible for dimerization and DNA binding (48, 49). Studies found that high glucose concentrations could induce USF2 binding to the *TGF-β1* promoter region -1013/-1002, enhancing *TGF-β1* promoter activity (50, 51). In addition, two specific binding sites for USF were identified in the *TGF-β1* promoter: -1,846 approximately -1,841 (CACATG) and -621 approximately -616 (CATGTG) (52), which did not include the positions -509 and -800. Thus, the current study provides no evidence that *TGF-β1*-509C/T and -800G/A could influence the transcriptional regulation of USF2 on the *TGF-β1* gene.

JUN is a transcription factor that recognizes and binds to the activator protein-1 (AP-1) consensus motif (53). Studies have validated that TGF-β1 could induce transcription of JUN mRNA through SMAD7 dependent/independent feedback manner (54, 55). Moreover, one study found that JUN could be involved in the promoter of *TGF-β1*, while its role and binding site in the *TGF-β1* promoter were unknown (56). More investigations should be taken to uncover the binding site of JUN in the *TGF-β1* promoter, then to determine if the binding sites covered the position of *TGF-β1*-509C/T and -800G/A genetic variants, and finally to figure out the underlying mechanism by which *TGF-β1* polymorphism regulated the binding activity between transcription factors and *TGF-β1* promoter to affect *TGF-β1* transcription.

Structural analysis of TGF-β1 protein

The *TGF-β1* codon 10 (CTG > CCG), codon 25 (CGG > CCG), and codon 263 (ACC > ATC) variants lead to amino-acid substitutions Leu10Pro, Arg25Pro, and Thr263Ile (Table S5). We investigated these codon variants based on the TGF-β1 crystal structure. TGF-β1 encodes a polypeptide comprising a signal peptide with 29 residues, a 249-residue pro-domain (latency-associated peptide), and a 112-residue growth factor (GF) domain (Figure 6A) (57, 58). And TGF-β1 is covalently linked to form dimers in the endoplasmic reticulum (58, 59). We modeled the overall crystal structure of TGF-β1 using the GalaxyHomomer method of GalaxyWeb (39, 40) and selected the best-predicted model for further analysis.

As illustrated in Figure 6B, *TGF-β1* codon 10 and codon 25 were located in the signal peptide of TGF-β1, which domain hasn't been confirmed based on experiments. We could not conclude any more results on how *TGF-β1* codon 10 and codon 25 variants affect the 3D structure of TGF-β1. Our results showed that the *TGF-β1* codon 263 was located in the pro-domain, close to the region where the TGF-β1 dimerization interacts, implying that the *TGF-β1* codon 263 variant may alter the dimerization of TGF-β1. Latent TGF-β1 is covalently linked to form disulfide dimers and binds to the latent TGF-β binding protein (LTBP) (57–59). Once TGF-β1 was released from the LTBP, TGF-β1 could be secreted and interact with membrane receptors to initiate signal transduction (58, 60). Therefore, the *TGF-β1* codon 263 variant might affect the binding of TGF-β1 to LTBP by altering the dimerization of TGF-β1, thus affecting TGF-β1 secretion and signal transduction.

Discussion

In the present study, we pooled 35 studies and conducted a meta-analysis to evaluate the frequency of *TGF-β1* SNPs in CLD patients and healthy individuals. To our knowledge, this is the first systematic review and meta-analysis to comprehensively assess all *TGF-β1* SNPs associated with CLDs. Our results revealed that the *TGF-β1*-509C/T and codon 10 were significantly associated with CLD risk. Individuals with the *TGF-β1*-509 (TT or CT allele) or codon 10 (Pro/Pro allele) showed an increased risk of CLDs in the overall population. In particular, we identified that *TGF-β1*-509C/T was strongly associated with patients with cirrhosis or CHC, while *TGF-β1* codon 10 was more associated with patients with CHB. *TGF-β1* codon 25 exhibited a relationship with AIH risk. Moreover, we identified that the mRNA level of *TGF-β1* was significantly higher in a variety of CLDs, and explored the potential mechanisms by which *TGF-β1* polymorphisms influence CLD risk based on transcription factors and protein structure of TGF-β1.

CLDs are extremely common clinical conditions caused by diverse etiologies, such as CHB, CHC, AIH, cirrhosis, NASH, ALD, PBC and HCC, affecting the health of millions of people (1, 2). When the inflammatory balance is disrupted in the liver, sustained inflammation responses can lead to the occurrence of CLDs. TGF-β1 encoded by *TGF-β1* is a multifunctional immune regulator that contributes to various immunologic processes in CLDs (9). TGF-β1 not only shows the anti-inflammatory and immune surveillance properties in HCC but could also promote T cell differentiation and activation in CHB, CHC and NASH (11–15). Studies have indicated that *TGF-β1* genetic variants could trigger the susceptibility of CLDs, acting as a potential candidate for predicting CLD risk. Up to now, a few studies have investigated the relationship between *TGF-β1*-509C/T and codon 10 polymorphisms and the risk of HBV/HCV-induced cirrhosis and HCC. However, these results were inconsistent and controversial (Table S6). Some studies showed that the *TGF-β1*-

A

Feature key	Positions	Description	Graphical view	Length
Signal peptide	1-29	-		29
Pro-domain	30-278	Latency-associated peptide		249
Growth factor (GF) domain	279-390	Transforming growth factor beta-1		112

B

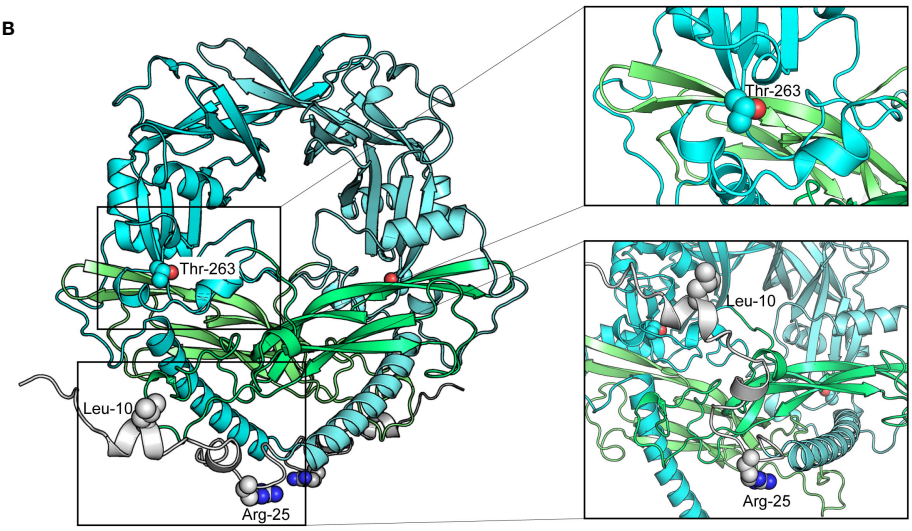

FIGURE 6
Peptide features and structure of TGF-β1. **(A)** Peptide features of TGF-β1; **(B)** Overall structure of TGF-β1. Protein structures and residues are shown in cartoon and sphere representation, respectively.

509 TT genotype showed an association with HCV-induced cirrhosis and HCC (20, 23, 24), and the *TGF-β1* codon 10 Pro/Pro genotype had a slight effect on HCC risk (20). But more studies just did not detect a significant association between *TGF-β1* polymorphisms and cirrhosis or HCC susceptibility (19, 21, 22, 25). As a whole, there was no systematic study to evaluate the association of *TGF-β1* polymorphisms in CLDs. Our study consolidated all available data with *TGF-β1* polymorphisms associated with diverse etiologies of CLDs and identified that *TGF-β1*-509C/T and codon 10 polymorphisms were highly associated with an increased risk of CLDs for the first time. *TGF-β1*-509C/T was significantly associated with CLD susceptibility under all genetic models except the recessive model (TT vs CC+CT; Table 5). For *TGF-β1* codon 10, the fixed-effect meta-analysis showed that the Pro/Pro genotype conferred a significantly increased risk to CLDs under the allele contrast model (pooled OR = 1.28, 95% CI: 1.06-1.54; Table 5). Lamentedly, the *TGF-β1* codon 25 showed no relationship with LCD risk (Table 5).

In the subgroup analysis based on etiologies, we found that *TGF-β1*-509C/T had a statistical association with cirrhosis and CHC under all genetic models (Table 6), consistently with the previous study (24). The *TGF-β1* codon 10 was significantly associated with CHB under allele model (pooled OR = 1.35, 95% CI: 1.05-1.75), homozygote model (pooled OR = 2.33, 95% CI: 1.28–4.22), heterozygote model (pooled OR = 2.58, 95% CI: 1.52-4.37) and dominant model (pooled OR = 2.51, 95% CI: 1.50-4.18) (Table 7). Interestingly, *TGF-β1* codon 25 Pro/Pro genotype showed a statistically significant association with AIH risk under homozygote model (pooled OR = 14.73, 95% CI: 3.92-55.37) and recessive model (pooled OR = 14.69, 95% CI: 3.98-54.23) (Table 8). Taken together, our data demonstrated that *TGF-β1*-509C/T and codon 10 polymorphisms could be feasible to screen for individuals at risk for CLDs, especially for cirrhosis, CHB, and CHC.

Studies have observed that *TGF-β1*-509C/T and codon 10 polymorphisms were associated with HCC risk (20). However, we didn't reveal similar results based on the involved 35 eligible studies (Tables 6 and 7). To get clear on which *TGF-β1* polymorphism could affect HCC risk, we analyzed the *TGF-β1* variants on the cBioPortal database. Our results showed that the most common variants of *TGF-β1* in HCC were missense mutations in G29E, A105S, D191N, and F321L, which might be the more precise genetic factors of *TGF-β1* to influence HCC susceptibility (Figure S1).

The fact that CLDs have different pathogenic and pathogenesis and are regulated by various genes. Based on our findings that *TGF-β1* polymorphisms contribute differently to CLD susceptibility, we hypothesized that *TGF-β1* polymorphism might be associated with CLD-related genes and play distinct regulatory roles. Lamentedly, the relationship between *TGF-β1* polymorphism and CLD-related

genes has not been identified, except the different interactions between TGF-β1 signaling and CLD-related genes, such as *Ki67* and *P53*, well-known HCC-related genes (61). A positive correlation between the activated TGF-β1 signaling pathway and high Ki67 expression due to the abnormal proliferation of cancer cells in tumor tissues (62). *P53* mutants affected the transcriptional activation of TGF-β (63, 64). Overall, the interactions between *TGF-β1* polymorphism and different CLD-related genes are interesting and undiscovered, which is worth further studies.

To reduce sampling bias in case-control studies, studies in which *TGF-β1* SNPs demonstrated a departure from HWE in controls were excluded. Furthermore, sensitivity analysis was also applied to evaluate the potential source of heterogeneity of *TGF-β1*-509C/T and codon 25 (Tables S3, S4). After removing a single study at a time under the random-effects model, the positive association between *TGF-β1*-509C/T and the CLD risk was not changed (Table S3). In the current study, we did not observe any publication bias in *TGF-β1*-509C/T and codon 10 (Table 5; Figure 4), confirming our findings that *TGF-β1*-509C/T and codon 10 were positively associated with CLD risk.

Studies have shown that the mRNA and protein levels of TGF-β1 were significantly upregulated in patients with cirrhosis (26, 27), and TGF-β1 expression was higher in tumor tissues of HCC (28–30). Clinic studies revealed that *TGF-β1* gene variants could affect TGF-β1 levels in individuals. For instance, individuals with *TGF-β1*-509C/T or codon 10 showed an increased level of TGF-β1 expression (31–33). However, the underlying mechanism is still unclear. Accordingly, we comprehensively analyzed the *TGF-β1* mRNA levels in different etiologies of CLDs and observed that *TGF-β1* was higher in patients with CHB, AIH, NASH and cirrhosis, compared to healthy controls (Figures 5A-D). Moreover, we integrated the different types of CLDs and validated that *TGF-β1* was significantly upregulated in CLD patients (Figure 5H). Collectively, these results suggested that high *TGF-β1* expression may be a promising biomarker for CLD diagnosis.

The *TGF-β1*-509C/T and -800G/A are located in the promoter region at positions -509 and -800, separately, which might change the transcription of *TGF-β1* by affecting the binding between transcription factors and *TGF-β1*. We explored the potential transcription factors of *TGF-β1* based on publicly available databases and observed three crucial transcription factors of *TGF-β1* (Figure 5M). Studies have reported the binding sites of SP-1 and USF2 in the *TGF-β1* promoter, which did not cover the position of *TGF-β1*-509C/T and -800G/A genetic variants. Based on the current results, transcriptional regulation of SP-1 or USF2 in *TGF-β1* did not affect *TGF-β1* expression associated with *TGF-β1*-509C/T and -800G/A. On the other hand, studies have found that JUN was occupied in the *TGF-β1* promoter, but the binding sites haven't been reported (56). Guess that if we could figure out the vital transcription factors of *TGF-β1* with the binding sites covering -509 or -800 in the *TGF-β1* promoter region, we might uncover the underlying mechanisms by which *TGF-β1*-509C/T and -800G/A affect TGF-β1 levels in patients with CLDs. Nevertheless, our findings could provide an idea of how *TGF-β1* genetic variants in the promoter affect *TGF-β1* expression.

In the endoplasmic reticulum, the pro-domain and GF domain of latent TGF-β1 are covalently linked to form disulfide dimers (57–59). At the same time, the pro-domain binds to the potential TGF-β binding protein to form disulfide connections. And after being released from its latent form, TGF-β1 is secreted and directly interacts with membrane receptors to initiate signal transduction (58, 60). *TGF-β1* codon 10, codon 25, and codon 263 change the amino-acid substitutions, possibly leading to changes in TGF-β1 expression and secretion. We investigated the potential effects of *TGF-β1* codon variants based on the crystal structure of the TGF-β1 protein. The 1-29 of the TGF-β1 domain as a signal peptide hasn't been solved based on experiments. Thus, we can't conclude any useful results for *TGF-β1* codon 10 and codon 25 variants. As shown in Figure 6, codon 263 was located close to where the dimerization of TGF-β1 interacts. Consequently, we had a hypothesis that the *TGF-β1* codon 263 variant may affect the dimerization of TGF-β1 in the endoplasmic reticulum and then change the TGF-β1 secretion, which remains further defined.

Conclusion

Our analysis provides evidence supporting *TGF-β1*-509C/T (rs1800469) and *TGF-β1* codon 10 (rs1800470) as susceptibility factors for CLD occurrence for the first time (Figure 7). *TGF-β1*-509 TT genotype and T allele were correlated with increased CLD risk, specifically with cirrhosis and CHC-induced CLD individuals. The *TGF-β1* codon 10 polymorphism was also correlated with increased CLD susceptibility, playing a more significant role in predicting the occurrence of CHB. Our exploration of the underlying mechanisms by which *TGF-β1* polymorphisms affect CLD risk by regulating TGF-β1 expression would provide a better understanding of the association between the immune regulator and CLD pathogenesis. Notwithstanding the significant findings obtained from the current study, several limitations should still be considered. First, the pathogenesis of CLDs is sophisticated and engages potential interactions between genes and the environment. More studies with sufficient statistics are required for a more thorough assessment. Second, except for etiology, *TGF-β1* polymorphisms on CLD susceptibility could be affected by ethnicity, sex, age, etc. We did not carry out a subgroup analysis to assess these effects on the association between *TGF-β1* polymorphisms and CLD risk. Third, the sample size of our study was relatively small, and we had two studies with NOS scores of 6, which were of intermediate quality. Finally,

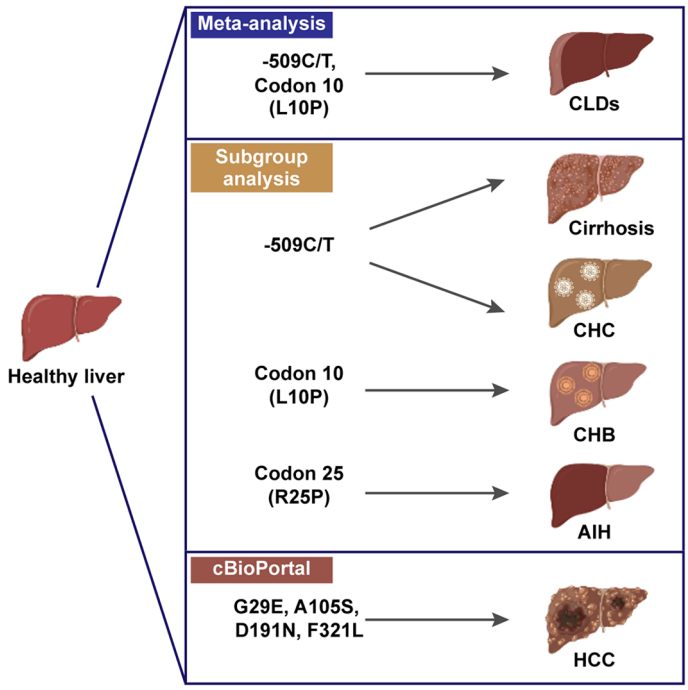

FIGURE 7
Schematic of *TGF-β1* polymorphisms in susceptibility of CLDs, created in BioRender.com.

we did not perform a meta-analysis on *TGF-β1*-800G/A and codon 263 for the small sample size of aggregate analysis. Further investigation should be carried out to verify this relationship and explore other aspects of the CLD risk.

Data availability statement

The original contributions presented in the study are included in the article/Supplementary Material. Further inquiries can be directed to the corresponding authors.

Author contributions

Conceptualization, QW, JW, QH, BY, and XC. methodology, XC, HZ, ZY and YD. software, XC and ZY. validation, HZ, ZY, YD and XD. investigation, XC and ZY. data curation, JW, XC and ZY. writing—original draft preparation, QW, JW and XC. writing—review and editing, QW, JW and XC. All authors contributed to the article and approved the submitted version.

Funding

This research was funded by the Zhejiang Provincial Natural Science Foundation (No. LY22H310001, No. LR21H310001) and the Fundamental Research Funds for the Central Universities.

Conflict of interest

The authors declare that the research was conducted in the absence of any commercial or financial relationships that could be construed as a potential conflict of interest.

Publisher's note

All claims expressed in this article are solely those of the authors and do not necessarily represent those of their affiliated organizations, or those of the publisher, the editors and the reviewers. Any product that may be evaluated in this article, or claim that may be made by its manufacturer, is not guaranteed or endorsed by the publisher.

Supplementary material

The Supplementary Material for this article can be found online at: https://www.frontiersin.org/articles/10.3389/fimmu.2022.1058532/full#supplementary-material

References

1. Marcellin P, Kutala BK. Liver diseases: A major, neglected global public health problem requiring urgent actions and large-scale screening. *Liver Int* (2018) 38:2–6. doi: 10.1111/liv.13682

2. Ramachandran P, Matchett KP, Dobie R, Wilson-Kanamori JR, Henderson NC. Single-cell technologies in hepatology: new insights into liver biology and disease pathogenesis. *Nat Rev Gastroenterol Hepatol* (2020) 17:457–72. doi: 10.1038/s41575-020-0304-x

3. Sepanlou SG, Safiri S, Bisignano C, Ikuta KS, Merat S, Saberifiroozi M, et al. The global, regional, and national burden of cirrhosis by cause in 195 countries and territories, 1990-2017: a systematic analysis for the global burden of disease study 2017. *Lancet Gastroenterol* (2020) 5:245–66. doi: 10.1016/S2468-1253(19)30349-8

4. Purohit V, Brenner DA. Mechanisms of alcohol-induced hepatic fibrosis: A summary of the Ron Thurman symposium. *Hepatology* (2006) 43:872–8. doi: 10.1002/hep.21107

5. Kim YJ, Lee HS. Single nucleotide polymorphisms associated with hepatocellular carcinoma in patients with chronic hepatitis b virus infection. *Intervirology* (2005) 48:10–5. doi: 10.1159/000082089

6. Han ZG. Functional genomic studies: Insights into the pathogenesis of liver cancer. *Annu Rev Genom Hum G* (2012) 13:171–205. doi: 10.1146/annurev-genom-090711-163752

7. Batlle E, Massague J. Transforming growth factor-beta signaling in immunity and cancer. *Immunity* (2019) 50:924–40. doi: 10.1016/j.immuni.2019.03.024

8. Matsuzaki K, Seki T, Okazaki K. TGF-beta signal shifting between tumor suppression and fibro-carcinogenesis in human chronic liver diseases. *J Gastroenterol* (2014) 49:971–81. doi: 10.1007/s00535-013-0910-2

9. Gough NR, Xiang XY, Mishra L. TGF-beta signaling in liver, pancreas, and gastrointestinal diseases and cancer. *Gastroenterology* (2021) 161:434–+. doi: 10.1053/j.gastro.2021.04.064

10. Larson C, Oronsky B, Carter CA, Oronsky A, Knox SJ, Sher D, et al. TGF-beta: a master immune regulator. *Expert Opin Ther Targets* (2020) 24:427–38. doi: 10.1080/14728222.2020.1744568

11. Gomes AL, Teijeiro A, Buren S, Tummala KS, Yilmaz M, Waisman A, et al. Metabolic inflammation-associated IL-17A causes non-alcoholic steatohepatitis and hepatocellular carcinoma. *Cancer Cell* (2016) 30:161–75. doi: 10.1016/j.ccell.2016.05.020

12. Chen J, Gingold JA, Su X. Immunomodulatory TGF-beta signaling in hepatocellular carcinoma. *Trends Mol Med* (2019) 25:1010–23. doi: 10.1016/j.molmed.2019.06.007

13. Paquissi FC. Immunity and fibrogenesis: The role of Th17/IL-17 axis in HBV and HCV-induced chronic hepatitis and progression to cirrhosis. *Front Immunol* (2017) 8. doi: 10.3389/fimmu.2017.01195

14. Li N, Yamamoto G, Fuji H, Kisseleva T. Interleukin-17 in liver disease pathogenesis. *Semin Liver Dis* (2021) 41:507–15. doi: 10.1055/s-0041-1730926

15. Karimi-Googheri M, Daneshvar H, Nosratabadi R, Zare-Bidaki M, Hassanshahi G, Ebrahim M, et al. Important roles played by TGF-beta in hepatitis b infection. *J Med Virol* (2014) 86:102–8. doi: 10.1002/jmv.23727

16. Tsuchida T, Friedman SL. Mechanisms of hepatic stellate cell activation. *Nat Rev Gastroenterol Hepatol* (2017) 14:397–411. doi: 10.1038/nrgastro.2017.38

17. Cai XY, Wang JJ, Wang JC, Zhou Q, Yang B, He QJ, et al. Intercellular crosstalk of hepatic stellate cells in liver fibrosis: New insights into therapy. *Pharmacol Res* (2020) 155:104720. doi: 10.1016/j.phrs.2020.104720

18. Kisseleva T, Brenner D. Molecular and cellular mechanisms of liver fibrosis and its regression. *Nat Rev Gastroenterol Hepatol* (2021) 18:151–66. doi: 10.1038/s41575-020-00372-7

19. Xiang TX, Cheng N, Li XN, Wu XP. Association between transforming growth factor-beta 1 polymorphisms and hepatocellular cancer risk: A meta-analysis. *Hepatol Res* (2012) 42:583–90. doi: 10.1111/j.1872-034X.2011.00958.x

20. Guo Y, Zang CB, Li YJ, Yuan L, Liu QJ, Zhang LY, et al. Association between TGF-beta 1 polymorphisms and hepatocellular carcinoma risk: A meta-analysis. *Genet Test Mol Bioma* (2013) 17:814–20. doi: 10.1089/gtmb.2013.0268

21. Wu XD, Zeng K, Gong CS, Chen JH, Chen YQ. Transforming growth factor-beta genetic polymorphisms on development of liver cirrhosis in a meta-analysis. *Mol Biol Rep* (2013) 40:535–43. doi: 10.1007/s11033-012-2090-1

22. Lu WQ, Qiu JL, Huang ZL, Liu HY. Enhanced circulating transforming growth factor beta 1 is causally associated with an increased risk of hepatocellular carcinoma: a mendelian randomization meta-analysis. *Oncotarget* (2016) 7:84695–704. doi: 10.18632/oncotarget.13218

23. Toshikuni N, Matsue Y, Minato T, Hayashi N, Tsuchishima M, Tsutsumi M. Association between transforming growth factor-beta 1-509 c > T variants and hepatocellular carcinoma susceptibility: A meta-analysis. *J Gastroen Hepatol* (2016) 31:423–3. doi: 10.4149/neo_2016_615

24. Guo P, Sun X, Feng X, Zhang C. Transforming growth factor-beta1 gene polymorphisms with liver cirrhosis risk: A meta-analysis. *Infect Genet Evol* (2018) 58:164–70. doi: 10.1016/j.meegid.2017.12.019

25. Zhang C, Ye Z, Zhang Z, Zheng J, Tang Y, Hou E, et al. A comprehensive evaluation of single nucleotide polymorphisms associated with hepatocellular carcinoma risk in Asian populations: A systematic review and network meta-analysis. *Gene* (2020) 735:144365. doi: 10.1016/j.gene.2020.144365

26. Gabriel A, Ziolkowski A, Radlowski P, Tomaszek K, Dziambor A. Hepatocyte steatosis in HCV patients promotes fibrosis by enhancing TGF-beta liver expression. *Hepatol Res* (2008) 38:141–6. 10.1111/j.1872-034X.2007.00258.x

27. Mohagheghi S, Geramizadeh B, Nikeghbalian S, Khodadadi I, Karimi J, Khajehahmadi Z, et al. Intricate role of yes-associated protein1 in human liver cirrhosis: TGF-beta1 still is a giant player. *IUBMB Life* (2019) 71:1453–64. doi: 10.1002/iub.2052

28. Wang B, Liu T, Wu JC, Lou SZ, Chen R, Lu LG, et al. STAT3 aggravates TGF-beta1-induced hepatic epithelial-to-mesenchymal transition and migration. *BioMed Pharmacother* (2018) 98:214–21. doi: 10.1016/j.biopha.2017.12.035

29. Peng L, Yuan XQ, Zhang CY, Ye F, Zhou HF, Li WL, et al. High TGF-beta1 expression predicts poor disease prognosis in hepatocellular carcinoma patients. *Oncotarget* (2017) 8:34387–97. doi: 10.18632/oncotarget.16166

30. Ning J, Ye Y, Bu D, Zhao G, Song T, Liu P, et al. Imbalance of TGF-beta1/BMP-7 pathways induced by M2-polarized macrophages promotes hepatocellular carcinoma aggressiveness. *Mol Ther* (2021) 29:2067–87. doi: 10.1016/j.ymthe.2021.02.016

31. Grainger DJ, Heathcote K, Chiano M, Snieder H, Kemp PR, Metcalfe JC, et al. Genetic control of the circulating concentration of transforming growth factor type beta1. *Hum Mol Genet* (1999) 8:93–7. doi: 10.1093/hmg/8.1.93

32. Dunning AM, Ellis PD, McBride S, Kirschenlohr HL, Healey CS, Kemp PR, et al. A transforming growth factor beta 1 signal peptide variant increases secretion *in vitro* and is associated with increased incidence of invasive breast cancer. *Cancer Res* (2003) 63:2610–5.

33. Taubenschuss E, Marton E, Mogg M, Frech B, Ehart L, Muin D, et al. The L10P polymorphism and serum levels of transforming growth factor beta1 in human breast cancer. *Int J Mol Sci* (2013) 14:15376–85. doi: 10.3390/ijms140815376

34. Moher D, Liberati A, Tetzlaff J, Altman DG, Grp P. Preferred reporting items for systematic reviews and meta-analyses: The PRISMA statement. *J Clin Epidemiol* (2009) 62:1006–12. doi: 10.1016/j.jclinepi.2009.06.005

35. GA Wells BS, O'Connell D, Peterson J, Welch V, Losos PT M, et al. The Newcastle-Ottawa Scale (NOS) for assessing the quality of nonrandomised studies in meta-analyses. (2011). Availabe at: http://www.ohri.ca/programs/clinical_epidemiology/oxford.asp.

36. Gao JJ, Aksoy BA, Dogrusoz U, Dresdner G, Gross B, Sumer SO, et al. Integrative analysis of complex cancer genomics and clinical profiles using the cBioPortal. *Sci Signal* (2013) 6:pl1. doi: 10.1126/scisignal.2004088

37. Ramachandran P, Dobie R, Wilson-Kanamori JR, Dora EF, Henderson BEP, Luu NT, et al. Resolving the fibrotic niche of human liver cirrhosis at single-cell level. *Nature* (2019) 575:512–8. doi: 10.1038/s41586-019-1631-3

38. Aran D, Looney AP, Liu L, Wu E, Fong V, Hsu A, et al. Reference-based analysis of lung single-cell sequencing reveals a transitional profibrotic macrophage. *Nat Immunol* (2019) 20:163–72. doi: 10.1038/s41590-018-0276-y

39. Ko J, Park H, Heo L, Seok C. GalaxyWEB server for protein structure prediction and refinement. *Nucleic Acids Res* (2012) 40:W294–297. doi: 10.1093/nar/gks493

40. Baek M, Park T, Heo L, Park C, Seok C. GalaxyHomomer: a web server for protein homo-oligomer structure prediction from a monomer sequence or structure. *Nucleic Acids Res* (2017) 45:W320–4. doi: 10.1093/nar/gkx246

41. Higgins JP, Thompson SG, Deeks JJ, Altman DG. Measuring inconsistency in meta-analyses. *BMJ* (2003) 327:557–60. doi: 10.1136/bmj.327.7414.557

42. Begg CB, Mazumdar M. Operating characteristics of a rank correlation test for publication bias. *Biometrics* (1994) 50:1088–101. doi: 10.2307/2533446

43. Egger M, Davey Smith G, Schneider M, Minder C. Bias in meta-analysis detected by a simple, graphical test. *BMJ* (1997) 315:629–34. doi: 10.1136/bmj.315.7109.629

44. Shih SC, Claffey KP. Role of AP-1 and HIF-1 transcription factors in TGF-beta activation of VEGF expression. *Growth Factors* (2001) 19:19–34. doi: 10.3109/08977190109001073

45. Martin-Gallausiaux C, Beguet-Crespel F, Marinelli L, Jamet A, Ledue F, Blottiere HM, et al. Butyrate produced by gut commensal bacteria activates TGF-

beta1 expression through the transcription factor SP1 in human intestinal epithelial cells. *Sci Rep-Uk* (2018) 8:9742. doi: 10.1038/s41598-018-28048-y

46. Datto MB, Li JM, Shen X, Hu PP, Yu Y, Wang XF. Sp1, but not Sp3, functions to mediate promoter activation by TGF-beta through canonical Sp1 binding sites. *Nucleic Acids Res* (1998) 26:2449–56. doi: 10.1093/nar/26.10.2449

47. Chen H, Zhou Y, Chen KQ, An G, Ji SY, Chen QK, et al. Anti-fibrotic effects *via* regulation of transcription factor Sp1 on hepatic stellate cells. *Cell Physiol Biochem* (2012) 29:51–60. doi: 10.1159/000337586

48. Littlewood TD, Evan GI. Transcription factors 2: helix-loop-helix. *Protein Profile* (1995) 2:621–702.

49. Zhu Y, Casado M, Vaulont S, Sharma K. Role of upstream stimulatory factors in regulation of renal transforming growth factor-beta1. *Diabetes* (2005) 54:1976–84. doi: 10.2337/diabetes.54.7.1976

50. Wang SX, Skorczewski J, Feng X, Mei L, Murphy-Ullrich JE. Glucose up-regulates thrombospondin 1 gene transcription and transforming growth factor-beta activity through antagonism of cGMP-dependent protein kinase repression via upstream stimulatory factor 2. *J Biol Chem* (2004) 279:34311–22. doi: 10.1074/jbc.M401629200

51. Weigert C, Brodbeck K, Sawadogo M, Haring HU, Schleicher ED. Upstream stimulatory factor (USF) proteins induce human TGF-beta 1 gene activation via the glucose-response element-1013/-1002 in mesangial cells - up-regulation of USF activity by the hexosamine biosynthetic pathway. *J Biol Chem* (2004) 279:15908–15. doi: 10.1074/jbc.M313524200

52. Kim KS, Jung HS, Chung YJ, Jung TS, Jang HW, Lee MS, et al. Overexpression of USF increases TGF-beta1 protein levels, but G1 phase arrest was not induced in FRTL-5 cells. *J Korean Med Sci* (2008) 23:870–6. doi: 10.3346/jkms.2008.23.5.870

53. Qing J, Zhang Y, Derynck R. Structural and functional characterization of the transforming growth factor-beta -induced Smad3/c-jun transcriptional cooperativity. *J Biol Chem* (2000) 275:38802–12. doi: 10.1074/jbc.M004731200

54. Thakur N, Hamidi A, Song J, Itoh S, Bergh A, Heldin CH, et al. Smad7 enhances TGF-beta-Induced transcription of c-jun and HDAC6 promoting invasion of prostate cancer cells. *iScience* (2020) 23:101470. doi: 10.1016/j.isci.2020.101470

55. Liu F, Shang YX. Sirtuin 6 attenuates epithelial-mesenchymal transition by suppressing the TGF-beta1/Smad3 pathway and c-jun in asthma models. *Int Immunopharmacol* (2020) 82:106333. doi: 10.1016/j.intimp.2020.106333

56. Yue J, Mulder KM. Requirement of Ras/MAPK pathway activation by transforming growth factor beta for transforming growth factor beta 1 production in a smad-dependent pathway. *J Biol Chem* (2000) 275:35656. doi: 10.1016/S0021-9258(20)88877-2

57. Shi M, Zhu J, Wang R, Chen X, Mi L, Waltz T, et al. Latent TGF-beta structure and activation. *Nature* (2011) 474:343–9. doi: 10.1038/nature10152

58. Hinck AP, Mueller TD, Springer TA. Structural biology and evolution of the TGF-beta family. *Cold Spring Harb Perspect Biol* (2016) 8:a022103. doi: 10.1101/cshperspect.a022103

59. ten Dijke P, Arthur HM. Extracellular control of TGFbeta signalling in vascular development and disease. *Nat Rev Mol Cell Biol* (2007) 8:857–69. doi: 10.1038/nrm2262

60. Tzavlaki K, Moustakas A. TGF-beta signaling. *Biomolecules* (2020) 10.

61. Xu LX, He MH, Dai ZH, Yu J, Wang JG, Li XC, et al. Genomic and transcriptional heterogeneity of multifocal hepatocellular carcinoma. *Ann Oncol* (2019) 30:990–7. doi: 10.1093/annonc/mdz103

62. Moretti S, Pinzi C, Berti E, Spallanzani A, Chiarugi A, Boddi V, et al. *In situ* expression of transforming growth factor beta is associated with melanoma progression and correlates with Ki67, HLA-DR and beta 3 integrin expression. *Melanoma Res* (1997) 7:313–21. doi: 10.1097/00008390-199708000-00006

63. Vousden KH, Prives C. Blinded by the light: The growing complexity of p53. *Cell* (2009) 137:413–31. doi: 10.1016/j.cell.2009.04.037

64. Morris SM, Baek JY, Koszarek A, Kanngurn S, Knoblaugh SE, Grady WM, et al. Transforming growth factor-beta signaling promotes hepatocarcinogenesis induced by p53 loss. *Hepatology* (2012) 55:121–31. doi: 10.1002/hep.24653

frontiers | Frontiers in Immunology

TYPE Original Research
PUBLISHED 07 December 2022
DOI 10.3389/fimmu.2022.1069196

OPEN ACCESS

EDITED BY
Yanbo Wang,
Nanjing University, China

REVIEWED BY
Qinghai Zeng,
Central South University, China
Ya-fei Qin,
Tianjin Medical University General Hospital, China

*CORRESPONDENCE
Shuli Li
lishli@fmmu.edu.cn
Chunying Li
lichying@fmmu.edu.cn

†These authors have contributed equally to this work and share first authorship

SPECIALTY SECTION
This article was submitted to Cytokines and Soluble Mediators in Immunity, a section of the journal Frontiers in Immunology

RECEIVED 13 October 2022
ACCEPTED 21 November 2022
PUBLISHED 07 December 2022

CITATION
He K, Wu W, Wang X, Dai W, Wang S, Li C and Li S (2022) Circulatory levels of alarmins in patients with non-segmental vitiligo: Potential biomarkers for disease diagnosis and activity/severity assessment. *Front. Immunol.* 13:1069196. doi: 10.3389/fimmu.2022.1069196

Circulatory levels of alarmins in patients with non-segmental vitiligo: Potential biomarkers for disease diagnosis and activity/severity assessment

Kaiqiao He[1†], Wei Wu[1†], Xinju Wang[1], Wei Dai[2], Sijia Wang[2], Chunying Li[1*] and Shuli Li[1*]

[1]Department of Dermatology, Xijing Hospital, Fourth Military Medical University, Xi'an, China, [2]Department of Dermatology and Venereology, Nanfang Hospital, Southern Medical University, Guangzhou, China

Background: Non-segmental vitiligo (NSV) is an autoimmune skin disorder that is difficult to determine disease activity/severity and thus to treat. Alarmins have emerged as promising biomarkers in various diseases, so further confirmation of their potential roles in NSV would be of considerable value. With the present work, we aimed to determine the serum levels of alarmins in patients with NSV, correlate these alarmins with disease activity and severity, and analyze the predictive value of the combination of these markers.

Methods: 104 NSV patients and 56 healthy controls were enrolled at the Xijing Hospital of Fourth Military Medical University between September 1, 2018, and June 30, 2019. The serum levels of alarmins (including IL-33, IL-1α, S100A9, S100A12, S100B, and HMGB1) were measured with enzyme-linked immunosorbent assays. The predictive performance of these biomarkers was evaluated with the area under the receiver operating characteristic curve (AUC), sensitivity, specificity, and other representative statistics.

Results: A total of 104 patients with NSV (mean [SD] age, 34.2 [13.0] years; 62 [59.6%] male) and 56 healthy controls (mean [SD] age, 34.8 [13.5] years; 34 [60.7%] male) were enrolled. For vitiligo diagnosis, S100B had the highest sensitivity (92.31%), whereas HMGB1 had the highest specificity (85.71%); the combination of IL-1α, S100B, S100A9, and HMGB1 increased the AUC value to 0.925, with a sensitivity of 87.50% and a specificity of 85.71%. Multivariate logistic regression analysis showed S100B (OR, 1.019; 95% CI, 1.002-1.038; P =0.03), S100A9 (OR, 1.002; 95% CI, 1.001-1.003; P<0.001), and HMGB1 (OR, 1.915; 95% CI, 1.186-3.091; P =0.008) were significantly associated with vitiligo activity. S100A9 had the highest accuracy in discriminating patients at the active stage from the stable stage, with an AUC value of 0.827. The combination of these alarmins had an AUC value of 0.860 to assess disease activity, with a sensitivity of 90.00% and a specificity of 72.97%. Furthermore, S100B (r=0.61, P <0.001),

S100A9 (r=0.33, P <0.001), and HMGB1 (r = 0.51, P <0.001) levels were positively correlated with the affected body surface area (BSA) in NSV patients.

Conclusions: Serum S100B, S100A9, and HMGB1 might be biomarkers for diagnosing and assessing the activity/severity of NSV, either used alone or in combination.

KEYWORDS

vitiligo, alarmins, biomarkers, diagnose, disease activity, disease severity

Introduction

Vitiligo is a common depigmented skin disease with a worldwide prevalence of 0.5%-2% (1, 2). It can be classified into two major forms: non-segmental vitiligo (NSV, also known as vitiligo) and segmental vitiligo (SV). SV only accounts for 5% to 16% of all vitiligo cases and is characterized by sudden onset with rapid stabilization, whereas NSV is the most common form with unpredictable course, which brings patients significant psychosocial and economic detriment (3, 4). The burden imposed by vitiligo is further exacerbated by a lack of objective methods to gauge the activity and severity of the disease and subsequently a belated or imprecise management. Clinically, the diagnosis and assessment of vitiligo are highly dependent on the physician's subjective judgment, which mainly rely on cutaneous symptoms like the trichrome sign, confetti-like depigmentation, and the Koebner phenomenon (5). However, cutaneous symptoms cannot be recognized in all patients and are always imperceptible at the onset, making it imperative to establish biomarkers that may be detected early and reliably assess the disease status. Recent studies have discovered several serum biomarkers for vitiligo, including sCD25 and sCD27 (6). The use of such serum markers for vitiligo assessment would help guide better management.

Alarmins are endogenous, constitutively expressed, chemotactic, and immune-activating proteins/peptides. They have been thought to be initiators of both innate and adaptive immunity, as well as influencing the types of adaptive immune responses (7, 8). In response to cell injury or death, alarmins are released to galvanize immune cells both in host defense and disease (9). Increasing studies have discovered that alarmins could also serve as biomarkers for the diagnosis, prognosis, and treatment response in several autoimmune diseases, including rheumatoid arthritis, systemic lupus erythematosus, and psoriatic arthritis (10–12). Among these alarmins, HMGB1 and S100B have been reported to be involved in the pathogenesis of vitiligo and could even serve as potential therapeutic targets for vitiligo (13, 14). The serum concentrations of IL-1α and IL-33 were reported higher in vitiligo patients than that in healthy subjects (15, 16). S100A9 and S100A12, the two alarmins are prone to rise after oxidative stress which is an important inducer for vitiligo initiation, and then involved in the aberrant immune response (17, 18). Therefore, in this study we would like to detect the serum expression of these above alarmins (HMGB1, S100B, IL-1α, IL-33, S100A9, and S100A12) in NSV patients and healthy controls, to further investigate their clinical significance in the diagnosis and assessment of disease activity/severity in vitiligo.

Materials and methods

Participants

In this cross-sectional study, one hundred and four patients with NSV were enrolled at the Department of Dermatology, Xijing Hospital of Fourth Military Medical University between September 1, 2018, and June 30, 2019. Exclusion criteria included a diagnosis of other autoimmune diseases aside from vitiligo, and with any immunosuppressive or narrow band Ultra Violet B (NB-UVB) therapy within 6 weeks before enrollment to the study. In addition, fifty-six age and sex-matched healthy controls were recruited from the physical examination. None of the healthy subjects had a personal history of autoimmune disorder or any previous treatment influencing inflammatory response. Written informed consent was obtained from each patient and healthy control before the study. The study was designed and executed according to the principles of the Declaration of Helsinki and approved by the ethics committee of Xijing Hospital of Fourth Military Medical University.

Assessment of vitiligo disease activity

Disease activity was assessed by three dermatologists according to "Diagnosis and treatment of vitiligo: an expert

consensus statement (2018)" published in Chinese Journal of Dermatology and classified into three categories: stable, mild-moderate active, and very active (19).

Stable vitiligo may be determined if at least two items were identified: VIDA score ≤ 0; clinical feature of lesions with clear edges or signs of repigmentation; no Koebner phenomenon within 1 year; white lesion with sharply clear borders, smaller than or equal to the visual area under Wood's light.

Any one of the following four characteristics might indicate active vitiligo: VIDA score 1 to 4; clinical features, including poorly defined borders and inflammatory signs (such as trichromatic vitiligo, confetti-like depigmentation, and hypopigmentation); Koebner phenomenon in the past 1 year; In the Wood's light examination, poorly demarcated borders associated with hypomelanotic edging or larger hypochromia area than the visual area. Among active vitiligo, mild-moderate active vitiligo was scored with VIDA score 1 to 3, and very active vitiligo in patients with VIDA score equal to 4 or obvious clinical markers.

Assessment of vitiligo disease severity

Disease severity was assessed based on the affected body surface area (BSA) and evaluated by three experts independently. One hand unit is about 1% of the BSA; one finger unit accounts for 0.1% of the BSA; one fingertip unit is equal to 0.03% of the BSA approximately. The final BSA values were averaged among the experts.

Blood samples collection and laboratory measurements

The samples of peripheral blood from patients with NSV and healthy controls were collected, and the serum was isolated by centrifugation for 5 minutes at 1000×g. After that, samples were stored under -80°C until analysis. Repeated thawing and freezing were avoided. Commercial enzyme-linked immunosorbent assays (ELISA) were used to measure the serum level of IL-33, IL-1α, S100A12 (Beijing 4A Biotech Co., Ltd), S100A9, S100B (R&D Systems), and HMGB1 (IBL, Japan).

Statistical analysis

Statistical analysis was conducted using SPSS, version 26 (IBM Corporation), and GraphPad Prism, version 9 (GraphPad Software). Continuous variables were expressed as mean (SD) or median (interquartile range) and discrete variables were expressed as percentage distributions. Two independent samples t-test and chi-square test were used to compare the differences between NSV and healthy controls. Mann-Whitney U test and Kruskal-Wallis H test were used to compare the differences between two or more than two groups. The receiver operating characteristic curve was used to investigate the sensitivity and specificity of alarmins as biomarkers. Adjustment of possible confounding factors was performed using multivariate logistic regression. For correlation analysis, Pearson correlation analyses were performed. In all cases, $P<0.05$ was considered statistically significant.

Results

Clinical characteristics of the participants

A total of 104 patients with NSV (mean [SD] age, 34.2 [13.0] years; 62 [59.6%] male) and 56 healthy controls (mean [SD] age, 34.8 [13.5] years; 34 [60.7%] male) were included in the study. Subjects were well-matched for age and sex. In addition, 30 of 104 patients (28.8%) had stable vitiligo, 37 of 104 patients (35.6%) had mild-moderate active vitiligo, and the 37 remaining patients (35.6%) had very active vitiligo (Table 1).

Serum levels of IL-1α, S100B, S100A9, and HMGB1 are increased in patients with NSV

Regarding the expression of alarmins, serum levels of IL-1α, S100B, S100A9, and HMGB1 were significantly elevated in patients with NSV compared with healthy controls, whereas the expression of IL-33 and S100A12 showed no change (Table 1). The ROC curve analysis for identifying disease diagnostic value was significant for IL-1α, S100B, S100A9, and HMGB1, with AUC values of 0.784, 0.723, 0.750, and 0.800, respectively. Among these alarmins, S100B had the highest sensitivity of 92.31% and HMGB1 had the highest specificity of 85.71%. The diagnosis accuracy for each combination of IL-1α, S100B, S100A9, and HMGB1 was also carried out. When the four biomarkers were combined, the AUC value was 0.925, with a sensitivity of 87.50% and a specificity of 85.71%, which was superior to using any biomarker alone or any kind of combination (Table 2, Figure 1).

Serum levels of S100B, S100A9, and HMGB1 are increased in active patients with NSV

In terms of disease activity evaluated by physicians, we found that the serum levels of S100A12, S100B, S100A9, and HMGB1 in patients with very active vitiligo were significantly higher than those in patients in stable phase (S100A12, $P=0.046$; S100B, $P=0.018$; S100A9, $P<0.001$; HMGB1, $P<0.001$). In

TABLE 1 Baseline demographics and clinical characteristics.

Characteristics	Patients with NSV (n=104)	Controls (n=56)	*P*-value
Age (years), mean (SD)	34.2 (13.0)	34.8 (13.5)	0.76[a]
Sex, n (%)			0.89[b]
Female	42 (40.4%)	22 (39.3)	NA
Male	62 (59.6%)	34 (60.7)	NA
Age at disease onset (years), mean (SD)	24.5 (13.0)	NA	NA
Disease duration (months), median (IQR)	72 (36-165)	NA	NA
Activity, n (%)		NA	NA
Stable	30 (28.8%)	NA	NA
Mild-moderate active	37 (35.6%)	NA	NA
Very active	37 (35.6%)	NA	NA
Affected BSA (%), median (IQR)	6 (2-25.9)	NA	NA
Serum alarmins, median (IQR)	NA	NA	NA
IL-33, pg/ml	19.0 (16.0-25.7)	19.0 (15.7-27.3)	0.818[c]
IL-1α, pg/ml	6.7 (5.5-9.7)	4.9 (4.3-5.6)	**<0.001**[c]
S100A12, ng/ml	9.4 (8.5-10.3)	8.8 (7.4-10.4)	0.109[c]
S100B, pg/ml	31.3 (20.8-47.2)	19.9 (7.5-30.9)	**<0.001**[c]
S100A9, ng/ml	1171.4 (790.1-1690.3)	623.7 (396.8-1169.7)	**<0.001**[c]
HMGB1, ng/ml	1.5 (0.9-2.0)	0.8 (0.5-1.1)	**<0.001**[c]

BSA, body surface area; SD, standard deviation; IQR, interquartile range; NA, not applicable.
[a]P value was calculated by Independent samples t-test.
[b]P value was calculated by Chi-square test.
[c]P value was calculated by Mann-Whitney U test p-value <0.05 was represented in bold.

addition, patients in mild-moderate phase had higher levels of S100B and S100A9 than those in stable phase (S100B, P =0.025; S100A9, P<0.001). However, no obvious difference was observed between patients in mild-moderate active phase and very active phase (Figure 2). To further eliminate the impact of confounding factors on our results, including age, age at disease onset, and disease duration, we conducted multivariate logistic regression. Our results showed that the serum levels of S100B (OR, 1.019; 95% CI, 1.002-1.038; P =0.03), S100A9 (OR, 1.002; 95% CI, 1.001-1.003; P<0.001), and HMGB1 (OR, 1.915; 95% CI, 1.186-3.091; P =0.008) were significantly associated with disease activity (Table 3).

We then found that the ROC curve analysis for assessing disease activity was significant for S100B, S100A9, and HMGB1,

TABLE 2 Diagnostic values of biomarkers in patients with NSV.

Alarmins	Cut-off value	AUC (95%CI)	Sensitivity, %	Specificity, %	PPV, %	NPV, %
IL-1α, pg/ml	5.647	0.784 (0.711,0.857)	73.08	80.36	87.36	61.65
S100B, pg/ml	15.32	0.723 (0.640,0.806)	92.31	42.86	75.0	75.01
S100A9, ng/ml	628.544	0.750 (0.673,0.828)	85.58	53.57	77.39	66.67
HMGB1, ng/ml	1.227	0.800 (0.733,0.867)	61.54	85.71	88.89	54.55
IL-1α+S100B		0.823 (0.758,0.888)	75.96	76.77	85.86	63.23
IL-1α+S100A9		0.848 (0.787,0.908)	88.46	67.86	83.64	76.00
IL-1α+HMGB1		0.890 (0.841,0.939)	78.85	85.71	91.11	68.57
S100B+S100A9		0.805 (0.739,0.871)	59.62	94.64	95.38	55.79
S100B+HMGB1		0.848 (0.789,0.907)	62.50	92.86	94.21	57.14
S100A9+HMGB1		0.863 (0.808,0.918)	69.23	89.29	92.31	60.98
IL-1α+S100B+S100A9		0.864 (0.808,0.919)	71.15	85.71	90.24	61.53
IL-1α+S100B+HMGB1		0.900 (0.854,0.947)	84.62	80.36	88.89	73.78
S100B+S100A9+HMGB1		0.884 (0.834,0.934)	77.88	87.50	92.05	68.05
all combined		0.925 (0.886,0.965)	87.50	85.71	91.92	78.69

AUC, area under the curve; PPV, positive predictive value; NPV, negative predictive value.
The diagnostic cut-off value corresponds to the maximum point of the Youden index.
The all combined represents the combination of IL-1α, S100B, S100A9, and HMGB1.

10.3389/fimmu.2022.1069196

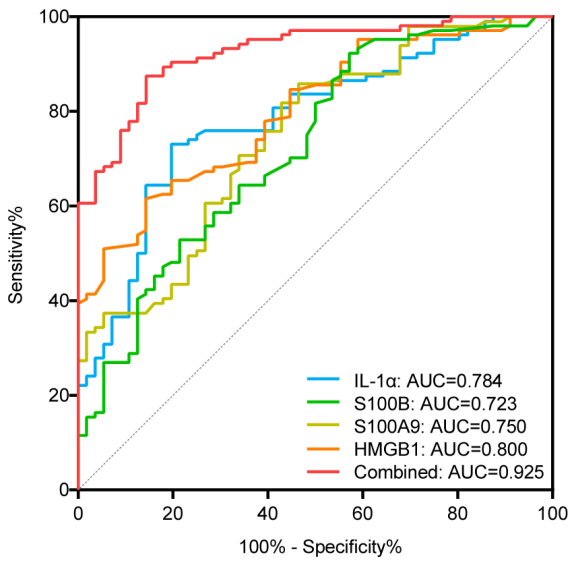

FIGURE 1
ROC curves of IL-1α, S100B, S100A9, and HMGB1 for diagnosing vitiligo. AUC indicates the area under the receiver operating characteristic curve. The blue, green, yellow, orange curve represents the ROC curve of IL-α, S100B, S100A9, and HMGB1, respectively; the red curve represents the ROC curve of the combination of IL-1α, S100B, S100A9, and HMGB1.

with AUC values of 0.691, 0.827, and 0.646, respectively. Importantly, the AUC value increased to 0.860 when the three alarmins mentioned above were combined, with a sensitivity of 90.00% and a specificity of 72.97% (Figure 3, Table 4). Although the diagnostic value of the combined model has a superimposed effect, the difference in actual values of S100A9 between the active and stable vitiligo patients is remarkable, indicating that the assessment of vitiligo activity based on the model with only one predictor is promising.

Serum levels of S100B, S100A9, and HMGB1 correlate with the affected body surface area in patients with NSV

We found that the serum levels of S100B, S100A9, and HMGB1 were positively correlated with increased BSA in NSV patients (r=0.61, P <0.001; r=0.33, P <0.001; r = 0.51, P <0.001, respectively) (Figure 4A). The heatmap also showed that the disease activity and severity of vitiligo were significantly correlated. Thus, we explored the association between S100B, S100A9, and HMGB1 and vitiligo severity in various disease activity phases (Figures 4B–G). The findings demonstrated that although S100B was only correlated with the affected BSA in active vitiligo (r =0.60, P <0.001) (Figures 4B, E), HMGB1 was

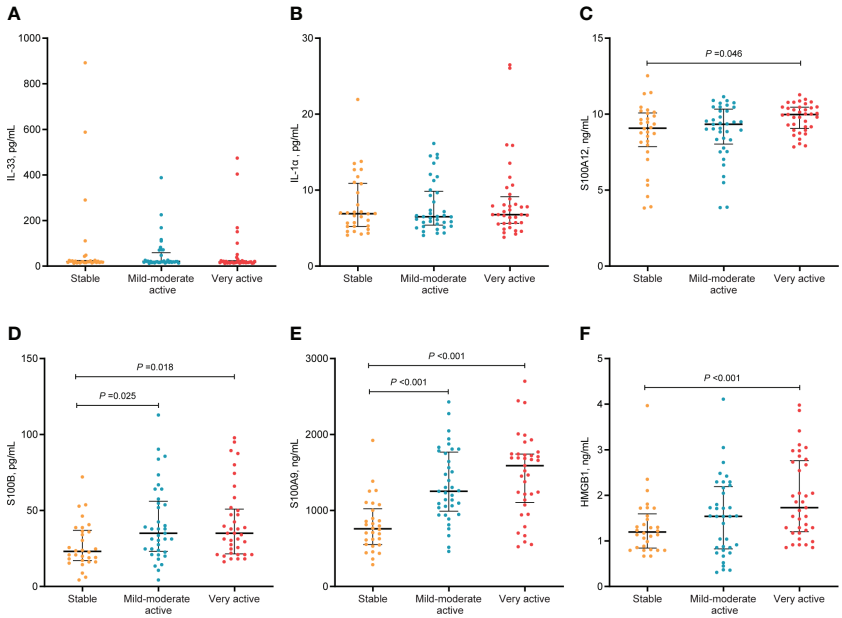

FIGURE 2
Serum levels of alarmins in different activity stage in patients with NSV. The median and IQR were represented by the middle black line, and the lower and upper black lines, respectively. Serum levels of IL-33 **(A)**, IL-α **(B)**, S100A12 **(C)**, S100B **(D)**, S100A9 **(E)**, HMGB1 **(F)** in patients with NSV at stable, mild-moderate active, and very active stage.

10.3389/fimmu.2022.1069196

TABLE 3 Multivariate models investigating the association of S100A12, S100B, S100A9, HMGB1, and disease activity.

Independent variable	Coefficient	Wald test	OR (95% CI)	*P*-value
Model 1				
Age	1.414	2.065	4.111 (0.598, 28.272)	0.15
Disease duration	-0.112	1.884	0.894 (0.763, 1.049)	0.17
Age at disease onset	-1.393	2.003	0.248 (0.036, 1.710)	0.16
S100A12	0.214	3.458	1.238 (0.989, 1.550)	0.06
Model 2				
Age	1.577	2.592	4.840 (0.710, 33.007)	0.11
Disease duration	-0.124	2.364	0.883 (0.753, 1.035)	0.12
Age at disease onset	-1.556	2.521	0.211 (0.031, 1.440)	0.11
S100B	0.019	4.652	1.019 (1.002, 1.038)	**0.03**
Model 3				
Age	1.640	2.441	5.156 (0.659, 40.347)	0.12
Disease duration	-0.130	2.234	0.878 (0.741, 1.041)	0.14
Age at disease onset	-1.620	2.377	0.198 (0.025,1.552)	0.12
S100A9	0.002	21.816	1.002 (1.001,1.003)	**<0.001**
Model 4				
Age	1.280	1.721	3.598 (0.531, 24.364)	0.19
Disease duration	-0.100	1.535	0.905 (0.773, 1.060)	0.22
Age at disease onset	-1.264	1.674	0.283 (0.042, 1.917)	0.20
HMGB1	0.650	7.063	1.915 (1.186, 3.091)	**0.008**

OR, odds ratio.
p-value <0.05 was represented in bold.

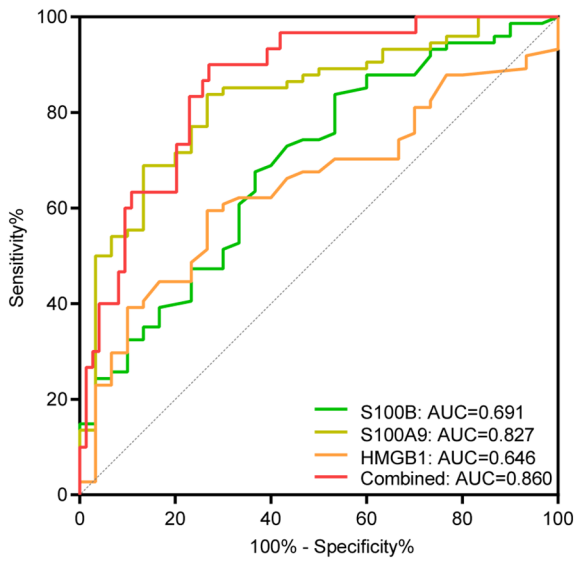

FIGURE 3
ROC curve analysis of S100B, S100A9, and HMGB1 for assessing disease activity. AUC indicates the area under the receiver operating characteristic curve. The green, yellow, and orange curve represents the ROC curve of S100B, S100A9 and HMGB1, respectively; the red curve represents the ROC curve of the combination of S100B, S100A9, and HMGB1.

associated with the vitiligo severity in both the stable and active stages (stable phase, r=0.60, P <0.001; active phase, r=0.50, P <0.001) (Figures 4D, G). However, no correlation was shown between affected BSA and S100A9 serum levels in patients with active and stable vitiligo (Figures 4C, F).

Discussion

In the current study, we have evaluated six alarmins and demonstrated that S100B, S100A9, and HMGB1 as possible promising candidates for the biomarkers of NSV with high accuracy. In addition, the predictive accuracy for disease diagnosis and assessment was significantly improved when various alarmins were used in combination. This finding has special clinical and practical significance.

The clinical diagnosis of vitiligo is often determined by the appearance of reduced or lost skin pigmentation. However, this is not always the case. Vitiligo lesions at onset might be challenging to distinguish from adjacent normal skin due to the slight loss of pigmentation. Although histopathology is the gold standard for diagnosis and blister fluid testing could more accurately reflect the changes in the skin inflammatory microenvironment, these invasive examinations may induce the Koebner phenomenon in patients at the active stage. In contrast, circulating biomarkers are

TABLE 4 Diagnostic values of biomarkers for the prediction of vitiligo activity.

Alarmins	Cut-off value	AUC (95%CI)	Sensitivity, %	Specificity, %	PPV, %	NPV, %
S100B, pg/ml	26.606	0.691 (0.580,0.802)	67.57	63.33	77.39	51.26
S100A9, ng/ml	917.498	0.827 (0.742,0.913)	83.78	73.33	85.37	70.88
HMGB1, ng/ml	1.476	0.646 (0.537,0.755)	59.46	73.33	80.55	49.34
S100B+S100A9		0.850 (0.772,0.929)	96.67	70.27	85.79	91.91
S100B+HMGB1		0.718 (0.613,0.824)	80.00	58.11	78.01	61.01
S100A9+HMGB1		0.848 (0.770,0.925)	86.67	75.68	86.87	75.35
all combined		0.860 (0.786,0.933)	90.00	72.97	86.08	79.71

AUC, area under the curve; PPV, positive predictive value; NPV, negative predictive value.
The diagnostic cut-off value corresponds to the maximum point of the Youden index.
The all combined represents the combination of S100B, S100A9, and HMGB1.

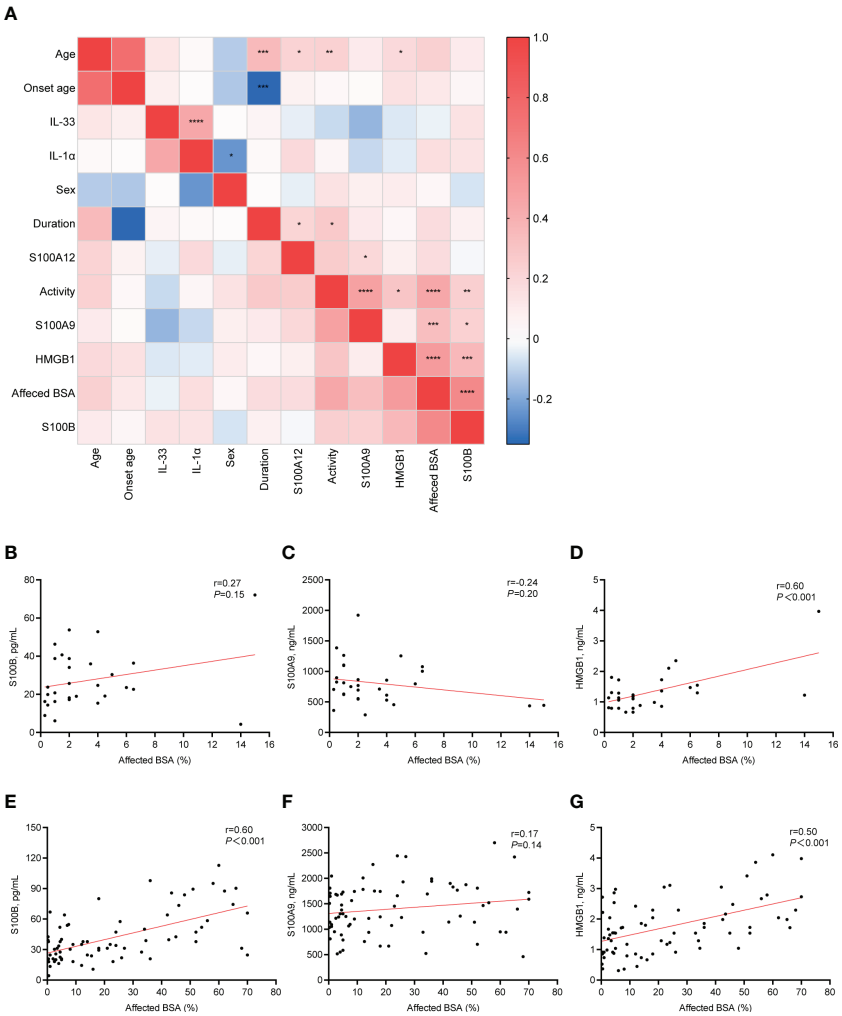

FIGURE 4
Correlation between clinical characteristics and serum alarmins. **(A)**, The correlation heatmap of clinical characteristics and serum alarmins by using Pearson correlations. **(B–D)**, Correlation changes in serum level of S100B, S100A9, and HMGB1 with changes in the affected BSA (%) of patients with stable vitiligo. **(E–G)**, Correlation changes in serum level of S100B, S100A9, and HMGB1 with changes in the affected BSA (%) of patients with active vitiligo. *P* values were calculated by Pearson correlation. **P* < 0.05, ***P* < 0.01, ****P* < 0.001, *****P* < 0.0001.

easier to collect and more acceptable for patients. Our ROC analysis revealed that serum IL-1α, S100B, S100A9, and HMGB1 had predictive capacity on the diagnosis of vitiligo. Of these, by using the cut-off value of serum S100B, approximately 92% of patients with NSV could be identified. Although these alarmins are also upregulated in other autoimmune diseases, we could infer that the overall diagnostic accuracy of vitiligo could be significantly improved by combining these biomarkers with the patients' disease features and physical examination.

With the dual guarantee of multivariate logistic regression and ROC analysis, we found that serum HMGB1, S100B, and S100A9 can efficiently discriminate between patients with stable and active vitiligo, and can be used as potential biomarkers for the prediction of disease activity. It is now widely accepted that alarmins (such as HMGB1 and certain S100 proteins) can stimulate innate immunity, trigger antigen-presenting cells, and activate adaptive immune responses, playing a key role in the pathogenesis of inflammatory and autoimmune diseases (8, 20, 21). Our previous study has demonstrated that HMGB1 is released from melanocytes under oxidative stress, and then promotes the skin migration of $CD8^+$ T cells and the maturation of dendritic cells, thus contributing to the formation of oxidative stress-induced autoimmunity in vitiligo (13). Therefore, the elevated serum levels of HMGB1 indicate a hyperactive immune state in patients with vitiligo. Consistent with our study, a recent study by Speeckaert et al. has also confirmed the elevated serum S100B levels in NSV patients at the active stage, and the *in vitro* experiments have shown that the release of S100B by stressed melanocytes may be the most plausible source of serum S100B in patients with NSV (14). Moreover, S100B inhibitor pentamidine could stop hair graying in the monobenzone-induced depigmentation mice model, suggesting S100B as a potential therapeutic target for vitiligo (14).

Importantly, our research revealed for the first time that circulating level of S100A9 was significantly elevated in NSV patients, and displayed high accuracy in disease activity assessment (AUC = 0.827), superior to sCD27 (AUC = 0.649) and sCD25 (AUC = 0.716) reported in the previous studies (6). More importantly, S100A9 is highly expressed and easily measured in serum samples, with expression levels hundreds of times higher than soluble CDs and chemokines such as CXCL10, thus might be expected to be one of the most valuable biomarkers of vitiligo activity (6, 22). A close correlation between elevated S100 proteins and disease activity has also been demonstrated in many inflammatory diseases, including rheumatoid arthritis, inflammatory bowel disease, as well as Alzheimer's disease (23). It has been well accepted that S100A9 interacts with and actives Toll-like receptor-4 (TLR-4)-expressing cells *via* a specific binding site, thus promoting the pro-inflammatory signaling cascade (24). However, S100A9 usually exists as heterodimeric complexes with S100A8 and forms heterotetramers in the presence of calcium (25). Due to an autoinhibitory feedback mechanism induced by calcium-dependent tetramerization, the alarmins S100A8/S100A9 are just temporarily active in the local microenvironment (26). Therefore, restricting the activity of S100A8/S100A9 *via* blocking a specific TLR4-binding site is not only a specific anti-inflammatory therapy but also minimizing systemic side effects (26). Thus the exact function and intervention mechanism of S100A9 in the development of vitiligo is of great importance to be investigated.

Unlike our study, Li et al. (27) and Vaccaro et al. (16) demonstrated that serum levels of IL-33 were elevated in patients, and positively correlated with disease activity. The reason for the difference may be attributed to the baseline characteristics of participants, the sample size, as well as other confounding factors.

Identifying the factors that affect the severity of vitiligo is also crucial for the treatment of vitiligo. Our study showed that S100B was only correlated with affected BSA in active vitiligo, but HMGB1 was associated with the vitiligo severity in both the active and stable stages. It should be noted that we used the affected BSA to assess disease severity, which can be affected by inter- and intra-assessor variability. More accurate and reliable methods of assessing disease severity need to be investigated, to further validate the potential of candidate serum markers as indicators of disease severity.

In our study, we excluded the patients receiving immunosuppressive or NB-UVB therapy within 6 weeks before sample detection, thus to some extent excluding the potential effects of treatments on the serum level of alarmins. Importantly, increasing studies have suggested that alarmins could also be used as biomarkers to monitor the efficacy of treatment in several autoimmune diseases. In patients with rheumatoid arthritis, serum S100A8/A9 and IL-33 levels were reduced after infliximab or anti-TNF-α treatment, respectively (10, 28); and in Juvenile Idiopathic Arthritis patients, serum concentrations of S100A8/S100A9 decreased significantly after intraarticular triamcinolone therapy (29); serum HMGB1 levels were decreased after the treatment with statins or prednisolone in patients with granulomatous polyangiitis (30). The prognosis and recurrence of patients could also be predicted by serum alarmins. Serum levels of IL-33 have been found higher in eosinophilic granulomatosis patients with polyangiitis and Behçet disease patients with uveitis at relapse than that at the onset or during remission (31, 32). The recurrence of ANCA-associated vasculitis was also closely associated with the levels of S100A8/A9 (33). Therefore, future studies are needed to determine whether alarmins can serve as clinical bio-indicators for the prediction of treatment response, prognosis, and recurrence of vitiligo.

There are several limitations in our study. First, the cohort size was relatively small, and the single-center design may limit the generalizability of these results. Furthermore, the cross-sectional design and observational study did not allow causal inference. Additionally, our study focused mainly on the role of alarmins in the diagnosis and assessment of vitiligo and was unable to determine their potential contribution to the prognosis and prediction of treatment response in vitiligo. Moreover, our study only detected a few specific alarmins but did not screen all the alarmins. Above all, future studies based on multicenter and

longitudinal samples are needed to explore the association between serum alarmins and clinical progression and prognosis.

Conclusion

In conclusion, this study discovers the potential significance of serum IL-1α, S100B, S100A9, and HMGB1 in the auxiliary diagnosis of patients with NSV. Additionally, it is highlighted that serum S100B, S100A9, and HMGB1 might be potential biomarkers for assessing the activity and severity of NSV. Thereby, alarmins offer a versatile, noninvasive way for diagnosis and clinical condition monitoring of vitiligo.

Data availability statement

The raw data supporting the conclusions of this article will be made available by the authors, without undue reservation.

Ethics statement

The studies involving human participants were reviewed and approved by ethics committee of Xijing Hospital of the Fourth Military Medical University. The patients/participants provided their written informed consent to participate in this study. Written informed consent was obtained from the individual(s) for the publication of any potentially identifiable images or data included in this article.

Author contributions

KH and WW have contributed equally to this work. WD and SW collected the blood samples. KH, WW, SL, and CL conceived and designed the experiments. KH, WW, and XW performed statistical analysis. KH and WW drafted the manuscript. SL and CL revised the manuscript. All authors contributed to the article and approved the submitted version.

Funding

This research was funded by the National Natural Science Foundation of China (No. 82222059, No. 82173416, No. 81930087, and No. 12126606).

Acknowledgments

We gratefully acknowledge all vitiligo patients and healthy volunteers for their selfless donation of samples used in this study.

Conflict of interest

The authors declare that the research was conducted in the absence of any commercial or financial relationships that could be construed as a potential conflict of interest.

Publisher's note

References

1. Ezzedine K, Eleftheriadou V, Whitton M, van Geel N. Vitiligo. *Lancet* (2015) 386:74–84. doi: 10.1016/S0140-6736(14)60763-7

2. Wang Y, Li S, Li C. Clinical features, immunopathogenesis, and therapeutic strategies in vitiligo. *Clin Rev Allergy Immunol* (2021) 61:299–323. doi: 10.1007/s12016-021-08868-z

3. Speeckaert R, Lambert J, Bulat V, Belpaire A, Speeckaert M, van Geel N. Autoimmunity in segmental vitiligo. *Front Immunol* (2020) 11:568447. doi: 10.3389/fimmu.2020.568447

4. Salman A, Kurt E, Topcuoglu V, Demircay Z. Social anxiety and quality of life in vitiligo and acne patients with facial involvement: A cross-sectional controlled study. *Am J Clin Dermatol* (2016) 17:305–11. doi: 10.1007/s40257-016-0172-x

5. Rodrigues M, Ezzedine K, Hamzavi I, Pandya AG, Harris JE, Vitiligo Working G. New discoveries in the pathogenesis and classification of vitiligo. *J Am Acad Dermatol* (2017) 77:1–13. doi: 10.1016/j.jaad.2016.10.048

6. Speeckaert R, Lambert J, van Geel N. Clinical significance of serum soluble CD molecules to assess disease activity in vitiligo. *JAMA Dermatol* (2016) 152:1194–200. doi: 10.1001/jamadermatol.2016.2366

7. Danieli MG, Antonelli E, Piga MA, Claudi I, Palmeri D, Tonacci A, et al. Alarmins in autoimmune diseases. *Autoimmun Rev* (2022) 21:103142. doi: 10.1016/j.autrev.2022.103142

8. Yang, Han Z, Oppenheim JJ. Alarmins and immunity. *Immunol Rev* (2017) 280:41–56. doi: 10.1111/imr.12577

9. Oppenheim JJ, Yang D. Alarmins: Chemotactic activators of immune responses. *Curr Opin Immunol* (2005) 17:359–65. doi: 10.1016/j.coi.2005.06.002

10. Garcia-Arias M, Pascual-Salcedo D, Ramiro S, Ueberschlag ME, Jermann TM, Cara C, et al. Calprotectin in rheumatoid arthritis: Association with disease activity in a cross-sectional and a longitudinal cohort. *Mol Diagn Ther* (2013) 17:49–56. doi: 10.1007/s40291-013-0016-9

11. Ma CY, Jiao YL, Zhang J, Yang QR, Zhang ZF, Shen YJ, et al. Elevated plasma level of HMGB1 is associated with disease activity and combined alterations with IFN-α and TNF-α in systemic lupus erythematosus. *Rheumatol Int* (2012) 32:395–402. doi: 10.1007/s00296-010-1636-6

12. O'Reilly S. Pound the alarm: Danger signals in rheumatic diseases. *Clin Sci (Lond)* (2015) 128:297–305. doi: 10.1042/CS20140467

13. Cui T, Zhang W, Li S, Chen X, Chang Y, Yi X, et al. Oxidative stress-induced HMGB1 release from melanocytes: A paracrine mechanism underlying the cutaneous inflammation in vitiligo. *J Invest Dermatol* (2019) 139:2174–84.e4. doi: 10.1016/j.jid.2019.03.1148

14. Speeckaert R, Voet S, Hoste E, van Geel N. S100B is a potential disease activity marker in nonsegmental vitiligo. *J Invest Dermatol* (2017) 137:1445–53. doi: 10.1016/j.jid.2017.01.033

15. Gholijani N, Yazdani MR, Dastgheib L. Predominant role of innate pro-inflammatory cytokines in vitiligo disease. *Arch Dermatol Res* (2020) 312:123–31. doi: 10.1007/s00403-019-01996-9

16. Vaccaro M, Cicero F, Mannucci C, Calapai G, Spatari G, Barbuzza O, et al. IL-33 circulating serum levels are increased in patients with non-segmental generalized vitiligo. *Arch Dermatol Res* (2016) 308:527–30. doi: 10.1007/s00403-016-1675-2

17. Hofmann Bowman M, Wilk J, Heydemann A, Kim G, Rehman J, Lodato JA, et al. S100A12 mediates aortic wall remodeling and aortic aneurysm. *Circ Res* (2010) 106:145–54. doi: 10.1161/CIRCRESAHA.109.209486

18. Lim SY, Raftery MJ, Geczy CL. Oxidative modifications of DAMPs suppress inflammation: The case for S100A8 and S100A9. *Antioxid Redox Signal* (2011) 15:2235–48. doi: 10.1089/ars.2010.3641

19. Li S, Dai W, Wang S, Kang P, Ye Z, Han P, et al. Clinical significance of serum oxidative stress markers to assess disease activity and severity in patients with non-segmental vitiligo. *Front Cell Dev Biol* (2021) 9:739413. doi: 10.3389/fcell.2021.739413

20. Chan JK, Roth J, Oppenheim JJ, Tracey KJ, Vogl T, Feldmann M, et al. Alarmins: Awaiting a clinical response. *J Clin Invest* (2012) 122:2711–9. doi: 10.1172/JCI62423

21. Murao A, Aziz M, Wang H, Brenner M, Wang P. Release mechanisms of major DAMPs. *Apoptosis* (2021) 26:152–62. doi: 10.1007/s10495-021-01663-3

22. Strassner JP, Rashighi M, Ahmed Refat M, Richmond JM, Harris JE. Suction blistering the lesional skin of vitiligo patients reveals useful biomarkers of disease activity. *J Am Acad Dermatol* (2017) 76:847–55.e5. doi: 10.1016/j.jaad.2016.12.021

23. Holzinger D, Tenbrock K, Roth J. Alarmins of the S100-family in juvenile autoimmune and auto-inflammatory diseases. *Front Immunol* (2019) 10:182. doi: 10.3389/fimmu.2019.00182

24. Singh P, Ali SA. Multifunctional role of S100 protein family in the immune system: An update. *Cells* (2022) 11(15):2274. doi: 10.3390/cells11152274

25. Leukert N, Vogl T, Strupat K, Reichelt R, Sorg C, Roth J. Calcium-dependent tetramer formation of S100A8 and S100A9 is essential for biological activity. *J Mol Biol* (2006) 359:961–72. doi: 10.1016/j.jmb.2006.04.009

26. Vogl T, Stratis A, Wixler V, Völler T, Thurainayagam S, Jorch SK, et al. Autoinhibitory regulation of S100A8/S100A9 alarmin activity locally restricts sterile inflammation. *J Clin Invest* (2018) 128:1852–66. doi: 10.1172/JCI89867

27. Li P, Ma H, Han D, Mou K. Interleukin-33 affects cytokine production by keratinocytes in vitiligo. *Clin Exp Dermatol* (2015) 40:163–70. doi: 10.1111/ced.12464

28. Mu R, Huang HQ, Li YH, Li C, Ye H, Li ZG. Elevated serum interleukin 33 is associated with autoantibody production in patients with rheumatoid arthritis. *J Rheumatol* (2010) 37:2006–13. doi: 10.3899/jrheum.100184

29. Frosch M, Strey A, Vogl T, Wulffraat NM, Kuis W, Sunderkotter C, et al. Myeloid-related proteins 8 and 14 are specifically secreted during interaction of phagocytes and activated endothelium and are useful markers for monitoring disease activity in pauciarticular-onset juvenile rheumatoid arthritis. *Arthritis Rheum* (2000) 43:628–37. doi: 10.1002/1529-0131(200003)43:3<628::AID-ANR20>3.0.CO;2-X

30. Souza AW, de Leeuw K, van Timmeren MM, Limburg PC, Stegeman CA, Bijl M, et al. Impact of serum high mobility group box 1 and soluble receptor for advanced glycation end-products on subclinical atherosclerosis in patients with granulomatosis with polyangiitis. *PLoS One* (2014) 9:e96067. doi: 10.1371/journal.pone.0096067

31. Takeuchi M, Karasawa Y, Harimoto K, Tanaka A, Shibata M, Sato T, et al. Analysis of Th cell-related cytokine production in Behçet disease patients with uveitis before and after infliximab treatment. *Ocul Immunol Inflamm* (2017) 25:52–61. doi: 10.3109/09273948.2016.1158276

32. Tsurikisawa N, Oshikata C, Watanabe M, Tsuburai T, Kaneko T, Saito H. Innate immune response reflects disease activity in eosinophilic granulomatosis with polyangiitis. *Clin Exp Allergy* (2018) 48:1305–16. doi: 10.1111/cea.13209

33. Pepper RJ, Hamour S, Chavele KM, Todd SK, Rasmussen N, Flint S, et al. Leukocyte and serum S100A8/S100A9 expression reflects disease activity in ANCA-associated vasculitis and glomerulonephritis. *Kidney Int* (2013) 83:1150–8. doi: 10.1038/ki.2013.2

frontiers | Frontiers in Immunology

TYPE Original Research
PUBLISHED 14 December 2022
DOI 10.3389/fimmu.2022.1079259

OPEN ACCESS

EDITED BY
Tao Liu,
Brigham and Women's Hospital and Harvard Medical School, United States

REVIEWED BY
Sajad Karampoor,
Iran University of Medical Sciences, Iran
Dawei Cui,
Zhejiang University School of Medicine, China

*CORRESPONDENCE
Chen-Yu Zhang
cyzhang@nju.edu.cn
Meng Ding
vikkiding@163.com
Chunni Zhang
zchunni27@hotmail.com
Jun-Jun Wang
wangjunjun9202@163.com

†These authors have contributed equally to this work

SPECIALTY SECTION
This article was submitted to Cytokines and Soluble Mediators in Immunity, a section of the journal Frontiers in Immunology

RECEIVED 25 October 2022
ACCEPTED 29 November 2022
PUBLISHED 14 December 2022

CITATION
Wang C, Zhu Y, Chen P, Wang C, Zhou W, Zhang C, Wang J, Chen X, Ding M, Zhang C, Wang J-J and Zhang C-Y (2022) Altered serum human cytomegalovirus microRNA levels are common and closely associated with the inflammatory status in patients with fever. *Front. Immunol.* 13:1079259. doi: 10.3389/fimmu.2022.1079259

Altered serum human cytomegalovirus microRNA levels are common and closely associated with the inflammatory status in patients with fever

Cheng Wang[1,2†], Yunhua Zhu[1,2†], Penglu Chen[1,2†], Chen Wang[2], Wanqing Zhou[1,2], Cuiping Zhang[1], Jing Wang[1], Xi Chen[2], Meng Ding[1,2*], Chunni Zhang[1,2*], Jun-Jun Wang[1*] and Chen-Yu Zhang[1,2*]

[1]Department of Clinical Laboratory, Jinling Hospital, State Key Laboratory of Pharmaceutical Biotechnology, NJU Advanced Institute for Life Sciences (NAILS), School of Life Sciences, Nanjing University, Nanjing, China, [2]Nanjing Drum Tower Hospital Center of Molecular Diagnostic and Therapy, Chinese Academy of Medical Sciences Research Unit of Extracellular RNA, State Key Laboratory of Pharmaceutical Biotechnology, Jiangsu Engineering Research Center for MicroRNA Biology and Biotechnology, NJU Advanced Institute of Life Sciences (NAILS), Institute of Artificial Intelligence Biomedicine, School of Life Sciences, Nanjing University, Nanjing, China

Background: Fever has a complicated etiology, and diagnosing its causative factor is clinically challenging. Human cytomegalovirus (HCMV) infection causes various diseases. However, the clinical relevance, prevalence, and significance of HCMV microRNAs (miRNA) in association with fever remain unclear. In the present study, we analyzed the HCMV miRNA expression pattern in the serum of patients with fever and evaluate its clinical associations with occult HCMV infection status in immune disorders.

Methods: We included serum samples from 138 patients with fever and 151 age-gender-matched controls in this study. First, the serum levels of 24 HCMV miRNAs were determined using a hydrolysis probe-based stem-loop quantitative reverse transcription polymerase chain reaction (RT-qPCR) assay in the training set. The markedly altered miRNAs were verified in the validation and testing sets. The serum HCMV IgG/IgM and DNA titers in the testing cohort were also assessed using enzyme-linked immunosorbent assay (ELISA) and RT-qPCR, respectively.

Results: The majority of HCMV miRNAs were markedly upregulated in the serum of fever patients. We selected the five most significantly altered HCMV miRNAs: hcmv-miR-US4-3p, hcmv-miR-US29-3p, hcmv-miR-US5-2-3p, hcmv-miR-UL112-3p, and hcmv-miR-US33-3p for validation. These miRNAs were also significantly elevated in the serum of fever patients in the validation and testing sets compared with the controls. Logistic regression analysis

revealed that the five miRNAs were novel potential risk factors for fever. Notably, the serum levels of four of the five confirmed HCMV miRNAs were significantly associated with blood C-reaction protein concentrations. Moreover, the five HCMV miRNA levels were closely correlated with the HCMV DNA titers in the testing cohort.

Conclusion: HCMV infection and activation are common in fever patients and could be novel risk factors for fever. These differentially expressed HCMV miRNAs could enable HCMV activation status monitoring in immune disorders.

KEYWORDS

HCMV, human cytomegalovirus, serum, fever, risk factor, immune disorders, microRNA

1 Introduction

Fever, including undifferentiated fever and fever of unknown origin (FUO), is frequently observed in patients seeking health care in China. However, the complex etiology of fever and its delayed diagnosis complicates the treatment (1–3). Recent epidemiological surveys have demonstrated that fever is prevalent in both developing and developed countries, and the causes of fever vary depending on the region and time (4). Nowadays, the most frequently reported etiologies of fever include infection, non-infectious inflammatory disease (NIID), and malignancy. However, these factors cause fever in about 60–80% of fever patients, and many patients remain undiagnosed (5, 6). The most frequently used diagnostic procedures for fever are imaging methods, blood tests, blood cultures, and molecular detection (7). Blood cultures and serum procalcitonin tests can discriminate fever resulting from bacterial infection from other fevers, but the unfulfilled positive rate and time-consuming procedures often obscure and delay the diagnosis of fever (8). Thus, accurate diagnosis and timely management of fever remain a challenge for physicians in clinical therapy.

Reportedly, human herpes virus (HHV) infection is an important etiological agent for fever, especially for FUO (9). The study highlights an association between HHV infection and the clinical signs of fever, providing direct evidence that HHV cell-free nucleic acids detected in circulation might help in the diagnosis and treatment of fever. As one of the largest and most complex members of the human beta herpes virus family, human cytomegalovirus (HCMV) is a ubiquitous human pathogen. The seroprevalence data revealed that > 90% of people have been infected with HCMV, and the infection risk increases with age. Once infected, the infection persists lifelong and may undergo periodic reactivation (10). HCMV infection and activation can cause congenital birth defects and morbidity in immunocompromised patients and allogeneic bone marrow or organ-transplant recipients. However, the molecular mechanism by which HCMV infects the host, maintains latency, and reactivates remains unclear (10). Patients with fever frequently present with immunocompromised conditions or immunodepression during the disease. However, the clinical association between HCMV and fever has rarely been explored. Moreover, the high prevalence of HCMV IgG and a short window period for HCMV IgM detection in blood limits HCMV infection and reactivation surveillance.

MicroRNAs are small noncoding RNA molecules that bind to the 3′ untranslated region (3′-UTR) of a target messenger RNA and repress its translation, thus controlling protein expression at the post-transcriptional level in virtually all eukaryotic organisms and some virus, including HCMV (11). HCMV encodes 26 known mature miRNAs. Some of the HCMV-encoded miRNAs target both viral and host genes, including important immune modulators. Furthermore, infections with HCMV can alter the expression of host miRNAs to benefit virus replication (11, 12). Human body fluids also contain stable miRNAs, and dysregulated serum miRNAs are blood-based biomarkers for various diseases, such as cancer, diabetes, and infectious diseases (13). These pieces of evidence imply that expression profiles of altered host miRNAs combined with HCMV miRNAs in the serum might serve as potential diagnostic tools for HCMV-related diseases and be involved in disease occurrence and progression. A pioneering study reported that a circulating miRNA profile comprising two host miRNAs and one HCMV miRNA, hcmv-miR-UL112, is a novel noninvasive biomarker for essential hypertension (14). Subsequently, another group found the same HCMV miRNA (hcmv-miR-UL112) more prevalent in the serum of diabetes mellitus and glioblastoma multiform patients as compared with rheumatoid arthritis patients and healthy subjects (15). Furthermore, our group also found that dysregulated HCMV miRNAs in circulation were closely associated with oral lichen

Abbreviations: miRNA, microRNA; HCMV, human cytomegalovirus; NIID, non-infectious inflammatory disease; RT-qPCR, quantitative reverse transcription polymerase chain reaction; Cq, quantification cycle; AUC, the area under the ROC curve; ELISA, enzyme linked immunosorbent assay.

planus, adverse pregnancy outcomes, and treatment efficacy of chronic hepatitis B patients (16–18). Additionally, circulating HCMV miRNAs could be encapsulated by extracellular vesicles and participate in immune disorders (16, 19, 20).

Currently, despite the high infection rates of HCMV in human beings, little is known about the HCMV-encoded miRNA patterns in the serum of fever patients with immune disorders. The clinical relevance of HCMV miRNAs in fever also remains incompletely characterized. Thus, in the present study, we used hydrolysis probe-based reverse transcription quantitative real-time PCR (RT-qPCR) to examine the comprehensive expression profile of serum HCMV miRNAs in a cohort of fever patients to analyze the relations between HCMV and fever. We also aimed to evaluate the possible clinical significance and associated pathogenesis of serum HCMV miRNAs, which could provide useful information for fever management.

2 Materials and methods

2.1 Study population, sample collection, and study design

The present study complies with the World Medical Association Declaration of Helsinki and is approved by the ethics committee board of Jinling hospital. Written informed consent was obtained from all participants. For the patients who had a compromised capacity to consent, written informed consent was obtained from the legally authorized representative on the behalf of the participant. A total of 138 fever patients who were treated at the Department of Integration of Traditional Chinese and Western Medicine of Jinling Hospital (Nanjing, China) between November 2013 and November 2016 were enrolled in this study. The inclusion criterion in the study was: patients with a fever (≥ 37.3 °C) with no apparent diagnosis after an initial outpatient or hospital evaluation, including a careful history, physical examination, and initial laboratory assessment. Patient details, including demographic characteristics, medical history, blood parameters, blood cultures (if performed), imaging and endoscopy (if performed), final diagnostic, and outcome data were collected and retrospectively analyzed. In addition, 151 age-gender-matched individuals from the Healthy Physical Examination Centre of Jinling Hospital showing no evidence of fever and/or other abnormalities were selected as normal controls.

A multiphase case-control study was designed to explore the dysregulated HCMV miRNA profile in the serum of fever patients. We initially screened the 24 HCMV miRNAs and their expression patterns in a cohort (the training set) constituting 33 patients and 38 healthy controls. Subsequently, the most markedly altered HCMV miRNAs were further confirmed in another cohort (the validation set) containing 65 patients and 68 controls. Finally, the selected miRNAs were examined in a cohort (the testing set), including 40 patients and 45 controls. Moreover, we also measured the peripheral blood HCMV DNA titers and serum anti-HCMV IgG/IgM content in the testing set. A schematic representation of the study design and workflow is shown in Figure 1.

2.2 Serum RNA isolation and RT-qPCR assay of HCMV-encoded miRNAs

Total RNA was extracted from 100 μL of serum using a one-step phenol/chloroform purification method and precipitated using isopropyl alcohol as previously described (21). Hydrolysis probe-based RT-qPCR was carried out using a TaqMan miRNA PCR kit (Applied Biosystems, Foster City, CA, USA) according to the manufacturer's instructions with a minor modification as previously described (21). Briefly, 2 μL of total RNA was reverse transcribed to cDNA using AMV reverse transcriptase (TaKaRa, Dalian, China) and the stem-loop RT primer (Applied Biosystems, Foster City, CA, USA). Real-time PCR was performed using hydrolysis miRNA probes on a Roche LightCycler® 480 II PCR System (Roche Diagnostics, Mannheim, Germany). All reactions, including no-template controls, were performed in triplicates. The quantification cycle (Cq) values were determined using the fixed threshold settings. To control the variability in RNA extraction and purification procedures, an exogenous plant small molecular RNA, MIR2911 (5′-GGCCGGGGGACGGGCUGGGA-3′), was spiked into each sample with a final concentration of 10^6 fmol/L during RNA isolation as a synthetic external reference for the normalization of serum miRNAs. Relative levels of HCMV miRNAs were then normalized to the exogenous MIR2911 and calculated using the comparative Cq method ($2^{-\Delta Cq}$).

2.3 HCMV titers, anti-HCMV IgG, and IgM antibodies determination

We examined the copy number of HCMV DNA using qRT-PCR in the peripheral blood samples of fever patients and controls in the testing set as previously described (14, 16). Briefly, the sequences of the sense and antisense primers for HCMV DNA quantification were 5′-CACGGTCCCGGTTTAGCA-3′ and 5′-CGTAACGTGGACCTGACGTTT-3′. The probe sequence was 5′-TATCTGCCCGAGGATCGCGGTTACA-3′. The 5′ and 3′ ends of the probe were labeled with FAM and TAMRA dyes, respectively. HCMV DNA was extracted from the peripheral blood leukocytes (PBLs) using the QIAamp Min Elute Virus Spin (Qiagen, Hilden, Germany) and QIAamp DNA Mini kit (Qiagen, Hilden, Germany) according to the manufacturer's protocol. We tested 20 μL of each DNA extract with TaqMan PCR assays on a 96-well plate for < 45 cycles. A ten-fold diluted recombinant plasmid containing the HCMV target sequence was used as a template for standard curve preparation.

ELISA tests for anti-HCMV IgG and IgM antibodies in serum were performed with a commercially available ELISA kit

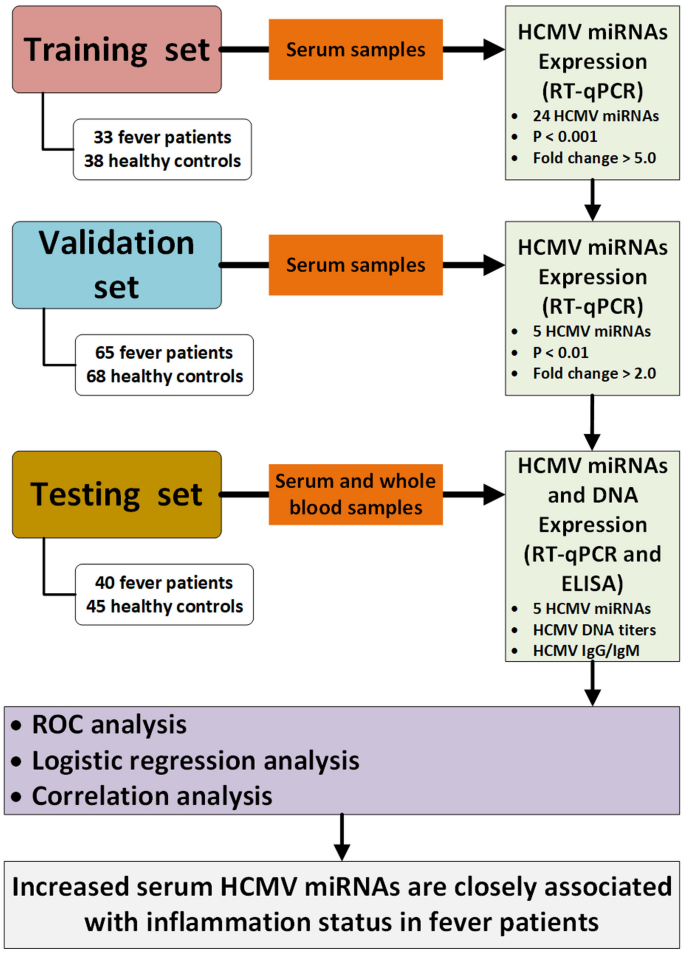

FIGURE 1
Flow chart of the experimental design. HCMV, human cytomegalovirus; Cq, quantification cycle; RT-qPCR, quantitative reverse transcription polymerase chain reaction; ELISA, enzyme-linked immunosorbent assay; ROC, receiver operating characteristic.

(MEDSON, NJ, USA) according to the manufacturer's instructions. Briefly, for anti-HCMV IgG testing, the absorbance of serum anti-HCMV IgG was assessed using the ELISA kit, and its absolute concentrations were calculated from the calibration curve. For anti-HCMV IgM testing, ELISA values of < 1.0, 1.0–1.2, and > 1.2 were considered as a negative result, an equivocal infection, and a positive result, indicating prior exposure to HCMV (for anti-HCMVIgG) or acute infection with HCMV (for anti-HCMV IgM), respectively.

2.4 Statistical analysis

Statistical analysis was performed with GraphPad Prism 9.0 software or SPSS statistical software (version 23.0). The miRNA levels are represented as means and standard errors (Mean ± SEM) and other clinical variables as mean ± SD. The data analyses were performed using the non-parametric Mann–Whitney tests or Kruskal-Wallis test with statistical significance set at $P < 0.05$. Forward stepwise univariate and multivariate logistic regression analyzes were conducted to evaluate the influences of serum HCMV miRNAs on fever patients. ROC curves were constructed, and the areas under the ROC curves (AUCs) were calculated to evaluate the discrimination ability of serum HCMV miRNA for fever prediction. Spearman rank correlation analysis was used to analyze the relationship between the miRNA concentrations and clinical features or other parameters.

3 Results

3.1 Study population and final diagnosis

The present study enrolled 138 fever patients, including 87 (63%) males and 51 (37%) females, with a mean age of 58.00 ± 23.57 years (Table 1). Based on the medical records, 122 (88.4%)

patients ultimately had their underlying disease diagnosed, of which 87 (63%) had infectious diseases, 20 (14.5%) had non-infectious connective tissue diseases, four (2.9%) had hematological malignancies, 11 (8.0%) had non-infectious inflammatory diseases, and 16 (11.6%) remained undiagnosed. As shown in Table 1, pulmonary infection, upper respiratory tract infection, vasculitis, and connective tissue diseases were the most common diagnoses. Laboratory test results, including hematological index and serological and immunological parameters (if performed), are also listed in Table 1.

3.2 Expression profiles of HCMV-encoded miRNAs in the serum of fever patients

To fully characterize the serum HCMV miRNA expression signature in fever patients, we measured the expression pattern of 24 HCMV miRNAs (miRBase 22.0) in 33 randomly assigned fever patients and 38 matched controls (referred to as the training set) using RT-qPCR analysis. The RT-qPCR results showed that HCMV miRNAs were readily detected in both fever patients and controls. Of the 24 HCMV miRNAs examined, 17 miRNAs were significantly upregulated in the serum of fever patients compared with the controls ($P < 0.05$). The relative expression levels of the 24 HCMV-encoded miRNAs in fever patients and controls are shown in Supplemental Data Table 1.

Of the 17 markedly altered miRNAs, five with a high elevation (fold change > 5 and $P < 0.001$), including hcmv-miR-US4-3p, hcmv-miR-US29-3p, hcmv-miR-US5-2-3p, hcmv-miR-UL112-3p, and hcmv-miR-US33-3p, were then selected for further verification (Table 2). These miRNAs are reported to be related to CMV latency, reactivation, and immune evasion.

We examined the five selected HCMV miRNAs in a larger cohort comprising 66 fever patients and 68 controls (referred to as the validation set). The RT-qPCR results showed the alteration pattern of the five candidate miRNAs in the fever case group was consistent with that from the training set ($P < 0.01$ for all miRNAs) (Table 2), thus confirming the stability of the expression profile.

3.3 Confirmation of altered HCMV miRNAs in the serum samples of the testing set

The changes in the five selected HCMV miRNAs expression were further confirmed in a cohort referred to as the testing set of 40 fever patients and 45 controls. As shown in Figure 2, the levels of the five selected HCMV miRNAs in the testing set were significantly elevated in the fever patients in comparison with the healthy controls (all with $P < 0.0001$), consistent with the results of the training and validation sets.

3.4 ROC curve analysis

To assess the diagnostic value of the five HCMV miRNAs in discriminating fever patients from control subjects, we conducted the ROC curve analysis in the all samples enrolled in the training, validation, and testing sets. As shown in Figure 3, the area under the ROC curves (AUCs) of the five HCMV miRNAs for discriminating fever patients from controls ranged from 0.721–0.789, indicating the practical usefulness of individual HCMV miRNAs in the auxiliary diagnosis of the fever patients.

3.5 Association between serum HCMV miRNA expression levels and fever status

We then tested the predictive effects of the five HCMV miRNAs for fever among all patients and controls enrolled in the training, validation, and testing sets. Using the control group as the reference category and fever status as a dependent two-category variable, forward stepwise univariate logistic regression analysis demonstrated the five selected miRNAs were independent risk factors for FUO. The odds ratios (ORs) of these miRNAs for FUO were hcmv-miR-US4-3p: OR = 8.688, 95% CI, 4.923–15.331, $P < 0.001$, hcmv-miR-US29-3p: OR = 9.13, 95% CI, 5.268–15.826, $P < 0.001$, hcmv-miR-US5-2-3p: OR = 6.144, 95% CI, 3.580–10.546, $P < 0.001$, hcmv-miR-UL112-3p: OR = 4.303, 95% CI, 2.620–7.068, $P < 0.001$, and hcmv-miR-US33-3p: OR = 4.153, 95% CI, 2.510–6.870, $P < 0.001$ (Table 3).

Next, we investigated whether the altered HCMV miRNAs were still independently associated with fever in the same cohort samples when age, gender, and other clinical parameters were included. Using a dependent two-category variable multivariate logistic regression analysis and after adjusting for age, gender, and hematological index, we observed that hcmv-miR-US29-3p: OR = 6.47, 95% CI, 2.893–14.470, $P < 0.001$ and hcmv-miR-US33-3p: OR = 3.2, 95% CI, 7.9–19.7, $P < 0.001$ remained independent risk factors in fever (Table 3).

Taken together, these results revealed that the five overexpressed miRNAs facilitate the diagnosis of fever and might serve as novel potential risk factors for fever.

3.6 Relative expression levels of the selected serum HCMV miRNA in fever patients with different etiology

We next explored the difference in the concentrations of the 5 HCMV miRNA among fever patients that were caused by different etiology. As shown in the Supplementary Figure 1, none of the five HCMV-encoded miRNAs has any statistically difference among patients with different etiology by Kruskal-Wallis's test (Supplementary Figure 1). These results indicated that the altered HCMV miRNAs in fever patients may not affect by different etiology, but may associate with immune disorders.

10.3389/fimmu.2022.1079259

TABLE 1 Demographic and clinical information of the fever patients and healthy controls.[a]

Variables		Control (n = 151)	Fever (n = 138)	P value
Age (years)		53.87 ± 10.44	58.00 ± 23.57	0.052[b]
Sex				0.799[c]
	Male	93	87	
	Female	58	51	
Hematological index				
	WBC (× 10^9/L)	5.79 ± 1.50	8.48 ± 5.43	< 0.0001[d]
	Lymphocyte (%)	35.33 ± 8.05	21.99 ± 14.12	< 0.0001[d]
	Monocytes (%)	5.80 ± 1.53	7.93 ± 3.98	< 0.0001[d]
	Neutrophil (%)	55.79 ± 8.98	68.01 ± 15.82	< 0.0001[d]
	Acidophilicgranulocyte (%)	2.47 ± 1.71	1.76 ± 2.65	< 0.0001[d]
	Basophil (%)	0.41 ± 0.23	0.32 ± 0.35	< 0.0001[d]
C-reactive protein (mg/L)		< 0.50	48.16 ± 50.42	
Procalcitonin (μg/L)			2.03 ± 7.92	
Interleukin-6 (ng/L)			44.18 ± 49.07	
Final diagnosis for fever				
	Infection			87 (63 %)
			Tuberculosis	1
			Bacteremia	2
			Brucellosis	1
			Sepsis	3
			Pulmonary infection	34
			Mycoplasma pneumonia	2
			Upper respiratory tract infection	32
			Urinary tract infection	4
			Intracranial infection	1
			Infective endocarditis	2
			Gastrointestinal tract infection	1
			Monocytic angina	2
			Influenza viruses	1
			Herpes	1
	Autoimmunological disease			20 (14.5 %)
			Vasculitis	7
			Adult still disease	1
			Sjogren syndrome	1
			Systemic lupus erythematosus	2
			Overlap syndrome	1
			Undifferentiated connective tissue disease	6
			Erythema nodosum	2
	Hematological malignancies			4 (2.9 %)
			Lymphoma	3
			Malignant plasma cell dyscrasia	1
	Non-infectious inflammatory diseases			11 (8.0 %)
			Necrotizing lymphadenitis	4
			Thyroiditis	1
			Other	6
	Undiagnosed			16 (11.6 %)

[a]Data are mean (SD) or number (%). [b]Compared with control group. [c]Two sides χ^2 test. [d]P values were calculated by the Mann-Whitney U test.

10.3389/fimmu.2022.1079259

TABLE 2 Serum levels of the markedly altered HCMV-encoded miRNAs in fever patients arranged into the training and validation sets.[a]

HCMV miRNA	Control	Fever	P value	Fold change
Training set	**(n = 38)**	**(n = 33)**		
hcmv-miR-US4-3p	29.87 ± 5.55	209.7 ± 61.02	< 0.0001	7.02
hcmv-miR-US29-3p	6.56 ± 1.52	34.12 ± 9.72	< 0.0001	5.2
hcmv-miR-US5-2-3p	2.74 ± 0.60	14.17 ± 4.07	0.0001	5.17
hcmv-miR-UL112-3p	123.3 ± 15.92	867.7 ± 312.0	0.0003	7.03
hcmv-miR-US33-3p	12.43 ± 1.63	83.83 ± 29.92	0.0003	6.74
Validation set	**(n = 68)**	**(n = 65)**		
hcmv-miR-US4-3p	30.35 ± 4.19	153.7 ± 49.20	0.0007	5.06
hcmv-miR-US29-3p	9.32 ± 1.38	43.00 ± 10.96	0.0009	4.61
hcmv-miR-US5-2-3p	6.53 ± 1.32	18.75 ± 4.22	0.0037	2.87
hcmv-miR-UL112-3p	180.8 ± 23.21	741.7 ± 205.8	0.0012	4.1
hcmv-miR-US33-3p	21.09 ± 3.32	80.88 ± 26.96	0.0086	3.83

[a]The relative expression of miRNA to spiked-in exogenous MIR2911($\times 10^{-5}$) was calculated using the $2^{-\Delta Cq}$ method. The data are presented as the mean ± SEM. P-value was calculated with a nonparametric Mann-Whitney test. The bold values represent the sample size of control subjects and fever patients in each set.

3.7 Detection of HCMV in the peripheral blood and serum samples

We then measured the HCMV DNA in peripheral blood leukocytes (PBLs) of the samples in the testing set using RT-qPCR assays. Using the TaqMan assay, we found that the HCMV DNA was significantly higher in the fever patients than in the controls (Figure 4). Furthermore, we also performed ELISA assays to determine the anti-HCMV IgG and IgM concentrations in the serum samples of the same cohort (Figure 4). Our results showed that 100% of fever patients and 97.8% of controls were anti-HCMV IgG positive, while 97.5% of fever patients and 97.8% of controls were anti-HCMV IgM negative. No significant differences were found between the fever patients and the controls (Figure 4).

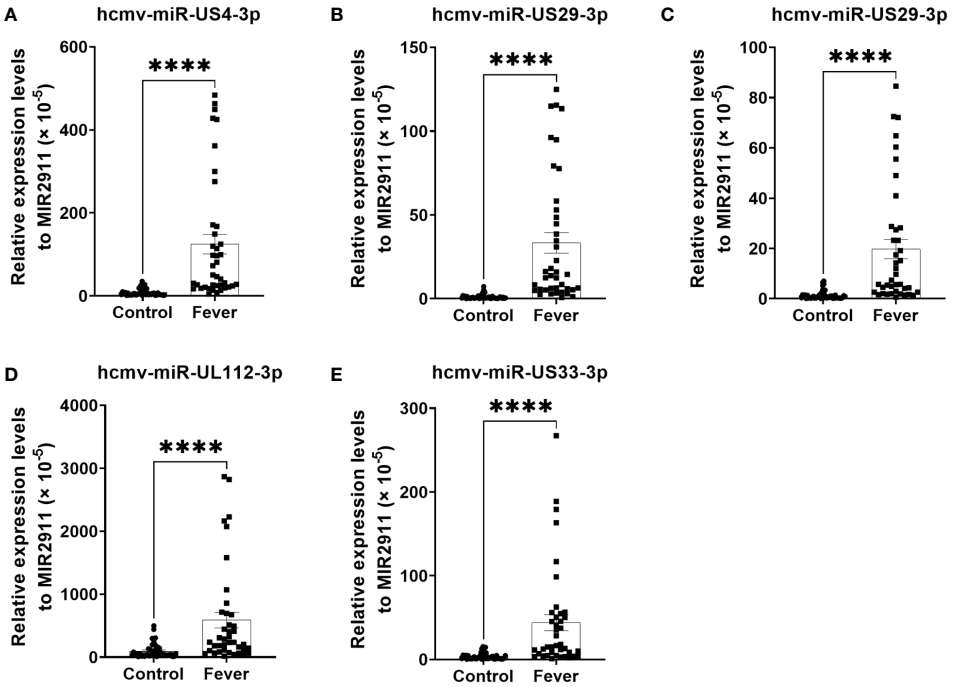

FIGURE 2
Relative levels of the five HCMV miRNAs in the serum of fever patients and healthy controls of the testing set **(A–E)**. Cq values were converted to relative concentrations normalized to MIR2911 values ($\times 10^{-5}$) and were calculated using the comparative Cq method ($2^{-\Delta Cq}$). P values were calculated by the Mann-Whitney U test. ****P < 0.0001.

10.3389/fimmu.2022.1079259

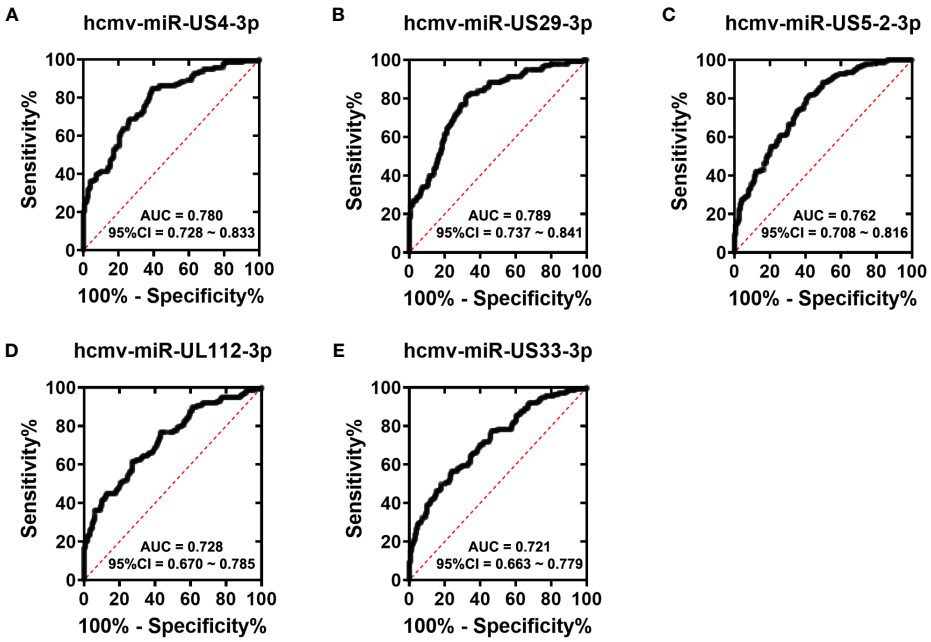

FIGURE 3
ROC curves analysis of the five selected HCMV miRNAs **(A–E)**. Receiver operating characteristic (ROC) curves for the ability of five individual HCMV miRNAs to discriminating fever patients from controls subjects in all the samples that were enrolled in the training set, validation set and the testing sets.

3.8 Correlations between the concentration of serum HCMV miRNAs and hematological parameters

To further examine the clinical association between the five selected HCMV miRNAs and hematological indices, we conducted a multiple nonparametric correlation analysis. The results showed that the concentrations of four of the five HCMV miRNAs were significantly negatively correlated with the blood C-reaction protein (CRP) concentrations in all fever patients (standardized coefficient R ranged from −0.151 to −0.217; $P < 0.05$) (Table 4). These data indicate that increased HCMV virus

TABLE 3 Univariate and multivariate logistic regression analyses of the five selected serum HCMV miRNAs as potential risk factors for patients with fever.

Variable	Univariate analysis			Multivariate analysis		
	OR	95% CI	P value	OR	95% CI	P value
Age	1.013	1.000-1.026	0.053	–	–	0.103
Sex	1.064	0.661-1.713	0.799	–	–	0.289
hcmv-miR-US4-3p	8.688	4.923-15.331	< 0.001	–	–	0.215
hcmv-miR-US29-3p	9.13	5.268-15.826	< 0.001	6.47	2.893-14.470	< 0.001
hcmv-miR-US5-2-3p	6.144	3.580-10.546	< 0.001	–	–	0.868
hcmv-miR-UL112-3p	4.303	2.620-7.068	< 0.001	–	–	0.517
hcmv-miR-US33-3p	4.153	2.510-6.870	< 0.001	2.753	1.255-6.043	0.012
WBC	1.257	1.147-1.377	< 0.001	1.311	1.123-1.530	0.001
Lymphocyte	0.904	0.881-0.928	< 0.001	0.928	0.899-0.957	< 0.001
Monocytes	1.347	1.205-1.506	< 0.001	1.617	1.346-1.942	< 0.001
Neutrophil	1.079	1.056-1.104	< 0.001	–	–	0.732
Acidophilicgranulocyte	0.839	0.737-0.955	0.008	0.797	0.685-0.927	0.003
Basophil	0.341	0.141-0.824	0.017	–	–	0.292

titers or virus reactivation were correlated with the severity of the immune response of fever patients. Nevertheless, no significant association was observed between the concentrations of the candidate miRNAs and other blood parameters (Table 4).

We also analyzed the association between the concentrations of the five serum HCMV miRNAs and the contents of HCMV DNA titers and serum HCMV IgG/IgM in the testing set samples. As expected, there was no significant statistical correlation between HCMV miRNAs and HCMV IgG/IgM indicators ($P > 0.05$) (Figure 5). Notably, the serum levels of the five HCMV miRNA were significantly correlated with the contents of HCMV DNA titers ($P < 0.05$) (Figure 5).

3.9 Target gene analysis of HCMV miRNA

To explore the potential biological function of the five HCMV miRNAs, target genes prediction analyzes for the five HCMV miRNAs were performed by using TargetScan Human 5.2 Custom (https://www.targetscan.org/vert_50/seedmatch.html). As showed in Supplementary Table 2, a total of 143, 10, 117, 33, and 7 genes were predicted as potential target of hcmv-miR-US4-3p, hcmv-miR-US29-3p, hcmv-miR-US5-2-3p, hcmv-miR-UL112-3p and hcmv-miR-US33-3p, respectively. Notably, five genes including NUFIP2, ANKH, TNPO1, BCL11A, and LRRC59 were the common targets of hcmv-miR-US4-3p, hcmv-miR-UL112-3p and hcmv-miR-US5-2-3p.

4 Discussion

Despite the rapid progress in the comprehensive physical examination and exhaustive workup in the hospital, fever remains a diagnostic and therapeutic challenge for expert physicians, especially in primary treatment (22). This is because the etiologies of fever vary with the region and time. Infections and NIID are the leading cause of fever. However, reportedly, the ratios of undiagnosed fever cases have gradually increased (4, 23). This led us to explore the potential etiology and diagnostic methods for fever. HCMV is a highly prevalent virus in the human population and an important infectious pathogen that induces morbidity and mortality in immunocompromised individuals. Unfortunately, the mechanism of HCMV pathogenesis remains obscure (10). Patients with fever usually have significantly immunocompromised signs, which can be induced by many pathogens (24). Many studies have demonstrated that miRNAs—small non-coding RNAs—are involved in HCMV pathogenesis. These miRNAs alter the host immune system. However, the clinical relevance between HCMV-encoded miRNAs and fever has rarely been investigated. We designed a retrospective case-control study to uncover the potential association between HCMV and fever. By conducting a comprehensive profiling analysis of HCMV miRNAs in the serum of fever patients using RT-qPCR, we found a higher prevalence of HCMV miRNAs in fever patients, and 17 out of 24 (70.8%) measured HCMV miRNAs were markedly elevated in serum samples from fever patients compared with the normal controls. Moreover, ROC curves and multiple rank correlation analyses revealed a strong relationship between selected HCMV miRNAs and fever status. To date, this study is the first comprehensive analysis of circulating HCMV miRNA in fever patients. Our results not only reveal an increased number of novel risk factors for molecular assessment and management of fever but also provide potential etiology, pathogenesis, and progression mechanism of HCMV.

HCMV reactivates in response to immunosuppression, inflammation, infection, or stress (10). Evidence shows the potential link between HCMV infection and fever (25); however, the pathologic function of HCMV involved in these diseases remains relatively unexplored (26). A prospective multicenter

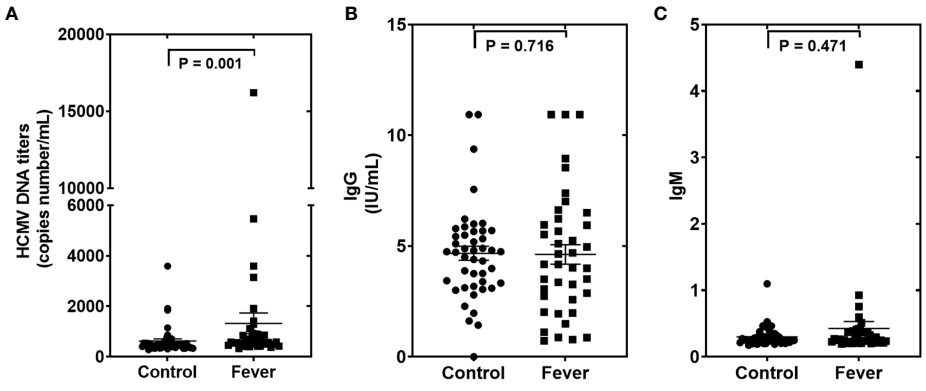

FIGURE 4
The human cytomegalovirus (HCMV) DNA, anti-HCMV IgG, and anti-HCMV IgM levels in patients with fever and healthy controls of the testing set **(A–C)**. Comparison of HCMV DNA copy numbers. **(A)**, anti-HCMV IgG **(B)**, and anti-HCMV IgM **(C)** in the fever patient's vs the control subjects. P values were calculated by the Mann-Whitney U test.

10.3389/fimmu.2022.1079259

TABLE 4 Relationship between the five selected HCMV miRNAs expression levels in serum and hematological and serological indices.[a]

miRNA		WBC	Lymphocyte	Monocytes	Neutrophil	Acidophilicgranulocyte	Basophil	CRP	Globularproteins	PCT	IL-6
hcmv-miR-US4-3p	*R*	-0.091	0.046	-0.089	-0.026	-0.066	-0.024	-0.151	-0.077	0.174	-0.209
	P value	0.291	0.591	0.299	0.765	0.443	0.781	0.084	0.377	0.131	0.116
hcmv-miR-US29-3p	*R*	-0.116	0.047	-0.032	-0.039	-0.017	-0.021	-0.199	-0.146	0.143	-0.220
	P value	0.174	0.588	0.713	0.654	0.846	0.807	0.023	0.091	0.215	0.098
hcmv-miR-US-5-2-3p	*R*	-0.098	0.053	-0.027	-0.047	-0.007	0.021	-0.217	-0.113	0.183	-0.186
	P value	0.255	0.539	0.751	0.588	0.940	0.803	0.013	0.194	0.112	0.161
hcmv-miR-UL112-3p	*R*	-0.046	0.027	-0.024	-0.031	0.008	0.007	-0.184	-0.082	0.137	-0.178
	P value	0.591	0.758	0.778	0.721	0.926	0.932	0.036	0.346	0.234	0.180
hcmv-miR-US33-3p	*R*	-0.071	0.064	-0.063	-0.052	-0.040	0.025	-0.181	-0.070	0.065	-0.159
	P value	0.411	0.457	0.463	0.550	0.645	0.776	0.039	0.417	0.572	0.234

[a]Spearman rank correlation analysis.

survey of 154 patients with fever in twelve Turkish tertiary care hospitals found five cases diagnosed as CMV infection (23). Another group found that HCMV reactivation was related to fever patients during neutropenia (27). HCMV was also detected in the colonic mucosa of patients with fever (28). As the second most common cause of fever, the pathologic mechanisms of CTD are still largely unknown, and HCMV infection has been reported to participate in CTD pathogenesis (29, 30). Studies have observed a higher prevalence or activity of HCMV in various autoimmune diseases, such as systemic lupus erythematosus (31) and systemic sclerosis (32). Collectively, these data further highlight the clinical relevance of HCMV and fever. We found that the levels of most HCMV miRNAs were increased in the blood of fever patients, elucidating a potential link between HCMV and fever. The univariate logistic regression analyses revealed that the five HCMV miRNAs were independently correlated with fever using the control group as the reference category. Moreover, after multivariate logistic regression with adjustment for age, gender, and other hematological indices, HCMV-encoded miR-US29-3p and miR-US33-3p remained a strong risk factor for fever. Additionally, four of the five miRNAs were significantly associated with CRP levels. The exact reason for the negative correlation between the serum HCMV miRNAs' levels and blood CRP contents remain unclear. One possible explanation is that HCMV under latent infection status in healthy subjects with normal immunity, however, fever patients with high CRP levels often exhibited immunocompromised status, and the HCMV can be reactive when the host organism immunity attenuate (33). Nevertheless, Further studies and direct evidences are still needed to clarify this issue. Thus, these results indicated that HCMV miRNAs might act as a novel auxiliary evaluation index for fever and are closely associated with immune response. Our findings contribute to the early implementation of medical treatment and provide useful information to help physicians refine their early therapeutic interventions.

The intrinsic mechanisms of HCMV miRNA upregulation in the circulation of fever patients are yet to be elucidated. Multiple studies from our group and others have documented that miRNAs are either selectively packed into microvesicles and actively secreted or they passively leak from broken cells into the circulation (34). Moreover, HCMV can deliver its miRNAs through virions and dense bodies (35, 36). We speculated that activated HCMV in the infected cells might release miRNAs into the blood. However, we did not study the state of HCMV in the present study. Emerging studies have reported the presence of cell-free viral miRNAs in the plasma derived from the active release of viral particles or lysis of infected cells. The viral miRNAs were detectable in systemically circulating exosomes in EBV and KSHV-associated malignancies patients (37, 38). Moreover, human JC polyomavirus-encoded miRNAs can be detected in the plasma and urine samples of progressive multifocal leukoencephalopathy patients (39). These studies further confirm our hypothesis. Although the cell types releasing

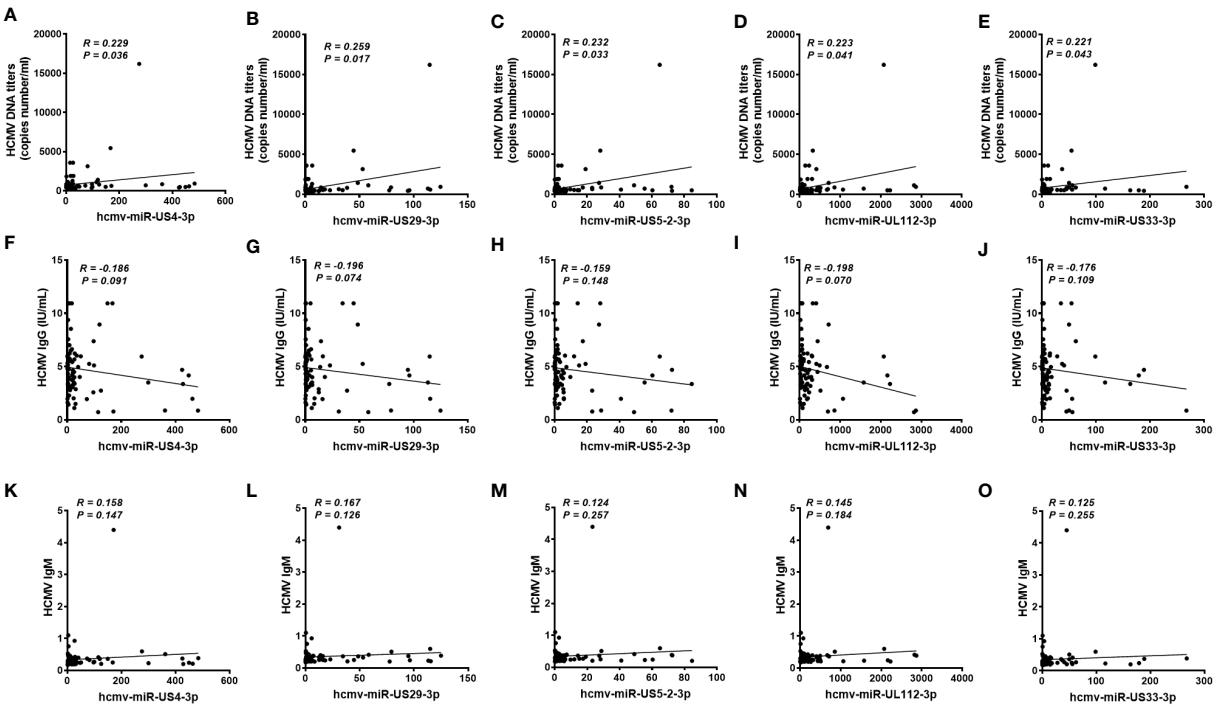

FIGURE 5
Correlation analysis of serum levels of the five selected HCMV miRNAs and the human cytomegalovirus (HCMV) DNA, anti-HCMV IgG, and anti-HCMV IgM levels in patients with fever and healthy controls of the testing set **(A–O)**. Correlations between the serum levels of the five selected HCMV miRNAs and HCMV DNA contents **(A-E)**, anti-HCMV IgG **(F-J)** and anti-HCMV IgM **(K-O)**.

HCMV miRNAs into the blood remain unclear, HCMV might target the highly susceptible cell types, such as endothelial cells, macrophages, and monocytes. However, further studies need to confirm the exact origin of these miRNAs.

Our study confirmed five of the 17 upregulated HCMV miRNAs to be significantly elevated in the serum of fever patients. Of the five altered miRNAs, miR-UL112-3p was the most reported miRNA. It is ectopically expressed early after infection and accumulates during viral infection. Many studies suggest that this miRNA might be involved in regulating both host and viral gene expression during viral infection to establish and maintain latency through targeting genes, such as MICB, immediate-early (IE) gene products, Toll-Like Receptor (TLR), and Interleukin-32 (IL-32) (11). Remarkably, two recent studies highlighted that serum levels of miR-UL112-3p were significantly elevated in patients with essential hypertension, diabetes mellitus, and glioblastoma (14, 15). In addition, immune and inflammation-associated interferon regulatory factor 1 was demonstrated to be a direct target of miR-UL112-3p (14). Abundant expression of miR-US5-2-3p was observed during HCMV lytic infection in human embryo lung fibroblasts, suggesting that these miRNAs function in the HCMV replication cycle and viral DNA synthesis (40). miR-US5-2-3p was also reported to regulate the viral gene US7 later in the infection (41). A recent study found that the two HCMV miRNAs identified in our study can cooperatively target multiple genes belonging to the cell secretory pathway to limit cytokine release and aid in the proper assembly and release of the viral particles (42). Currently, we are unaware of the role of miR-US4-3p, miR-US29-3p, and miR-US33-3p. Our results and the abovementioned findings suggest that the HCMV miRNAs identified in our study might be involved in the pathological process of fever and immune disorders by regulating HCMV infection-related genes. This idea will be further validated in ongoing *in vitro* and *in vivo* studies.

Our bioinformatic analysis results revealed that a number of genes could be regulated by the five HCMV miRNAs. More interestingly, of these predicted targets, five genes including NUFIP2, ANKH, TNPO1, BCL11A, and LRRC59 were recognized as the common targets of hcmv-miR-US4-3p, hcmv-miR-UL112-3p and hcmv-miR-US5-2-3p. Performing the literature survey for the five genes, NUFIP2 were found to be closely associated with immune disease, including rheumatoid arthritis, and may participate in immune response-regulating signaling pathway as well as immune cell function (43, 44). Like NUFIP2, ANKH was also reported to be involved in the pathogenesis of arthritis, immune and inflammatory response (45, 46). For TNPO1, reports found that this gene was associated with protein localization and transport, inflammatory-immune response, and tumor immune evasion (47–49). BCL11A was reported to be associated with adaptive and innate immunity,

especially for dendritic cell and lymphoid development, and genome-wide association studies demonstrated that this gene is participated in immune-mediated inflammatory disease such as COVID-19 and autoimmune diseases (50–53). LRRC59 was identified as a vital positive regulator of type I IFN signaling upon virus infection and acted role in innate antiviral responses (54). Moreover, upregulated LRRC59 protein levels were reported after immune stimulation and would greatly facilitate the processes of lymphocytes immune phenotypes occurring (55). Collectively, these evidences further indicated that the altered HCMV miRNAs are therefore likely to be play pivot roles in inflammatory-immune disorders.

Our study has some limitations. First, we observed no significant difference in the levels of sera IgG and IgM in fever patients when compared with controls, and these results revealed no direct evidence for CMV activation in those fever patients. The high positive rate for IgG and high negative rate for IgM were also reported in other similar pioneer studies (14, 15). These studies and our findings suggest that the detected IgG/IgM may not reflect the actual virus activation in the HCMV-infected and reactivation population. Nevertheless, HCMV DNA titers were elevated in the serum samples of fever patients compared with the controls and were positively correlated with the levels of the five HCMV miRNAs. These results can partially prove that HCMV reactivation occurs in fever patients with immune disorders. Another weak point of the present study is that all the fever patients and controls in our study were Chinese Han from one medical center. Since the causes of fever vary depending on the region and time, we cannot assume that the HCMV miRNA profiles will be consistent in other ethnicities and medical centers.

In conclusion, our study demonstrated for the first time that HCMV miRNAs can be detected in the circulation of fever patients and altered HCMV miRNAs are common in fever patients with immune disorders. Moreover, altered HCMV miRNAs could be novel risk factors for fever, allowing further auxiliary diagnosis and management of fever patients. Our data reveal a novel phenomenon that HCMV miRNA expression patterns might reflect the immune response of the host, and provide new clues and direction to explore the etiology of fever.

Data availability statement

The original contributions presented in the study are included in the article/Supplementary Material. Further inquiries can be directed to the corresponding authors.

Ethics statement

The studies involving human participants were reviewed and approved by the ethics committee board of Jinling hospital. Written informed consent to participate in this study was provided by the participants' legal guardian/next of kin.

Author contributions

Conceptualization, C-YZ, CNZ, and J-JW. Data curation, ChengW, MD, YZ, PC, and CPZ. Formal analysis, ChengW, WZ, ChenW, and JW. Funding acquisition, ChengW and CNZ. Methodology, ChengW, MD, XC, CNZ, and C-YZ. Resources, J-JW, C-YZ, YZ, and CNZ. Supervision, CNZ, C-YZ, and J-JW. Roles/writing and original draft, ChengW and CNZ. Writing, review and editing, J-JW, ChenW, and C-YZ. All authors contributed to the article and approved the submitted version.

Funding

This work was supported by grants from National Natural Science Foundation of China (no. 81772282 and 82072376), Fund of State Key Laboratory of Analytical Chemistry for Life Science (no. 5431ZZXM1907), Natural Science Foundation of Jiangsu Provincial (BK20211132), and Fund of Jiangsu Postdoctoral Science Foundation (2021K322C). The funder played no role in the study.

Acknowledgments

We would like to thank Editage (www.editage.com) for English language editing.

Conflict of interest

The authors declare that the research was conducted in the absence of any commercial or financial relationships that could be construed as a potential conflict of interest.

Publisher's note

Supplementary material

The Supplementary Material for this article can be found online at: https://www.frontiersin.org/articles/10.3389/fimmu.2022.1079259/full#supplementary-material

References

1. Petersdorf RG, Beeson PB. Fever of unexplained origin: report on 100 cases. *Medicine* (1961) 40:1–30. doi: 10.1097/00005792-196102000-00001

2. Phuong HL, Nga TT, Giao PT, Hung le Q, Binh TQ, Nam NV, et al. Randomised primary health center based interventions to improve the diagnosis and treatment of undifferentiated fever and dengue in Vietnam. *BMC Health Serv Res* (2010) 10:275. doi: 10.1186/1472-6963-10-275

3. Charlier C, Perrodeau E, Levallois C, Cachina T, Dommergues M, Salomon LJ, et al. Causes of fever in pregnant women with acute undifferentiated fever: a prospective multicentric study. *Eur J Clin Microbiol Infect Dis* (2020) 39:999–1002. doi: 10.1007/s10096-019-03809-3

4. Yamanouchi M, Uehara Y, Yokokawa H, Hosoda T, Watanabe Y, Shiga T, et al. Analysis of 256 cases of classic fever of unknown origin. *Internal Med* (2014) 53:2471–5. doi: 10.2169/internalmedicine.53.2218

5. Mir T, Nabi Dhobi G, Nabi Koul A, Saleh T. Clinical profile of classical fever of unknown origin (FUO). *Caspian J Internal Med* (2014) 5:35–9. http://caspjim.com/article-1-40-en.html

6. Bleeker-Rovers CP, van der Meer JW, Oyen WJ. Fever of unknown origin. *Semin Nucl Med* (2009) 39:81–7. doi: 10.1053/j.semnuclmed.2008.10.002

7. Naito T, Mizooka M, Mitsumoto F, Kanazawa K, Torikai K, Ohno S, et al. Diagnostic workup for fever of unknown origin: a multicenter collaborative retrospective study. *BMJ Open* (2013) 3:e003971. doi: 10.1136/bmjopen-2013-003971

8. Mahmoudi S, Mehrazmay A, Salesi M, Mamishi S. Fever of unknown origin: a retrospective study of 95 children in an Iranian referral hospital. *Br J Biomed Sci* (2014) 71:40–2. doi: 10.1080/09674845.2014.11669961

9. Zhou W, Tan X, Li Y, Tan W. Human herpes viruses are associated with classic fever of unknown origin (FUO) in Beijing patients. *PloS One* (2014) 9: e101619. doi: 10.1371/journal.pone.0101619

10. Crough T, Khanna R. Immunobiology of human cytomegalovirus: from bench to bedside. *Clin Microbiol Rev* (2009) 22:76–98. doi: 10.1128/CMR.00034-08

11. Hook L, Hancock M, Landais I, Grabski R, Britt W, Nelson JA. Cytomegalovirus microRNAs. *Curr Opin Virol* (2014) 7:40–6. doi: 10.1016/j.coviro.2014.03.015

12. Dhuruvasan K, Sivasubramanian G, Pellett PE. Roles of host and viral microRNAs in human cytomegalovirus biology. *Virus Res* (2011) 157:180–92. doi: 10.1016/j.virusres.2010.10.011

13. Chen X, Ba Y, Ma L, Cai X, Yin Y, Wang K, et al. Characterization of microRNAs in serum: a novel class of biomarkers for diagnosis of cancer and other diseases. *Cell Res* (2008) 18:997–1006. doi: 10.1038/cr.2008.282

14. Li S, Zhu J, Zhang W, Chen Y, Zhang K, Popescu LM, et al. Signature microRNA expression profile of essential hypertension and its novel link to human cytomegalovirus infection. *Circulation* (2011) 124:175–84. doi: 10.1161/CIRCULATIONAHA.110.012237

15. Mohammad AA, Rahbar A, Lui WO, Davoudi B, Catrina A, Stragliotto G, et al. Detection of circulating hcmv-miR-UL112-3p in patients with glioblastoma, rheumatoid arthritis, diabetes mellitus and healthy controls. *PloS One* (2014) 9: e113740. doi: 10.1371/journal.pone.0113740

16. Ding M, Wang X, Wang C, Liu X, Zen K, Wang W, et al. Distinct expression profile of HCMV encoded miRNAs in plasma from oral lichen planus patients. *J Transl Med* (2017) 15:133. doi: 10.1186/s12967-017-1222-8

17. Gao Z, Zhou L, Bai J, Ding M, Liu D, Zheng S, et al. Assessment of HCMV-encoded microRNAs in plasma as potential biomarkers in pregnant women with adverse pregnancy outcomes. *Ann Transl Med* (2021) 9:638. doi: 10.21037/atm-20-7354

18. Pan Y, Wang N, Zhou Z, Liang H, Pan C, Zhu D, et al. Circulating human cytomegalovirus-encoded HCMV-miR-US4-1 as an indicator for predicting the efficacy of IFNalpha treatment in chronic hepatitis b patients. *Sci Rep* (2016) 6:23007. doi: 10.1038/srep23007

19. Sadeghipour S, Mathias RA. Herpesviruses hijack host exosomes for viral pathogenesis. *Semin Cell Dev Biol* (2017) 67:91–100. doi: 10.1016/j.semcdb.2017.03.005

20. Zhang J, Huang Y, Wang Q, Ma Y, Qi Y, Liu Z, et al. Levels of human cytomegalovirus miR-US25-1-5p and miR-UL112-3p in serum extracellular vesicles from infants with HCMV active infection are significantly correlated with liver damage. *Eur J Clin Microbiol Infect Dis* (2020) 39:471–81. doi: 10.1007/s10096-019-03747-0

21. Wang C, Hu J, Lu M, Gu H, Zhou X, Chen X, et al. A panel of five serum miRNAs as a potential diagnostic tool for early-stage renal cell carcinoma. *Sci Rep* (2015) 5:7610. doi: 10.1038/srep07610

22. Gafter-Gvili A, Raibman S, Grossman A, Avni T, Paul M, Leibovici L, et al. [18F]FDG-PET/CT for the diagnosis of patients with fever of unknown origin. *QJM Monthly J Assoc Physicians* (2015) 108:289–98. doi: 10.1093/qjmed/hcu193

23. Kucukardali Y, Oncul O, Cavuslu S, Danaci M, Calangu S, Erdem H, et al. The spectrum of diseases causing fever of unknown origin in Turkey: a multicenter study. *Int J Infect Dis IJID* (2008) 12:71–9. doi: 10.1016/j.ijid.2007.04.013

24. Cunha BA, Hage JE, Nouri Y. Fever of unknown origin (FUO) in an immunocompetent adult due to cytomegalovirus (CMV) with polyclonal gammopathy. *Infection* (2012) 40:327–30. doi: 10.1007/s15010-011-0191-8

25. Herbein G. Tumors and cytomegalovirus: An intimate interplay. *Viruses* (2022) 14:812. doi: 10.3390/v14040812

26. Saltoglu N, Tasova Y, Midikli D, Aksu HS, Sanli A, Dundar IH. Fever of unknown origin in Turkey: evaluation of 87 cases during a nine-year-period of study. *J Infect* (2004) 48:81–5. doi: 10.1016/j.jinf.2003.08.006

27. Persson L, Dahl H, Linde A, Engervall P, Vikerfors T, Tidefelt U. Human cytomegalovirus, human herpesvirus-6 and human herpesvirus-7 in neutropenic patients with fever of unknown origin. *Clin Microbiol Infect* (2003) 9:640–4. doi: 10.1046/j.1469-0691.2003.00578.x

28. Nihashi T, Ito K, Kato T, Kato R, Okuda M, Arima T, et al. An abnormal accumulation of fluorine-18-FDG PET in cytomegalovirus enteritis–a case report. *Ann Nucl Med* (2006) 20:75–8. doi: 10.1007/BF02985595

29. Gugliesi F, Pasquero S, Griffante G, Scutera S, Albano C, Pacheco SFC, et al. Human cytomegalovirus and autoimmune diseases: Where are we? *Viruses* (2021) 13:260. doi: 10.3390/v13020260

30. Davignon JL, Combe B, Cantagrel A. Cytomegalovirus infection: friend or foe in rheumatoid arthritis? *Arthritis Res Ther* (2021) 23:16. doi: 10.1186/s13075-020-02398-3

31. Zhang J, Dou Y, Zhong Z, Su J, Xu D, Tang F, et al. Clinical characteristics and therapy exploration of active human cytomegalovirus infection in 105 lupus patients. *Lupus* (2014) 23:889–97. doi: 10.1177/0961203314532560

32. Namboodiri AM, Rocca KM, Kuwana M, Pandey JP. Antibodies to human cytomegalovirus protein UL83 in systemic sclerosis. *Clin Exp Rheumatol* (2006) 24:176–8. https://www.clinexprheumatol.org/article.asp?a=2816

33. Zhou W, Wang C, Ding M, Bian Y, Zhong Y, Shen H, et al. Different expression pattern of human cytomegalovirus-encoded microRNAs in circulation from virus latency to reactivation. *J Transl Med* (2020) 18:469. doi: 10.1186/s12967-020-02653-w

34. Chen X, Liang H, Zhang J, Zen K, Zhang CY. Secreted microRNAs: a new form of intercellular communication. *Trends Cell Biol* (2012) 22:125–32. doi: 10.1016/j.tcb.2011.12.001

35. Mohammad AA, Costa H, Landazuri N, Lui WO, Hultenby K, Rahbar A, et al. Human cytomegalovirus microRNAs are carried by virions and dense bodies and are delivered to target cells. *J Gen Virol* (2017) 98:1058–72. doi: 10.1099/jgv.0.000736

36. Bergamelli M, Martin H, Aubert Y, Mansuy JM, Marcellin M, Burlet-Schiltz O, et al. Human cytomegalovirus modifies placental small extracellular vesicle composition to enhance infection of fetal neural cells *in vitro*. *Viruses* (2022) 14:2030. doi: 10.3390/v14092030

37. Chugh PE, Sin SH, Ozgur S, Henry DH, Menezes P, Griffith J, et al. Systemically circulating viral and tumor-derived microRNAs in KSHV-associated malignancies. *PloS Pathog* (2013) 9:e1003484. doi: 10.1371/journal.ppat.1003484

38. Meckes DGJr., Shair KH, Marquitz AR, Kung CP, Edwards RH, Raab-Traub N. Human tumor virus utilizes exosomes for intercellular communication. *Proc Natl Acad Sci United States America* (2010) 107:20370–5. doi: 10.1073/pnas.1014194107

39. Lagatie O, Van Loy T, Tritsmans L, Stuyver LJ. Viral miRNAs in plasma and urine divulge JC polyomavirus infection. *Virol J* (2014) 11:158. doi: 10.1186/1743-422X-11-158

40. Shen ZZ, Pan X, Miao LF, Ye HQ, Chavanas S, Davrinche C, et al. Comprehensive analysis of human cytomegalovirus microRNA expression during lytic and quiescent infection. *PloS One* (2014) 9:e88531. doi: 10.1371/journal.pone.0088531

41. Tirabassi R, Hook L, Landais I, Grey F, Meyers H, Hewitt H, et al. Human cytomegalovirus US7 is regulated synergistically by two virally encoded microRNAs and by two distinct mechanisms. *J Virol* (2011) 85:11938–44. doi: 10.1128/JVI.05443-11

42. Hook LM, Grey F, Grabski R, Tirabassi R, Doyle T, Hancock M, et al. Cytomegalovirus miRNAs target secretory pathway genes to facilitate formation of

the virion assembly compartment and reduce cytokine secretion. *Cell Host Microbe* (2014) 15:363–73. doi: 10.1016/j.chom.2014.02.004

43. Wu C, Tan S, Liu L, Cheng S, Li P, Li W, et al. Transcriptome-wide association study identifies susceptibility genes for rheumatoid arthritis. *Arthritis Res Ther* (2021) 23:38. doi: 10.1186/s13075-021-02419-9

44. Rehage N, Davydova E, Conrad C, Behrens G, Maiser A, Stehklein JE, et al. Binding of NUFIP2 to roquin promotes recognition and regulation of ICOS mRNA. *Nat Commun* (2018) 9:299. doi: 10.1038/s41467-017-02582-1

45. Reginato AM, Olsen BR. Genetics and experimental models of crystal-induced arthritis. lessons learned from mice and men: is it crystal clear? *Curr Opin Rheumatol* (2007) 19:134–45. doi: 10.1097/BOR.0b013e328040c00b

46. Sun Y, Mauerhan DR, Honeycutt PR, Kneisl JS, Norton JH, Hanley ENJr., et al. Analysis of meniscal degeneration and meniscal gene expression. *BMC Musculoskelet Disord* (2010) 11:19. doi: 10.1186/1471-2474-11-19

47. Zhang X, Sun R, Liu L. Potentially critical roles of TNPO1, RAP1B, ZDHHC17, and PPM1B in the progression of coronary atherosclerosis through microarray data analysis. *J Cell Biochem* (2019) 120:4301–11. doi: 10.1002/jcb.27715

48. Yang B, Chen J, Teng Y. TNPO1-mediated nuclear import of FUBP1 contributes to tumor immune evasion by increasing NRP1 expression in cervical cancer. *J Immunol Res* (2021) 2021:9994004. doi: 10.1155/2021/9994004

49. Aladeokin AC, Akiyama T, Kimura A, Kimura Y, Takahashi-Jitsuki A, Nakamura H, et al. Network-guided analysis of hippocampal proteome identifies novel proteins that colocalize with abeta in a mice model of early-stage alzheimer's disease. *Neurobiol Dis* (2019) 132:104603. doi: 10.1016/j.nbd.2019.104603

50. Ippolito GC, Dekker JD, Wang YH, Lee BK, Shaffer AL, Lin 3J, et al. Dendritic cell fate is determined by BCL11A. *Proc Natl Acad Sci United States America* (2014) 111:E998–1006. doi: 10.1073/pnas.1319228111

51. Yu Y, Wang J, Khaled W, Burke S, Li P, Chen X, et al. Bcl11a is essential for lymphoid development and negatively regulates p53. *J Exp Med* (2012) 209:2467–83. doi: 10.1084/jem.20121846

52. Kousathanas A, Pairo-Castineira E, Rawlik K, Stuckey A, Odhams CA, Walker S, et al. Whole-genome sequencing reveals host factors underlying critical COVID-19. *Nature* (2022) 607:97–103. doi: 10.1038/s41586-022-04576-6

53. Dozmorov MG, Wren JD, Alarcon-Riquelme ME. Epigenomic elements enriched in the promoters of autoimmunity susceptibility genes. *Epigenetics* (2014) 9:276–85. doi: 10.4161/epi.27021

54. Xian H, Yang S, Jin S, Zhang Y, Cui J. LRRC59 modulates type I interferon signaling by restraining the SQSTM1/p62-mediated autophagic degradation of pattern recognition receptor DDX58/RIG-I. *Autophagy* (2020) 16:408–18. doi: 10.1080/15548627.2019.1615303

55. Kleinwort KJH, Degroote RL, Hirmer S, Korbonits L, Lorenz L, Scholz AM, et al. Bovine peripheral blood derived lymphocyte proteome and secretome show divergent reaction of bovine immune phenotypes after stimulation with pokeweed mitogen. *Proteomes* (2022) 10:7. doi: 10.3390/proteomes10010007

frontiers | Frontiers in Immunology

TYPE Mini Review
PUBLISHED 18 January 2023
DOI 10.3389/fimmu.2023.1082165

OPEN ACCESS

EDITED BY
Tao Liu,
Brigham and Women's Hospital and Harvard Medical School, United States

REVIEWED BY
Fangfang Jin,
Nanjing University of Chinese Medicine, China
Santosh Kumar Yadav,
University of Nebraska Medical Center, United States
Xiao Lin,
Wenzhou Medical University, China

*CORRESPONDENCE
Zhibin Zhang
Zzhang16@mdanderson.org

SPECIALTY SECTION
This article was submitted to Cytokines and Soluble Mediators in Immunity, a section of the journal Frontiers in Immunology

RECEIVED 27 October 2022
ACCEPTED 03 January 2023
PUBLISHED 18 January 2023

CITATION
Kong Q and Zhang Z (2023) Cancer-associated pyroptosis: A new license to kill tumor.
Front. Immunol. 14:1082165.
doi: 10.3389/fimmu.2023.1082165

Cancer-associated pyroptosis: A new license to kill tumor

Qing Kong and Zhibin Zhang*

Department of Immunology, The University of Texas MD Anderson Cancer Center, Houston, TX, United States

Pyroptosis is a programmed necrotic cell death mediated by pore-forming Gasdermin (GSDM) proteins. After being unleashed from the C-terminal auto-inhibitory domains by proteolytic cleavage, the N-terminal domains of GSDMs oligomerize and perforate on the plasma membrane to induce cytolytic pyroptosis, releasing immune mediators and alarming the immune system. Upon infection or danger signal perception, GSDMD that functions downstream of the inflammasome, a supramolecular complex for inflammatory caspase activation, is cleaved and activated by inflammasome-activated caspase-1/4/5/11 in immune cells and epithelial cells to trigger pyroptosis and exert anti-infection protection. Unlike this inflammasome-activated pyroptosis (IAP), recent studies also suggest an emerging role of cancer-associated pyroptosis (CAP), mediated by other GSDMs in cancer cells, in provoking anti-tumor immunity. IAP and CAP share common features like cell membrane rupture but also differ in occurrence sites, activating mechanisms, secreting cytokines and biological outcomes. Here we review the most recent knowledge of cancer-associated pyroptosis and present a promising avenue for developing therapeutic interventions to enhance anti-tumor immunity for cancer treatment.

KEYWORDS

pyroptosis, programmed cell death, killer lymphocyte, inflammasome, anti-tumor immunity, interleukin-1β, gasdermin

Introduction: Overview of Inflammasome-activated pyroptosis

Pyroptosis was first observed in 1986, when Friedlander reported that Anthrax lethal toxin induced rapid and massive cell death in mouse peritoneal macrophages (1). Similar observations were made by Zychlinsky and colleagues in macrophages challenged with *Shigella flexneri* and *Salmonella typhimurium* (2, 3), and their studies revealed that those pathogen-induced macrophage deaths featured caspase-1 activation and were accompanied by IL-1β and IL-18 release (2, 4), but these cell deaths were classified into apoptosis (2, 3). In 2000, Cookson and Brennan reported *Salmonella*-induced cell death as caspase-1-dependent necrosis (5), which exhibits distinct features compared to apoptosis. Pyroptosis displays giant membrane ballooning, while apoptosis exhibits cell shrinkage and small blebbing. In 2001, they named this proinflammatory cell death "pyroptosis", in which

the Greek root "pyro" means fire or fever, and "ptosis" denotes falling (6). Later studies confirmed that Anthrax lethal toxin treatment, *Shigella* challenge and *Salmonella* infection all induce pyroptosis in macrophages (7, 8). Thus, pyroptosis could be originally defined as a caspase-1-mediated inflammatory cell death triggered by sensing of invasive pathogens and danger signals in macrophages. Later on, this pyroptosis was also reported in other immune and non-immune cells, such as epithelial cells and cardiomyocytes.

This classical caspase-1-dependent pyroptosis is mediated by inflammasome, manifesting IL-1β/IL-18 secretion and cell membrane rupture. The inflammasome is a multi-protein platform responsible for caspase-1 activation, proposed by Tschop and coworkers in 2002 (9). Recognition of pathogen-associated molecular patterns (PAMPs) or danger-associated molecular patterns (DAMPs) by cytosolic pattern recognition receptors (PRRs) initiate the assembly of inflammasome, during which the PRR recruits an adaptor protein called ASC (Apoptosis-associated speck-like protein containing a CARD) as well as pro-caspase-1 to form a supramolecular complex, the inflammasome. ASC contains a pyrin domain (PYD) and a caspase recruitment domain (CARD), bridging the upstream PYD-containing PRR receptor and downstream CARD-containing caspase-1. The proximity-induced auto-processing of pro-caspase-1 leads to its activation, and active caspase-1 further maturates IL-1β and IL-18, and triggers pyroptosis (10). The most studied inflammasomes include but are not limited to NLRP1b inflammasome that is activated by lethal toxin (11, 12), AIM2 inflammasome for cytoplasmic double-strand DNA recognition (13–15), NLRP3 inflammasome that detects multiple danger signal molecules such as crystalline material, extracellular ATP and pore-forming toxins (16, 17), NLRC4 inflammasome that recognizes bacterial flagellin or type III secretion system components (18, 19), and Pyrin inflammasome that monitors the modification or inactivation of Rho GTPases by pathogens (20).

In addition to caspase-1-dependent canonical inflammasomes, a non-canonical inflammasome pathway has recently been identified (21–23), in which human caspase-4/5 and mouse caspase-11 act as cytosolic receptors for lipopolysaccharides (LPS) (24), a cell wall component from Gram-negative bacteria. Upon LPS binding, pro-caspase-4/5/11 oligomerize and are auto-activated to trigger pyroptosis. Although caspase-4/5/11 do not process IL-1β or IL-18, secretion of those cytokines are also detected during non-canonical inflammasome activation, which could be attributed to the secondary activation of NLRP3 inflammasome (25–27). The extensive studies on inflammasome pathways have been reviewed in detail (10, 28) and will not be further discussed here.

Inflammasome-activated pyroptosis (IAP) is a primary defense mechanism against intracellular bacterial infections (29). During lytic pyroptosis, intracellular pathogens, immune alarmins and other cellular components are released from the dead cells. Pyroptosis promotes the clearance of bacteria by disrupting the bacterial intracellular replication niche (30), directly damaging or eliminating the bacteria (31, 32), and enhancing host immune responses such as neutrophil-mediated bacterial killing (30, 31). Nonetheless, the molecular mechanism underlying pyroptosis remained unknown for decades until the seminal discovery of gasdermin D (GSDMD) in 2015.

Identification of Gasdermins: The pyroptosis executioners

Through unbiased genome-wide CRISPR-Cas9 screens and a forward genetic screen with ethyl-*N*-nitrosourea-mutagenized mice, respectively, Shao and Dixit group independently identified gasdermin D (GSDMD) as the executor of pyroptosis in 2015 (33, 34). GSDMD is cleaved after D276 by inflammatory caspase-1/4/5/11, and the resulting GSDMD N-terminal (NT) fragment is required for pyroptosis. Later on, Shao, Lieberman and other groups discovered that GSDMD-NT induces pyroptosis by forming membrane pores (32, 35–38). GSDMD consists of a pore-forming N-terminal domain (GSDM-NT) and an autoinhibitory C-terminal domain (GSDM-CT), connected by a flexible linker. The cleavage of GSDMD in the linker by inflammatory caspases unleashes GSDM-NTs, which oligomerize and perforate on the plasma membrane, leading to the disruption of the plasma membrane and pyroptosis. The structure of the GSDMD-NT membrane pore further validated these discoveries (39).

Human GSDMD belongs to a gasdermin family of six proteins, namely GSDM A-D, GSDME (a.k.a. DFNA5) and DFNB59 (40). Gasdermin A was initially named in 2000 based on its selective expression in the gastrointestinal tract and dermis (41). In mice, there are no *GSDMB* counterpart but 3 *gsdmas* (*gsdma* 1-3) and 4 *gsdmcs* (*gsdmc 1-4*). GSDM A-E exhibit pore-forming activity because overexpressing the NT domains of those GSDMs trigger pyroptosis in HEK293T cells (36). GSDM-mediated pyroptotic cell death can be triggered by proteases other than inflammatory caspases, including apoptotic caspases, serine protease granzymes secreted by cytotoxic lymphocytes, proteases from neutrophil granules and pathogens (40). For instance, cysteine protease SpeB from *Streptococcus pyogenes* cuts GSDMA to induce pyroptosis in keratinocytes (42, 43). GSDMB can be cut and activated by GzmA (44). Both GSDMC and GSDMD could be cleaved and activated by caspase-8 (45–47), and GSDMD is also cleaved by neutrophil elastase (48, 49) and cathepsin G (50), which are implicated in neutrophil pyroptosis (netosis). GSDME is processed and activated by both Caspase-3 (51, 52) and GzmB (53, 54). More details can be found in other reviews (40). All those proteolytic cleavages similarly release the pore-forming GSDM-NTs to activate pyroptotic cell death. Therefore, pyroptosis has been redefined as gasdermin-mediated programmed necrotic cell death (55, 56), which means any cells expressing GSDMs could undergo pyroptosis, no matter through what activating mechanisms. From another perspective, GSDMs act as intracellular sensors of mislocalized cytosolic proteases. If considering SpeB as a PAMP from bacteria and Gzms as DAMPs from within, the GSDMs function as unconventional PRRs that sense danger-associated proteases and alarm the immune system by triggering pyroptosis. It will also be interesting to investigate whether GSDMs could be activated through mechanisms other than proteolytic cleavage.

The cancer-associated pyroptosis in tumors

The identification of gasdermin family proteins and their pore-forming activities decouples the inflammasome pathways and

pyroptosis, which sets the stage for subsequent discoveries of various forms of pyroptosis that are implicated in distinct biological and pathological processes, like cancer. Although GSDMD-mediated IAP has attracted considerable attention, an era of cancer-associated pyroptosis (CAP) mediated by other GSDM proteins is in sight (Figure 1). In contrast to IAP, this CAP is independent of inflammasome or caspases. It occurs in tumor cells but not immune cells and is essential in igniting anti-tumor immunity.

GSDME-mediated CAP

Among the gasdermin family, GSDME, also known as DFNA5, is the most ancient member that first appeared in invertebrate lancelets (57). It was initially identified as a mutated gene in patients with nonsyndromic hearing impairment (58). Mutations of *GSDME* from those patients all result in the skipping of exon 8, which disrupts the autoinhibition and generates an auto-active GSDME protein that causes pyroptosis in cochlear cells (52, 58). GSDME can be cleaved and activated by apoptotic caspase-3, which converts apoptosis to pyroptosis in cells highly expressing GSDME (52), and mediates post-apoptotic secondary necrosis in cells with a low level of GSDME (51). *GSDME* is silenced by promoter hypermethylation (41, 59, 60) and mutated in multiple cancers including gastric, breast, colorectal tumors and melanoma (54), suggesting GSDME could function in tumor suppression (61). Indeed, *GSMDE* expression in breast tumor, colorectal tumor and melanoma suppresses tumor growth and enhances the number and functions of tumor-infiltrated NK and CD8 T cytotoxic lymphocytes (54). This tumor inhibition depends on both infiltrating lymphocytes and the pore-forming activity of GSDME. Mechanistically, NK and CD8 T cytotoxic lymphocytes deliver granzyme B (GzmB) into GSDME-expressing tumor cells, where GzmB cuts GSDME to induce pyroptosis. This process is amplified by caspase-3 because GzmB also activates caspase-3 to cleave GSDME. The resulting pyroptosis further activates killer cell-mediated anti-tumor response, creating a positive feedback anti-tumor loop, leading to tumor suppression (54). GSDME-mediated pyroptosis can be similarly induced by Chimeric Antigen Receptor T (CAR-T) cells (53). In GSDME-expressing melanoma, the combination of BRAF inhibitors and MEK inhibitors treatment, FDA-approved therapy for BRAF V600E/K mutant melanoma, activates caspase-3 and triggers GSDME pyroptosis. This pyroptosis in melanoma cells further increases the number and function of dendritic cells and T cells in tumors, leading to tumor suppression (62).

GSDMB-mediated CAP

Killer lymphocyte-mediated tumor cell killing is a vital and final step of anti-tumor immune protection. CD8+ cytotoxic T and NK cells eliminate infected or transformed cells by releasing cytotoxic granules, which contain the pore-forming protein perforin (PFN) and cytotoxic proteases called granzymes (Gzms) (63). Gzms, delivered by PFN into target cells, cleave multiple substrates to induce cell death (63). There are 5 human granzymes, including Gzm A, B, M, H and K. GzmA and GzmB are the most abundant and best-studied Gzms.

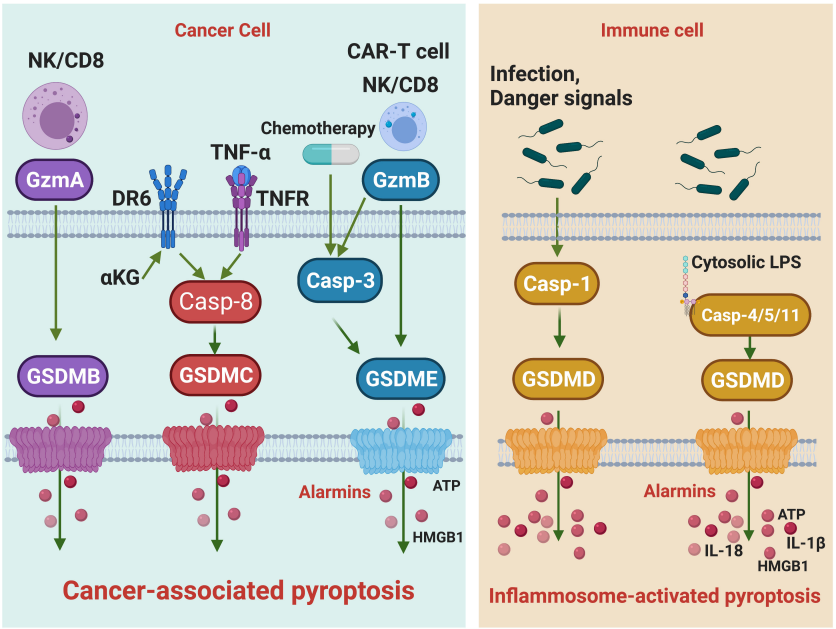

FIGURE 1
The signaling pathways of cancer-associated pyroptosis and inflammasome-activated pyroptosis. Killer lymphocytes, including NK cells and CD8 T cells, can release Gzms to activate GSDMs and trigger cancer-associated pyroptosis. GzmB cuts GSDME and GzmA cleaves GSDMB. The GzmB-induced pyroptosis can be amplified by caspase-3. In addition, chemotherapy drugs activating caspase-3 can also trigger GSDME pyroptosis. TNF-α and α-KG activate caspase-8 to initiate GSDMC-mediated cancer-associated pyroptosis, respectively. Alarmins such as ATP and HMGB1 are released during cancer-associated pyroptosis. Upon infection or danger signal perception, the assembly of canonical inflammasome leads to caspase-1 activation, which processes GSDMD to trigger inflammasome-activated pyroptosis. In the non-canonical inflammasome pathway, caspase-1/4/5 act as cytosolic receptors for lipopolysaccharide, a conserved component of Gram-negative bacterial cell wall. Recognition of LPS will activate caspase-1/4/5 to cleave GSDMD, leading to inflammasome-activated pyroptosis. Cytokines such as IL18 and IL-1β are released during inflammasome-activated pyroptosis.

GzmB cleaves after Asp residues like the caspases, and it also cleaves and activates caspase-3, which amplifies GzmB-mediated death (64). All the Gzms independently trigger cell death by different pathways (63, 65–70), which ensures that target cells resistant to any one pathway are killed. Based on those observations, one would speculate that, in addition to the GzmB/GSDME pathway, multiple Gzm pathways could lead to pyroptosis, a safeguard mechanism to ensure that GSDM-expressing target cells resistant to any one pathway are killed by pyroptosis. Indeed, shortly after identifying the GzmB/GSDME pathway, GzmA/GSDMB pathway was also reported to mediate killer cell-triggered pyroptosis (44). GzmA cleaves GSDMB after a major site K244 and a minor site K229. Human GSDMB has no counterpart in mice. However, human GSDMB expression combined with anti-PD-1 treatment significantly suppresses the growth of mouse CT26 colorectal carcinoma and B16 melanoma (44), suggesting that pyroptosis can function synergistically with immune checkpoint blockade. GSDMB expression is mainly detected in the gastrointestinal tract. GSDMB can be induced by interferon gamma (IFN-γ) and tumor necrosis factor alpha (TNF-α), which could be released by tumor-infiltrating CD8 T cells and other immune cells, thus providing a positive feedback loop. Although both GSDMB and GSDME can be activated by killer cells, it seems that GSDME is a more potent tumor suppressor than GSDMB, probably due to the initiation and amplification of GSDME pyroptosis by Caspase-3 in tumors. Whether other Gzms and GSDMs are also implicated in killer cell-triggered pyroptosis awaits further investigation.

GSDMC-mediated CAP

In addition to killer lymphocytes, cytokines and metabolites can also trigger cancer-associated pyroptosis mediated by GSDMC. A recent study revealed that upon TNF-α treatment, the active caspase-8 cleaves GSDMC, which unleashes the pore-forming GSDMC-NT to trigger pyroptosis in tumor cells (45). Of note, GSDMC normally does not express but can be induced under hypoxic stress through a PD-L1-STAT3 axis. Thus this CAP is closely related to hypoxia and restrained by PD-L1 expression and TNF-α secretion. It was proposed that GSDMC-mediated CAP promotes tumor progression by generating necrosis in tumors. However, most related experiments were performed in nude mice using human and mouse breast cancer cells, excluding the impacts of immune responses. α-Ketoglutarate (α-KG), an essential metabolite in the tricarboxylic acid (TCA) cycle, could also induce GSDMC-mediated pyroptosis in tumor cells. Mechanistically, α-KG induces the oxidation and internalization of the plasma membrane-localized death receptor DR6, which further recruits caspase-8 and GSDMC, leading to caspase-8-mediated GSDMC cleavage and pyroptosis (47). Not like TNF-α, α-KG activates DR6 from within the cells. Treatment of dimethyl-α-ketoglutarate (DM-α-KG), a cell membrane permeable analog of α-KG, suppressed the growth and metastasis of murine B16 melanoma. However, if the tumor suppressive effect of DM-α-KG depends on the immune system has not been determined yet. Further investigation is also required on the activation of GSDMC by caspase-8, because two different cleavage sites, Asp365 and Asp240, have been identified in those two studies, respectively.

CAP and anti-tumor immunity

Multiple lines of evidence suggest that CAP activates anti-tumor immunity (71). In GSDME-expression tumors, the number and function of dendritic cells, T cells and NK cells are increased (54, 62). More importantly, the tumor suppressive effect of GSMDE depends on those immune cells and is abolished in immune-deficient mice. Of note, GSDME is silenced and mutated in multiple tumors (41, 59, 60, 71), underscoring its essential role in tumor suppression. Moreover, GSDMB expression in tumors significantly increases the efficacy of immune checkpoint blockade (ICB), suggesting pyroptosis can synergize with ICB to promote anti-tumor immunity (44). A recent study has delivered GSDMA3-NT in tumor cells to induce pyroptosis (72). Phenylalanine trifluoroborate (Phe-BF3) is a cancer-imaging probe that can concentrate in tumor cells and desilylate and 'cleave' a designed linker that contains a silyl ether. GSDMA3-NT was conjugated by such a linker to the nanoparticle and was delivered and released into tumor cells by Phe-BF3-mediated desilylation. The release of GSDMA3-NT in tumors led to pyroptosis in around 10% of tumor cells, but the whole 4T1 mammary tumor graft was rejected. The tumor rejection was absent in immune-deficient mice or upon T cell depletion, suggesting pyroptosis in tumor cells activates anti-tumor immunity.

Non-pyroptotic functions of GSDMs

GSDM-mediated cancer-associated pyroptosis, in many cases, play a critical role in activating anti-tumor immunity. However, the pathological roles of GSDMs in cancers seem to be context- and cancer-type-dependent. For instance, high expression of GSDMB correlates with either better or worse survival rates in patients in a cancer-type-dependent manner (44). It is worth noting that GSDM expressions are not simply equal to pyroptosis since GSDMs can also exert non-pyroptotic functions. For example, GSDMB is implicated in epithelial immigration and regulates cell adherence (73). It also promotes tumor cell migration and breast cancer metastasis (74). GSDMD modulates mucin granule secretion in goblet cells and plays an essential role in mucus layer formation (75). GSDMD can also translocate to the nucleus and act as a PARP-1 inhibitor to induce DNA damage and apoptosis in colorectal cancer cells (76). Furthermore, GSDME transports a transcriptional factor YBX1 into the nucleus, which increases mucin expression and promotes the formation of a mucus barrier that prevents chymotrypsin-mediated destruction of pancreatic ductal adenocarcinoma (77). Therefore, the effects of GSDM expressions on tumor growth may be determined by both the pyroptosis and non-pyroptotic functions, which sometimes have opposite impacts on tumorigenesis.

IL-1β secretion in IAP and CAP

Although both are mediated by GSDM proteins, IAP and CAP are distinct from each other (Figure 1): 1) IAP mainly occurs in immune cells, and CAP mainly occurs in cancer cells. 2) IAP is mainly mediated by the inflammasome pathway, and CAP is triggered by various cytosolic proteases. 3) IAP is accompanied by the maturation

and secretion of IL-1β (and IL-18), but CAP is not. 4) IAP and CAP may lead to distinct outcomes in tumor growth. The secretion of IL-1β seemly distinguishes IAP from CAP. IL-1β plays dual roles in tumorigenesis (78). It is essential for the establishment of anti-tumor immunity in some contexts. IL-1β produced by NLRP3 IAP in dendritic cells is required to prime IFN-γ–producing CD8 T cells by dying tumor cells (79). Administration of IL-1β increased the population size and functionality of adoptively transferred T cells within the tumor (80). IL-1β is also protective in colitis-associated cancer (81) and myeloma and B-cell lymphoma (82). Nonetheless, it is well documented that IL-1β promotes tumorigenesis. Polymorphisms in the *IL-1β* gene resulting in elevated IL-1β production are associated with an increased risk of gastric cancers (83) and shorter survival in pancreatic cancer patients (84). Chemical carcinogen-induced tumorigenesis is significantly impaired in *IL-1β* knockout mice (85). Indeed, overexpressing human IL-1β in mouse stomachs leads to spontaneous gastric inflammation and cancer, possibly caused by early recruitment of myeloid-derived suppressor cells (MDSCs). Increased IL-1β production is also observed in head and neck squamous cell carcinoma (HNSCC) patients. Pharmacological inhibition of NLRP3 inflammasome in HNSCC mouse models significantly reduces the IL-1β production, which reduces MDSCs, regulatory T cells (Tregs) and tumor-associated macrophages (TAMs) but increases CD4 and CD8 T cells in tumors to improve anti-tumor immunity (86). Therefore, the recruitment of immunosuppressive cells could be a primary mechanism underlying IL-1β-mediated tumorigenesis. IL-1β may also contribute to angiogenesis and invasiveness of the tumor (87–90). The multifaceted roles of IL-1β reflect the roles of IAP and, broadly, inflammation in tumorigenesis. Chronic inflammation, caused by infection, autoimmunity, and environmental or dietary exposure, is believed to promote tumorigenesis. While acute inflammation, induced by therapy drugs or therapy-boosted killer cell attacks, usually enforces anti-tumor immunity and suppresses tumor growth (91). In this regard, IAPs, which are usually activated during infection and autoimmunity, are more likely to generate a pro-tumor chronic inflammatory environment. While CAP, as we discussed before, is mainly initiated by chemotherapy drugs and killer cell attacks that lead to acute inflammation to promote anti-tumor immunity.

Of note, CAP itself does not release IL-1β (no expression and/or activation of inflammasome components in most tumors), but IL-1β production has been observed in tumors with CAP. In CAR-T-cell-treated tumor cells, the robust CAP released a large amount of ATP, which activated NLRP3-mediated inflammasome and pyroptosis in tumor-infiltrating macrophages, leading to the release of cytokines such as IL-1β (53). This IL-1β production is reminiscent of IL-1β secretion in non-canonical inflammasome, which does not generate IL-1β but can trigger secondary NLRP3 inflammasome activation and IL-1β production. When delivering and specifically releasing an active GSDMA3 fragment into tumor cells, GSDMA3-NT similarly triggered CAP as well as IL-1β production. This IL-1β secretion could also be attributed to the secondary activation of IAP (72). Secondary IAP activation and IL-1β secretion may require robust CAP induction, and no IL-1β secretion was reported in other CAPs.

Harness cancer-associated pyroptosis to ignite anti-tumor immunity

Cancer-associated pyroptosis, rather than immunosilent apoptosis, not only directly kills some susceptible tumor cells, but also elicits robust tumor-specific immune responses, leading to the control or rejection of the entire tumor (54, 72). The role of pyroptosis in anti-tumor immunity makes GSDM proteins attractive therapeutic targets for cancer treatment. Because GSDME could be cleaved and activated by caspase-3, multiple caspase-3-activating chemotherapy drugs have been used to activate GSDME pyroptosis in tumors (92). For instance, BRAF inhibitors plus MEK inhibitors treatment can activate GSDME pyroptosis to enhance anti-tumor immunity in GSDME-expressing melanoma (62). Similar strategies have also been reported for pyroptosis mediated by other GSDMs. As mentioned, α-KG has shown its ability to trigger GSDMC-mediated pyroptosis and suppress tumor growth (47). Serine dipeptidase DPP8/9 inhibitors, which activate GSDMD-mediated pyroptosis in human myeloid cells, induce pyroptosis in most human acute myeloid leukemia cell lines and primary cells but not cells from other lineages, presenting a novel therapeutic strategy for acute myeloid leukemia (93). Multiple nano-technology-based strategies have also been developed to activate pyroptosis in tumor cells (94, 95).

Nonetheless, it is well documented that tumors can evade CAP by suppressing the expression of GSDMs, which hampers the usage of pyroptosis-activating drugs. *GSDME* is suppressed by promoter hypermethylation in gastric, colorectal and breast cancers (41, 59, 60). GSDMA and GSDMB are similarly silenced by methylation in some cancer cell lines (96, 97). DNA methyltransferase inhibitor 5-aza-2'-deoxycytosine (decitabine) upregulates *GSDME* expression and restores pyroptosis in culture cells (52, 60). Decitabine combined with chemotherapy nano-drugs triggers GSDME-mediated pyroptosis and enhances the efficacy of chemotherapy in mice (98). Thus similar strategies might also be used to increase the expressions of other GSDMs in tumors. In addition, some cytokines, chemokines and other signaling molecules could upregulate the expression of GSDMs. For instance, GSDMA is upregulated by transforming growth factor-β (TGF-β) (99), GSDMB by interferons and TNF-α (44), and GSDME by corticosteroid dexamethasone and forskolin (100). It is worth testing whether these GSDM transcriptional modulators could be combined with pyroptosis-inducing drugs to de-repress CAP and potentiate tumor-specific immune responses.

Regardless of endogenous GSDM expressions and activating mechanisms, strategy to directly introduce active GSDM proteins into tumor cells has also been proposed. A recent study described nanoparticle delivery combined with the desilylation-based release of GSDMA3-NT in tumors (72). Phenylalanine trifluoroborate (Phe-BF3) is a cancer-imaging probe that can enter cells to desilylate and 'cleave' a designed linker that contains a silyl ether. GSDMA3-NT proteins were conjugated to nanoparticles by a triethylsilyl linker, which can be cleaved by Phe-BF3. Those nanoparticles and Phe-BF3 were both concentrated in tumors, leading to the selective release of GSDMA3-NT in tumor cells to trigger CAP. Interestingly, pyroptosis of around 15% of tumor cells was sufficient to reject the entire

transplanted tumor in a T cell-dependent manner, confirming the potential of CAP in activating anti-tumor immunity and eliminating tumors.

While there are great therapeutic benefits of targeting GSDMs and pyroptosis for tumor suppression, the safety of those strategies needs to be carefully evaluated. Uncontrolled and excess activation of pyroptosis may cause severe tissue damage and other adverse effects. DPP8/9 inhibitors, which induce pyroptosis in acute myeloid leukemia, also activate pyroptosis in other cells, such as B cells and CD34+ cells (93) and augment treatment-associated toxicity. Nonspecific activation of GSDME-mediated pyroptosis in normal tissues resulted in extensive tissue damage upon chemotherapy treatments in mice (52). Secondary activation of GSDMD pyroptosis by CAP alarmins in tumor-associated macrophages lies at the root of CAR-T cell-triggered cytokine release syndrome, a severe adverse effect of CAR-T immunotherapy (53). Those observations represent the possible limitations of pyroptosis-based immunotherapeutic strategies. Thus, CAP induction *in vivo* needs to be finely controlled to achieve the specific targeting of tumor cells, which is a major challenge for pyroptosis-based immunotherapeutics.

Discussion

Identifying GSDMs and their pore-forming activity has revolutionized our understanding of pyroptosis. Pyroptosis has been redefined as a gasdermin-mediated programmed necrotic cell death. In addition to classical inflammasome-activated pyroptosis, recent studies have identified many novel forms of pyroptosis mediated by different GSDMs and activated by various proteases, most of which occur in tumor cells. Pyroptosis in tumors is a highly immunogenic cell death that activates anti-tumor immune protection. Therefore, inducing pyroptosis in tumor cells could have therapeutic utility. Nonetheless, many questions about cancer-associated pyroptosis remain elusive. 1) How does pyroptosis activate anti-tumor immunity? It has been shown that CAP is associated with more active tumor-infiltrating immune cells such as dendritic cells, CD4 and CD8 T cells and NK cells (54, 62), which lead to the control or rejection of the implanted tumors. However, the exact mechanism underlying how pyroptosis recruits and activates those immune cells remains largely unknown. 2) How do cancer cells evade anti-tumor pyroptosis? It is well documented that GSDME is silenced or mutated in multiple tumors (41, 59, 60, 71). However, GSDMB is overexpressed in multiple tumors, and it is controversial if it acts as a pore-forming protein (44, 73, 101). Further investigation is required to clarify if GSDMB-mediated pyroptosis activates anti-tumor immunity and how tumors evade this CAP. 3) How is pyroptosis regulated in cells? The regulation of IAP has been extensively studied (10, 102), but how cancer-associated pyroptosis, mediated by GSDMB, C, and E, is regulated remains elusive and awaits further investigation. 4) How can we harness pyroptosis to ignite anti-tumor immunity to treat tumors, and how can we block pyroptosis-associated toxicity? As we discussed, many strategies have been proposed to employ pyroptosis to kill tumor cells and activate the tumor-specific immune response. How to efficiently and specifically induce pyroptosis in tumor cells is the key to suppressing tumor growth but reducing pyroptosis-associated toxicity. Tumor-targeting GSDM agonists could be a possible way to address the problem.

Author contributions

ZZ and QK wrote and revised the manuscript. Both authors contributed to the article and approved the submitted version.

Funding

This study was supported by the UT system Rising STARs Award and Elsa U. Pardee Research Grant Award to ZZ.

Conflict of interest

The authors declare that the research was conducted in the absence of any commercial or financial relationships that could be construed as a potential conflict of interest.

Publisher's note

References

1. Friedlander AM. Macrophages are sensitive to anthrax lethal toxin through an acid-dependent process. *J Biol Chem* (1986) 261:7123–6. doi: 10.1016/S0021-9258(17)38364-3

2. Hersh D, Monack DM, Smith MR, Ghori N, Falkow S, Zychlinsky A. The salmonella invasin SipB induces macrophage apoptosis by binding to caspase-1. *Proc Natl Acad Sci USA* (1999) 96:2396–401. doi: 10.1073/pnas.96.5.2396

3. Zychlinsky A, Prevost MC, Sansonetti PJ. Shigella flexneri induces apoptosis in infected macrophages. *Nature* (1992) 358:167–9. doi: 10.1038/358167a0

4. Chen Y, Smith MR, Thirumalai K, Zychlinsky A. A bacterial invasin induces macrophage apoptosis by binding directly to ICE. *EMBO J* (1996) 15:3853–60. doi: 10.1002/j.1460-2075.1996.tb00759.x

5. Brennan MA, Cookson BT. Salmonella induces macrophage death by caspase-1-dependent necrosis. *Mol Microbiol* (2000) 38:31–40. doi: 10.1046/j.1365-2958.2000.02103.x

6. Cookson BT, Brennan MA. Pro-inflammatory programmed cell death. *Trends Microbiol* (2001) 9:113–4. doi: 10.1016/S0966-842X(00)01936-3

7. Fink SL, Bergsbaken T, Cookson BT. Anthrax lethal toxin and salmonella elicit the common cell death pathway of caspase-1-dependent pyroptosis *via* distinct mechanisms. *Proc Natl Acad Sci U.S.A.* (2008) 105:4312–7. doi: 10.1073/pnas.0707370105

8. Suzuki T, Franchi L, Toma C, Ashida H, Ogawa M, Yoshikawa Y, et al. Differential regulation of caspase-1 activation, pyroptosis, and autophagy *via* ipaf and ASC in shigella-infected macrophages. *PloS Pathog* (2007) 3:e111. doi: 10.1371/journal.ppat.0030111

9. Martinon F, Burns K, Tschopp J. The inflammasome: a molecular platform triggering activation of inflammatory caspases and processing of proIL-beta. *Mol Cell* (2002) 10:417–26. doi: 10.1016/S1097-2765(02)00599-3

10. Broz P, Dixit VM. Inflammasomes: mechanism of assembly, regulation and signalling. *Nat Rev Immunol* (2016) 16:407–20. doi: 10.1038/nri.2016.58

11. Boyden ED, Dietrich WF. Nalp1b controls mouse macrophage susceptibility to anthrax lethal toxin. *Nat Genet* (2006) 38:240–4. doi: 10.1038/ng1724

12. Levinsohn JL, Newman ZL, Hellmich KA, Fattah R, Getz MA, Liu S, et al. Anthrax lethal factor cleavage of Nlrp1 is required for activation of the inflammasome. *PloS Pathog* (2012) 8:e1002638. doi: 10.1371/journal.ppat.1002638

13. Fernandes-Alnemri T, Yu JW, Datta P, Wu J, Alnemri ES. AIM2 activates the inflammasome and cell death in response to cytoplasmic DNA. *Nature* (2009) 458:509–13. doi: 10.1038/nature07710

14. Hornung V, Ablasser A, Charrel-Dennis M, Bauernfeind F, Horvath G, Caffrey DR, et al. AIM2 recognizes cytosolic dsDNA and forms a caspase-1-activating inflammasome with ASC. *Nature* (2009) 458:514–8. doi: 10.1038/nature07725

15. Roberts TL, Idris A, Dunn JA, Kelly GM, Burnton CM, Hodgson S, et al. HIN-200 proteins regulate caspase activation in response to foreign cytoplasmic DNA. *Science* (2009) 323:1057–60. doi: 10.1126/science.1169841

16. Kelley N, Jeltema D, Duan Y, He Y. The NLRP3 inflammasome: An overview of mechanisms of activation and regulation. *Int J Mol Sci* (2019) 20. doi: 10.3390/ijms20133328

17. Swanson KV, Deng M, Ting JP. The NLRP3 inflammasome: molecular activation and regulation to therapeutics. *Nat Rev Immunol* (2019) 19:477–89. doi: 10.1038/s41577-019-0165-0

18. Kofoed EM, Vance RE. Innate immune recognition of bacterial ligands by NAIPs determines inflammasome specificity. *Nature* (2011) 477:592–5. doi: 10.1038/nature10394

19. Zhao Y, Yang J, Shi J, Gong YN, Lu Q, Xu H, et al. The NLRC4 inflammasome receptors for bacterial flagellin and type III secretion apparatus. *Nature* (2011) 477:596–600. doi: 10.1038/nature10510

20. Xu H, Yang J, Gao W, Li L, Li P, Zhang L, et al. Innate immune sensing of bacterial modifications of rho GTPases by the pyrin inflammasome. *Nature* (2014) 513:237–41. doi: 10.1038/nature13449

21. Hagar JA, Powell DA, Aachoui Y, Ernst RK, Miao EA. Cytoplasmic LPS activates caspase-11: implications in TLR4-independent endotoxic shock. *Science* (2013) 341:1250–3. doi: 10.1126/science.1240988

22. Kayagaki N, Warming S, Lamkanfi M, Vande Walle L, Louie S, Dong J, et al. Non-canonical inflammasome activation targets caspase-11. *Nature* (2011) 479:117–21. doi: 10.1038/nature10558

23. Kayagaki N, Wong MT, Stowe IB, Ramani SR, Gonzalez LC, Akashi-Takamura S, et al. Noncanonical inflammasome activation by intracellular LPS independent of TLR4. *Science* (2013) 341:1246–9. doi: 10.1126/science.1240248

24. Shi J, Zhao Y, Wang Y, Gao W, Ding J, Li P, et al. Inflammatory caspases are innate immune receptors for intracellular LPS. *Nature* (2014) 514:187–92. doi: 10.1038/nature13683

25. Baker PJ, Boucher D, Bierschenk D, Tebartz C, Whitney PG, D'Silva DB, et al. NLRP3 inflammasome activation downstream of cytoplasmic LPS recognition by both caspase-4 and caspase-5. *Eur J Immunol* (2015) 45:2918–26. doi: 10.1002/eji.201545655

26. Ruhl S, Broz P. Caspase-11 activates a canonical NLRP3 inflammasome by promoting k(+) efflux. *Eur J Immunol* (2015) 45:2927–36. doi: 10.1002/eji.201545772

27. Schmid-Burgk JL, Gaidt MM, Schmidt T, Ebert TS, Bartok E, Hornung V. Caspase-4 mediates non-canonical activation of the NLRP3 inflammasome in human myeloid cells. *Eur J Immunol* (2015) 45:2911–7. doi: 10.1002/eji.201545523

28. Zheng D, Liwinski T, Elinav E. Inflammasome activation and regulation: toward a better understanding of complex mechanisms. *Cell Discovery* (2020) 6:36. doi: 10.1038/s41421-020-0167-x

29. Jorgensen I, Miao EA. Pyroptotic cell death defends against intracellular pathogens. *Immunol Rev* (2015) 265:130–42. doi: 10.1111/imr.12287

30. Miao EA, Leaf IA, Treuting PM, Mao DP, Dors M, Sarkar A, et al. Caspase-1-induced pyroptosis is an innate immune effector mechanism against intracellular bacteria. *Nat Immunol* (2010) 11:1136–42. doi: 10.1038/ni.1960

31. Jorgensen I, Zhang Y, Krantz BA, Miao EA. Pyroptosis triggers pore-induced intracellular traps (PITs) that capture bacteria and lead to their clearance by efferocytosis. *J Exp Med* (2016) 213:2113–28. doi: 10.1084/jem.20151613

32. Liu X, Zhang Z, Ruan J, Pan Y, Magupalli VG, Wu H, et al. Inflammasome-activated gasdermin d causes pyroptosis by forming membrane pores. *Nature* (2016) 535:153–8. doi: 10.1038/nature18629

33. Kayagaki N, Stowe IB, Lee BL, O'Rourke K, Anderson K, Warming S, et al. Caspase-11 cleaves gasdermin d for non-canonical inflammasome signalling. *Nature* (2015) 526:666–71. doi: 10.1038/nature15541

34. Shi J, Zhao Y, Wang K, Shi X, Wang Y, Huang H, et al. Cleavage of GSDMD by inflammatory caspases determines pyroptotic cell death. *Nature* (2015) 526:660–5. doi: 10.1038/nature15514

35. Chen X, He WT, Hu L, Li J, Fang Y, Wang X, et al. Pyroptosis is driven by non-selective gasdermin-d pore and its morphology is different from MLKL channel-mediated necroptosis. *Cell Res* (2016) 26:1007–20. doi: 10.1038/cr.2016.100

36. Ding J, Wang K, Liu W, She Y, Sun Q, Shi J, et al. Pore-forming activity and structural autoinhibition of the gasdermin family. *Nature* (2016) 535:111–6. doi: 10.1038/nature18590

37. Gaidt MM, Hornung V. Pore formation by GSDMD is the effector mechanism of pyroptosis. *EMBO J* (2016) 35:2167–9. doi: 10.15252/embj.201695415

38. Sborgi L, Ruhl S, Mulvihill E, Pipercevic J, Heilig R, Stahlberg H, et al. GSDMD membrane pore formation constitutes the mechanism of pyroptotic cell death. *EMBO J* (2016) 35:1766–78. doi: 10.15252/embj.201694696

39. Xia S, Zhang Z, Magupalli VG, Pablo JL, Dong Y, Vora SM, et al. Gasdermin d pore structure reveals preferential release of mature interleukin-1. *Nature* (2021) 593:607–11. doi: 10.1038/s41586-021-03478-3

40. Liu X, Xia S, Zhang Z, Wu H, Lieberman J. Channelling inflammation: gasdermins in physiology and disease. *Nat Rev Drug Discov* (2021) 20:384–405. doi: 10.1038/s41573-021-00154-z

41. Saeki N, Kuwahara Y, Sasaki H, Satoh H, Shiroishi T. Gasdermin (Gsdm) localizing to mouse chromosome 11 is predominantly expressed in upper gastrointestinal tract but significantly suppressed in human gastric cancer cells. *Mamm Genome* (2000) 11:718–24. doi: 10.1007/s003350010138

42. Deng W, Bai Y, Deng F, Pan Y, Mei S, Zheng Z, et al. Streptococcal pyrogenic exotoxin b cleaves GSDMA and triggers pyroptosis. *Nature* (2022) 602:496–502. doi: 10.1038/s41586-021-04384-4

43. LaRock DL, Johnson AF, Wilde S, Sands JS, Monteiro MP, LaRock CN. Group a streptococcus induces GSDMA-dependent pyroptosis in keratinocytes. *Nature* (2022) 605:527–31. doi: 10.1038/s41586-022-04717-x

44. Zhou Z, He H, Wang K, Shi X, Wang Y, Su Y, et al. Granzyme a from cytotoxic lymphocytes cleaves GSDMB to trigger pyroptosis in target cells. *Science* (2020) 368:eaaz7548. doi: 10.1126/science.aaz7548

45. Hou J, Zhao R, Xia W, Chang CW, You Y, Hsu JM, et al. PD-L1-mediated gasdermin c expression switches apoptosis to pyroptosis in cancer cells and facilitates tumour necrosis. *Nat Cell Biol* (2020) 22:1264–75. doi: 10.1038/s41556-020-0575-z

46. Orning P, Weng D, Starheim K, Ratner D, Best Z, Lee B, et al. Pathogen blockade of TAK1 triggers caspase-8-dependent cleavage of gasdermin d and cell death. *Science* (2018) 362:1064–9. doi: 10.1126/science.aau2818

47. Zhang JY, Zhou B, Sun RY, Ai YL, Cheng K, Li FN, et al. The metabolite alpha-KG induces GSDMC-dependent pyroptosis through death receptor 6-activated caspase-8. *Cell Res* (2021) 31(9):980–97. doi: 10.1038/s41422-021-00506-9

48. Kambara H, Liu F, Zhang X, Liu P, Bajrami B, Teng Y, et al. Gasdermin d exerts anti-inflammatory effects by promoting neutrophil death. *Cell Rep* (2018) 22:2924–36. doi: 10.1016/j.celrep.2018.02.067

49. Sollberger G, Choidas A, Burn GL, Habenberger P, Di Lucrezia R, Kordes S, et al. Gasdermin d plays a vital role in the generation of neutrophil extracellular traps. *Sci Immunol* (2018) 3. doi: 10.1126/sciimmunol.aar6689

50. Burgener SS, Leborgne NGF, Snipas SJ, Salvesen GS, Bird PI, Benarafa C. Cathepsin G inhibition by Serpinb1 and Serpinb6 prevents programmed necrosis in neutrophils and monocytes and reduces GSDMD-driven inflammation. *Cell Rep* (2019) 27:3646–3656 e3645. doi: 10.1016/j.celrep.2019.05.065

51. Rogers C, Fernandes-Alnemri T, Mayes L, Alnemri D, Cingolani G, Alnemri ES. Cleavage of DFNA5 by caspase-3 during apoptosis mediates progression to secondary necrotic/pyroptotic cell death. *Nat Commun* (2017) 8:14128. doi: 10.1038/ncomms14128

52. Wang Y, Gao W, Shi X, Ding J, Liu W, He H, et al. Chemotherapy drugs induce pyroptosis through caspase-3 cleavage of a gasdermin. *Nature* (2017) 547:99–103. doi: 10.1038/nature22393

53. Liu Y, Fang Y, Chen X, Wang Z, Liang X, Zhang T, et al. Gasdermin e-mediated target cell pyroptosis by CAR T cells triggers cytokine release syndrome. *Sci Immunol* (2020) 5. doi: 10.1126/sciimmunol.aax7969

54. Zhang Z, Zhang Y, Xia S, Kong Q, Li S, Liu X, et al. Gasdermin e suppresses tumour growth by activating anti-tumour immunity. *Nature* (2020) 579:415–20. doi: 10.1038/s41586-020-2071-9

55. Galluzzi L, Vitale I, Aaronson SA, Abrams JM, Adam D, Agostinis P, et al. Molecular mechanisms of cell death: recommendations of the nomenclature committee on cell death 2018. *Cell Death Differ* (2018) 25:486–541. doi: 10.1038/s41418-017-0012-4

56. Shi J, Gao W, Shao F. Pyroptosis: Gasdermin-mediated programmed necrotic cell death. *Trends Biochem Sci* (2017) 42:245–54. doi: 10.1016/j.tibs.2016.10.004

57. Zhang Z, Lieberman J. Lighting a fire on the reef. *Sci Immunol* (2020) 5. doi: 10.1126/sciimmunol.abf0905

58. Van Laer L, Huizing EH, Verstreken M, van Zuijlen D, Wauters JG, Bossuyt PJ, et al. Nonsyndromic hearing impairment is associated with a mutation in DFNA5. *Nat Genet* (1998) 20:194–7. doi: 10.1038/2503

59. Croes L, de Beeck KO, Pauwels P, Vanden Berghe W, Peeters M, Fransen E, et al. DFNA5 promoter methylation a marker for breast tumorigenesis. *Oncotarget* (2017) 8:31948–58. doi: 10.18632/oncotarget.16654

60. Kim MS, Chang X, Yamashita K, Nagpal JK, Baek JH, Wu G, et al. Aberrant promoter methylation and tumor suppressive activity of the DFNA5 gene in colorectal carcinoma. *Oncogene* (2008) 27:3624–34. doi: 10.1038/sj.onc.1211021

61. de Beeck KO, Van Laer L, Van Camp G. DFNA5, a gene involved in hearing loss and cancer: a review. *Ann otol rhinol laryngol* (2012) 121:197–207. doi: 10.1177/000348941212100310

62. Erkes DA, Cai W, Sanchez IM, Purwin TJ, Rogers C, Field CO, et al. Mutant BRAF and MEK inhibitors regulate the tumor immune microenvironment via pyroptosis. *Cancer Discovery* (2020) 10:254–69. doi: 10.1158/2159-8290.CD-19-0672

63. Chowdhury D, Lieberman J. Death by a thousand cuts: granzyme pathways of programmed cell death. *Annu Rev Immunol* (2008) 26:389–420. doi: 10.1146/annurev.immunol.26.021607.090404

64. Darmon AJ, Nicholson DW, Bleackley RC. Activation of the apoptotic protease CPP32 by cytotoxic T-cell-derived granzyme b. *Nature* (1995) 377:446–8. doi: 10.1038/377446a0

65. Beresford PJ, Xia Z, Greenberg AH, Lieberman J. Granzyme a loading induces rapid cytolysis and a novel form of DNA damage independently of caspase activation. *Immunity* (1999) 10:585–94. doi: 10.1016/S1074-7613(00)80058-8

66. Heusel JW, Wesselschmidt RL, Shresta S, Russell JH, Ley TJ. Cytotoxic lymphocytes require granzyme b for the rapid induction of DNA fragmentation and apoptosis in allogeneic target cells. *Cell* (1994) 76:977–87. doi: 10.1016/0092-8674(94)90376-X

67. Hua G, Zhang Q, Fan Z. Heat shock protein 75 (TRAP1) antagonizes reactive oxygen species generation and protects cells from granzyme m-mediated apoptosis. *J Biol Chem* (2007) 282:20553–60. doi: 10.1074/jbc.M703196200

68. Lu H, Hou Q, Zhao T, Zhang H, Zhang Q, Wu L, et al. Granzyme m directly cleaves inhibitor of caspase-activated DNase (CAD) to unleash CAD leading to DNA fragmentation. *J Immunol* (2006) 177:1171–8. doi: 10.4049/jimmunol.177.2.1171

69. Shi L, Kraut RP, Aebersold R, Greenberg AH. A natural killer cell granule protein that induces DNA fragmentation and apoptosis. *J Exp Med* (1992) 175:553–66. doi: 10.1084/jem.175.2.553

70. Shresta S, Graubert TA, Thomas DA, Raptis SZ, Ley TJ. Granzyme a initiates an alternative pathway for granule-mediated apoptosis. *Immunity* (1999) 10:595–605. doi: 10.1016/S1074-7613(00)80059-X

71. Zhang Z, Zhang Y, Lieberman J. Lighting a fire: Can we harness pyroptosis to ignite anti-tumor immunity? *Cancer Immunol Res* (2020) 9(1):2–7. doi: 10.1126/science.aaz7548

72. Wang Q, Wang Y, Ding J, Wang C, Zhou X, Gao W, et al. A bioorthogonal system reveals antitumour immune function of pyroptosis. *Nature* (2020) 579:421–6. doi: 10.1158/2326-6066.CIR-20-0525

73. Rana N, Privitera G, Kondolf HC, Bulek K, Lechuga S, De Salvo C, et al. GSDMB is increased in IBD and regulates epithelial restitution/repair independent of pyroptosis. *Cell* (2022) 185:283–298 e217. doi: 10.1038/s41586-020-2079-1

74. Hergueta-Redondo M, Sarrio D, Molina-Crespo A, Megias D, Mota A, Rojo-Sebastian A, et al. Gasdermin-b promotes invasion and metastasis in breast cancer cells. *PloS One* (2014) 9:e90099. doi: 10.1016/j.cell.2021.12.024

75. Zhang J, Yu Q, Jiang D, Yu K, Yu W, Chi Z, et al. Epithelial gasdermin d shapes the host-microbial interface by driving mucus layer formation. *Sci Immunol* (2022) 7:eabk2092. doi: 10.1371/journal.pone.0090099

76. Peng X, Na R, Zhou W, Meng X, Yang Y, Amini S, et al. Nuclear translocation of gasdermin d sensitizes colorectal cancer to chemotherapy in a pyroptosis-independent manner. *Oncogene* (2022) 41(47):5092–106. doi: 10.1126/sciimmunol.abk2092

77. Lv J, Liu Y, Mo S, Zhou Y, Chen F, Cheng F, et al. Gasdermin e mediates resistance of pancreatic adenocarcinoma to enzymatic digestion through a YBX1-mucin pathway. *Nat Cell Biol* (2022) 24:364–72. doi: 10.1038/s41388-022-02503-7

78. Bent R, Moll L, Grabbe S, Bros M. Interleukin-1 beta-a friend or foe in malignancies? *Int J Mol Sci* (2018) 19. doi: 10.1038/s41556-022-00857-4

79. Ghiringhelli F, Apetoh L, Tesniere A, Aymeric L, Ma Y, Ortiz C, et al. Activation of the NLRP3 inflammasome in dendritic cells induces IL-1beta-dependent adaptive immunity against tumors. *Nat Med* (2009) 15:1170–8. doi: 10.3390/ijms19082155

80. Lee PH, Yamamoto TN, Gurusamy D, Sukumar M, Yu Z, Hu-Li J, et al. Host conditioning with IL-1beta improves the antitumor function of adoptively transferred T cells. *J Exp Med* (2019) 216:2619–34. doi: 10.1038/nm.2028

81. Allen IC, TeKippe EM, Woodford RM, Uronis JM, Holl EK, Rogers AB, et al. The NLRP3 inflammasome functions as a negative regulator of tumorigenesis during colitis-associated cancer. *J Exp Med* (2010) 207:1045–56. doi: 10.1084/jem.20181218

82. Haabeth OA, Lorvik KB, Hammarstrom C, Donaldson IM, Haraldsen G, Bogen B, et al. Inflammation driven by tumour-specific Th1 cells protects against b-cell cancer. *Nat Commun* (2011) 2:240. doi: 10.1084/jem.20100050

83. El-Omar EM, Carrington M, Chow WH, McColl KE, Bream JH, Young HA, et al. Interleukin-1 polymorphisms associated with increased risk of gastric cancer. *Nature* (2000) 404:398–402. doi: 10.1038/ncomms1239

84. Heils A, Haug K, Kunz WS, Fernandez G, Horvath S, Rebstock J, et al. Interleukin-1beta gene polymorphism and susceptibility to temporal lobe epilepsy with hippocampal sclerosis. *Ann Neurol* (2000) 48:948–50. doi: 10.1038/35006081

85. Krelin Y, Voronov E, Dotan S, Elkabets M, Reich E, Fogel M, et al. Interleukin-1beta-driven inflammation promotes the development and invasiveness of chemical carcinogen-induced tumors. *Cancer Res* (2007) 67:1062–71. doi: 10.1002/1531-8249(200012)48:6<948::AID-ANA21>3.0.CO;2-G

86. Chen L, Huang CF, Li YC, Deng WW, Mao L, Wu L, et al. Blockage of the NLRP3 inflammasome by MCC950 improves anti-tumor immune responses in head and neck squamous cell carcinoma. *Cell Mol Life Sci* (2018) 75:2045–58. doi: 10.1158/0008-5472.CAN-06-2956

87. Carmi Y, Dotan S, Rider P, Kaplanov I, White MR, Baron R, et al. The role of IL-1beta in the early tumor cell-induced angiogenic response. *J Immunol* (2013) 190:3500–9. doi: 10.1007/s00018-017-2720-9

88. Giavazzi R, Garofalo A, Bani MR, Abbate M, Ghezzi P, Boraschi D, et al. Interleukin 1-induced augmentation of experimental metastases from a human melanoma in nude mice. *Cancer Res* (1990) 50:4771–5. doi: 10.4049/jimmunol.1202769

89. Vidal-Vanaclocha F, Fantuzzi G, Mendoza L, Fuentes AM, Anasagasti MJ, Martin J, et al. IL-18 regulates IL-1beta-dependent hepatic melanoma metastasis *via* vascular cell adhesion molecule-1. *Proc Natl Acad Sci USA* (2000) 97:734–9. doi: 10.1073/pnas.97.2.734

90. Voronov E, Shouval DS, Krelin Y, Cagnano E, Benharroch D, Iwakura Y, et al. IL-1 is required for tumor invasiveness and angiogenesis. *Proc Natl Acad Sci USA* (2003) 100:2645–50. doi: 10.1073/pnas.0437939100

91. Grivennikov SI, Greten FR, Karin M. Immunity, inflammation, and cancer. *Cell* (2010) 140:883–99. doi: 10.1016/j.cell.2010.01.025

92. Liao XX, Dai YZ, Zhao YZ, Nie K. Gasdermin e: A prospective target for therapy of diseases. *Front Pharmacol* (2022) 13:855828. doi: 10.1016/j.cell.2010.01.025

93. Johnson DC, Taabazuing CY, Okondo MC, Chui AJ, Rao SD, Brown FC, et al. DPP8/DPP9 inhibitor-induced pyroptosis for treatment of acute myeloid leukemia. *Nat Med* (2018) 24:1151–6. doi: 10.3389/fphar.2022.855828

94. Muppala V, Farran B, Nagaraju GP. Pyroptosis-based nanotherapeutics: Possible mechanisms for cancer treatment. *Life Sci* (2022) 308:120970. doi: 10.1038/s41591-018-0082-y

95. Wu D, Wang S, Yu G, Chen X. Cell death mediated by the pyroptosis pathway with the aid of nanotechnology: Prospects for cancer therapy. *Angew Chem Int Ed Engl* (2021) 60:8018–34. doi: 10.1016/j.lfs.2022.120970

96. Kothari PH, Qiu W, Croteau-Chonka DC, Martinez FD, Liu AH, Lemanske RFJr., et al. Role of local CpG DNA methylation in mediating the 17q21 asthma susceptibility gasdermin b (GSDMB)/ORMDL sphingolipid biosynthesis regulator 3 (ORMDL3) expression quantitative trait locus. *J Allergy Clin Immunol* (2018) 141:2282–6:e2286. doi: 10.1002/anie.202010281

97. Moussette S, Al Tuwaijri A, Kohan-Ghadr HR, Elzein S, Farias R, Berube J, et al. Role of DNA methylation in expression control of the IKZF3-GSDMA region in human epithelial cells. *PloS One* (2017) 12:e0172707. doi: 10.1016/j.jaci.2017.11.057

98. Fan JX, Deng RH, Wang H, Liu XH, Wang XN, Qin R, et al. Epigenetics-based tumor cells pyroptosis for enhancing the immunological effect of chemotherapeutic nanocarriers. *Nano Lett* (2019) 19:8049–58. doi: 10.1371/journal.pone.0172707

99. Saeki N, Kim DH, Usui T, Aoyagi K, Tatsuta T, Aoki K, et al. GASDERMIN, suppressed frequently in gastric cancer, is a target of LMO1 in TGF-beta-dependent apoptotic signalling. *Oncogene* (2007) 26:6488–98. doi: 10.1021/acs.nanolett.9b03245

100. Webb MS, Miller AL, Thompson EB. In CEM cells the autosomal deafness gene dfna5 is regulated by glucocorticoids and forskolin. *J Steroid Biochem Mol Biol* (2007) 107:15–21. doi: 10.1038/sj.onc.1210475

101. Hansen JM, de Jong MF, Wu Q, Zhang LS, Heisler DB, Alto LT, et al. Pathogenic ubiquitination of GSDMB inhibits NK cell bactericidal functions. *Cell* (2021) 184:3178–91:e3118. doi: 10.1016/j.jsbmb.2007.02.004

102. Latz E, Xiao TS, Stutz A. Activation and regulation of the inflammasomes. *Nat Rev Immunol* (2013) 13:397–411. doi: 10.1016/j.cell.2021.04.036

frontiers | Frontiers in Immunology

TYPE Original Research
PUBLISHED 08 February 2023
DOI 10.3389/fimmu.2023.1109381

OPEN ACCESS

EDITED BY
Yanbo Wang,
Nanjing University, China

REVIEWED BY
Wang Xiqiao,
Shanghai Jiao Tong University, China
Li Wenfeng,
First Affiliated Hospital of Wenzhou Medical University, China
Shufang Cui,
China Pharmaceutical University, China

*CORRESPONDENCE
Xu Luo
luoxu@wmu.edu.cn

SPECIALTY SECTION
This article was submitted to Cytokines and Soluble Mediators in Immunity, a section of the journal Frontiers in Immunology

RECEIVED 27 November 2022
ACCEPTED 10 January 2023
PUBLISHED 08 February 2023

CITATION
Lu W, Zhang J, Wu Y, Sun W, Jiang Z and Luo X (2023) Engineered NF-κB siRNA-encapsulating exosomes as a modality for therapy of skin lesions.
Front. Immunol. 14:1109381.
doi: 10.3389/fimmu.2023.1109381

Engineered NF-κB siRNA-encapsulating exosomes as a modality for therapy of skin lesions

Wei Lu[1], Jinzhong Zhang[1], Yungang Wu[2], Wenxue Sun[3], Zipei Jiang[4] and Xu Luo[5,6,7,8]*

[1]The Quzhou Affiliated Hospital of Wenzhou Medical University, Quzhou People's Hospital, Quzhou, Zhejiang, China, [2]Department of the Orthopedics of Traditional Chinese Medicine (TCM), the First Affiliated Hospital of Wenzhou Medical University, Wenzhou, Zhejiang, China, [3]Hemodialysis Room, Department of Nephrology, the First Hospital Affiliated of Wenzhou Medical University, Wenzhou, Zhejiang, China, [4]Department of Ophthalmology, the First Hospital Affiliated of Wenzhou Medical University, Wenzhou, Zhejiang, China, [5]Wenzhou Medical University, Wenzhou, Zhejiang, China, [6]Department of Wounds and Burns, The First Affiliated Hospital of Wenzhou Medical University, Wenzhou, Zhejiang, China, [7]Key Laboratory of Intelligent Treatment and Life Support for Critical Diseases of Zhejiang Province, The First Affiliated Hospital of Wenzhou Medical University, Wenzhou, Zhejiang, China, [8]Zhejiang Engineering Research Center for Hospital Emergency and Process Digitization, Wenzhou, Zhejiang, China

Introduction: Despite the protection and management of skin has been paid more and more attention, effective countermeasures are still lacking for patients suffering from UV or chemotherapy with damaged skin. Recently, gene therapy by small interfering RNA (siRNA) has emerged as a new therapeutic strategy for skin lesions. However, siRNA therapy has not been applied to skin therapy due to lack of effective delivery vector.

Methods: Here, we develop a synthetic biology strategy that integrates the exosomes with artificial genetic circuits to reprogram the adipose mesenchymal stem cell to express and assemble siRNAs into exosomes and facilitate in vivo delivery siRNAs for therapy of mouse models of skin lesions.

Results: Particularly, siRNA enriched exosomes (si-ADMSC-EXOs) could be directly taken up by the skin cells to inhibit the expression of skin injury related genes. When mice with skin lesions were smeared with si-ADMSC-EXOs, the repair of lesioned skin became faster and the expression of inflammatory cytokines were decreased.

Discussion: Overall, this study establishes a feasible therapeutic strategy for skin injury, which may offer an alternative to conventional biological therapies requiring two or more independent compounds.

KEYWORDS

engineered, siRNA, exosomes, UV, skin lesions, therapy

Introduction

Skin is the largest area organ in the human body, which has various functions such as regulating body temperature, preventing water loss, resisting the invasion of pathogens, and preventing body trauma (1, 2). In recent years, increased extreme weather and flourished means of chemoradiotherapy have damaged the skin by UV light and chemoradiotherapy drugs. The study confirmed that the skin of chemoradiotherapy patients, newborns, elderly people and long-term outdoor workers were more vulnerable (2, 3).

Chemotherapeutic drug extravasation is a common skin injury event in the clinic, however care guidelines developed for it can only alleviate the skin injury process in the manner of extrinsic intervention (4–7). UV light and radiation can cause irreversible damage to the skin such as photosensitivity and hyperpigmentation, and current anti-wrinkle, moisturizing, and whitening products only have reparative effects on the epidermal and dermal layers (8–10). Studies have confirmed that inhibiting the expression of key genes of skin lesions such as NF-κB, AP-1, and MMPs can improve cutaneous photosensitivity and dark pigmentation after chemotherapy (11, 12). Therefore, finding novel functional molecules that improve the body's skin self-healing ability is a boon for patients with UV and chemotherapy skin lesions.

Exosomes are double membrane structured extracellular vesicles with diameters in the range of 30-200 nm (13). The special structure of exosomes can protect internal molecules from degradation by enzymes and stress, while having the ability of intercellular communication, and thus are commonly used as carriers for small molecule drug delivery (14). The variety and quantity of "cargo" loaded by natural exosomes are difficult to control, and only modified engineered exosomes can have the ability to selectively package nucleic acid drugs that target a gene of interest. Small interfering RNA (siRNA) is a short strand RNA targeting the 3'UTR region of mRNA, and siRNA can be loaded in exosomes across cells leading to silencing of their target genes (14, 15). The researchers constructed siRNA spherical nano-nucleic acids by the method of click chemistry, which can perform gene regulation and therapy on a psoriasis mouse model (15). Adipose derived mesenchymal stem cells (ADMSCs) are less difficult to access than umbilical cord and bone marrow mesenchymal stem cells, and exosomes (ADMSC-EXOs) produced by them can promote endothelial cell survival and repair dermal cells (16–18). Therefore, using ADMSCs as a carrier to biosynthesize engineered ADMSC-EXOs loaded with target siRNAs may be a promising novel gene therapy for repairing skin lesions.

Here, we *in vitro* packaged lentivirus containing siRNA against key genes (NF-κB) in skin lesions, and constructed stable cell lines secreting exosomes with high levels of siRNA (si-ADMSC-EXOs) by lentiviral transfection of ADMSCs. Subsequently, the knockdown effects of the engineered si-ADMSC-EXOs on the target genes were validated in *in vitro* cell experiments, and the therapeutic effects of the engineered si-ADMSC-EXOs on UVB induced skin lesions were further evaluated *in vivo* experiments in mice. In conclusion, we demonstrated its reparative effects on skin lesions *in vivo* and *in vitro* experiments by synthesizing engineered ADMSC-EXOs containing siRNA.

Materials and methods

Materials

C57BL6 males were purchased from the model animal Institute of Nanjing Medical University (Nanjing, China). Adipose mesenchymal stem cells (ADMSCs), HEK 293T and RAW 264.7 cell were purchased from ATCC cell bank (Shanghai, China). The synthetic siRNA was purchased from GenScript (Nanjing, China), and serum, DMEM medium was purchased from Thermo Fisher (USA). CD63, CD9, Calnexin and ALIX antibodies were purchased from Abcam (USA).

Culture and engineering of ADMSC

Cells were cultured using DMEM medium containing 10% FBS. Lentiviral packaging plasmids containing siRNA and GFP fluorescent sequences, as well as lentiviral vectors containing puromycin, were transfected into logarithmically growing HEK 293T cells, changed 6 h later, and lentiviral supernatant 48 h after transfection was collected. Cells and cell debris were removed, and 50000 g was ultracentrifuged for 2 h to concentrate viral particles, which were resuspended using sterile PBS. At ADMSC cell density of 80%, approximately 10^7 viral particles were added to 10^6 cells for transfection. After 3 days, 10^{-3} of puromycin was added and siRNA containing stable ADMSC cells (si-ADMSCs) were selected.

Cell proliferation assay

CCK-8 assay was performed to analyze cell proliferation and viability. A density of 2×10^3 cells/well was seeded in 96 well plates. 10 μL of CCK-8 solution was added per well at 12, 24, 36, 48 and 60 (h), respectively, and then cell proliferation was determined at a wavelength of 450 nm using a microplate reader.

Identification of exosomes

When cells reached 80% confluence, 10% exosome free FBS DMEM was used for rehydration, and cell supernatants were collected after 48 h of culture. Next, exosomes were obtained by centrifugation at 300 g for 10 min, followed by centrifugation at 10000 g for 1 h and ultracentrifugation at 110000 g for 70 min and resuspension with appropriate amounts of PBS. To know the number of exosomes, their particle size distribution and concentration were detected using a nanoparticle size tracking analyzer (NTA). The morphology of exosomes was observed using transmission electron microscopy (TEM). 30 μg of exosomal protein was used to perform Western blot (WB) analysis.

Fluorescent tracing of MSC exosomes

Samples of freshly ultradissociated exosomes were diluted to 1 mL with diluent C and loaded with 6 μL PKH26 to the tube, mix gently

for 30 s, let stand at room temperature for 5min. The reaction was quenched by adding 10% BSA in 2 mL PBS configuration and brought to 8.5 mL with serum-free medium. 1.5 mL of sucrose solution (0.971 M) was slowly added dropwise with a gun to an ultracentrifuge tube, and the exosome-PKH26 labeling solution was added above the sucrose buffer layer. 110000 g for over dissociation 2 h at 4 °C. The medium and middle layer were carefully aspirated and exosomes were resuspended with 1x PBS and transferred inside 10 kDa MWCO ultrafiltration tubes. Add 9 mL PBS, 0.75 mL culture medium, and centrifuge at 3000 g for 40 min to a final volume of 0.5-1 mL. The stained exosomes were added dropwise to epithelial cells cultured in serum-free exosomes, and the cells were collected after 4 h of culture for observation under a fluorescence microscope. Meanwhile, the stained exosomes were applied on the surface of mouse skin, and the absorption of exosomes was photographed under a fluorescence imaging system after 4 h.

RT-qPCR

Total RNA from cells and tissues was extracted using Trizol as previously described (19). Reverse transcription and quantitative PCR primers for siRNAs were designed using miRNA design v1.01, and all primers were synthesized at GenScript Biotech (Nanjing, China). Briefly, 2 µL of total RNA was first mixed with 5 × gDNA wiper mix and incubated at 42°C for 2 min to remove contamination of genomic DNA. Incubate the mixture at 25°C for 5 min, 50°C for 15 min, and 85°C for 5 min. Finally, SYBR dye qPCR amplification was carried out on LightCyler 96 instrument. PCR program for tsRNAs included the following steps: 95°C for 10 min, followed by 40 cycles at 95°C for 15 s and 60°C for 1 min. The threshold cycle (CT) values were determined using a fixed threshold setting.

Western blot

Exosomes or tissues were homogenized by protease free Congo beads, protein lysates were prepared using an ice bath of Pierce RIPA buffer containing protease and phosphatase inhibitors for 30min, and samples were quantified using a BCA protein assay kit. Protein samples were denatured by addition of SDS at 99° C for 5 min and run at 80 V for 30 min on 12% bis-tris stacking gel and 120 V for 1 h on separating gel according to the manufacturer's recommended protocol. Proteins were transferred to 0.2 µm PVDF membranes. Membranes were blocked with 5% nonfat milk for 1 h at room temperature, incubated with antibodies against CD63, anti-CD9 as well as anti-AlIX in 1 x TBST overnight at 4°C, washed, and incubated with the corresponding secondary antibodies for 1 h at room temperature to detect target proteins. Finally, ECL luminescent liquid was added dropwise to expose in an exposure instrument.

Animals and treatment conditions

All animal experiments were approved by the Laboratory Animal Ethics Committee of Wenzhou Medical University. 8 weeks old male C57BL/6 mice were randomly divided into four groups (n = 5), and an area of 3 × 3 cm^2 just above the back of the mice was applied with hair removal cream, scraped off after 10 min, and 0.1 mg carprofen was administered to each mouse *via* drinking water. After 48 h, the UVB lamp height was set to 1 m (W = 10^7 µJ/cm^2), the mice in the 4 groups were irradiated for 0, 16, 32, and 64 (min) times per week until the mice developed macroscopic skin lesions in the skin. Twenty 8-week-old C57BL/6 males were UV induced for 32 min as described above until the appearance of skin lesions and randomly assigned to three groups: (1) Skin smeared with 200 µL PBS, (2) Skin smeared with 200 µL ADMSC-EXOs (1 ug/µL), (3) Skin ameared with 200 µL si-ADMSC-EXOs. Treatments were given 3 times per week for 2 weeks.

H&E staining

Mice were euthanized and UV irradiated and control skin were surgically removed, fixed using 4% paraformaldehyde. Skin tissues were embedded in paraffin, sectioned (8 µM thick), UV induced inflammation, cellular infiltration and skin damage were assessed with H & E staining.

ELISA

The cell supernatant and mouse skin tissues were collected and centrifuged at 1000 g for 10 min, followed by 10000 g for 30 min, and the supernatant was taken to a clean EP tube. The levels of cytokines in the samples were then analyzed using an inflammatory cytokine multi analyte ELISArray Kit (Qiagen, Germany) according to the manufacturer's instructions. Absorbance (450 nm) was measured using a multifunctional microplate reader.

Statistical analysis

All values are expressed as mean ± SEM or mean ± SD. Statistically significant differences between the groups were analyzed using one-way or two-way analysis of variance (ANOVA). Differences with $P < 0.05$ were considered statistically significant. (Statistical significance was designated as $^{*}P < 0.05$, $^{**}P < 0.01$, $^{***}P < 0.005$, and $^{****}P < 0.001$).

Results

ADMSC derived exosomes directly taken up by skin

Exosomal membrane is a kind of cell membrane like structure, and exosomes can be taken up by cells or tissues in the way of membrane fusion. To explore the contribution of skin uptake of ADMSC derived exosomes, we characterized ADMSC exosomes obtained by ultracentrifugation and applied the stained exosomes with epithelial cells and mice skin cells for fluorescence tracing. Transmission electron microscopy (TEM) observed that exosomes extracted from ADMSC cell culture fluid were vesicle like structures with diameters ranging between 100-200 nm (Figure 1A); Further

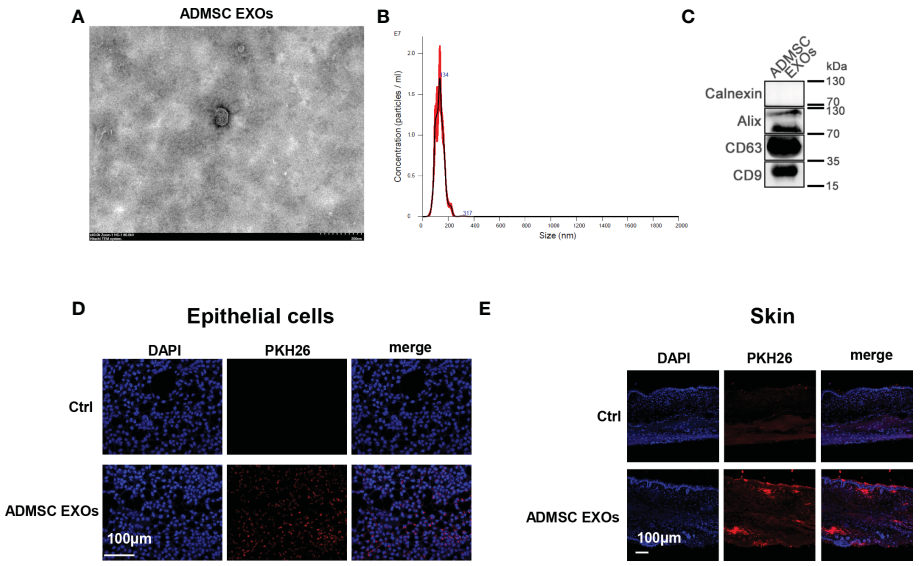

FIGURE 1
ADMSC derived exosomes directly taken up by skin. **(A, B)** Transmission electron microscopy **(A)** and nanoparticle size tracking **(B)** assay of exosomes extracted from ADMSC cell culture medium. **(C)** Analysis of the protein markers (CD9, CD63, and Alix) in ADMSC exosomes through western blot. **(D, E)** PKH26 stained ADMSC exosomes could be taken up by epithelial cells **(D)** and mouse skin tissues **(E)**.

analysis using nanoparticle size tracking (NTA) confirmed that the size distribution of ADMSC-EXOs was between 30-200 nm, with a peak size at 130 nm and a concentration of approximately 9×10^{11} particles/ml (Figure 1B). We next performed western blot (WB) analysis of membrane proteins from ADMSC-EXOs, which express CD9, CD63, and Alix characteristic of exosomes, but not calnexin, which is part of the cell membrane skeleton (Figure 1C). Next, we added the PKH26 stained exosomes into culture medium of epithelial cells, and exosomes could be absorbed by epithelial cells after 4 h incubation (Figure 1D). Besides, the stained exosomes were applied on the surface of mouse skin tissue, and the fluorescence could be detected in cuticle and dermal tissues of skin after 4 h (Figure 1E). These results suggested that ADMSC derived exosomes can be taken up by epithelial cells and mouse skin, and may function as carrier for drug delivery.

Biosynthesis of engineered si-ADMSC-EXOs

The therapeutic use of siRNA is limited by the inability of RNA molecules to reach their target cells. Recently, nature's own carriers of RNA, exosomes, are increasingly being considered as siRNA delivery vehicles due to their properties. NF-κB (nuclear factor kappa light chain enhancer of activated B cells), which is one of the key regulators of inflammatory immune responses and regulated cytokine production (e.g., interleukin-6 (IL-6) and TNF-α), plays an integral role in the pathogenesis of skin lesions. We therefore evaluated the therapeutic effects of the siRNA designed to specifically target NF-κB for the treatment of skin lesions. We constructed a genetic circuit consisting of two functional modules: the promoter module drives the transcription of siRNA, which leads to the package of saturated cytoplasmic siRNA into exosomes, while the siRNA expression cassette module maximises the expression of the siRNA guide strand and minimises the expression of undesired passenger strand. Besides, the cytomegalovirus (CMV) promoter was selected as the promoter module, and the pre-miR-155 backbone was selected as the optimal siRNA expression cassette to produce siRNA. To make the siRNA of target genes highly expressed in ADMSC exosomes, we constructed lentivirus containing these siRNA-expressed genetic circuit. After the lentivirus infected the cell, we could select the siRNA stablely expressed ADMSC cell line (si-ADMSCs). The si-ADMSC exosomes were then obtained by ultracentrifugation (Figure 2A). Quantitative PCR revealed that the siRNA expression of NF-κB was significantly higher in si-ADMSC exosomes (si-ADMSC-EXOs) than in normal ADMSC-EXOs (Figure 2B). TEM results confirmed that there was no obvious difference in the morphology between si-ADMSC-EXOs and ADMSC-EXOs, and NTA analysis also indicated that there were no significant differences in particle number and size distribution between the two types of exosomes (Figures 2C, D). Proteins of exosomes were also detected by WB, and the amount of protein expression of si-ADMSC-EXOs was similar with that of ADMSC-EXOs (Figure 2E). These results suggested the successful synthesis of siRNA overexpressed si-ADMSC-EXOs, and the characterization of si-ADMSC-EXOs and ADMSC-EXOs was not significantly different, providing the potential for gene therapy in skin lesions.

Evaluation of the activity of NF-κB siRNA-encapsulating exosomes *in vitro*

We evaluated whether the formation of NF-κB siRNA-encapsulating exosomes could reduce NF-κB expression *in vitro*. Macrophages play a central role in all stages of wound healing and orchestrate the wound healing process. Their functional phenotype is dependent on the wound microenvironment, which changes during

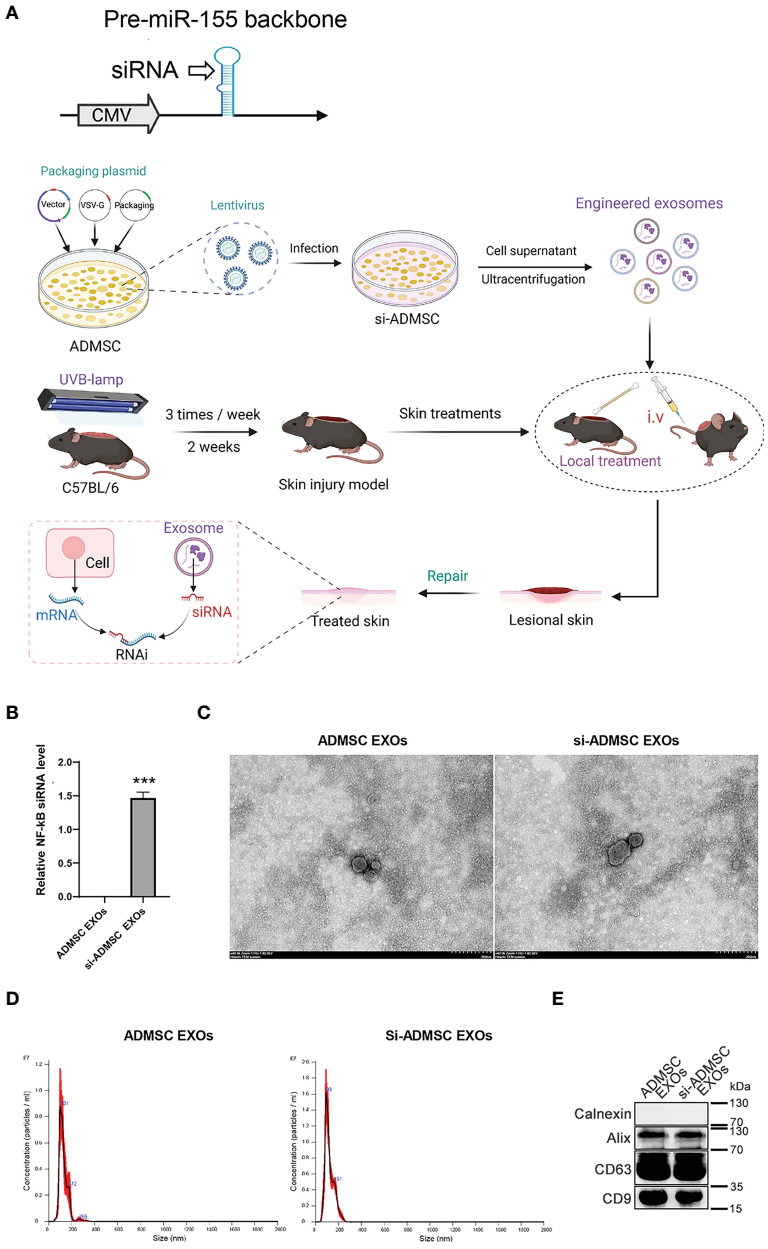

FIGURE 2
Biosynthesis of engineered si-ADMSC-EXOs. **(A)** Schematic of the experimental design. Genetic circuit were constructed consisting of two functional modules: the promoter module drives the transcription of siRNA, which leads to the package of saturated cytoplasmic siRNA into exosomes, while the siRNA expression cassette module maximises the expression of the siRNA guide strand and minimises the expression of undesired passenger strand. The cytomegalovirus (CMV) promoter was selected as the promoter module, and the pre-miR-155 backbone was selected as the optimal siRNA expression cassette to produce siRNA. We then constructed lentivirus containing these siRNA-expressed genetic circuit and infected with ADMSC cells. siRNA expressed-ADMSC cells were selected (si-ADMSCs) and the secreted exosomes were obtained through ultracentrifugation. The skin lesions were treated through swearing the si-ADMSC exosomes. **(B)** Quantitative PCR analysis the siRNA level of NF-κB in si-ADMSC exosomes and normal ADMSC exosomes. **(C-E)** Transmission electron microscopy **(C)**, nanoparticle size tracking **(D)**, western blot **(E)** assay of exosomes extracted from si-ADMSC and ADMSC cell culture medium. ***$p<0.001$.

healing, hereby altering macrophage phenotype. Pathological functioning of macrophages in the wound healing process can result in derailed wound healing, like the formation of ulcers, chronic wounds, hypertrophic scars and keloids. We first incubated si-ADMSC-EXOs with macrophage cells (RAW 264.7 cell lines) and epithelial cells, respectively, and detected the expression levels of the NF-κB. Significant decrease in NF-κB protein and mRNA expression was observed in both primary macrophages and epithelial cells (Figures 3A, B). We then explored the function of NF-κB siRNA-encapsulating exosomes in macrophage proliferation by CCK-8 assay. Compared with the mock or control group, the engineered si-ADMSC-EXOs significantly inhibited the proliferation of RAW 264.7 cells (Figure 3C). Next, we measured the levels of cytokines in RAW 264.7 cells through ELISA, and we found that the expression levels of IL-6 and TNF-α, but not IL-10, were decreased in RAW 264.7 cell relative to controls (Figure 3D). These results indicated that

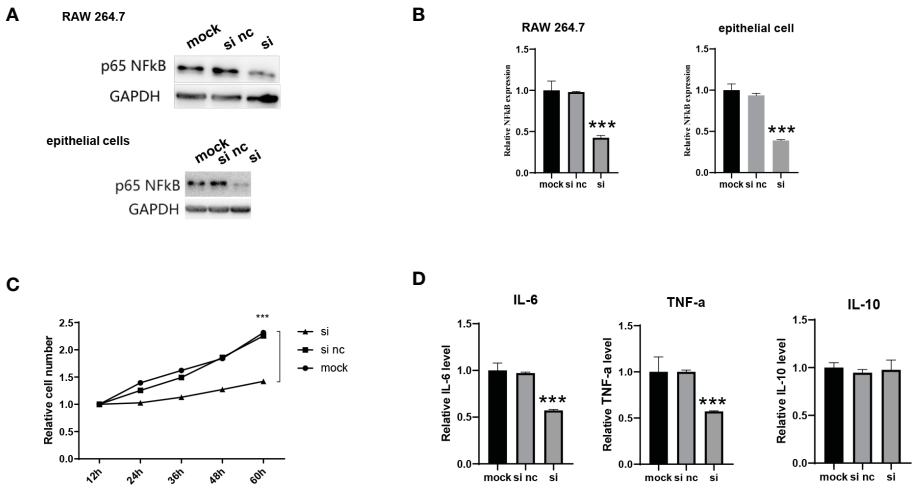

FIGURE 3
Evaluation of the activity of NF-κB siRNA-encapsulating exosomes *in vitro*. **(A, B)** The NF-κB protein **(A)** and mRNA **(B)** level of primary macrophages cells (RAW 264.7) and epithelial cells after incubating with si-ADMSC-EXOs (si) and nc-ADMSC-EXOs (si nc). **(C)** CCK-8 assay of RAW 264.7 cells after incubating with si-ADMSC-EXOs (si) and nc-ADMSC-EXOs (si nc). **(D)** ELISA assay of IL-6, TNF-α and IL-10 level in RAW 264.7 cells after incubating with si-ADMSC-EXOs (si) and nc-ADMSC-EXOs (si nc). ***$p<0.001$.

the biosynthesized engineered si-ADMSC-EXOs can effectively inhibit the expression of the target genes and inhibit the macrophage activation.

In vivo therapeutic effects of engineered si-ADMSC-EXOs in skin injury mice model

Above, we confirmed that si-ADMSC-EXOs could be taken up by epithelial cells and skin, while suppressing the expression of target genes and inhibiting the proliferation and cytokines of macrophages *in vitro*. Here, we constructed skin injury model in C57BL/6 mice by two weeks of UV irradiation and then treated by smearing ADMSC-EXOs or si-ADMSC-EXOs, respectively (Figure 2A), while negative control mice were treated without UV irradiation (vehicle). Comparing with vehicle group mice, two weeks of UV irradiation caused the mice acute skin redness and ulceration in both ADMSC-EXOs and si-ADMSC-EXOs group (Figure 4A). As expected, treating with si-ADMSC-EXOs could faster recovery the injury in skin comparing with ADMSC-EXOs group (Figure 4A). H&E staining was further employed to observe the skin pathological changes, and UV irradiation would change the nuclei of skin tissue into irregular morphology, and the epidermal layer became thicker, while the si-ADMSC-EXOs treatment group showed a higher rate of skin recovery than ADMSC-EXOs group (Figure 4B). WB analysis of the treated skin revealed that the expression of NF-κB was no significantly different between the ADMSC-EXOs and vehicle groups, but remarkably reduced in the si-ADMSC-EXOs group (Figure 4C). Consistently, the expression levels of IL-6 and TNF-α, but not IL-10 were decreased in si-ADMSC-EXOs group comparing to ADMSC-EXOs group (Figure 4D). Besides, the level of phosphorylated ERK protein (p-ERK) and c-Jun protein (p-c-Jun) were lower in si-ADMSC-EXOs group, indicating the skin inflammation was reduced (Figure 4E). Finally, by immunohistochemical analysis, the level of the macrophage marker F480 in the skin tissue was higher in the UV irradiated group than in the control group, whereas the level of the M2 type macrophage marker CD206 was higher after treatment with si-ADMSC-EXOs than in the other two groups (Figures 4F, G). These results suggested that UV irradiation promoted an increase in M1 macrophages in the skin, which secrete inflammatory cytokines; while si-ADMSC-EXOs treatment could ultimately induce M2 type macrophage activation and inhibit inflammatory responses, thereby repairing and remodeling damaged skin cells.

Discussion

Despite recent advancements in our knowledge of the pathogenic mechanisms of skin lesions, considerable unmet medical methods were needed for the repair of skin lesions for patients after UV light and chemotherapy drugs. Ectopic immune responses are one of the most promising therapeutic targets, and therapy using cytokines (e.g., TGF-β) has been specifically developed to alleviate immune responses (20). However, the weak therapeutic effect, high treatment costs and serious side effects remain serious problems for biological therapy. Therefore, it is urgent to develop an alternative strategy with high therapeutic efficiency and few side effects. Because siRNA is solely dependent on the mRNA sequence and inhibits immunological targets with strong specificity, RNAi therapy has the intrinsic ability to overcome the shortcomings of biological therapy (21). Unfortunately, the lack of safe and effective carriers for the delivery of siRNA therapeutics remains a major problem to its clinical application. For skin delivery, an ideal siRNA carrier must overcome a series of biological hurdles: it should protect siRNA from degradation by RNases in the skin surface, have proper permeability of the epidermis and no stimulatory effects on immune cells.

RNA interference is a sequence-specific, post-transcriptional gene silencing mechanism in animals and plants, offering an opportunity to inhibit mRNAs and modulate the expression of corresponding

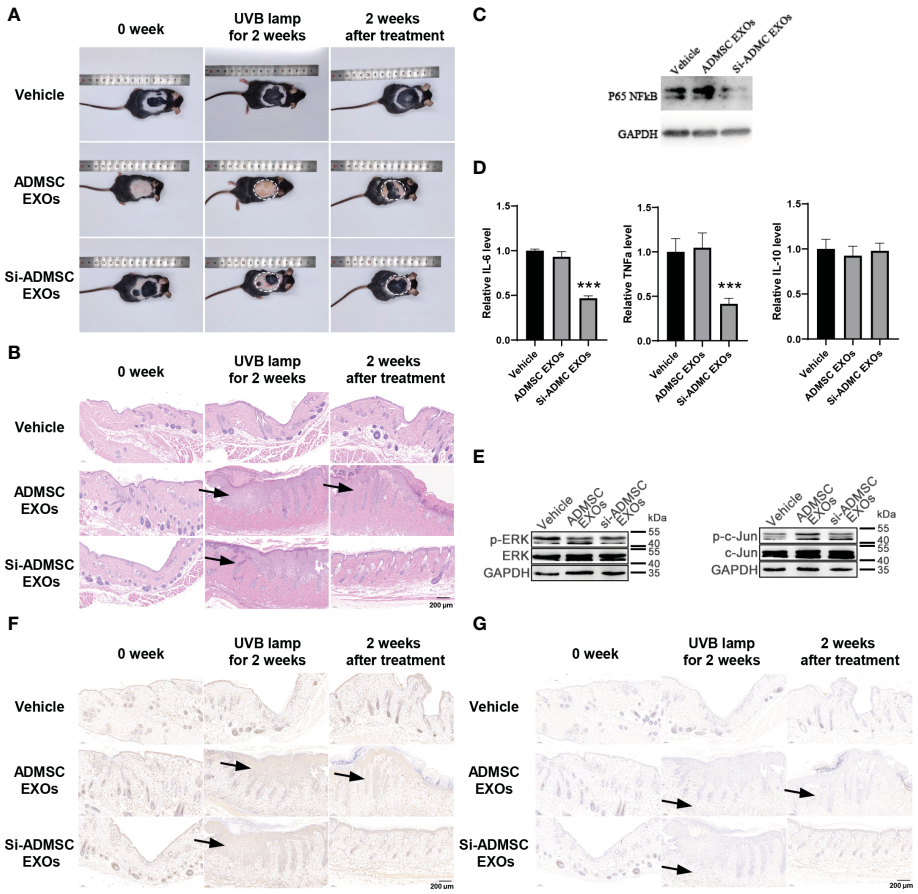

FIGURE 4
In vivo therapeutic effects of engineered si-ADMSC-EXOs in skin injury mice model. **(A)** Representative macroscopic features of skin injury. The skin injury model in C57BL/6 mice were constructed by two weeks of UV irradiation and then treated by smearing ADMSC-EXOs or si-ADMSC-EXOs exosomes; while control mice were set without UV irradiation (vehicle). **(B)** Representative images of H&E staining of mice skin injury tissues. **(C)** The protein level of NF-κB in the treated skin tissues. **(D)** ELISA assay of IL-6, TNF-α and IL-10 level in the treated skin tissues. **(E)** The protein level of phosphorylated ERK protein (p-ERK) and c-Jun protein (p-c-Jun) in the treated skin tissues. **(F, G)** Immunohistochemical analysis of the macrophage markers (F480 and CD206) in the treated skin tissues. ***$p<0.001$.

proteins, and RNAi have therefore greatly enlarged the proportion of human proteins that can be therapeutically manipulated (22, 23). The major challenge for RNAi-based therapy is the lack of an efficient *in vivo* delivery system, had elicited tremendous efforts to overcome this hurdle, including using delivery vehicles and conjugated ligands (24). In recent years, exosomes have emerged as potential drug carrier for RNA or protein, which can effectively delivery drug to recipient cells (25). Owing to their low immunogenicity, allogenic MSC- exosomes are available for repeated administration to patients without substantial side effects (25). Zhang et al. recently reported that hypoxic microenvironment induced microRNA-125b were packaged into MSC-derived exosomes, and exosomes can be taken up by endothelial cells and accelerate wound healing (11). This study demonstrated the superiority of the engineered exosomes platform for the delivery of siRNA/miRNA to targeted cell populations *in vivo*. We used a similar concept of self-assembly based on the nature of exosomes because exosomes and their cargoes are self-assembled by cells. Based on the intrinsic ability of the small RNA processing machinery of the MSCs to self-assemble siRNA into exosomes, we designed genetic circuits to engineer MSCs to self-assemble siRNAs into exosomes. Considering the short in cell half-life of the genetic circuits formed as naked DNA plasmids, we selected lentivirus as the carrier of genetic circuits because lentivirus is capable of establishing long-term transgene expression in adipose mesenchymal stem cells. Then we cultured the engineered adipose mesenchymal stem cells and collected the culture medium. We isolated the exosomes (*si-ADMSC-EXOs*) and daubed them to the sites of wounding, which resulted in significant target gene reduction and symptom alleviation in acute wounding models.

The molecular mechanism underlying the self-assembly of siRNAs into exosomes is not known. Recent studies on secretory miRNAs may provide some inspiration for this question. There are several evidences that cells selectively package certain miRNAs into EVs for active secretion (26). The promoter, miRNA/siRNA sequence and pre-miRNA structure may join together to decide the sorting route of siRNAs to exosomes in the genetic circuit design. According to previous reports, we selected CMV promoter and pre-miR-155 structure to express siRNA in MSC cells, and the siRNA were found enriched in the exosomes (26). However, there is much room for optimizing the structure of genetic circuits to guarantee the preferential sorting of siRNAs into exosomes rather than retaining them within cells.

Taken together, this study established a convenient, effective and safe strategy for assembling and delivery of siRNAs in mouse models of skin lesions. This technology has important theoretical significance and translational value because it may provide a significant therapeutic benefit for skin lesions.

Data availability statement

The raw data supporting the conclusions of this article will be made available by the authors, without undue reservation.

Ethics statement

The animal study was reviewed and approved by Laboratory Animal Ethics Committee of Wenzhou Medical University.

Author contributions

These authors were involved with this manuscript: WL and XL (study concept and design, analysis and interpretation of data); WL (drafting of the manuscript); WL, XL, YW, JZ and WS (acquisition of data; analysis and interpretation of data; statistical analysis); WL, WS and ZJ (technical or material support). All authors contributed to the article and approved the submitted version.

Funding

This work was supported by grants from the Project of Zhejiang Medical and Health Science and technology plan (Nos. 2022496777).

Conflict of interest

The authors declare that the research was conducted in the absence of any commercial or financial relationships that could be construed as a potential conflict of interest.

The reviewer LW declared a shared affiliation with the authors YW, WS, ZJ and XL to the handling editor at the time of review.

Publisher's note

References

1. Zhong J, Wang H, Yang K, Wang H, Duan C, Ni N, et al. Reversibly immortalized keratinocytes (iKera) facilitate re-epithelization and skin wound healing: Potential applications in cell-based skin tissue engineering. *Bioact Mater* (2022) 9:523–40. doi: 10.1016/j.bioactmat.2021.07.022

2. Wang L, Xian YF, Loo SKF, Ip SP, Yang W, Chan WY, et al. Baicalin ameliorates 2,4-dinitrochlorobenzene-induced atopic dermatitis-like skin lesions in mice through modulating skin barrier function, gut microbiota and JAK/STAT pathway. *Bioorg Chem* (2022) 119:105538. doi: 10.1016/j.bioorg.2021.105538

3. de Bengy AF, Lamartine J, Sigaudo-Roussel D, Fromy B. Newborn and elderly skin: Two fragile skins at higher risk of pressure injury. *Biol Rev Camb Philos Soc* (2022) 97:874–95. doi: 10.1111/brv.12827

4. Hennings H, Shores RA, Poirier MC, Reed E, Tarone RE, Yuspa SH. Enhanced malignant conversion of benign mouse skin tumors by cisplatin. *J Natl Cancer Inst* (1990) 82:836–40. doi: 10.1093/jnci/82.10.836

5. Rudolph R, Larson DL. Etiology and treatment of chemotherapeutic agent extravasation injuries: A review. *J Clin Oncol* (1987) 5:1116–26. doi: 10.1200/JCO.1987.5.7.1116

6. Olver IN, Aisner J, Hament A, Buchanan L, Bishop JF, Kaplan RS. A prospective study of topical dimethyl sulfoxide for treating anthracycline extravasation. *J Clin Oncol* (1988) 6:1732–5. doi: 10.1200/JCO.1988.6.11.1732

7. Ener RA, Meglathery SB, Styler M. Extravasation of systemic hemato-oncological therapies. *Ann Oncol* (2004) 15:858–62. doi: 10.1093/annonc/mdh214

8. Liu Z, Tang W, Liu J, Han Y, Yan Q, Dong Y, et al. A novel sprayable thermosensitive hydrogel coupled with zinc modified metformin promotes the healing of skin wound. *Bioact Mater* (2023) 20:610–26. doi: 10.1016/j.bioactmat.2022.06.008

9. Hartono SP, Bedell VM, Alam SK, O'Gorman M, Serres M, Hall SR, et al. Vascular endothelial growth factor as an immediate-early activator of ultraviolet-induced skin injury. *Mayo Clin Proc* (2022) 97:154–64. doi: 10.1016/j.mayocp.2021.08.018

10. Choi SI, Han HS, Kim JM, Park G, Jang YP, Shin YK, et al. Eisenia bicyclis extract repairs UVB-induced skin photoaging *In vitro* and *In vivo*: Photoprotective effects. *Mar Drugs* (2021) 19(12):693. doi: 10.3390/md19120693

11. Zhang XF, Wang T, Wang ZX, Huang KP, Zhang YW, Wang GL, et al. Hypoxic ucMSC-secreted exosomal miR-125b promotes endothelial cell survival and migration during wound healing by targeting TP53INP1. *Mol Ther Nucleic Acids* (2021) 26:347–59. doi: 10.1016/j.omtn.2021.07.014

12. Wang L, Kim HS, Je JG, Oh JY, Kim YS, Cha SH, et al. Protective effect of diphlorethohydroxycarmalol isolated from ishige okamurae against particulate matter-induced skin damage by regulation of NF-kappaB, AP-1, and MAPKs signaling pathways *In vitro* in human dermal fibroblasts. *Molecules* (2020) 25(5):1055. doi: 10.3390/molecules25051055

13. Su N, Hao Y, Wang F, Hou W, Chen H, Luo Y. Mesenchymal stromal exosome-functionalized scaffolds induce innate and adaptive immunomodulatory responses toward tissue repair. *Sci Adv* (2021) 7(20). doi: 10.1126/sciadv.abf7207

14. You DG, Lim GT, Kwon S, Um W, Oh BH, Song SH, et al. Metabolically engineered stem cell-derived exosomes to regulate macrophage heterogeneity in rheumatoid arthritis. *Sci Adv* (2021) 7(23). doi: 10.1126/sciadv.abe0083

15. Nemati H, Ghahramani MH, Faridi-Majidi R, Izadi B, Bahrami G, Madani SH, et al. Using siRNA-based spherical nucleic acid nanoparticle conjugates for gene regulation in psoriasis. *J Control Release* (2017) 268:259–68. doi: 10.1016/j.jconrel.2017.10.034

16. Xu J, Wang J, Liu M, Wang Y, Ashraf M, Xu M. Abstract 17239: miRNAs secreted by exosomes derived from adipose tissue mesenchymal stem cells overexpressing GATA-4 increase endothelial cell survival and promote angiogenesis. *Circulation* (2020) 142:A17239. doi: 10.1161/circ.142.suppl_3.17239

17. Squillaro T, Peluso G, Galderisi U. Clinical trials with mesenchymal stem cells: An update. *Cell Transplant* (2016) 25:829–48. doi: 10.3727/096368915X689622

18. Basu J, Ludlow JW. Exosomes for repair, regeneration and rejuvenation. *Expert Opin Biol Ther* (2016) 16:489–506. doi: 10.1517/14712598.2016.1131976

19. Jin F, Yang L, Wang W, Yuan N, Zhan S, Yang P, et al. A novel class of tsRNA signatures as biomarkers for diagnosis and prognosis of pancreatic cancer. *Mol Cancer* (2021) 20:95. doi: 10.1186/s12943-021-01389-5

20. Travis MA, Sheppard D. TGF-β activation and function in immunity. *Annurev Immunol* (2014) 32:51–82. doi: 10.1146/annurev-immunol-032713-120257

21. Setten RL, Rossi JJ, Han SP. The current state and future directions of RNAi-based therapeutics. *Nat Rev Drug Discovery* (2019) 18:421–46. doi: 10.1038/s41573-019-0017-4

22. Davidson BL, McCray PBJr. Current prospects for RNA interference-based therapies. *Nat Rev Genet* (2011) 12:329–40. doi: 10.1038/nrg2968

23. Kole R, Krainer AR, Altman S. RNA Therapeutics: Beyond RNA interference and antisense oligonucleotides. *Nat Rev Drug Discovery* (2012) 11:125–40. doi: 10.1038/nrd3625

24. Bora RS, Gupta D, Mukkur TKS, Saini KS. RNA Interference therapeutics for cancer: Challenges and opportunities (Review). *Mol Med Rep* (2012) 6:9–15. doi: 10.3892/mmr.2012.871

25. Lai RC, Chen TS, Lim SK. Mesenchymal stem cell exosome: A novel stem cell-based therapy for cardiovascular disease. *Regenerative Med* (2011) 6:481–92. doi: 10.2217/rme.11.35

26. Zhou X, Yu M, Ma L, Fu J, Guo J, Lei J, et al. *In vivo* self-assembled siRNA as a modality for combination therapy of ulcerative colitis. *Nat Commun* (2022) 13:5700. doi: 10.1038/s41467-022-33436-0

frontiers | Frontiers in Immunology

TYPE Original Research
PUBLISHED 09 February 2023
DOI 10.3389/fimmu.2023.1077645

OPEN ACCESS

EDITED BY
Tao Liu,
Brigham and Women's Hospital and Harvard Medical School, United States

REVIEWED BY
Masaki Shimizu,
Tokyo Medical and Dental University, Japan
Ke Rui,
Affiliated Hospital of Jiangsu University, China

*CORRESPONDENCE
Jun Liang
13505193169@139.com
Zhiyang Li
lizhiyangcn@qq.com
Ping Yang
pingyang@njglyy.com

†These authors have contributed equally to this work

SPECIALTY SECTION
This article was submitted to Cytokines and Soluble Mediators in Immunity, a section of the journal Frontiers in Immunology

RECEIVED 23 October 2022
ACCEPTED 30 January 2023
PUBLISHED 09 February 2023

CITATION
Chen S, Zhang X, Meng K, Sun Y, Shu R, Han Y, Feng Q, Li Z, Yang P and Liang J (2023) Urinary exosome tsRNAs as novel markers for diagnosis and prediction of lupus nephritis.
Front. Immunol. 14:1077645.
doi: 10.3389/fimmu.2023.1077645

Urinary exosome tsRNAs as novel markers for diagnosis and prediction of lupus nephritis

Shanshan Chen[1†], Xiaoshan Zhang[2†], Kaifang Meng[3], Yifan Sun[2], Ruilu Shu[1], Yan Han[1], Qingxiu Feng[1], Zhiyang Li[2*], Ping Yang[2*] and Jun Liang[1*]

[1]Department of Rheumatology and Immunology, Affiliated Nanjing Drum Tower Hospital, Medical School of Nanjing University, Nanjing, China, [2]Department of Clinical Laboratory, The Affiliated Drum Tower Hospital of Nanjing University Medical School, Nanjing, Jiangsu, China, [3]Department of Respiratory and Critical Care Medicine, Nanjing Drum Tower Hospital Clinical College of Nanjing Medical University, Nanjing, Jiangsu, China

Objective: Lupus nephritis (LN) is one of the most severe organ manifestations of systemic lupus erythematosus (SLE). Early identification of renal disease in SLE is important. Renal biopsy is currently recognized as the gold standard for diagnosing LN, however, it is invasive and inconvenient for dynamic monitoring. Urine has been considered more promising and valuable than blood in identifying inflamed kidney tissue. Here, we determine whether the signatures of tRNA-derived small noncoding RNA (tsRNA) in urinary exosomes can serve as novel biomarkers for the diagnosis of LN.

Methods: tsRNA sequencing was performed in exosome extracted from pooled urine of 20 LN patients and 20 SLE without LN, and the top 10 upregulated tsRNAs were screened as candidate markers of LN. The candidate urinary exosomal tsRNAs were primarily elected by TaqMan probe-based quantitative reverse transcription-PCR (RT-PCR) in 40 samples (20 LN and 20 SLE without LN) in the training phase. In the validation phase, selected tsRNAs from the training phase were further confirmed in a larger cohort (54 LN patients and 39 SLE without LN). Receiver operating characteristic curve (ROC) analysis was conducted to evaluate the diagnostic efficacy.

Results: Upregulated levels of tRF3-Ile-AAT-1 and tiRNA5-Lys-CTT-1 in the urinary exosomes were observed in LN compared with SLE without LN ($P < 0.0001$ and $P < 0.001$) and healthy controls ($P < 0.01$ and $P < 0.01$), with the area under the curve (AUC) of 0.777 (95% CI: 0.681-0.874, sensitivity 79.63%, specificity 66.69%) and 0.715 (95% CI: 0.610-0.820, sensitivity 66.96%, specificity 76.92%) for discriminating LN from SLE without LN patients. SLE patients with mild activity and moderate to severe activity had higher levels of urinary exosome derived tRF3-Ile AAT-1 ($P = 0.035$ and $P < 0.001$) and tiRNA5-Lys-CTT-1 ($P = 0.021$ and $P < 0.001$) compared with patients with no activity. Moreover, bioinformatics analysis revealed that both of the tsRNAs regulate the immune process by modulating metabolism and signal pathway.

Conclusion: In this study, we demonstrated that urinary exosome tsRNAs can be served as noninvasive biomarkers for the efficient diagnosis and prediction of nephritis in SLE.

KEYWORDS

Lupus nephritis, urinary exosomes, tsRNA, non-invasive biomarkers, diagnosis

Introduction

Systemic lupus erythematosus (SLE) is an autoimmune disease that predominantly affects women and typically has manifestations in multiple organs. Immune-system aberrations, heritable, hormonal, as well as environmental factors, contribute to the progression of organ damage (1). Lupus nephritis (LN) is a form of glomerulonephritis considered as a severe manifestation of the SLE and continues to be a major cause of morbidity and mortality for SLE patients (2, 3). Routine laboratory examinations such as proteinuria, anti–double-stranded DNA antibodies, and protein-to-creatinine ratio cannot fully reflect disease activity and present with the low diagnostic performance of LN (3–6). To date, renal biopsy was regarded as the gold standard for the diagnosis and classification of scarring and the extent of renal inflammation, but the invasiveness of this approach is not conducive to dynamic monitoring (7). Therefore, it is necessary to search and identify effective non-invasive biomarkers for the detection of LN in SLE.

Exosomes are extracellular vesicles (EVs) secreted by cells mainly consists of phospholipids bilayer structures, with a diameter range from 40 to 160 nm (average ~100 nm), existing in various body fluids including blood, urine and saliva, and plays important roles in remodeling extracellular matrix and transmitting signals and molecules to other cells (8, 9). Endogenous microRNAs (miRNAs), long non coding RNAs (lncRNAs), and tRNA-derived small noncoding RNA (tsRNAs) can be frequently transferred through exosomes from donor cells to recipient cells, displaying important immunomodulatory function in the pathogenesis of various autoimmune diseases, including SLE (10). Recently studies showed that abnormal expression of serum exosomal-miRNAs and lncRNAs was described in LN/SLE patients and both of them are associated with the activity of SLE, histological alterations, and the involvement of renal (11–13). Despite the growing interest in exploring serum exosome derived biomarkers for evaluating activity of disease and predicting the involvement of LN, few biomarkers have been used in clinical practice. Unlike other sample types like tissue or serum, urine testing can be truly non-invasive. Furthermore, the urine is physically close to the site of activity of the renal disease which may be promising specimens for monitoring the patients of SLE.

tsRNAs are novel noncoding small RNAs (14~40 nt in length), has rarely been described in SLE, including tRNA-derived fragments (tRFs) and tRNA halves (tiRNAs) originate from mature tRNAs or their precursors under the circumstance of enzymatic lysis and stress condition, and have been found stable in the exosome circulating in the biofluids, including urine (11). Furthermore, tsRNAs exert an essential role in the pathophysiology of biological processes by connecting with proteins or mRNA, regulating gene expression, and inhibiting translation (13). Mounting evidence has indicated that the aberrated expression of tsRNAs are deeply implicated in cancer, parasitic disease (12–16). Recently, a few studies including our previous research pay attention to the relationship between SLE and tsRNA (14, 17–19). However, the diagnostic values and biological functions of tsRNAs in urinary exosome, especially for LN, are still ambiguous and intriguing.

In this study, RNA sequencing, qRT-PCR validation, and ROC analysis were performed to identify LN-associated tsRNA signatures in urinary exosome. The urinary exosome derived tsRNA signatures showed enormous potentiality as novel non-invasive biomarkers for diagnosing and predicting LN in SLE.

Materials and methods

Subjects and study design

This study including 173 individuals was divided into three phases. In the discovery phase, tsRNA sequencing was conducted in exosomes extracted from pooled urine of 20 lupus nephritis patients (LN) and 20 SLE without LN, and the top 10 upregulated tsRNAs were screened as candidate marker of lupus nephritis. The candidate urinary exosomal tsRNAs were primary elected by qRT-PCR in 40 samples (20 LN and 20 SLE without LN patients) in the training phase. In the validation phase, selected tsRNAs in the training phase were further confirmed in a larger cohort (54 LN and 39 SLE without LN patients), and 24 sex-age matched healthy volunteers from the Center of Physical Examination were enrolled as controls. A total of 94 LN and 79 SLE without LN patients hospitalized in Nanjing Drum Tower Hospital between October 2020 and May 2022 were enrolled in this study (Figure 1). The clinical features of both cohorts in validation phase were shown in Table 1. The updated criteria of American College of Rheumatology (ACR) 1997 were used to diagnose SLE (20). The activity of disease was evaluated by the systemic lupus erythematosus disease activity index (SLEDAI) (21). Briefly, SLE patients with SLEDAI ≤ 4 were allocated to the stable-disease cohort, SLEDAI vary from 5 to 9 to the mild activity cohort, and SLEDAI ≥ 10 to the moderate-severe activity cohort. All participants provided informed consent and agreed to utilize their urine for research purposes. This study was approved by the ethics committee of Nanjing Drum Tower Hospital and conducted by the principles of the Declaration of Helsinki (1989).

RNA sequencing

The 5-adenylated, 3-blocked single-stranded DNA junction is used to connect to the RNAs purified and separated by PAGE electrophoresis cutting glue. One strand cDNA was synthesized by reverse transcription extension with RT primer with unique molecular identifiers (UMI) in the system. High-sensitivity polymerase was used to amplify the cDNA with both 3 'and 5' connectors. Eligible libraries were sequenced on a computer according to the instructions provided by the manufacturer company. A total of 50 cycles of sequencing were performed.

Isolation and characterization of exosomes

Exosomes were isolated from urine samples with Total Exosome Isolation (from urine) reagent (Thermo Fisher Scientific Baltics UAB) according to the manufacturer's instructions. First, 180uL urine mixing with 180uL Total Exosome Isolation (from urine) reagent was stored at 4°C for 24 hours. Then the supernatants were discards and the exosome pellets were resuspended in 100 μL 1× phosphate buffer saline (PBS) for further tsRNA extraction. The size and morphology of isolated exosomes were observed by particle size analyzer and transmission electron microscopy.

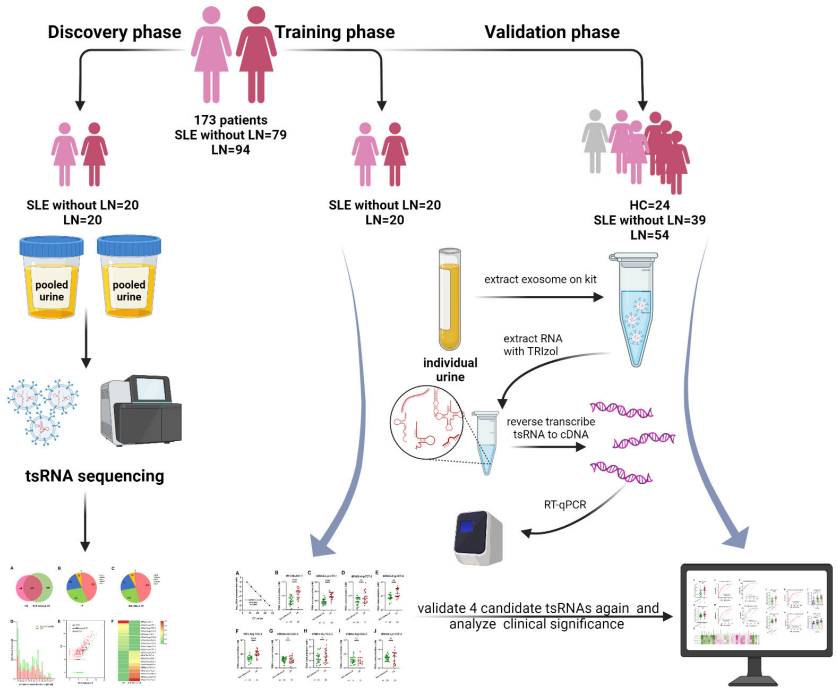

FIGURE 1
Workflow of the study.

Western blot was used to character exosomes with markers of anti-TSG101 (Abcam, UK), and anti-CD63 (three from Abcam, UK).

tsRNA extraction and RT-qPCR

Total tsRNAs were extracted from urinary exosomes using the Trizol reagent (Thermo Fisher scientific, US) and were dissolved in water treated by diethylpyrocarbonate (DEPC). The content and purity of acquired tsRNA were examed with OneDrop-2000 (NanoDrop Technologies). tsRNAs were reverse transcribed to cDNA using miRNA 1st Strand cDNA Synthesis Kit (Vazyme Biotech). The quantitative RT-PCR reaction was conducted in 96-well plates with the miRNA Universal SYBR qPCR Master Mix (Vazyme Biotech) in 96-well plates.

Pathway analysis

To gain insight into the function of the target genes of tsRNAs, we implemented gene ontology (GO), annotations Kyoto Encyclopedia of Genes and Genomes (KEGG) and wiki pathway enrichment analysis using the tRF target gene database (http://www.rnanut.net/tRFTar/). Significance was established on *P*-value ($P < 0.05$) and Q-values.

Statistical analysis

Continuous variables were presented as the median (interquartile range [IQR]) according to the normality test, and the differences between the groups were determined by the Mann-Whitney U test. Spearman rank test were employed to analyze the correlations between 4 tsRNAs and clinical variables. Receiver operator characteristic (ROC) analyses of variables were performed to calculate the areas under the ROC curves (AUCs) for identifying LN from SLE without LN. Statistical analyses were performed using GraphPad Prism version 8 (GraphPad Software Inc., La Jolla, CA, USA). A two-sided *P* less than 0.05 was considered statistically significant.

Data and materials availability

The raw data obtained from tsRNA sequencing have been deposited in GEO under registration code PRJNA890378. The primary discoveries of this study were summarized in the manuscript and raw data that support the results of this study are available from the corresponding author upon reasonable request.

Results

Characteristics of urinary exosomes

The urinary exosomes characterized by cup-shaped morphology with vesicles of 129 nm average diameters were examined using transmission electron microscopy (TEM) and nanoparticle tracking analysis (NTA) (Figures 2A, B). The presence of exosomes markers including CD63, and TSG101 (9) were verified by Western blot analysis (Figure 2C). Collectively, these results demonstrated the existence of exosomes in urine, which laid the foundation for further research on exosome biomarkers.

TABLE 1 Statistics of clinical information of validation phase specimens.

clinical characteristic	SLE without LN (n = 39)	LN (n = 54)	*p* value
Age, years	44.0 (32.0-54.0)	39.5(29.0-50.3)	0.286
Male, n (%)	4 (10.25)	5 (9.25)	1
Proteinuria, n (%)	0 (0)	21 (38.89)	<0.001***
Hematuria, n (%)	7 (17.95)	30 (55.56)	<0.001***
pyuria, n (%)	3 (7.69)	18 (33.33)	0.004**
Cylinderuria, n (%)	0 (0)	9 (16.67)	0.007**
24h proteinuria, median (IQR), mg/24h	253.5 (130.8-401.5)	3394.0 (1327.5-5396.5)	<0.001***
ACR, median (IQR), mg/g	32.25 (12.4-104.8)	1811.4 (661.9-4088.2)	<0.001***
WBC, median (IQR), ×10^9/L	4.3 (2.5-5.7)	4.9 (3.6-7.5)	0.015*
Lymphocytes, ×10^9/L	0.80 (0.6-1.2)	0.90 (0.6-1.4)	0.550
Hb, median (IQR), g/L	109.0 (83.0-124.0)	95.0 (70.0-110.0)	0.046*
PLT, median (IQR), ×10^9fL	148.0 (79.0-207.0)	198.0 (131.5-239.3)	0.036*
D-dimer, median (IQR), mg/L	1.2 (0.2-2.0)	1.0 (0.4-1.9)	0.504
ESR, median (IQR), mm/h	28.0 (16.0-59.3)	37.0 (22.0-59.8)	0.211
ALT, median(IQR), U/L	18.5 (12.1 -26.3)	12.1 (8.5-19.0)	0.004**
AST, median (IQR), U/L	18.6 (15.1-26.5)	16.2 (14.0-21.9)	0.042*
blood albumin, median (IQR), g/L	37.4 (34.7-39.0)	31.3 (27.5-34.4)	<0.001***
eGFR, median (IQR), ml/min/1.73m^2	130.5 (97.6-169.9)	90.5 (50.7-117.8)	<0.001***
C3, median (IQR), g/L	0.89 (0.55-1.08)	0.73 (0.49-1.03)	0.208
C4, median (IQR), g/L	0.15 (0.06-0.20)	0.13 (0.06-0.23)	0.694
IgG, median (IQR), IU/mL	13.4 (9.2-20.4)	10.2 (6.9-15.1)	0.017**
Th/Ts, median (IQR)	0.93 (0.65-1.23)	0.47 (0.47-0.97)	0.024*
anti-dsDNA, median (IQR)	67.68 (15.30-229.02)	108.94 (20.24-461.84)	0.260
25-(0H) D3, median (IQR), ng/ mL	16.51 (12.60-21.42)	11.32 (7.32-16.49)	0.001*
SLE-DAI, median (IQR)	4.0 (2.0-6.0)	9.5 (6.0-16.0)	<0.001***
tRF3-Ile-AAT-1, median (IQR)	0.19 (0.07-1.35)	1.88 (0.49-5.73)	<0.001***
tiRNA5-Lys-CTT-1, median (IQR)	0.24 (0.11-0.53)	0.76 (0.29-1.74)	<0.001***

ACR, albumin-to-creatinine ratio; WBC, white blood cells; Hb, hemoglobin; PLT, platelet; ESR, erythrocyte sedimentation rate; eGFR, glomerular filtration rate; C3, complement C3; C4, complement C4; IgG, immunoglobulin G; Th/Ts, helper T cells/suppressor T cells; anti-dsDNA, anti-double stranded DNA antibody; SLE-DAI, systemic lupus erythematosus disease activity index. *$p < 0.05$, **$p < 0.01$, and ***$p < 0.001$ (Mann-Whitney U test).

Ectopic urinary exosomes derived tsRNAs profiles in LN patients

To identify the tsRNAs profile in the urinary exosomes of LN patients, all participates were divided into two cohorts based on the clinical classification criteria, including LN and SLE without LN patients. Urine pooled from 20 LN patients and 20 SLE without LN patients were utilized to extract exosomes, followed by tsRNA sequencing (GEO number: PRJNA890378). The amount and classification of tsRNAs in urinary exosomes were described by Venn diagram and pie chart in both LN and SLE without LN (Figures 3A–C). Length distribution of tsRNAs was further analyzed and various number of bases of tsRNA exhibited significant bias between the two groups (Figure 3D). In scatter plot analysis, 275 upregulated and 171 downregulated tsRNAs, which satisfied the criterion that $\log_2$ fold-change > 1.5 by sequencing detection, were observed in LN compared with SLE without LN patients (Figure 3). The top 10 upregulated tsRNAs visualized using hierarchical clustering were selected as candidate markers of lupus nephritis (Figure 3F).

Identification of differentially expressed urinary exosomes derived tsRNAs in LN and SLE without LN patients

RT-qPCR assay was performed to validate the sequencing results of urinary exosomes from 20 LN and 20 SLE without LN patients in

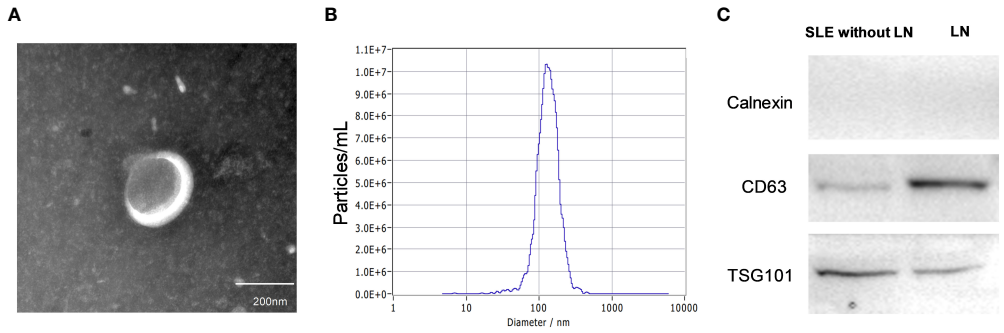

FIGURE 2
Characteristics of urinary exosomes. **(A, B)** Transmission electron micrograph and nanoparticle tracking analysis confirmed that the isolated small vesicles are urinary exosomes (with vesicle of 129 nm average diameters). **(C)** Western blotting showed the biomarkers of exosomes such as CD63, and TSG101.

the training phase. The absolute quantification for different expression of tsRNAs was determined by the linear standard curve from 10 f-mol/L to 1 nmol/L (Figure 4A). Specific primers were designed for the 10 candidate tsRNAs and the tsRNAs was successfully amplified except of tiRNA5-Arg-CCG-2, which could not be amplified and was thus eliminated from this study. Elevated expression of tRF3-Ile-AAT-1, tiRNA5-Lys-CTT-1, tiRNA5-Arg-CCT-4, and tRF5-Arg-TCG-3 were measured in the urinary exosomes of LN compared with SLE without LN patients (Figures 4B–J), implying urinary exosomes derived tsRNAs may serve as promising biomarkers for the diagnosis of LN.

Diagnostic value of urinary exosomes derived tsRNAs in the validation phase

We enrolled 54 LN, 39 SLE without LN patients and 24 healthy controls in the validation phase, in which tRF3-Ile-AAT-1 and tiRNA5-Lys-CTT-1 were remarkably increased in LN compared with SLE without LN patients ($P < 0.0001$ and $P < 0.001$) and healthy controls ($P < 0.01$ and $P < 0.01$) (Figures 5A, D), whereas tiRNA5-Arg-CCT-4 and tRF5-Arg-TCG-3 showed no difference among the three cohorts. The AUCs of tRF3-Ile-AAT-1 and tiRNA5-Lys-CTT-1 were 0.777 (95% confidence interval [CI]:

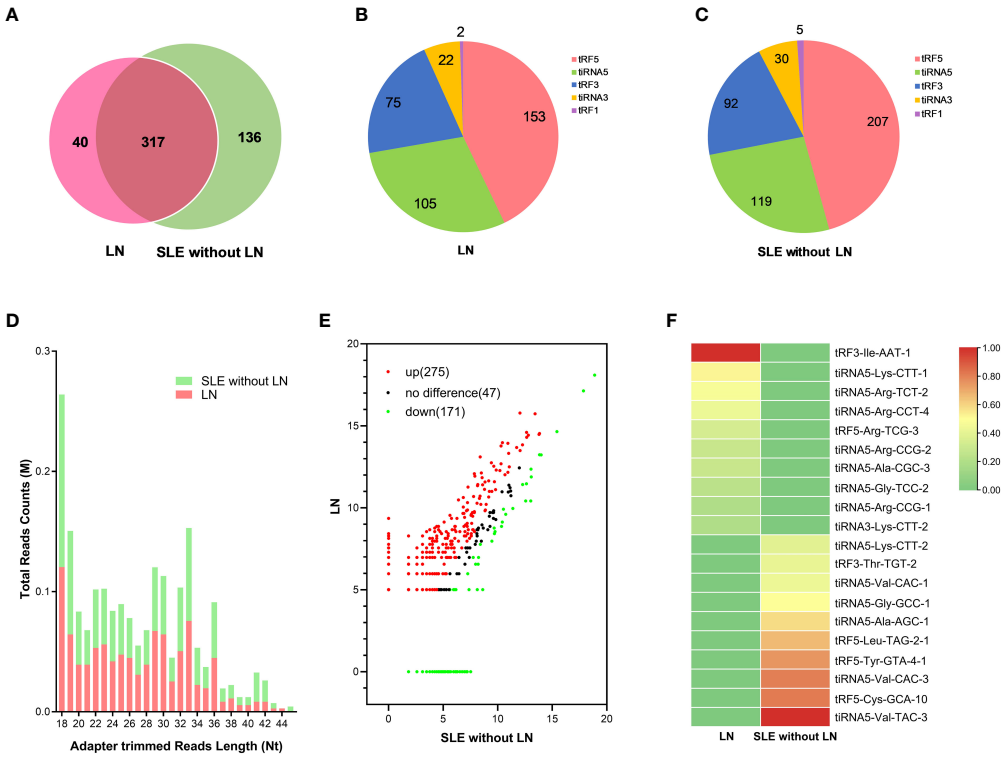

FIGURE 3
Analysis of differentially expressed tsRNAs in UEs of LN patients. **(A)** Venn diagram of urinary exosomes derived tsRNAs in LNs and SLE without LN patients. **(B, C)** The distribution of 5 types urinary exosomes derived tsRNAs in the two cohorts. **(D)** The profiles of various length of tsRNAs in urinary exosomes between the two cohorts. **(E)** Scatter plots of differentially expressed tsRNAs. Red and green dots indicated upregulated and downregulated tsRNAs (log2 fold-change > 1.5 between the two compared cohorts), and black dots indicated non-differentially expressed tsRNAs. **(F)** Hierarchical clustering indicated the profiles of top 10 upregulated and downregulated tsRNAs between two cohorts.

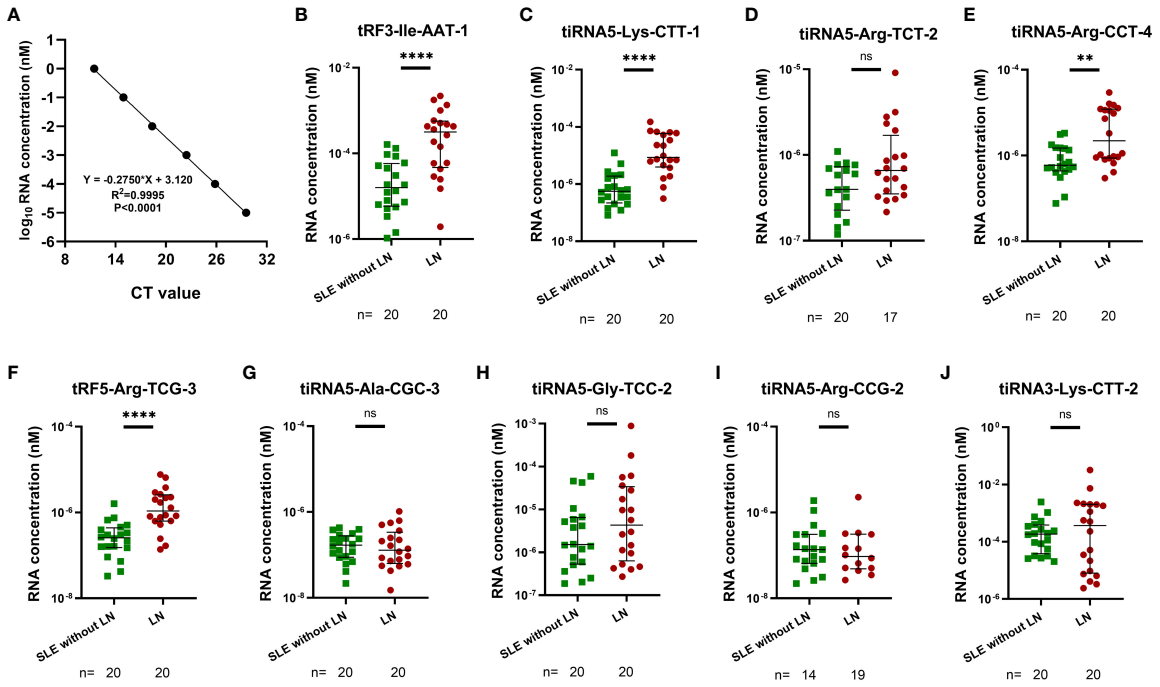

FIGURE 4
Identification of differentially expressed urinary exosomes derived tsRNAs in LNs and SLE without LN patients. **(A)** Linear standard curve of urinary exosomes derived tsRNAs concentration. **(B–J)** Differential expression of 9 tsRNAs verified by RT-qPCR in LN and SLE without LN patients. tRF3-Ile-AAT-1, tiRNA5-Lys-CTT-1, tiRNA5-Arg-CCT-4 and tRF5-Arg-TCG-3 were significantly upregulated in LNs compared with SLE without LN patients. P value of Mann Whitney U test: (**P < 0.01, ****P < 0.0001).

0.681-0.874, sensitivity 79.63%, specificity 66.69%) and 0.715 (95% CI: 0.610-0.820, sensitivity 66.96%, specificity 76.92%) for discriminating LN from SLE without LN patients (Figures 5B, E). In addition, 24-hour proteinuria showed good diagnostic value in identifying nephritis in SLE patients (AUC=0.94), whereas anti-dsDNA, complement C3 and C4 have limited diagnostic value in lupus nephritis (Figures 5G–I). To further demonstrate the clinical significance of tRF3-Ile-AAT-1 and tiRNA5-Lys-CTT-1 expression in SLE patients, we investigated the association between the tsRNAs levels and various clinical parameters in a total of 93 SLE patients. The results indicated that urinary exosomes derived tRF3-Ile-AAT-1 and tiRNA5-Lys-CTT-1 were positively correlated with ACR, SLEDAI and 24-hour proteinuria while negatively associated with albumin (Alb), complement C3 and Vitamin D3 (Figure 5J). Then we explored the predictive accuracy of the tRF3-Ile-AAT-1 and tiRNA5-Lys-CTT-1 combined with clinical indicators. The AUCs of tRF3-Ile-AAT-1 and Alb as well as tiRNA5-Lys-CTT-1 and Alb were 0.873 (95% CI: 0.802–0.944) and 0.880 (95% CI: 0.811–0.949) between individuals of LN and SLE without LN patients. As expected, integrated panel of tRF3-Ile-AAT-1, tiRNA5-Lys-CTT-1 and Alb resulted in the highest AUC of 0.881 (95% CI: 0.813-0.950, sensitivity 83.72%, specificity 94.19%) (Figure 5C). The AUCs of tRF3-Ile-AAT-1 and eGFR as well as tiRNA5-Lys-CTT-1 and eGFR were 0.783 (95% CI: 0.687-0.878) and 0.836 (95% CI: 0.754-0.917). Similarly, integrated panel of tRF3-Ile-AAT-1, tiRNA5-Lys-CTT-1 and eGFR resulted in the highest AUC of 0.838 (95% CI: 0.757-0.918, sensitivity 83.72%, specificity 94.19%) (Figure 5F).

Significance of tRF3-Ile-AAT-1 and tiRNA5-Lys-CTT-1 in clinical practice

Routine urinalysis usually utilized as indicators for monitoring the occurrence and progression of LN with a high specificity but low sensitivity. LN with weakly positive proteinuria (2+/1+) are commonly ignored and resulted in a delay of diagnosis in clinical practice. Elevated tRF3-Ile AAT-1 levels were observed in LN with proteinuria (2+)/(1+) compared with SLE without LN patients ($P < 0.001$), and the AUC of tRF3-Ile-AAT-1 were 0.749 (95% CI: 0.633-0.865, sensitivity 66.67%, specificity 78.79%) for discriminating LN with proteinuria (2+)/(1+) from SLE without LN patients (Figures 6A, B). Similarly, tiRNA5-Lys-CTT-1 levels were higher in LN with proteinuria (2+)/(1+) compared with SLE without LN patients ($P = 0.009$), and the AUC was 0.715 (95% CI: 0.554-0.804, sensitivity 76.92%, specificity 57.58%) (Figures 6D, E). Intriguingly, SLE patients with mild activity and moderate to severe activity had higher urinary exosomes derived tRF3-Ile AAT-1 ($P = 0.035$ and $P < 0.001$) and tiRNA5-Lys-CTT-1 ($P = 0.021$ and $P < 0.001$) levels compared with patients with no activity, whereas there was no difference of tRF3-Ile-AAT-1 and tiRNA5-Lys-CTT-1 between SLE patients with mild activity and moderate to severe activity (both $P > 0.05$) (Figures 6C, F).

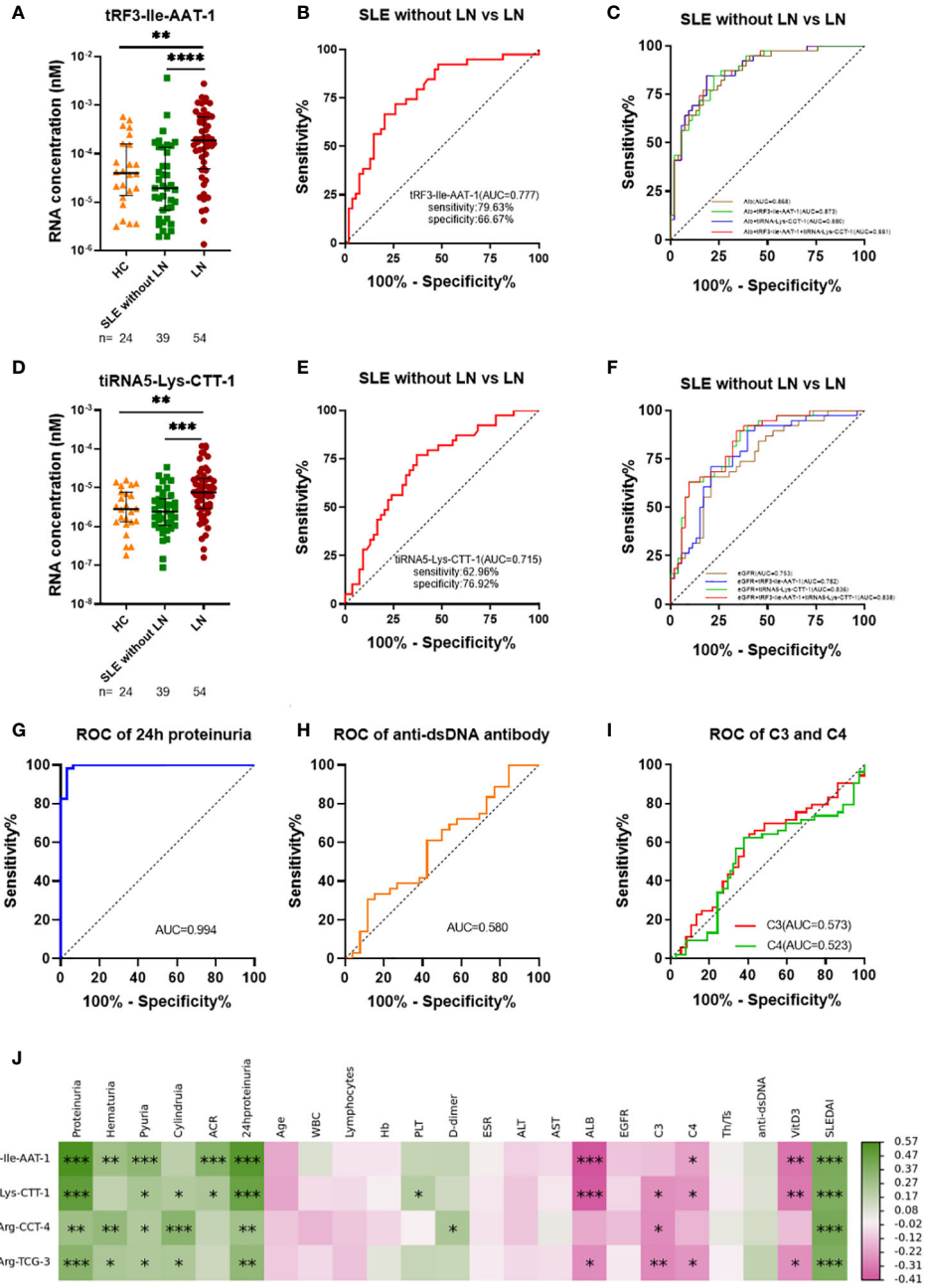

FIGURE 5
Diagnostic value of urinary exosomes derived tsRNAs in the validated stage. **(A)** Overexpression of tRF3-Ile AAT-1 in LNs compared with SLE without LN patients and healthy controls. **(B)** Receiver operator characteristic (ROC) curve of tRF3-Ile AAT-1 in distinguishing LNs from SLE without LN patients. **(C)** ROC combined diagnostic analyses of tRF3-Ile AAT-1and Alb, tiRNA5-Lys-CTT-1 and Alb, as well as tRF3-Ile AAT-1, tiRNA5-Lys-CTT-1 and Alb in discriminating LNs from SLE without LN patients.**(D)** Overexpression of tiRNA5-Lys-CTT-1 in LNs compared with SLE without LN patients and healthy controls. **(E)** ROC curve of tiRNA5-Lys-CTT-1 in distinguishing LNs from SLE without LN patients. **(F)** ROC combined diagnostic analyses of tRF3-Ile AAT-1and eGFR, tiRNA5-Lys-CTT-1 and eGFR, as well as tRF3-Ile AAT-1, tiRNA5-Lys-CTT-1 and eGFR in discriminating LNs from SLE without LN patients. **(G)** ROC curve of 24h proteinuria in distinguishing LNs from SLE without LN patients. **(H)** ROC curve of anti-dsDNA in distinguishing LNs from SLE without LN patients. **(I)** ROC curves of complement C3 and C4 in distinguishing LNs from SLE without LN patients. **(J)** Correlation analyses between tsRNAs and clinical variables. Green and red color represent the positive correlation and negative correlation, and the depth of the color represents the degree of correlation. *(*P < 0.05, **P < 0.01, ***P < 0.001, ****P < 0.0001).*

Enrichment analysis of tRF3-Ile AAT-1 and tiRNA5-Lys-CTT-1

To investigate the potential functions of tRF3-Ile AAT-1 and tiRNA5-Lys-CTT-1, we performed gene ontology analyses including cellular components, biological processes and molecular functions as well as signal pathway analyses containing KEGG and wiki pathways ($P < 0.05$). The GO project of tRF3-Ile AAT-1 were enriched in regulation of steroid biosynthetic process, embryo implantation, insulin-like growth factor binding, growth factor binding and so on (Figure 7A). Surprisingly, the KEGG showed that there may be some correlation between tRF3-Ile AAT-1 and coronavirus disease -

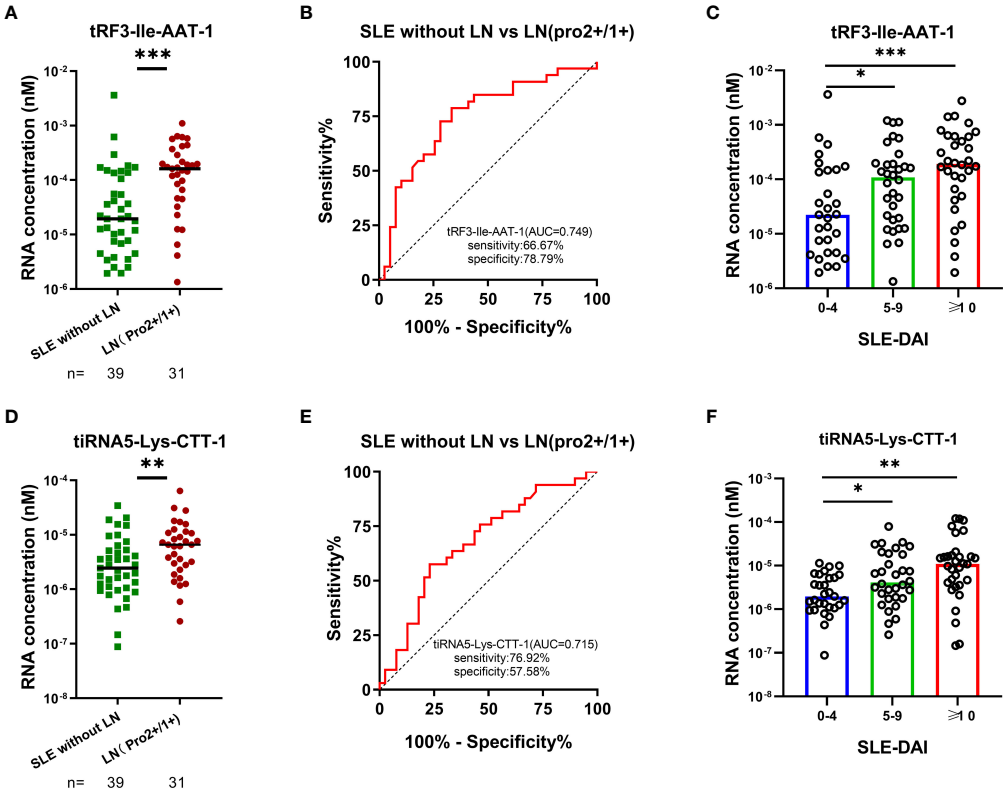

FIGURE 6
Significance of tRF3-Ile AAT-1 and tiRNA5-Lys-CTT-1 in clinical practice. **(A, B)** Diagnostic value of tRF3-Ile AAT-1 in LNs with proteinuria (2+)/ (1+) and SLE without LN patients. **(D, E)** Diagnostic value of tiRNA5-Lys-CTT-1 in LNs with proteinuria (2+)/ (1+) and SLE without LN patients. **(C, F)** Correlation between tRF3-Ile AAT-1, tiRNA5-Lys-CTT-1 and the activity of SLE measured by SLE-DAI 2000 (0-4, no activity; 5-9, mild activity; ≥10, moderate to severe activity).

COVID-19 (Figure 7B). GO terms targeted by tiRNA5-Lys-CTT-1 including cellular response to fibroblast growth factor stimulus, VCP-NPL4-UFD1 AAA ATPase complex, platelet-derived growth factor binding, and other GO stems was found to be enrich (Figure 7C). Signal pathway analysis of tiRNA5-Lys-CTT-1 showed the tsRNA was involved in the pathway of Human papillomavirus infection, Senescence and Autophagy in Cancer, EGF/EGFR Signaling Pathway (Figure 7D). Hence, these results remind us of the tsRNAs were likely to participate in the pathogenesis of lupus *via* affecting these functions.

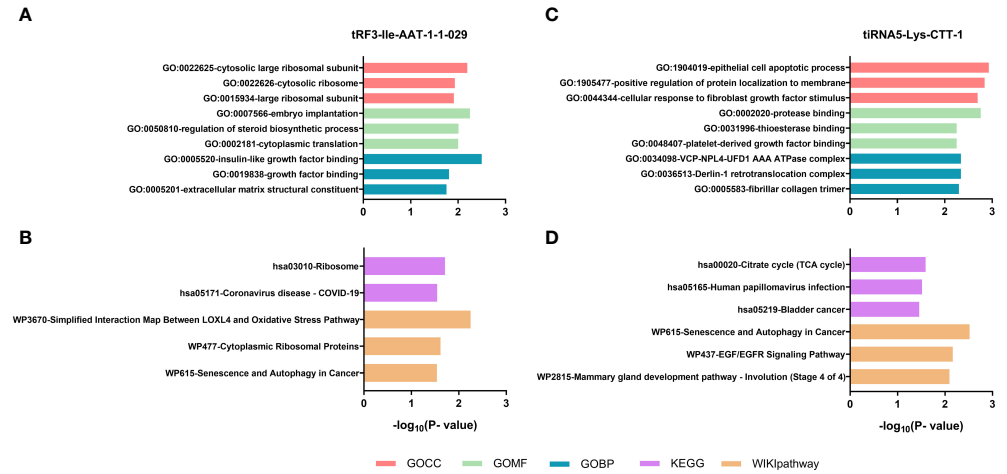

FIGURE 7
Enrichment analysis of tRF3-Ile AAT-1 and tiRNA5-Lys-CTT-1. GO terms analysis of tRF3-Ile AAT-1 **(A)**. Signal pathway analysis of tRF3-Ile AAT-1 **(B)**. GO terms analysis of tiRNA5-Lys-CTT-1 **(C)**. Signal pathway analysis of tiRNA5-Lys-CTT-1 **(D)**.

Discussion

SLE is an autoimmune disease characterized by abnormal activation of lymphocytes and abnormal accumulation of autoantibodies (22, 23). Lupus nephritis is one of the most devastating manifestations of SLE, during which 40% of them will develop chronic kidney disease and 10–20% of them will progress to end-stage renal disease within 5 years after diagnosis (14, 24). Thus, early detection and prediction of the progression of LN is critical for the management and treatment of SLE. As the main diagnostic criterion for LN, the 24-hour urinary protein provides good estimate of proteinuria. However, this method still has many drawbacks except for the inconvenience and the length time taken to undertake the test, such as inaccurate timing, partial urine sample loss during urine retention, poor patient compliance for urine protein test, physical activity, and not appropriate for outpatients or children (14, 24–28). Similarly, the usefulness of examining the urinary sediment has been the subject of debate because of the huge variation in quantifying the finding (3). In fact, protein-to-creatinine ratio in spot urine has replaced 24-hour urinary protein collections in many centers, while this approach has not been carefully validated (3). In addition, non-conventional biomarkers, like monocyte chemoattractant protein-1 (MCP-1) (29, 30), kidney injury molecule–1 (KIM-1) (30), vascular cell adhesion molecule-1 (VCAM-1) (31), neutrophil gelatinase-associated lipocalin (NGAL) (32), and microRNAs (33) have been described in the diagnosis and disease activity monitoring of LN, while the specificity and sensitivity are typically difficult to meet clinical practice standards. Therefore, reliable non-invasive biomarkers with higher sensitivity and specificity for the early detection and risk stratification of LN are urgently needed.

Urinary exosomes originated from glomerular podocytes or renal tubules epithelial cells enclose various species of RNA including tsRNAs (34, 35). Zhu et al. (36) found that the bladder, endothelial cell, basal cell, monocyte, and dendritic cell may closely participate in the formation of urine exosomes by investigating the genetic sources of urinary exosomes both at the levels of organs and cells. The evidence showed that the existence of CD47 on exosomes prolongs their half-life period in the circulation (37). In addtion, the tsRNAs were encapsulated in exosomes protecting them from degradation, and have a good deal of methylated modifications and terminal modifications making them stable in body fluids (38).The changes of urinary exosomal tsRNAs may reflect renal injury so that can be expected to be a potential clinical biomarker without need for an invasive tissue biopsy.

Recently, Park. Et al. reported that tsRNAs were capable of regulating the chromatin states in immune cells, indicating that tsRNAs involved critically in the occurrence and development of immune-related diseases (11). Chioyu et al. has described that tsRNA were enrich in exosomes released by T cells, which played a critical role in the organ involvement of SLE (39). More importantly, the content of tsRNAs in vesicles were significantly higher than miRNAs (39–41). tsRNAs in serum as biomarkers of SLE and LN patients were confirmed in our previous studies (14, 15).Based on the perspective of non-invasive liquid biopsy, this was the first report to explore whether urinary exosome derived tsRNA signatures could be considered as biomarkers for distinguishing LN from SLE patients

In our study, exosomes were characterized by TEM and NTA and double phospholipid bilayer cup-shaped vesicle structures with average particle about 129 nm were obtained, which was consistent with previous study (42). According to the sequencing results, we discovered 275 upregulated urinary exosomes derived tsRNAs in LN compared with SLE without LN patients. In training phase, 10 tsRNAs were verified increasing expression in LN. In validation phase, based on more clinical specimens, we further narrowed the candidates tsRNAs down to tRF3-Ile AAT-1 and tiRNA5-Lys-CTT-1. In addition, ROC curve analyses showed the high-precision discriminatory power of tRF3-Ile AAT-1 and tiRNA5-Lys-CTT-1 between SLE patients with and without LN. The evidence showed that angiogenin cleaves t-RNA into fragment as tsRNAs under conditions of cell stress, which contributes to immune system dysregulation, autoantibody production and fatal comorbidities of SLE patients (39, 40). tRFs and tiRNAs inhibit translation in a variety of ways (38), and possibly slow down the progression of some inflammatory reaction manifestation of SLE in the kidneys. In our study, tRF3-Ile-AAT-1 and tiRNA5-Lys-CTT-1 showed good diagnostic value in identifying LN in SLE patients, which are better than conventional biomarkers such as anti-dsDNA antibody, C3 and C4. We further created a panel consisted of both tsRNAs and clinical parameters such as Alb and EGFR, demonstrating higher diagnostic value in distinguishing LN from SLE patients. SLE-DAI is a reliable indicator reflecting SLE activity scored by clinical symptoms and auxiliary examination, while 24 hours proteinuria is considered as the main diagnostic criteria for LN contraindicated to renal biopsy (3, 21). The two tsRNAs were positively correlated with proteinuria and SLE-DAI score, implying that tsRNAs may be involved in the activity of SLE and progression of LN. In addition, LN often present with mild proteinuria (3), and our study analyzed the significance of tsRNAs in clinical practice and found that it could identify active LN who were often missed because the urine protein in routine examination did not reach strong positive. Besides, both tsRNAs in our study can distinguish active SLE from stable SLE patients, which can help rheumatologist judge the severity and risk of disease. Intriguingly, there was a strong correlation between the two tsRNAs, while mechanism of exactly how they cooperate in LN depends on further research. GO analysis showed tRF3-Ile AAT-1 was enriched in insulin-like growth factor binding, which influenced autoimmune by modulating signaling pathways relevant to Th17/Treg balance (42). tiRNA5-Lys-CTT-1 was found involved with platelet-derived growth factor (PDGF) binding, there were studies showed that PDGF family have been concerned as an autoantigen target in the serum of SLE patients and play role in the pathogenesis of renal fibrosis (43). On the strength of above, we can hypothesize that tsRNAs may be involved in the occurrence and development of LN by participating in these pathways.

In summary, we first identified novel urine exosome derived two-tsRNAs signature in SLE patients. We then demonstrated that urine exosome derived tRF3-Ile AAT-1, tiRNA5-Lys-CTT-1 could be used as novel promising biomarkers for distinguishing LN from SLE patients. Furthermore, our study also revealed the potential

biological functions of the two novel urine exosome derived tsRNAs. However, because of the limited samples and single-center experience of our study, randomized clinical trials will be needed to evaluate the possible application of the two-tsRNAs signature in the diagnosis and prognosis of LN in the future.

Data availability statement

The datasets presented in this study can be found in online repositories. The names of the repository/repositories and accession number(s) can be found in the article/Supplementary Material.

Ethics statement

The studies involving human participants were reviewed and approved by Ethics Committee of the Affiliated Drum Tower Hospital of Nanjing University Medical School. The patients/participants provided their written informed consent to participate in this study. Written informed consent was obtained from the individual(s) for the publication of any potentially identifiable images or data included in this article.

Author contributions

SC and XZ contributed equally to this work. SC and PY writing the original draft. XZ: methodology and data validation. ZL, JL: conceptualization and supervision. PY is the chief designer of the whole experiment. All authors contributed to the article and approved the submitted version.

Funding

This work was supported by Nanjing Drum Tower Hospital Clinical Research Special Fund project (No. 2022-LCYJ-PY-36).

Acknowledgments

The authors would like to thank all patients for sending their consents and sincerely acknowledge the staff of rheumatology department.

Conflict of interest

The authors declare that the research was conducted in the absence of any commercial or financial relationships that could be construed as a potential conflict of interest.

Publisher's note

Supplementary material

The Supplementary Material for this article can be found online at: https://www.frontiersin.org/articles/10.3389/fimmu.2023.1077645/full#supplementary-material

References

1. Tsokos GC. Systemic lupus erythematosus. *N Engl J Med* (2011) 365:2110–21. doi: 10.1056/NEJMra1100359

2. Almaani S, Meara A, Rovin BH. Update on lupus nephritis. *Clin J Am Soc Nephrol* (2017) 12:825–35. doi: 10.2215/CJN.05780616

3. Anders HJ, Saxena R, Zhao MH, Parodis I, Salmon JE, Mohan C. Lupus nephritis. *Nat Rev Dis Primers* (2020) 6:7. doi: 10.1038/s41572-019-0141-9

4. Moroni G, Radice A, Giammarresi G, Quaglini S, Gallelli B, Leoni A, et al. Are laboratory tests useful for monitoring the activity of lupus nephritis? a 6-year prospective study in a cohort of 228 patients with lupus nephritis. *Ann Rheum Dis* (2009) 68:234–7. doi: 10.1136/ard.2008.094508

5. Alvarado AS, Malvar A, Lococo B, Alberton V, Toniolo F, Nagaraja HN, et al. The value of repeat kidney biopsy in quiescent Argentinian lupus nephritis patients. *Lupus* (2014) 23:840–7. doi: 10.1177/0961203313518625

6. Mejia-Vilet JM, Malvar A, Arazi A, Rovin BH. The lupus nephritis management renaissance. *Kidney Int* (2022) 101:242–55. doi: 10.1016/j.kint.2021.09.012

7. Ubara Y, Kawaguchi T, Nagasawa T, Miura K, Katsuno T, Morikawa T, et al. Committee of practical guide for kidney b. kidney biopsy guidebook 2020 in Japan. *Clin Exp Nephrol* (2021) 25:325–64. doi: 10.1007/s10157-020-01986-6

8. Zhang L, Yu D. Exosomes in cancer development, metastasis, and immunity. *Biochim Biophys Acta Rev Cancer* (2019) 1871:455–68. doi: 10.1016/j.bbcan.2019.04.004

9. Kalluri R, LeBleu VS. The biology, function, and biomedical applications of exosomes. *Science* (2020) 367:eaau6977. doi: 10.1126/science.aau6977

10. Zheng C, Xie L, Qin H, Liu X, Chen X, Lv F, et al. The role of extracellular vesicles in systemic lupus erythematosus. *Front Cell Dev Biol* (2022) 10:835566. doi: 10.3389/fcell.2022.835566

11. Park J, Ahn SH, Shin MG, Kim HK, Chang S. tRNA-derived small RNAs: Novel epigenetic regulators. *Cancers (Basel)* (2020) 12:2773. doi: 10.3390/cancers12102773

12. Jin F, Yang L, Wang W, Yuan N, Zhan S, Yang P, et al. A novel class of tsRNA signatures as biomarkers for diagnosis and prognosis of pancreatic cancer. *Mol Cancer* (2021) 20:95. doi: 10.1186/s12943-021-01389-5

13. Pandey KK, Madhry D, Ravi Kumar YS, Malvankar S, Sapra L, Srivastava RK, et al. Regulatory roles of tRNA-derived RNA fragments in human pathophysiology. *Mol Ther Nucleic Acids* (2021) 26:161–73. doi: 10.1016/j.omtn.2021.06.023

14. Yang P, Zhang X, Chen S, Tao Y, Ning M, Zhu Y, et al. A novel serum tsRNA for diagnosis and prediction of nephritis in SLE. *Front Immunol* (2021) 12:735105. doi: 10.3389/fimmu.2021.735105

15. Zhang X, Yang P, Khan A, Xu D, Chen S, Zhai J, et al. Serum tsRNA as a novel molecular diagnostic biomarker for lupus nephritis. *Clin Transl Med* (2022) 12:e830. doi: 10.1002/ctm2.830

16. Artuyants A, Campos TL, Rai AK, Johnson PJ, Dauros-Singorenko P, Phillips A, et al. Extracellular vesicles produced by the protozoan parasite trichomonas vaginalis contain a preferential cargo of tRNA-derived small RNAs. *Int J Parasitol* (2020) 50:1145–55. doi: 10.1016/j.ijpara.2020.07.003

17. Xu H, Chen W, Zheng F, Tang D, Dai W, Huang S, et al. The potential role of tRNAs and small RNAs derived from tRNAs in the occurrence and development of systemic lupus erythematosus. *Biochem Biophys Res Commun* (2020) 527:561–7. doi: 10.1016/j.bbrc.2020.04.114

18. Dou R, Zhang X, Xu X, Wang P, Yan B. Mesenchymal stem cell exosomal tsRNA-21109 alleviate systemic lupus erythematosus by inhibiting macrophage M1 polarization. *Mol Immunol* (2021) 139:106–14. doi: 10.1016/j.molimm.2021.08.015

19. Liang Y, Zhang J, Qiu W, Chen B, Zhou Y, Chen X, et al. Dysregulation of tRNA-derived small RNAs and their potential roles in lupus nephritis. *Lupus* (2021) 30:2248–55. doi: 10.1177/09612033211061482

20. Hochberg MC. Updating the American college of rheumatology revised criteria for the classification of systemic lupus erythematosus. *Arthritis Rheum* (1997) 40:1725. doi: 10.1002/art.1780400928

21. Bombardier C, Gladman DD, Urowitz MB, Caron D, Chang CH. Derivation of the SLEDAI. a disease activity index for lupus patients. the committee on prognosis studies in SLE. *Arthritis Rheum* (1992) 35:630–40. doi: 10.1002/art.1780350606

22. Yu F, Haas M, Glassock R, Zhao MH. Redefining lupus nephritis: Clinical implications of pathophysiologic subtypes. *Nat Rev Nephrol* (2017) 13:483–95. doi: 10.1038/nrneph.2017.85

23. Yap DYH, Chan TM. B cell abnormalities in systemic lupus erythematosus and lupus nephritis-role in pathogenesis and effect of immunosuppressive treatments. *Int J Mol Sci* (2019) 20:6231. doi: 10.3390/ijms20246231

24. Aragon CC, Tafur RA, Suarez-Avellaneda A, Martinez MT, Salas AL, Tobon GJ. Urinary biomarkers in lupus nephritis. *J Transl Autoimmun* (2020) 3:100042. doi: 10.1016/j.jtauto.2020.100042

25. Fine DM, Ziegenbein M, Petri M, Han EC, McKinley AM, Chellini JW, et al. A prospective study of protein excretion using short-interval timed urine collections in patients with lupus nephritis. *Kidney Int* (2009) 76:1284–8. doi: 10.1038/ki.2009.344

26. Kobayashi S, Amano H, Terawaki H, Ogura M, Kawaguchi Y, Yokoo T. Spot urine protein/creatinine ratio as a reliable estimate of 24-hour proteinuria in patients with immunoglobulin a nephropathy, but not membranous nephropathy. *BMC Nephrol* (2019) 20:306. doi: 10.1186/s12882-019-1486-8

27. Akin D, Ozmen S. An unresolved issue: The relationship between spot urine protein-to-creatinine ratio and 24-hour proteinuria. *J Int Med Res* (2019) 47:1179–84. doi: 10.1177/0300060518819602

28. Rodby RA. Timed urine collections for albumin and protein: "The king is dead, long live the king!". *Am J Kidney Dis* (2016) 68:836–8. doi: 10.1053/j.ajkd.2016.06.025

29. Dong XW, Zheng ZH, Ding J, Luo X, Li ZQ, Li Y, et al. Combined detection of uMCP-1 and uTWEAK for rapid discrimination of severe lupus nephritis. *Lupus* (2018) 27:971–81. doi: 10.1177/0961203318758507

30. Ding Y, Nie LM, Pang Y, Wu WJ, Tan Y, Yu F, et al. Composite urinary biomarkers to predict pathological tubulointerstitial lesions in lupus nephritis. *Lupus* (2018) 27:1778–89. doi: 10.1177/0961203318788167

31. Spronk PE, Bootsma H, Huitema MG, Limburg PC, Kallenberg CG. Levels of soluble VCAM-1, soluble ICAM-1, and soluble e-selectin during disease exacerbations in patients with systemic lupus erythematosus (SLE); a long term prospective study. *Clin Exp Immunol* (1994) 97:439–44. doi: 10.1111/j.1365-2249.1994.tb06107.x

32. Rubinstein T, Pitashny M, Levine B, Schwartz N, Schwartzman J, Weinstein E, et al. Urinary neutrophil gelatinase-associated lipocalin as a novel biomarker for disease activity in lupus nephritis. *Rheumatol (Oxford)* (2010) 49:960–71. doi: 10.1093/rheumatology/kep468

33. Sole C, Moline T, Vidal M, Ordi-Ros J, Cortes-Hernandez J. An exosomal urinary miRNA signature for early diagnosis of renal fibrosis in lupus nephritis. *Cells* (2019) 8:773. doi: 10.3390/cells8080773

34. Pisitkun T, Johnstone R, Knepper MA. Discovery of urinary biomarkers. *Mol Cell Proteomics* (2006) 5:1760–71. doi: 10.1074/mcp.R600004-MCP200

35. Raposo G, Stoorvogel W. Extracellular vesicles: Exosomes, microvesicles, and friends. *J Cell Biol* (2013) 200:373–83. doi: 10.1083/jcb.201211138

36. Zhu Q, Cheng L, Deng C, Huang L, Li J, Wang Y, et al. The genetic source tracking of human urinary exosomes. *Proc Natl Acad Sci USA* (2021) 118. doi: 10.1073/pnas.2108876118

37. Kamerkar S, LeBleu VS, Sugimoto H, Yang S, Ruivo CF, Melo SA, et al. Exosomes facilitate therapeutic targeting of oncogenic KRAS in pancreatic cancer. *Nature* (2017) 546:498–503. doi: 10.1038/nature22341

38. Wang J, Ma G, Li M, Han X, Xu J, Liang M, et al. Plasma tRNA fragments derived from 5' ends as novel diagnostic biomarkers for early-stage breast cancer. *Mol Ther Nucleic Acids* (2020) 21:954–64. doi: 10.1016/j.omtn.2020.07.026

39. Chiou NT, Kageyama R, Ansel KM. Selective export into extracellular vesicles and function of tRNA fragments during T cell activation. *Cell Rep* (2018) 25:3356–70. doi: 10.1016/j.celrep.2018.11.073

40. Sharabi A, Tsokos GC. T Cell metabolism: New insights in systemic lupus erythematosus pathogenesis and therapy. *Nat Rev Rheumatol* (2020) 16:100–12. doi: 10.1038/s41584-019-0356-x

41. Shi J, Zhang Y, Tan D, Zhang X, Yan M, Zhang Y, et al. PANDORA-seq expands the repertoire of regulatory small RNAs by overcoming RNA modifications. *Nat Cell Biol* (2021) 23:424–36. doi: 10.1038/s41556-021-00652-7

42. Chen CY, Rao SS, Ren L, Hu XK, Tan YJ, Hu Y, et al. Exosomal DMBT1 from human urine-derived stem cells facilitates diabetic wound repair by promoting angiogenesis. *Theranostics* (2018) 8:1607–23. doi: 10.7150/thno.22958

43. Vanarsa K, Soomro S, Zhang T, Strachan B, Pedroza C, Nidhi M, et al. Quantitative planar array screen of 1000 proteins uncovers novel urinary protein biomarkers of lupus nephritis. *Ann Rheum Dis* (2020) 79:1349–61. doi: 10.1136/annrheumdis-2019-216312

frontiers | Frontiers in Immunology

TYPE Mini Review
PUBLISHED 24 February 2023
DOI 10.3389/fimmu.2023.1112811

OPEN ACCESS

EDITED BY
Yujing Zhang,
Nanjing University, China

REVIEWED BY
Vedrana Bulat,
Sisters of Charity Hospital, Zagreb, Croatia
John E Harris,
University of Massachusetts Medical School, United States

*CORRESPONDENCE
Reinhart Speeckaert
reinhart.speeckaert@uzgent.be

SPECIALTY SECTION
This article was submitted to Cytokines and Soluble Mediators in Immunity, a section of the journal Frontiers in Immunology

RECEIVED 30 November 2022
ACCEPTED 16 February 2023
PUBLISHED 24 February 2023

CITATION
Speeckaert R, Belpaire A, Speeckaert MM and van Geel N (2023) A meta-analysis of chemokines in vitiligo: Recruiting immune cells towards melanocytes.
Front. Immunol. 14:1112811.
doi: 10.3389/fimmu.2023.1112811

A meta-analysis of chemokines in vitiligo: Recruiting immune cells towards melanocytes

Reinhart Speeckaert[1]*, Arno Belpaire[1], Marijn M. Speeckaert[2] and Nanja van Geel[1]

[1]Department of Dermatology, Ghent University Hospital, Gent, Belgium, [2]Department of Nephrology, Ghent University Hospital, Gent, Belgium

Chemokine research offers insightful information on the pathogenesis of cutaneous immune disorders, such as vitiligo. Compared to cytokines, the higher detectable levels of chemokines display promising potential as future disease biomarkers. Nonetheless, some published study results are contradictory, which can be attributed to patient characteristics and methodological differences. In this study, a meta-analysis was performed to compare chemokine expression in blood and skin samples from vitiligo patients versus healthy controls. Furthermore, the relationship between chemokine expression and disease activity was evaluated. Chemokine levels were investigated in 15 articles in the circulation and in 9 articles in vitiligo skin. Overall, some clear trends were observed. CXCR3 signaling by CXCL10 and CXCL9 has been confirmed by several reports, although CXCL10 showed more robust findings in blood samples. In this meta-analysis, CCL5, CXCL8, CXCL12, and CXCL16 levels were also significantly elevated. This indicates a complex immune pathway activation in vitiligo that overall supports a Th1-dominant response. Chemokines linked to the Th2 and Th17 pathways were less prevalent. Despite these findings, study protocols that examine a broader range of chemokines are encouraged, because current research is mostly focused on a small number of chemokines that were differentially expressed in previous studies.

KEYWORDS

vitiligo, chemokine, disease activity, biomarker, CXCL

Introduction

Chemokines are signaling proteins regulating the recruitment of immune cells to the skin. Currently, around 50 chemokines and 18 receptors have been identified, often with overlapping functions leading to redundancy (1). Interestingly, different chemokines are involved in unfolding specific innate and targeted immune responses encountered in inflammatory skin disorders. Chemokines show great potential as disease biomarkers and provide important data to unravel the pathogenesis of complex immune responses. Chemokine levels are generally higher than cytokines allowing for more robust and reproducible results. Their short half-life ensures that changes can be detected rapidly. However, this trait may also introduce bias due to

temporary infectious diseases (e.g., viral infections) which may cloud the chronic level of inflammation in patients with autoimmune disorders (2, 3).

In recent years, a lot of research has been carried out on chemokines in vitiligo allowing for rapid progress in this field. Unraveling the signaling pathways facilitates the development of targeted therapies (2). In this study, we performed a meta-analysis of the published data on chemokines in the circulation and the skin of vitiligo patients.

Methods

A systematic search was done in PubMed and Embase to detect all articles investigating chemokines in vitiligo and comparing the values of vitiligo patients with healthy controls and/or active versus stable vitiligo patients. All articles from inception to October 2022 were eligible. The search was done between October 13th, 2022, and October 20th, 2022. The search strategy included the keywords 'chemokine' AND 'vitiligo' in all fields. The Prisma Flow Diagram can be found in the Supplementary Material (Supplementary Figure 2). Only human studies investigating chemokine levels in the blood and/or skin of vitiligo patients were included. Articles investigating animal models and abstracts were excluded. The aim was to investigate the difference in circulating and (peri-)lesional chemokine levels between vitiligo patients and healthy controls as well as between active and stable vitiligo patients. Results comparing chemokine levels before and after treatment were excluded because they may not be representative of the comparison of active versus stable disease. Meta-analysis was done in the case at least 2 articles performed an analysis of chemokines at the protein level using the same methodology. The meta-analysis was done with Review Manager 5.4.1 (The Cochrane Collaboration, 2020) using an inverse variant random effects model with the standardized mean difference as an effect measure. The standardized mean difference instead of the mean difference was used given the overall high variety in baseline chemokine concentrations in healthy controls pointing to an important difference in the results depending on the used lab kit and technology for measuring chemokine concentrations. When the difference between healthy controls and stable patients was less than 10%, the mean difference was used because this indicates that the methodology in these studies is likely comparable. The mean chemokine concentrations, standard deviation, and number of patients were extracted from each publication. When only the sample size, median, range, and/or interquartile range were provided, the mean was calculated based on the formula of Luo et al., 2018 and the standard deviation was based on Wan et al., 2014 (4, 5). For studies only displaying the results in graphs, data were extracted with GIMP 2.10.30 (GNU image manipulation program) using the method described by Van der Mierden et al., 2020 (6).

Results

21 articles were identified that compared the chemokine levels in vitiligo patients versus controls and/or between active and stable vitiligo patients (Supplementary Figure 1). Most results on chemokines in the circulation were found for CXCL10 (n=15), followed by CXCL9 (n=11), CCL5 (n=5), CXCL12 (n=4), CXCL8 (n=3), CXCL11 (n=4), CCL2 (n=2), CCL1 (n=1), CXCL1 (n=1), CCL3 (n=1), CCL4 (n=1), CXCL13 (n=1), CXCL16 (n=2), CCL17 (n=1), CCL20 (n=2), CCL22 (n=1), CCL27 (n=1), and CCL28 (n=1). Chemokine levels in the skin were measured in 10 studies for CXCL10 (n=9), CXCL9 (n=7), CXCL11 (n=4), CCL5 (n=2), CCL20 (n=2), CXCL8 (n=1), CCL17 (n=1), CCL22 (n=1).

Chemokines attracting CD8+ cytotoxic T lymphocytes

CXCR3 binding ligands: CXCL9, CXCL10 and CXCL11

Multiple chemokines can bind to the CXCR3 receptor leading to apparent functional redundancy (7). Three isoforms of CXCR3 exist: CXCR3-A, CXCR3-B and CXCR3-alt. CXCL9 and CXCL10 bind to CXCR3-A and CXCL9, CXCL10, CXCL11, CXCL4 bind to CXCR3-B (8). It should be noted that chemokine ligands binding to the same receptor can still exert a specific effect. due to differences in geographical expression leading to a tissue-specific role, and differences in timing of expression. The non-redundant roles of CXCL9, CXCL10 and CXCL11 have been confirmed by different reports (9, 10). CXCR3A is the predominant form produced by lymphocytes although CXCR3B expression has also been found in CXCL10 interferon-activated Th1 lymphocytes, CD8 T cells, NK cells, NKT cells, dendritic cells, and some endothelial cells (7). Stimulation of melanocytes by IFN-γ leads to the production of CXCL9, CXCL10, and to a lesser amount of CXCL11 and CXCL4 (11). Melanocytes express CXCR3B, although the exact levels of CXCR3-A and CXCR3-alt expression have not been determined. CXCR3 expression is elevated in vitiligo melanocytes compared to healthy pigment cells. Keratinocytes express also CXCR3, although this appears less prominent (11).

CXCL9

CXCL9 expression is upregulated by IFN-γ and in contrast to CXCL10 and CXCL11 not by IFN-α/β (12). CXCL9 has been extensively studied in vitiligo (497 vitiligo patients vs 257 healthy controls), although the data have been variable (Figure 1). 4/11 studies mentioned increased CXCL9 concentration in the circulation of vitiligo patients compared to healthy controls (13–23). Meta-analysis showed an overall non-significant result (P = 0.16). Only 1/5 reports found elevated circulating CXCL9 levels in active compared to stable vitiligo patients, although the final results of studies investigating CXCL9 in blister fluid were borderline significant (P = 0.05). CXCL9 is overexpressed in vitiligo skin compared to healthy skin (5 studies: 2 blister fluid, 2 mRNA of the skin, 1 immunohistochemistry) (17–19, 23, 24). A dramatic increase in CXCL9 concentrations in the actively progressing lesions compared to stable vitiligo skin became apparent

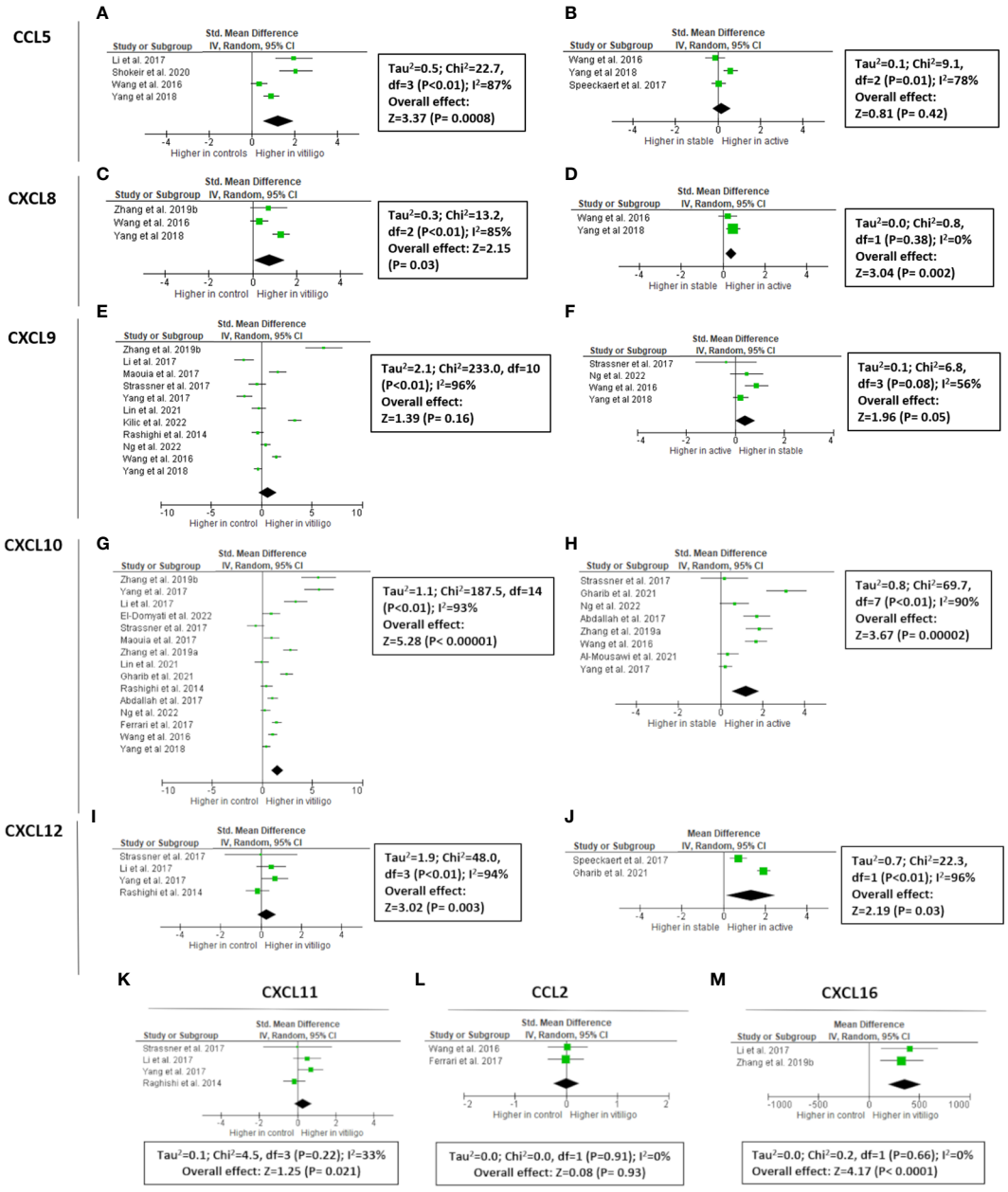

FIGURE 1
Meta-analysis of circulating chemokines of vitiligo patients versus controls or active versus stable patients for CCL5 **(A**, **B**, respectively), CXCL8 (**C**, **D**, respectively), CXCL9 (**E**, **F**, respectively), CXCL10 (**G**, **H**, respectively), CXCL11 **(K)**, CXCL12 (**I**, **J**, respectively), CCL2 **(L)**, and CXCL16 **(M)**. CCL: chemokine (C-C motif) ligand; CXCL: chemokine (C-X-C motif) ligand.

from 2 studies (5.3-12.3 fold increase; 19 active vs 36 stable; concentrations in blister fluid) (16, 18).

CXCL10

Vitiligo melanocytes have a higher constitutive CXCL10 production compared to healthy controls (11). A total of 709 patients and 362 controls were investigated in 15 studies. 12/15 studies (80%) reported significantly higher CXCL10 levels in vitiligo patients compared to controls, resulting in an overall highly significant CXCL10 concentration in the blood of vitiligo patients ($P < 0.00001$) (13–20, 22, 23, 25–28). The difference between patients and controls varied in the different studies with one study reporting a 7.8-fold increase (15). The largest study by Yang et al., 2018 (160 vitiligo patients versus 40 controls) found only a 1.3-fold increase (13). The baseline values of controls and vitiligo patients were very different depending on the publication. The mean values of CXCL10 ranged from 21.5 pg/ml to 1619 pg/ml in healthy controls and 40.09 pg/ml to 916.9 pg/ml in vitiligo patients. Although the higher expression of CXCL10 was confirmed by 12/15 studies, it is impossible to reliably estimate the magnitude

of the difference due to the marked variety between study results. 8 studies compared active versus stable vitiligo patients, with 5 pointing to significantly increased serum CXCL10 concentrations in case of disease activity. This resulted in a P value = 0.0004 by meta-analysis. 6 studies analyzed CXCL10 expression in the skin with a comparison between vitiligo patients and healthy controls: 3 analyzing CXCL10 concentrations in blister fluid, 2 mRNA of the skin and 1 evaluating skin biopsies by immunohistochemistry (Supplementary Figure 2) (13, 17–19, 26). All findings resulted in a higher CXCL10 expression in vitiligo compared to healthy skin. 3 studies analyzed the chemokine concentration in blister fluid of active versus stable vitiligo skin, also pointing to dramatically increased values in progressive vitiligo lesions (3.04-11.7 fold increase) (13, 16, 18).

CXCL11

Compared to CXCL9 and CXCL10, the expression of CXCL11 seems less pronounced in skin diseases. Some epidermal expression has been documented in CDLE and dermal expression in Jessner's lymphocytic infiltration (29). CXCL11 is induced by IFN-γ, IFN-β, and to a lesser extent by IFN-α. In contrast to CXCL10, CXCL11 induces the polarization of IL10-secreting T-regulatory type 1 cells, restraining autoimmunity (1). CXCL11 has the highest affinity for CXCR3 compared to CXCL10 and CXCL9 (12). In vitiligo, CXCL11 has little data including 4 studies with in total of 62 vitiligo patients and 67 controls (17, 18, 20, 23). The overall meta-analyses detected no significant increase in vitiligo patients (P = 0.21). Two studies found no clearly increased mRNA CXCL11 levels in vitiligo skin, while one study did (17, 18, 23).

CXCL16/CXCR6 receptor

Circulating CXCL16 levels were elevated in vitiligo in 2 studies (40 vitiligo patients and 24 healthy controls) (15, 20). Oxidative stress (H_2O_2) is correlated with CXCL16 mRNA levels in the skin of progressive vitiligo patients and serum CXCL16 decreases following successful therapy (15, 20). CXCL16 is produced by keratinocytes by ROS *via* an unfolded protein response. CXCL16-CXCR6 signaling regulates the recruitment of CD8+ T cells to vitiligo skin (20).

Chemokines recruiting both innate and adaptive immune cells

CXCL12: A CXCR4 binding chemokine

CXCL12 binds to two receptors, namely CXCR4 and ACKR3. CXCL12 is also known by its former name stromal cell-derived factor-1α (SDF-1α). It plays a homeostatic role in many tissues but has also a proinflammatory role and assists in T lymphocyte homing. Additionally, the recruitment of neutrophils, immature DCs, macrophages, innate lymphoid cells, and NK cells is promoted by CXCL12 (30). CXLCL12 can induce the expression of iNOS in CD8 T lymphocytes (31). iNOS is increased in vitiligo lesions and has been linked to melanocyte destruction (32). All 4 studies (177 vitiligo patients versus 82 controls) on circulating CXCL12 in vitiligo reported increased values in vitiligo patients compared to controls, resulting in a highly significant P-value of the meta-analysis (P = 0.003) (15, 19, 25, 33). Compared to other chemokines, the reported concentrations were relatively similar between the different reports. CXCL12 concentrations are also 1.2-1.7 higher in active vitiligo (2 studies; 45 active vs 65 stable) (25, 33).

Elevated CXCL12 expression has been demonstrated in many inflammatory and autoimmune skin diseases including psoriasis, rheumatoid arthritis, systemic lupus erythematosus, and inflammatory bowel disease. Furthermore, CXCL12 antagonists can delay disease onset and/or disease progression in inflammatory disorders (34). Melanocytes carry CCR4 and produce CXCL12 upon stimulation with LPS (35). Vitiligo melanocytes exhibited a 55.3 times upregulation based on RNA analysis compared to normal melanocytes (36). CXCL12 is one of the top secretary proteins upregulated in vitiligo (37). Additionally, CXCL12 regulates the migration and differentiation of melanocyte precursors and may play a role in the repigmentation of vitiligo lesions. On the other hand, some authors have hypothesized that CXCL12 may be responsible for hair graying or poliosis by the migration of melanocyte precursors out of the immune protective environment of the hair bulb (38, 39).

CCL5/RANTES: CCR5 signaling

CCL5 is a strong recruiting cytokine of NK cells, eosinophils, monocytes, effector memory T cells, B cells, and immature dendritic cells (Figure 2). CCL5 is induced by IFN-γ. 3/5 studies (266 patients versus 111 controls) reported significantly increased CCL5 concentrations in the circulation of vitiligo patients compared to healthy controls. The overall value of the meta-analysis was significant (P = 0.0008), although this result has to be interpreted with caution given the high variability in results ranging from no significant difference to an 11-fold difference in CCL5 levels (13, 20, 22, 33, 40). 3 studies investigated whether CCL5 was linked to disease activity with 2 studies documenting no significant difference and 1 report pointing to a small but significantly higher CCL5 concentration in active vitiligo (1.23-fold higher).

Yang et al., 2018 found increased CCL5 levels in the blister fluid of vitiligo patients compared to controls and higher values in active vitiligo versus stable vitiligo (13). Rashighi et al., 2014 detected increased CCL5 expression in lesional vitiligo skin compared to healthy controls (23). RNA analysis showed that *in vitro* cultured vitiligo melanocytes display a 23.5-fold upregulation of CCL5 (36). CCL5 can bind to CCR1, CCR3, and CCR4, although its highest affinity is with CCR5 (41). Gellatly et al., 2021 found that CCL3/4/5-CCR5 interaction is one the most affected pathways in vitiligo skin. CCR5 is upregulated on regulatory T cells (Tregs) in vitiligo promoting its function to suppress CD8+T cells (42).

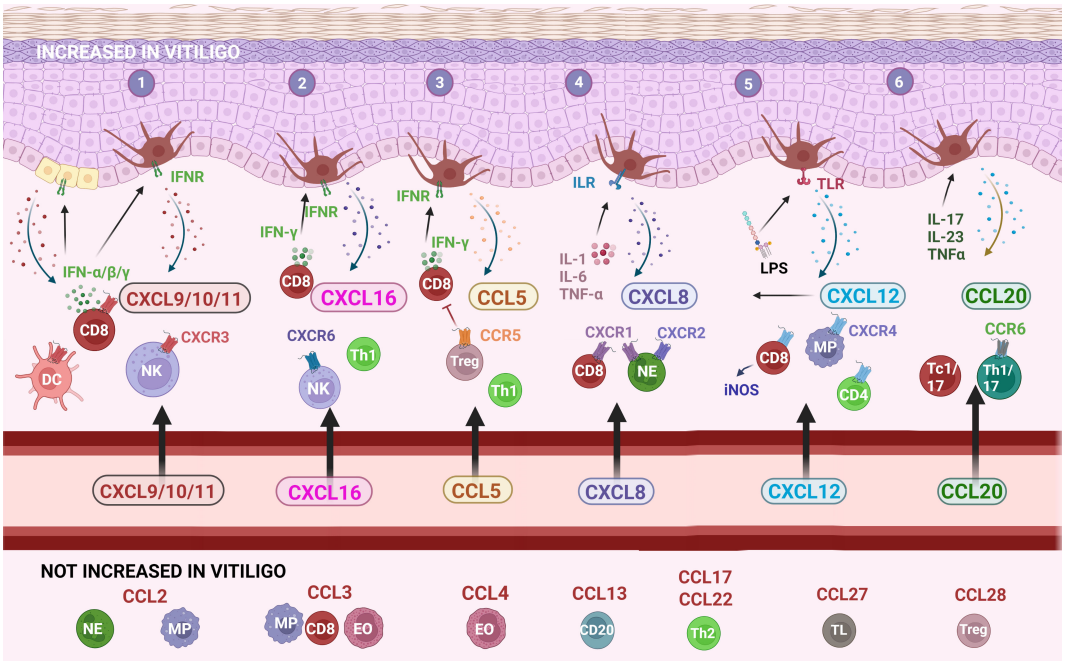

FIGURE 2
The main chemokines and receptors and their recruitment of immune cells into vitiligo skin. (1) CXCL9/10/11 chemokines bind to the CXCR3 receptor that plays a key role in the development of a cytotoxic CD8 response *via* IFN-γ, (2) CXCL16-CXCR6 signaling recruits NK cells, CD8 and CD4 lymphocytes; (3) the CCL5-CCR5 pathway attracts a broader range of immune cells into the skin; (4) CXCL8 is mostly recognized for its effect on neutrophils although a subset of CD8 lymphocytes also responds to this chemokine; (5) CXCL12 recruits several immune cells including macrophages and NK cells and also stimulates melanocyte migration; (6) CCL20 possibly involved in the recruitment of Tc1/17 and Th1/17 towards the skin. CCL: chemokine (C-C motif) ligand; CCR: chemokine (C-C motif) receptor; CD: cluster of differentiation; CXCL: chemokine (C-X-C motif) ligand; CXCR: chemokine (C-X-C motif) receptor; DC: dendritic cell; EO: eosinophil; IFN: interferon; IFNR: interferon receptor; IL: interleukin; ILR: interleukin receptor; iNOS: inducible nitric oxide synthase; LPS: lipopolysaccharides; MP: macrophage/monocyte; NE: neutrophil; NK: natural killer cell; Tc: cytotoxic T lymphocyte; Th: T helper lymphocyte; TL: skin-homing T lymphocyte; TLR: Toll-like receptor; TNF: tumor-necrosis factor; Treg: regulatory T cells. Created with Biorender.com.

CXCR1 and CXCR2 pathway: CXCL8

CXCL8 (= IL-8) is a proinflammatory cytokine expressed by a variety of cell types such as monocytes, macrophages, fibroblasts, endothelial, and epithelial cells including melanocytes (35). 3 studies (264 patients and 88 healthy controls) reported higher circulating CXCL8 values, although only one was statistically significant (13, 15, 22). A meta-analysis demonstrated also a significant overall effect (P = 0.03). CXCL8 levels were higher in active compared to stable vitiligo in 2 studies (P = 0.002). In one study, higher concentrations of CXCL8 were present in the blister fluid of vitiligo patients compared to healthy controls with increasing values in patients with progressive disease (13).

Vitiligo melanocytes seem to produce more CXCL8 compared to normal melanocytes (36). CXCL8 is produced upon stimulation of cells by different cytokines (e.g., IL-1, IL-6, and TNF-α) but also by other chemokines (e.g., CXCL12), reactive oxygen species, environmental stress, and bacteria. CXCL8 binds to CXCR1 and CXCR2, resulting in the chemotaxis and activation of neutrophils (43). CXCR1+ CD8 cells responding to CXCL8 have been linked with immediate cytotoxicity and early migration after innate immune activation (44). CXCL8 induces an oxidative burst, enhancing further inflammatory responses. It also induces endothelial cell permeability and angiogenesis (45). Unsurprisingly, this chemokine has been implicated in a variety of inflammatory disorders including psoriasis, asthma, inflammatory bowel syndrome, cystic fibrosis, and chronic obstructive pulmonary disorder (43).

Chemokine at the crossroads of Th17 and Th1 responses

CCL20/CCR6 receptor

Zhang et al., 2019 documented increased serum CCL20 values in vitiligo vs healthy controls and found slightly higher values depending on disease activity (46). Additionally, CCL20 concentrations were increased in the blister fluid of vitiligo patients compared to controls. CCL20 is induced by IL-17A, IL-23, and TNF-α and secreted by keratinocytes (46). The CCL20-CCR6 axis attracts IL-17A-producing cells to the skin and is elevated in chronic inflammatory diseases including psoriasis, inflammatory bowel disease and arthritis (46). However, the authors hypothesized that CCL20 may be involved in the recruitment of dual producing IL-17 and IFN-γ cells (CCR6+

Th1/17 cells and Tc1/17 cells) to vitiligo skin (46). Another study confirmed higher serum CCL20 concentrations in patients with active disease (47). In contrast, Rashighi et al., 2014 did not found increased CCL20 expression in lesional vitiligo skin versus controls (n=5 per group) (23). CCL20/CCR6 signaling recruits also Tregs to the skin and Tregs lacking CCR6 have a decreased capacity to migrate to vitiligo skin and suppress depigmentation (48).

Chemokines attracting neutrophils

CCL2/CCR2 receptor signaling

CCL2 is involved in the Th2 response and regulated by IL-4. CCL2 mainly attracts neutrophils and monocytes (49). CCL2 and IL-6 promote the survival of myeloid monocytes and trigger the differentiation towards M2-type macrophages (50). Additionally LPS-activated melanocytes have a high expression of CCL2 (35). No difference in serum CCL2 concentrations were found in vitiligo (170 vitiligo vs 90 control) (22, 28). Similarly, no higher values were found in progressive vitiligo (22).

Other chemokines

Several chemokines have to date only been investigated in one study and lack confirmation data.

Elevated chemokines without confirmatory data

Serum CCL3 levels were also higher in vitiligo patients although no link with disease activity was found (15). Nonetheless, a decreased production of CCL3 by vitiligo melanocytes has been reported (36). CCL3 is produced by a variety of hematopoietic and non-hematopoietic cells and recruits macrophages, eosinophils, and lymphocytes *via* the CCR1 or CCR5 receptor with preferential activity on activated CD8+ T cells (51). CCL3 was upregulated in CD8+ T cells of lesional and non-lesional vitiligo skin (42). Proteomic profiling of plasma (28 vitiligo patients versus 28 controls) showed elevated CXCL4 and CXCL7 levels (52). Higher CXCL4 levels would be in line with the increased CXCR3 signaling found in vitiligo.

Non-elevated chemokines without confirmatory data

No significantly elevated values were detected for CCL1, CXCL1, CCL4, CXCL13, CCL17, CCL22, CCL27, and CCL28 in the circulation of vitiligo patients. Most of these chemokines act on innate immune cells (e.g. neutrophils or eosinophils: CXCL1, CCL28), Th2 lymphocytes (CCL4, CCL17, CCL22), B lymphocytes (CXCL13), or Tregs (CCL28) (Figure 2). These cell types are therefore less likely to play a crucial role in the pathogenesis of vitiligo.

Conclusion

A substantial number of studies have confirmed the specific chemokine profile associated with vitiligo. Prominent CXCR3 signaling has been uncovered by the increased expression of CXCL9, CXCL10, CXCL11, and CXCL4. Of these chemokines, CXCL10 seems to display the most notable change in the blood circulation of vitiligo patients and is elevated in patients with active disease. In contrast, the levels of CXCL9 and CXCL11 tend to be more variable. The relevance of the CXCL12-CXCR4 pathway in vitiligo has also been confirmed although its differential expression in the skin has only been investigated to a limited extent. CXCL12 induces CXCL8 production which is also more pronounced in vitiligo patients. CCL5-CCR5 expression is elevated in vitiligo patients compared to healthy controls although a link with disease activity could not be confirmed. The CXCL16-CXCR6 pathway is another important pathogenic mechanism driving the progression of vitiligo by the recruitment of CD8+ lymphocytes (20). Most vitiligo studies have concentrated on a small number of chemokines based on previous findings, as evidenced by the large number of studies on CXCL9 and CXCL10. This method runs the risk of leaving key chemokines undiscovered for the time being. A possible role for CXCL4, CXCL7, and CCL18 has been suggested (42, 52). Broad chemokine profile studies are advisable to offer a non-biased approach.

Author contributions

RS performed the literature search, meta-analysis and wrote the draft of the article. AB created Figure 2. AB, MS, and NvG did a critical review of the manuscript. All authors contributed to the article and approved the submitted version.

Funding

The research activities of R. Speeckaert and N. van Geel are supported by the Scientific Research Foundation-Flanders (FWO Senior Clinical Investigator: 18B2721N and 1831512N, respectively). The research activitities of R. Speeckaert are supported by the Special Research Fund (Bijzonder Onderzoeksfonds, BOF) of Ghent University and Ghent University Hospital.

Conflict of interest

The authors declare that the research was conducted in the absence of any commercial or financial relationships that could be construed as a potential conflict of interest.

Publisher's note

All claims expressed in this article are solely those of the authors and do not necessarily represent those of their affiliated organizations, or those of the publisher, the editors and the reviewers. Any product that may be evaluated in this article, or claim that may be made by its manufacturer, is not guaranteed or endorsed by the publisher.

Supplementary material

The Supplementary Material for this article can be found online at: https://www.frontiersin.org/articles/10.3389/fimmu.2023.1112811/full#supplementary-material

SUPPLEMENTARY FIGURE 1
PRISMA flow diagram.

SUPPLEMENTARY FIGURE 2
Meta-analysis of chemokines at the protein level in skin blister fluid of vitiligo skin.

References

1. Karin N, Razon H. Chemokines beyond chemo-attraction: CXCL10 and its significant role in cancer and autoimmunity. *Cytokine* (2018) 109:24–8. doi: 10.1016/j.cyto.2018.02.012

2. Kunkel SL, Godessart N. Chemokines in autoimmunity: From pathology to therapeutics. *Autoimmun Rev* (2002) 1(6):313–20. doi: 10.1016/s1568-9972(02)00085-x

3. Melchjorsen J, Sørensen LN, Paludan SR. Expression and function of chemokines during viral infections: from molecular mechanisms to *in vivo* function. *J Leukoc Biol* (2003) 74(3):331–43. doi: 10.1189/jlb.1102577

4. Luo D, Wan X, Liu J, Tong T. Optimally estimating the sample mean from the sample size, median, mid-range, and/or mid-quartile range. *Stat Methods Med Res* (2018) 27(6):1785–805. doi: 10.1177/0962280216669183

5. Wan X, Wang W, Liu J, Tong T. Estimating the sample mean and standard deviation from the sample size, median, range and/or interquartile range. *BMC Med Res Methodol* (2014) 14:135. doi: 10.1186/1471-2288-14-135

6. Van der Mierden S, Spineli LM, Talbot SR, Yiannakou C, Zentrich E, Weegh N, et al. Extracting data from graphs: A case-study on animal research with implications for meta-analyses. *Res Synthesis Methods* (2021) 12(6):701–10. doi: 10.1002/jrsm.1481

7. Kuo PT, Zeng Z, Salim N, Mattarollo S, Wells JW, Leggatt GR. The role of CXCR3 and its chemokine ligands in skin disease and cancer. *Front Med (Lausanne)* (2018) 5:271. doi: 10.3389/fmed.2018.00271

8. Keeley EC, Mehrad B, Strieter RM. CXC chemokines in cancer angiogenesis and metastases. *Adv Cancer Res.* (2010). 106:91–111. doi: 10.1016/S0065-230X(10)06003-3

9. Metzemaekers M, Vanheule V, Janssens R, Struyf S, Proost P. Overview of the mechanisms that may contribute to the non-redundant activities of interferon-inducible CXC chemokine receptor 3 ligands. *Front Immunol* (2017) 8:1970. doi: 10.3389/fimmu.2017.01970

10. Dyer DP. Understanding the mechanisms that facilitate specificity, not redundancy, of chemokine-mediated leukocyte recruitment. *Immunology* (2020) 160 (4):336–44. doi: 10.1111/imm.13200

11. Tulic MK, Cavazza E, Cheli Y, Jacquel A, Luci C, Cardot-Leccia N, et al. Innate lymphocyte-induced CXCR3B-mediated melanocyte apoptosis is a potential initiator of T-cell autoreactivity in vitiligo. *Nat Commun* (2019) 10:2178. doi: 10.1038/s41467-019-09963-8

12. Tokunaga R, Zhang W, Naseem M, Puccini A, Berger MD, Soni S, et al. CXCL9, CXCL10, CXCL11/CXCR3 axis for immune activation - a target for novel cancer therapy. *Cancer Treat Rev* (2018) 63:40–7. doi: 10.1016/j.ctrv.2017.11.007

13. Yang L, Yang S, Lei J, Hu W, Chen R, Lin F, et al. Role of chemokines and the corresponding receptors in vitiligo: A pilot study. *J Dermatol* (2018) 45(1):31–8. doi: 10.1111/1346-8138.14004

14. Maouia A, Sormani L, Youssef M, Helal AN, Kassab A, Passeron T. Differential expression of CXCL9, CXCL10, and IFN-γ in vitiligo and alopecia areata patients. *Pigment Cell Melanoma Res* (2017) 30(2):259–61. doi: 10.1111/pcmr.12559

15. Zhang L, Xu X, Chen S, Kang Y, Wang X, Zhang C, et al. Increased circulating CXCL10 in non-segmental vitiligo concomitant with autoimmune thyroid disease and alopecia areata. *Ann Dermatol* (2019) 31(4):393–402. doi: 10.5021/ad.2019.31.4.393

16. Lin F, Hu W, Xu W, Zhou M, Xu A. CXCL9 as a key biomarker of vitiligo activity and prediction of the success of cultured melanocyte transplantation. *Sci Rep* (2021) 11:18298. doi: 10.1038/s41598-021-97296-2

17. Yang Y, Li S, Zhu G, Zhang Q, Wang G, Gao T, et al. A similar local immune and oxidative stress phenotype in vitiligo and halo nevus. *J Dermatol Sci* (2017) 87(1):50–9. doi: 10.1016/j.jdermsci.2017.03.008

18. Strassner JP, Rashighi M, Ahmed Refat M, Richmond JM, Harris JE. Suction blistering the lesional skin of vitiligo patients reveals useful biomarkers of disease activity. *J Am Acad Dermatol* (2017) 76(5):847–855.e5. doi: 10.1016/j.jaad.2016.12.021

19. Ng CY, Chiu Y-C, Chan Y-P, Lin Y-J, Chung P-H, Chung W-H, et al. Skin interstitial fluid and plasma multiplex cytokine analysis reveals IFN-γ signatures and granzyme b as useful biomarker for activity, severity and prognosis assessment in vitiligo. *Front Immunol* (2022) 13:872458. doi: 10.3389/fimmu.2022.872458

20. Li S, Zhu G, Yang Y, Jian Z, Guo S, Dai W, et al. Oxidative stress drives CD8+ T-cell skin trafficking in patients with vitiligo through CXCL16 upregulation by activating the unfolded protein response in keratinocytes. *J Allergy Clin Immunol* (2017) 140 (1):177–189.e9. doi: 10.1016/j.jaci.2016.10.013

21. Kılıc S, Şehitoğlu H, Gül C. Assessment of ADAM17 and ADAM10 proteins with CXCL10 and thyroid autoimmunity in vitiligo pathogenesis. *Postepy Dermatol Alergol* (2022) 39(2):397–400. doi: 10.5114/ada.2022.115891

22. Wang XX, Wang QQ, Wu JQ, Jiang M, Chen L, Zhang CF, et al. Increased expression of CXCR3 and its ligands in patients with vitiligo and CXCL10 as a potential clinical marker for vitiligo. *Br J Dermatol* (2016) 174(6):1318–26. doi: 10.1111/bjd.14416

23. Rashighi M, Agarwal P, Richmond JM, Harris TH, Dresser K, Su M-W, et al. CXCL10 is critical for the progression and maintenance of depigmentation in a mouse model of vitiligo. *Sci Transl Med* (2014) 6(223):223ra23. doi: 10.1126/scitranslmed.3007811

24. Bertolotti A, Boniface K, Vergier B, Mossalayi D, Taieb A, Ezzedine K, et al. Type I interferon signature in the initiation of the immune response in vitiligo. *Pigment Cell Melanoma Res* (2014) 27(3):398–407. doi: 10.1111/pcmr.12219

25. Gharib K, Gadallah H, Elsayed A. Chemokines in vitiligo pathogenesis: CXCL10 and 12. *J Clin Aesthet Dermatol* (2021) 14(9):27–32.

26. El-Domyati M, El-Din WH, Rezk AF, Chervoneva I, Lee JB, Farber M, et al. Systemic CXCL10 is a predictive biomarker of vitiligo lesional skin infiltration, PUVA, NB-UVB and corticosteroid treatment response and outcome. *Arch Dermatol Res* (2022) 314(3):275–84. doi: 10.1007/s00403-021-02228-9

27. Abdallah M, El-Mofty M, Anbar T, Rasheed H, Esmat S, Al-Tawdy A, et al. CXCL-10 and interleukin-6 are reliable serum markers for vitiligo activity: A multicenter cross-sectional study. *Pigment Cell Melanoma Res* (2018) 31(2):330–6. doi: 10.1111/pcmr.12667

28. Ferrari SM, Fallahi P, Santaguida G, Virili C, Ruffilli I, Ragusa F, et al. Circulating CXCL10 is increased in non-segmental vitiligo, in presence or absence of autoimmune thyroiditis. *Autoimmun Rev* (2017) 16(9):946–50. doi: 10.1016/j.autrev.2017.07.006

29. Flier J, Boorsma DM, van Beek PJ, Nieboer C, Stoof TJ, Willemze R, et al. Differential expression of CXCR3 targeting chemokines CXCL10, CXCL9, and CXCL11 in different types of skin inflammation. *J Pathol* (2001) 194(4):398–405. doi: 10.1002/1096-9896(200108)194:4<397::aid-path899>3.0.co;2-s

30. Zielińska KA, Katanaev VL. The signaling duo CXCL12 and CXCR4: Chemokine fuel for breast cancer tumorigenesis. *Cancers (Basel)* (2020) 12(10):3071. doi: 10.3390/cancers12103071

31. Choy JC, Yi T, Rao DA, Tellides G, Fox-Talbot K, Baldwin WM, et al. CXCL12 induction of iNOS in human CD8 T cells. *J Heart Lung Transplant* (2008) 27(12):1333–9. doi: 10.1016/j.healun.2008.08.014

32. Vaccaro M, Irrera N, Cutroneo G, Rizzo G, Vaccaro F, Anastasi GP, et al. Differential expression of nitric oxide synthase isoforms nNOS and iNOS in patients with non-segmental generalized vitiligo. *Int J Mol Sci* (2017) 18(12):2533. doi: 10.3390/ijms18122533

33. Speeckaert R, Ongenae K, van Geel N. Alterations of CXCL12 in serum of patients with vitiligo. *J Invest Dermatol* (2017) 137(7):1586–8. doi: 10.1016/j.jid.2017.02.012

34. García-Cuesta EM, Santiago CA, Vallejo-Díaz J, Juarranz Y, Rodríguez-Frade JM, Mellado M. The role of the CXCL12/CXCR4/ACKR3 axis in autoimmune diseases. *Front Endocrinol (Lausanne)* (2019) 10:585. doi: 10.3389/fendo.2019.00585

35. Tam I, Dzierżęga-Lęcznar A, Stępień K. Differential expression of inflammatory cytokines and chemokines in lipopolysaccharide-stimulated melanocytes from lightly and darkly pigmented skin. *Exp Dermatol* (2019) 28(5):551–60. doi: 10.1111/exd.13908

36. Rezk AF, Kemp DM, El-Domyati M, El-Din WH, Lee JB, Uitto J, et al. Misbalanced CXCL12 and CCL5 chemotactic signals in vitiligo onset and progression. *J Invest Dermatol* (2017) 137(5):1126–34. doi: 10.1016/j.jid.2016.12.028

37. Malhotra AG, Singh S, Jha M, Pandey KM. A parametric targetability evaluation approach for vitiligo proteome extracted through integration of gene ontologies and protein interaction topologies. *IEEE/ACM Trans Comput Biol Bioinform* (2019) 16 (6):1830–42. doi: 10.1109/TCBB.2018.2835459

38. Yamada T, Hasegawa S, Hasebe Y, Kawagishi-Hotta M, Arima M, Iwata Y, et al. CXCL12 regulates differentiation of human immature melanocyte precursors as well as their migration. *Arch Dermatol Res* (2019) 311(1):55–62. doi: 10.1007/s00403-018-1880-2

39. Liao Z-K, Hu S-H, Han B-Y, Qiu X, Jiang S, Lei T-C. Pro-pigmentary action of 5-fluorouracil through the stimulated secretion of CXCL12 by dermal fibroblasts. *Chin Med J* (2021) 134(20):2475–82. doi: 10.1097/CM9.0000000000001689

40. Shokeir1 HA, Emam2 H, Latif3 YA, Zeid4 OOA, Shoeib4 M, Hanafy4 NS, et al. Evaluation of serum level of RANTES among vitiligo patients before and after treatment by fractional carbon dioxide laser. *Indian J Public Health Res Dev* (2020) 11(3):145–51. doi: 10.37506/ijphrd.v11i3.3945

41. Appay V, Rowland-Jones SL. RANTES: A versatile and controversial chemokine. *Trends Immunol* (2001) 22(2):83–7. doi: 10.1016/s1471-4906(00)01812-3

42. Gellatly KJ, Strassner JP, Essien K, Refat MA, Murphy RL, Coffin-Schmitt A, et al. scRNA-seq of human vitiligo reveals complex networks of subclinical immune activation and a role for CCR5 in treg function. *Sci Transl Med* (2021) 13(610): eabd8995. doi: 10.1126/scitranslmed.abd8995

43. Ha H, Debnath B, Neamati N. Role of the CXCL8-CXCR1/2 axis in cancer and inflammatory diseases. *Theranostics* (2017) 7(6):1543–88. doi: 10.7150/thno.15625

44. Hess C, Means TK, Autissier P, Woodberry T, Altfeld M, Addo MM, et al. IL-8 responsiveness defines a subset of CD8 T cells poised to kill. *Blood* (2004) 104 (12):3463–71. doi: 10.1182/blood-2004-03-1067

45. Petreaca ML, Yao M, Liu Y, Defea K, Martins-Green M. Transactivation of vascular endothelial growth factor receptor-2 by interleukin-8 (IL-8/CXCL8) is required for IL-8/CXCL8-induced endothelial permeability. *Mol Biol Cell* (2007) 18 (12):5014–23. doi: 10.1091/mbc.e07-01-0004

46. Zhang L, Kang Y, Chen S, Wang L, Jiang M, Xiang L. Circulating CCL20: A potential biomarker for active vitiligo together with the number of Th1/17 cells. *J Dermatol Sci* (2019) 93(2):92–100. doi: 10.1016/j.jdermsci.2018.12.005

47. AL-Mousawi ZR, Alattabi AS, Hamza DM, AL-Hussiny FA. Serum level of CCL20 and CXCL 10 in patients with vitiligo and their association with disease activity. *Indian J Forensic Med Toxicol* (2021) 15(3):1147–56. doi: 10.37506/ijfmt.v15i3.15468

48. Essien KI, Katz EL, Strassner JP, Harris JE. Regulatory T cells require CCR6 for skin migration and local suppression of vitiligo. *J Invest Dermatol* (2022) 142(12):3158–3166.e7. doi: 10.1016/j.jid.2022.05.1090

49. Ratthé C, Ennaciri J, Garcês Gonçalves DM, Chiasson S, Girard D. Interleukin (IL)-4 induces leukocyte infiltration *in vivo* by an indirect mechanism. *Mediators Inflammation* (2009) 2009:193970. doi: 10.1155/2009/193970

50. Roca H, Varsos ZS, Sud S, Craig MJ, Ying C, Pienta KJ. CCL2 and interleukin-6 promote survival of human CD11b+ peripheral blood mononuclear cells and induce M2-type macrophage polarization *. *J Biol Chem* (2009) 284(49):34342–54. doi: 10.1074/jbc.M109.042671

51. Bhavsar I, Miller CS, Al-Sabbagh M. Macrophage inflammatory protein-1 alpha (MIP-1 alpha)/CCL3: As a biomarker. *Gen Methods biomark Res their Appl* (2015), 223–49. doi: 10.1007/978-94-007-7696-8_27

52. Liang L, Li Y, Tian X, Zhou J, Zhong L. Comprehensive lipidomic, metabolomic and proteomic profiling reveals the role of immune system in vitiligo. *Clin Exp Dermatol* (2019) 44(7):e216–23. doi: 10.1111/ced.13961

frontiers | Frontiers in Immunology

TYPE Review
PUBLISHED 24 February 2023
DOI 10.3389/fimmu.2023.1098570

OPEN ACCESS

EDITED BY
Yujing Zhang,
Nanjing University, China

REVIEWED BY
Jing Li,
Nanjing University, China
Dina H. Kassem,
Ain Shams University, Egypt

*CORRESPONDENCE
Hui Shen
shenhuicam@sohu.com

†These authors have contributed equally to this work

SPECIALTY SECTION
This article was submitted to Cytokines and Soluble Mediators in Immunity, a section of the journal Frontiers in Immunology

RECEIVED 15 November 2022
ACCEPTED 10 February 2023
PUBLISHED 24 February 2023

CITATION
Li Z, Gao Z, Sun T, Zhang S, Yang S, Zheng M and Shen H (2023) Meteorin-like/Metrnl, a novel secreted protein implicated in inflammation, immunology, and metabolism: A comprehensive review of preclinical and clinical studies. *Front. Immunol.* 14:1098570. doi: 10.3389/fimmu.2023.1098570

Meteorin-like/Metrnl, a novel secreted protein implicated in inflammation, immunology, and metabolism: A comprehensive review of preclinical and clinical studies

Zhuoqi Li[1†], Ziyu Gao[2†], Tao Sun[1], Shipeng Zhang[1], Shengnan Yang[1], Meilin Zheng[1] and Hui Shen[1*]

[1]Department of Rheumatology and Immunology, The First Hospital of China Medical University, China Medical University, Shen Yang, China, [2]Department of Thyroid Surgery, The First Hospital of China Medical University, China Medical University, Shen Yang, China

Meteorin-like, also known as Metrnl, Meteorin-β, Subfatin, and Cometin, is a novel secreted protein exerting pleiotropic effects on inflammation, immunology, and metabolism. Earlier research on this hormone focused on regulating energy expenditure and glucose homeostasis. Consequently, several studies attempted to characterize the molecule mechanism of Metrnl in glucose metabolism and obesity-related disorders but reported contradictory clinical results. Recent studies gradually noticed its multiple protective functions in inflammatory immune regulations and cardiometabolic diseases, such as inducing macrophage activation, angiogenesis, tissue remodeling, bone formation, and preventing dyslipidemias. A comprehensive understanding of this novel protein is essential to identify its significance as a potential therapeutic drug or a biomarker of certain diseases. In this review, we present the current knowledge on the physiology of Metrnl and its roles in inflammation, immunology, and metabolism, including animal/cell interventional preclinical studies and human clinical studies. We also describe controversies regarding the data of circulation Metrnl in different disease states to determine its clinical application better.

KEYWORDS

Metrnl, inflammation, metabolism, immunity, bone, heart, obesity, diabetes

Introduction

Secreted proteins play an important role in certain physiological or pathological processes to reflect and regulate the organism's state at the molecular level. Exploring the secreted protein's mechanism, which may be applied as a targeted agent or a predictive biomarker, would help diagnose and treat clinical diseases. Metrnl, also known as

Meteorin-like, Meteorin-β, Subfatin, and Cometin, is a novel secretory protein that shares 46% amino acid sequence homology with a neurotrophic factor named Meteorin. Unlike Meteorin's brain-specific expression in the central nervous system, Metrnl is abundant in metabolism-related organs and barrier tissues (1). Besides, its secretion and regulation depend not on the fixed model of cell types but on the concrete physiological and pathological context.

When Metrnl was described in early studies as an identity of adipokine, exerting pleiotropic effects on glucose homeostasis, such as improving insulin sensitivity, facilitating adipose tissue browning, and increasing energy expenditure (2). While recent research results suggested that Metrnl may play protective roles in several cardio-metabolic and other inflammatory immune diseases. Different physiological activities could also regulate Metrnl expression, including exercise, temperature variation, bariatric surgery, and high-fat diets. A comprehensive understanding of Metrnl is essential to determine its significance as a potential therapeutic agent or biomarker for certain diseases. As such, this present review would offer an overview of the valid evidence on the effects of Metrnl in inflammation, immunology, metabolism, and related diseases, including animal/cell interventional preclinical studies and human clinical studies.

Physiology of Metrnl

Metrnl is located on regions of human chromosome 17q25.3 and mouse chromosome 11qE2, consisting of 311 amino acids encoded by 936 base pairs (3). There is a 45 amino acid sequence at the amino terminus, but Metrnl does not have a membrane-spanning region. Since Metrnl was the only gene on the q-arm terminal end of chromosome 17, it may regulate a mild clinical phenotype of a rare disorder named Mild Ring 17 Syndrome (4). This phenotype presented as growth delay and intellectual disability and was presumed to be associated with abnormal expression of genes (including Metrnl) related to proximal telomere side neurogenesis. Interestingly, 17q25.3 was a susceptibility locus of cardiovascular disease (5), psoriasis (6), and atopic dermatitis (7), where its fragment deletion could result in cardiovascular deficiencies or cardiac phenotype changes. Notably, Metrnl has been studied preliminarily in these diseases, thus providing a genomic rationale for involvement in pathogenesis development. However, its intracellular localization and distribution still need to be clarified. Its molecular structure and family ligands are also poorly studied, which poses an obstacle to exploring the relationship between Metrnl structure and function.

Metrnl was highly conservative in its evolution and 40% homologous to the neurotrophic factor Meteorin (8). Unlike Meteorin's concentrated expression in the central nervous system (CNS), Metrnl was highly expressed in adipose, skin, and mucosal barrier tissue, whereas less in CNS (1, 9). Nevertheless, several studies still attempted to explore Metrnl functions in CNS. Based on original bioinformatics, Ramialison et al. (10) detected Metrnl as one of the direct downstream targets of PAX2/5/8 genes involved in inner ear growth. A similar study was reported by Jørgensen et al. (3) that Metrnl exclusively in dorsal root ganglions and inner ear during early mouse development but not in the adult CNS. These studies suggest Metrnl may be involved in inner ear development.

As a new neurotrophic factor, Metrnl could promote neurite outgrowth, migration, and neuroprotection (3, 11). Of note, Metrnl was able to cross the human blood-brain barrier to migrate into the CNS, as well as Metrnl levels in human cerebrospinal fluid were significantly correlated with its serum levels and albumin CSF/serum ratios (12). Considering Metrnl could induce significantly upon exercise and muscle contraction, prompting that Metrnl may migrate from the periphery tissues into the CNS under these activities. However, to address the effect of *de novo* innervation on human skeletal muscle cells, Jan et al. (13) found that co-culture myotubes with the embryonic rat spinal cord explants did not affect Metrnl mRNA expression. It may be interesting to explore whether Metrnl directly influences the muscle-brain axis or whether Metrnl involves in neuromuscular transmission. Recently, Hong et al. (14) reported that Metrnl could regulate cognitive dysfunction in D-galactose-induced aging models as Metrnl deficiency significantly aggravated the cognitive impairment and decreased hippocampal BDNF, TrkB, and GFAP levels. It would be promising that exploring Metrnl as a candidate treatment and alleviation of aging-related cognitive dysfunction. But further studies are required to clarify the specific mechanisms among Metrnl, neurons and other glial cells.

Metrnl and immunology

Considering Metrnl is involved in modulating the immune response, several studies have explored its implications in abnormal immune conditions, detected the expression of Metrnl in autoimmune diseases, and analyzed its relationship with these diseases. In this part, we described current knowledge of Metrnl's role in immunology, including regulations of innate or adaptive immunity and involvement in autoimmune diseases. We also summarized main findings of Metrnl-related preclinical (Table 1) and clinical studies (Table 2) on immunology to understand better.

Metrnl and immune system

Metrnl was first described in the immune field when Albert et al. (9) sought to discover a novel or uncharacterized gene associated with the immune system through bioinformatics analyses of the BIGE database (a comprehensive human gene expression database) (38, 39). Therefore, Metrnl was identified, and it is strongly produced by various macrophages. Importantly, Metrnl$^{-/-}$ mice exhibited B-cell immune system defects, including lower serum IgG levels (mainly because of IgG2b and IgG3 low levels) (17). Besides, its splenocytes showed an inability to secret some chemokines like CCL3 and CCL4, as well as a significant reduction in IFN levels. This study also reported that Metrnl could inhibit the expression of class MHC-II in peritoneal macrophages during IFN-γ induction (17). According to the ImmGen Datasets (https://www.immgen.org/), Metrnl could be produced by thymic

10.3389/fimmu.2023.1098570

TABLE 1 Summary of preclinical studies associated with Metrnl in inflammation and immunology.

Year	Ref.	Methods	Main findings	
			Immunology	Inflammation
2014	(15)	Mouse; *in vitro*	Trigger Type 2 immune cascade activation, promote M2 alternative activation of macrophages	Increase anti-inflammatory cytokines
2015	(9)	*In vitro*	Produced by M2-like macrophages	Overexpression in skin lesions of skin inflammatory diseases
2016	(16)	Mouse	Intestinal epithelial cells Metrnl-KO mouse: decrease gut antimicrobial peptides	–
2018	(17)	Mouse; *in vitro*	Metrnl$^{-/-}$ mice: develop inflammatory lesions easier, B-cell immune system defects	Induced by IL-4, IL-12, IL-17α, and TNF-α; inhibited by IFN-γ and TGF-β
2019	(18)	Mouse	Metrnl treatment in Crohn's disease-like mouse: ameliorate mesenteric lesions *via* STAT5/PPAR-γ	Decrease inflammatory score and pro-inflammatory cytokines
2020	(19)	Mouse	Intestinal epithelial cells Metrnl-KO mouse: deteriorate ulcerative colitis *via* autophagy-related AMPK-mTOR-p70S6K pathway	Increase TNF-α, IL-6, and IL-1β
2020	(20)	*In vitro*	Metrnl overexpression in H9C2 cells: attenuate cardiomyocytes apoptosis *via* AMPK-PAK2	Inhibit inflammation and endoplasmic reticulum stress
2020	(21)	Mouse; *in vitro*	Improve muscle regeneration by infiltrating immune cells *via* Stat3/IGF-1	Induce macrophage differentiate into inflammatory phenotype
2021	(22)	Mouse	Metrnl treatment in non-obese diabetic mice: delay onset, ameliorate islet lymphocyte infiltration	Increase IL-4, IL-10, and Foxp3; decrease IL-2, IL-17, and IFN-γ; suppress Treg cells
2021	(23)	Mouse; *in vitro*	–	Inhibit IL-1β in macrophages; associated with NLRP3 inflammasome activation
2021	(24)	*In vitro*	LPS-treated cells: ameliorate endothelial inflammation *via* AMPK and PPARδ-pathways	Suppress TNF-α, MCP-1, NFκB and IκB phosphorylations, and inflammatory markers
2022	(25)	Mouse; *in vitro*	Impair the maturation and functions of DCs, block the development of airway hyper-reactivity	Decrease DC-mediated Th2 immune responses and inflammation
2022	(26)	*In vitro* (fish)	Up-regulate Type 1 immune response	Increase IL-1β, IL-6, IL-8, IL-17A and TNF-α

TABLE 2 Metrnl-related circulation levels and tissue expressions of human clinical studies on inflammation and immunology.

Year	Ref.	Methods	Diseases	Main findings
2019	(27)	Tissue expression	PsA, RA, OA	Highly expressed in PsA synovial tissue and fluid than OA and RA
2020	(28)	Tissue expression	Malignant mesothelioma	Immunoreactivity more prominent than mesothelial hyperplasia
2020	(29)	Serum level	Inflammatory bowel disease	Lower in UC and CD patients than controls
2020	(30)	Tissue expression	NAFLD	Hepatic Metrnl expression decrease after bariatric surgery
2021	(31)	Serum and synovial fluid levels	OA	Lower serum levels and higher synovial fluid levels in OA patients than non-OA controls
2022	(32)	Tissue expression	Invasive ductal breast cancer	Immunoreactivity increased than normal breast tissues
2022	(33)	Tissue expression	Basal cell carcinoma	Immunoreactivity increased than control and trichoblastoma
2022	(34)	Tissue expression	Serous ovarian tumors	Immunoreactivity deteced in parenchymal areas of cancer tissues, localized in epithelial areas of normal tissues
2022	(35)	Serum level	Graves' disease	Lower in GD patients than healthy control
2022	(36)	Serum level	RA	Higher in RA patients than controls
2022	(37)	Gene expression	Bariatric surgery, obese	Increased significantly after bariatric surgery

medullary epithelial cells, suggesting Metrnl may also affect T-cell development.

While exploring specific mechanisms, Metrnl seems to be associated with Type 2 immune responses. Rao et al. (15) observed that Metrnl overexpression could trigger Type 2 immune cascade activation and secret cytokines IL-4/IL-13, promoting M2 macrophage activation to produce catecholamines (40). In an allergic asthma mice study, Metrnl could impair dendritic cells (DCs) maturation and function of antigen presentation both *in vitro* and vivo, thereby reducing Type 2 inflammatory responses (25). This study provided a novel treatment strategy for targeting Metrnl in allergic asthma. Besides, Legaki et al. (41) have recently identified Metrnl as one differentially methylated loci biomarker in asthma or rhinitis, which provides epigenetics evidence of Metrnl's involvement in asthma molecularly mechanisms. It is noteworthy that injecting recombinant Metrnl could not affect B-cell class switching or production of IgE but significantly decreased T-cell proliferation if coculturing splenic $CD4^+$ T cells with bone marrow-derived DCs (25). Interestingly, human helminth infections shared similar pathways with allergic asthma, a change in Type 2 phenotype differentiation (42, 43). In this state, Th2 cells develop a PD-1/PD-L2-dependent intrinsically hypo-responsive phenotype, denoted by parasite killing or impaired functionality. Furthermore, microarray data analysis revealed that Metrnl was identified as one immune regulatory gene associated with Th2 cell-intrinsic hypo-responsiveness transcriptional changes (44).

Given the immunomodulatory properties of Metrnl, it may influence tumorigenesis. Actually, Metrnl exerting pro-tumor and pro-apoptotic effects has been observed in pancreatic cancer (45, 46). But studies on Metrnl and tumor immune mechanisms are fewer, while other studies only preliminarily investigated Metrnl immunoreactivity and its relation with tumor prognosis. Metrnl immunoreactivity was increased significantly in invasive ductal breast cancer tissue compared with normal breast tissues, but no difference among the breast cancer grades (32). Similar elevation was also observed in tumor and stromal tissues of basal cell carcinoma and trichoblastoma (33), malignant mesothelioma (28), and serous ovarian tumors (34). Besides, a recent study on bladder cancer identified Metrnl as a target gene in epigenetic synergistic interactions between miRNA and DNA methylation, which was associated with the survival of potential prognostic markers in bladder cancer (47). However, this study did not provide any clinical data supporting it. Interestingly, tumor growth and metastasis depend on angiogenesis, while Metrnl has been identified as a driver of heart postinfarction angiogenesis (48). It would be a promising research orientation to explore Metrnl's roles in tumor growth, angiogenesis, invasion, and metastasis, thus determining whether Metrnl might be a target in tumor therapy.

Metrnl and autoimmune diseases

Metrnl was involved in multiple autoimmune disorders. As Type 1 diabetes (T1DM) is occurred by autoimmune progressive attacking pancreatic beta cells, a recent study by Zhina et al. (22) observed that intravenous administration of Metrnl could postpone the onset of diabetes in non-obese diabetic mice. This study further explored the mechanism and showed that Metrnl treatment could decrease islet lymphocyte infiltration and modulate immune cell responses. It would be prospective to combine Metrnl-related research results in T1DM patients to determine the possibility as a drug agent. Recently, Gong et al. (35) detected Metrnl levels in thyroid autoimmune diseases and found that Metrnl was significantly lower in Graves' disease (GD) patients than in healthy controls, positively correlated with CRP and WBC. Besides, Ushach et al. (9) calculated that Metrnl expression was up-regulated in rheumatoid arthritis (RA) synovial membranes by using a gene expression database of RA they constructed before (49). Further investigation proved this finding as Metrnl was significantly increased in the synovial fluid of psoriatic arthritis (PsA) and RA compared to osteoarthritis (OA) patients, and synovial biopsies also mirrored this expression (27, 50). In contrast, Metrnl levels reduced in OA serum (31). Importantly, our academic team recently reported that Metrnl serum level was higher in RA patients than in OA and healthy controls, positively correlated with disease activity indices (36). These results suggested the close relationship between Metrnl and autoimmune-associated arthritis, but the specific mechanism mediating this role remains to be found.

Using tissue microarray, Li et al. (16) found Metrnl highly expressed in the gastrointestinal tract and the intestinal epithelium. Interestingly, a study by Gholamrezayi et al. (29) reported that Metrnl circulation concentration was lower in both Crohn's disease (CD) and Ulcerative Colitis (UC) patients and inversely related with TNF-α and IL-6. To further figure out the mechanism, scholars generate the intestinal epithelial cell-specific Metrnl-KO mice, where Metrnl levels in the gut fluid and antimicrobial peptides release decreased significantly but did not influence colon length, intestinal permeability, or mucus content. However, UC was more prone to be induced in intestinal $Metrnl^{-/-}$ mice than in WT mice (19). In this study, intestinal Metrnl deficiency was related to reduced autophagy in epithelial cells *via* the AMPK-mTOR-p70S6K pathway. Similar to this study, Zuo et al. (18) showed that Metrnl was increased in CD mesenteric adipose tissue and that injecting Metrnl into $IL\text{-}10^{-/-}$ mice (CD-like model) could decrease the disease activity index and inflammatory score, indicating Metrnl mediated protective effects. In this study, Metrnl activated STAT5/PPAR-γ signaling and promoted adipocyte function, thereby ameliorating chronic colitis. Collectively, maybe different tissues produce Metrnl with different environmental regulatory mechanisms, and Metrnl may be a therapeutic target for UC and CD.

Metrnl and inflammation

Similar to inflammary factor, Metrnl also play roles in immune inflammatory response. In this part, we first overviewed Metrnl developments with inflammatory factor network in multiple diseases. Then we discussed its role of inflammation regulation in different tissues. We also summarized main findings of preclinical

studies and clinical studies in inflammation (Tables 1, 2). Finally, considering that Metrnl regulated several functions with the help of macrophages, we drew relationships among these relevant cells to better understand (Figure 1).

Metrnl and inflammatory factor network

Many studies presented so far indicate that Metrnl is associated with inflammation. Metrnl$^{-/-}$ mice, generated by Ushach et al. (17), were prone to develop inflammatory lesions (including uterus unilateral horn, kidneys, and liver) and endotoxin shock, suggesting Metrnl deficiency promotes inflammation development. It may play an anti-inflammatory role during sepsis. Metrnl was diffusely in activated macrophages (1, 9), as well as its production can be induced by several cytokines and inversely regulate other chemokines and cytokine production. Bone marrow macrophages can produce Metrnl by IL-4, IL-12, IL-17α, and TNF-α stimulating, of which TNF-α is the most potent inducer and can inhibit by IFN-γ and TGF-β (17). Incubating macrophages with Metrnl can also increase IL-6, IL-10, CXCL1, and CCL2 expression. Another study with similar findings by Junya et al. (26) reported that Metrnl homologues upregulated pro-inflammatory cytokines (TNF-α, IL-17A, IL-1β, IL-6, and IL-8) and promoted Type 1 immune response (IFN-γ and IL-2) *via* NF-κB dependent pathway in grass carp head kidney leukocytes. In addition, Metrnl overexpression inhibited inflammation and alleviated endoplasmic reticulum stress in injured H9C2 cells by activating AMPK-PAK2 signaling, playing an anti-inflammation role (20).

Several studies have reported that Metrnl serum levels were negatively associated with inflammatory cytokines like TNF-α and IL-6 in many metabolic diseases (20, 29, 51–53). A study on human umbilical vein endothelial cells (HUVECs) with Metrnl deficiency reported that pro-inflammatory cytokines IL-6, IL-1β, and MCP-1 were increased under normal conditions, and IL-6, IL-1β, TNF-α were elevated under ox-LDL stimulation (24). In this study, Metrnl could ameliorate LPS-induced endothelial cell inflammation through AMPK and PPAR-γ dependent pathways as endothelial injury inducing many metabolic diseases. Besides, disease activity index CRP and hs-CRP were also negatively correlated with Metrnl circulation in polycystic ovarian syndrome (PCOS), CAD, impaired glucose tolerance (IGT), GD, and type 2 diabetes Mellitus (T2DM) (35, 52, 54, 55). In contrast to these findings, two studies found that Metrnl serum levels were positively correlated with inflammation factors in chronic obstructive pulmonary diseases (COPD) and neurological disease patients (12, 56). Thus, larger participants should be involved in determining the correlation between Metrnl and the network of inflammation factors.

Metrnl and adipose tissue inflammation

Adipose tissue eosinophils (ATEs) distribution and function are important in controlling age-related and obesity-related inflammation (57). Metrnl could stimulate an eosinophil-

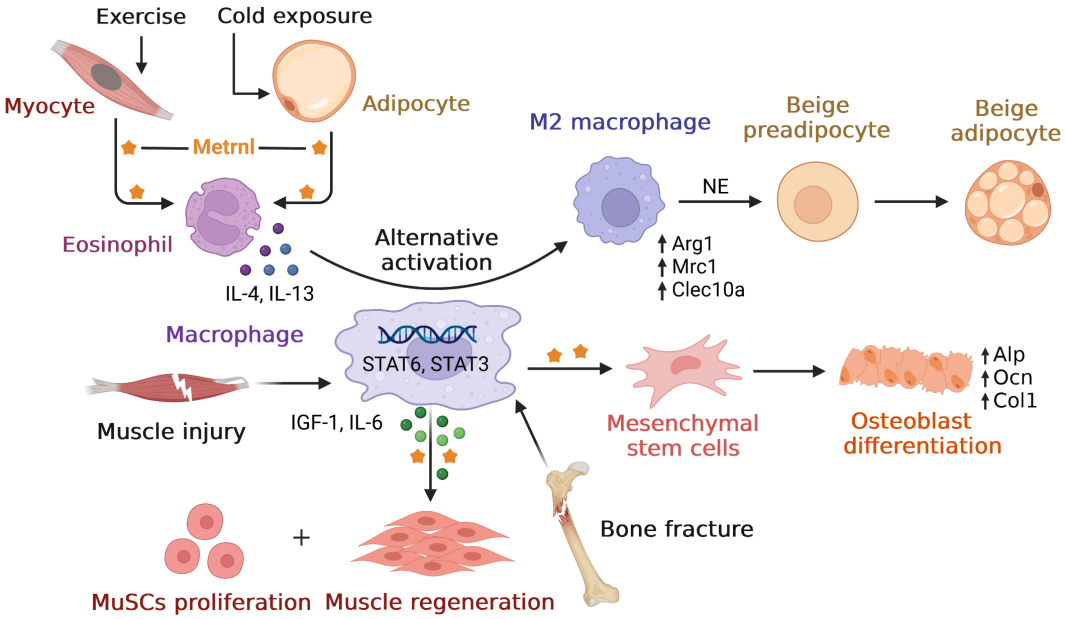

FIGURE 1
Overview of relationships between Metrnl and macrophages. Metrnl could induce IL-4 and IL-13 secretions by eosinophil upon exercise in myocytes and cold exposure in adipocytes. These cytokines stimulated macrophages' alternative activation to M2 type *via* STAT6 signaling, which released norepinephrine (NE) and promoted adipocyte browning to increase thermogenesis. After muscle injury, macrophage-derived Metrnl activated STAT3 signal to induce IGF-1 and IL-6 secretions, thus promoting muscle stem cells (MuSCs) proliferation and skeletal muscle regeneration. Metrnl was highly expressed at regions of osteoblast active and bone depositions during bone fracture healing. Besides, Metrnl could promote mesenchymal stem cells differentiating into osteoblasts with increasing osteogenic transcripts.

dependent increase in IL-4/IL-13 secreting, which promoted alternate activation of M2 macrophages to act as an anti-inflammatory function (15). Meanwhile, overexpression in Metrnl mice increases eosinophils in adipose tissue, and injecting an antibody against Metrnl prevents eosinophil accumulation (15, 40). Because Metrnl could not directly activate macrophages or adipocytes, eosinophils are indeed required for this mechanism (15). Interestingly, it is reported that transferring young mice eosinophils into an aged host can inhibit adipose tissue age-related inflammation and improve immune fitness, partially mediated by eosinophil-derived IL-4 (57). Many studies proved Metrnl can attenuate inflammation in adipose tissue (17, 18, 23, 24, 58, 59), and adipose tissue function was crucial in contributing to age-related metabolic diseases (60). Importantly, Ushach et al. (17) observed that older Metrnl-KO mice were prone to develop inflammatory lesions, especially unilateral inflammatory lesions of one uterus horn, while white adipose tissue developed no lesions. Furthermore, Metrnl played essential roles in body inflammation regulation and adipose tissue inflammation homeostasis. Beyond that, Metrnl may also slow adipose tissue inflammation associated with aging by affecting eosinophils.

Metrnl and skeletal muscle inflammation

Increasing evidence suggests that skeletal muscle inflammation is accompanied by obesity and metabolic disorders development, which is manifested by proinflammatory activation and immune cell infiltration in intramyocellular and perimuscular adipose tissue (61). Exercise has many beneficial effects on metabolic disorders partly attributed to its anti-inflammatory effect. Metrnl, one of the myokines, can be induced in the skeletal muscle upon exercise (15), especially during muscle contractions (62). Javaid et al. (23) showed that exercise could significantly enhance Metrnl expression in various muscle depots, inhibiting NLRP3 inflammasome activation and downregulating IL-1β and IL-18 in adipose tissue. Further *in vitro* macrophage experiments also confirmed this anti-inflammation role. Moreover, Jung et al. (58) found that treating high-fat-diet (HFD) mice with Metrnl can suppress inflammatory markers and attenuate the impaired insulin response in mouse skeletal muscle and differentiated C2C12 cells.

Of note, Metrnl also played a role in regenerating damaged muscle, as it was increased sharply (30-fold) after muscle injury 24h in murine models of muscle regeneration (21). Subsequently, single-cell RNA-seq demonstrated that the most robust Metrnl transcript was by macrophage clusters in the injured muscle. Meanwhile, the LysM Cre mouse and macrophage-specific Metrnl-KO mice experiments confirmed the essential role of macrophage-secreted Metrnl in successful muscle regeneration. Moreover, Metrnl can directly signal to macrophages through Stat3 to result in differentiation to an anti-inflammatory phenotype and indirectly to primary muscle satellite cells by IGF-1 and IL-6 secretion to promote muscle stem cell expansion (21, 63). Besides, we summarized main signal pathways of Metrnl in myocytes. Collectively, Metrnl has exerted a healing and anti-inflammation effect on skeletal muscle damage, indicating that Metrnl may be a novel therapeutic target for treating aging or other inflammatory myopathies.

Metrnl regulations in glucose metabolism

In humans, secretory proteins such as adipokines could modulate glucose uptake and release to regulate glucose homeostasis directly. Once a long-term lack of physical activities or a chronic high-fat diet induces obesity may result in disturbances of glucose metabolism, which leads to the development of insulin resistance and diabetes. In this section, we described the roles of Metrnl in glucose homeostasis, including glucose uptake, thermogenesis, and adipose browning. We also summarized regulations of Metrnl in related metabolic diseases, including insulin sensitivity, polycystic ovarian syndrome, and diabetes. Regarding controversial data in clinical studies, we analyzed it from multiple angles and summarized it in Supplementary Table 1.

Metrnl and glucose homeostasis

The human body can adapt to external and internal environment variations by adjusting metabolism in peripheral tissues, such as cold exposure could induce skeletal muscle and adipose tissue a switch of glucose and fat metabolism (64). This adaptation to acute environment change might be a protective mechanism to ensure enough glucose priority for the central nervous system, whereas fatty acids and amino acids are allocated to other peripheral metabolic organs (65). Metrnl can be strongly induced in the adipose tissue upon acute cold exposure and muscle upon exercise, leading to increased energy expenditure by stimulating the browning of white adipose tissue. Unlike most adipokines identified in obesity models, Metrnl was first described in the PGC-1α4 transgenics mice model (15). PGC-1α4 is an exercise-induced splice isoform of PPARγ coactivator 1a, and skeletal muscle-specific PGC-1α4-KO transgenics mice were lean and showed an increase in basal energy expenditure (66). Given that adipose thermogenesis can augment whole-body energy expenditure, this study analyzed adipose tissues for expression of genes related to thermogenesis or involved in imparting adipose tissue browning, so METRNL was the candidate gene (15). Besides, Metrnl may promote thermogenesis function through activations of the UCP family in brown adipose tissue (67). Recently, Şekerci et al. (68) reported that central administrating of Metrnl could activate hypothalamus-pituitary-thyroid axis hormones *via* peripheral UCPs. UCPs and PGC-1α were typical thermogenic genes in the nucleus, so Metrnl played roles in body energy homeostasis regulation.

Metrnl's ability to stimulate the browning of white adipose tissue seemed not to act directly on adipocytes but was dependent on the eosinophils-mediated IL-4/IL-13 signaling cascade of M2 alternately activated macrophages (15). This academic team subsequently demonstrated that eosinophils are indeed required for Metrnl-induced brownin. Owing to this mechanism, Metrnl has

been distinguished from other adipokines with similar functions, such as irisin (69), asprosin (70), and Fgf-21 (71), as they directly stimulated adipocytes to thermogenesis. Furthermore, Zhiyong et al. (59) used inguinal subcutaneous white adipose tissue in adipocyte-specific Metrnl-KO mice to verify these effects. However, there existed no Metrnl-induced adipose browning or no thermogenesis-associated gene change. Notably, the former report showed that Metrnl-induced adipose browning occurred briefly and disappeared in one week (15). So maybe using different experimental models (relatively acute and chronic models) caused this contradiction.

Both modest cold exposure and exercise could promote the conversion of white to brown adipose tissue, increasing the body's metabolism and helping weight loss (72). Metrnl could adapt to cold temperatures by regulating immune-adipose interactions to increase thermogenesis. Interestingly, a recent study based on Zebrafish using CRISPR/Cas9 system knockout gluk2, a protein that perceived cold in the periphery sensory neuron, revealed Metrnl was one of the differentially expressed genes (73). Although cold exposure induces no-shivering thermogenesis, long-term periods of negative caloric balance would diminish physiological resilience. In a recent study focusing on athletes in extreme cold during continuous physical activity, Coker et al. (74) observed that Metrnl serum levels remained stable throughout the 430-mile distance in temperature -45°C. In contrast to this finding, Saghebjoo et al. (75) investigated serum Metrnl changes in exercises with different temperature conditions on overweight young women. They observed that Metrnl was increased when exercising in temperate and warm water and decreased in cold water. Taking effects that the duration of exposure temperatures, the intensity of exercise, and the physical fitness of participants also affect the response of Metrnl, further investigations are required to clear appropriate temperature to enhance Metrnl expression.

Metrnl and insulin sensitivity

Insulin resistance is a risk factor for many metabolic disorders such as obesity and diabetes. Adipose tissue regulates insulin function *via* secreting adipokines and sequestering lipids, which or else would accumulate in other tissues and produce bad effects (76). Actually, the major participant to insulin resistance is exact the excessive deposition of lipids in other organs (77). Therefore, adipokines play crucial roles in lipid-associated insulin resistance. Researchers have established many animal models to explore the relationship between Metrnl and insulin resistance. In specific-adipocyte Metrnl-KO mice, though the plasma concentration of Metrnl remained unchanged, Metrnl expression was increased in adipose tissue with its phenotypes of insulin resistance induced by high-fat-diet exacerbated a lot (59). On the contrary, overexpression Metrnl of adipocyte-specific mice could antagonize insulin resistance induced by HFD or hyperphagia (leptin knockout). These results supported that Metrnl was associated with mice's overall insulin resistance.

Recently, in an injecting recombinant Metrnl to treat HFD-fed mice study, Metrnl ameliorated the impaired insulin response in skeletal muscle and C2C12 myoblast cells *via* AMPK/PPARδ-mediated signaling (58). Similar studies also concentrated on T2D mice; injection of Metrnl protein can reduce the high glucose-induced insulin secretion and promote the islet β-cell function recovery by activating pancreatic islet β-cell proliferation in mice and inhibiting β-cell apoptosis (78). This function was achieved *via* the WNT/β-catenin pathway, where β-catenin could protect apoptosis of islet microvascular endothelium role (79), which also pointed to the importance of the WNT/β-catenin pathway in maintaining β-cell function. In addition, Lee et al. (62) found that Metrnl treatment with C2C12 myoblasts could increase glucose uptake *via* the calcium-dependent AMPKα2 and p38 MAPK pathways, as well as in an AMPKα2-dependent manner to regulate the binding of HDAC5 to the GLUT4 promoter. In this study, Metrnl treatment could not elevate glucose tolerance in AMPK β1β2-KO mice, demonstrating the necessity of the AMPK pathway. Notably, Wang et al. (80) reported that serum Metrnl level was correlated with insulin resistance merely, but not with β-cell function (Figure 2). These animal studies suggested that Metrnl has strong insulin sensitization and antagonizes insulin resistance *in vitro*; its specific dosage, duration, effects, and mechanism need further study.

HOMA-IR (Homeostatic Model Assessment of Insulin Resistance) can quantitatively assess how much insulin your pancreas needs to keep your blood sugar levels in check (81). Although HOMA-IR is an indirect measure by calculating body fasting glucose and fasting insulin levels, it is still the most popular used model in clinical research as a direct measure is impractical (82). Many clinical researchers have analyzed the correlation between Metrnl and insulin resistance in diabetes or prediabetes *via* calculating this index, but the results seemed a little controversial. A study on healthy Iranian adults found plasma Metrnl in recreational athletes increased significantly compared to sedentary subjects after correcting the insulin resistance degree (83). In contrast, baseline plasma Metrnl remained no different. Corresponding to the former study, another report on T2DM patients observed that after adjusting for HOMA-IR, Metrnl did not correlate with increased OR for T2DM. Besides, this study concluded an increase in Metrnl levels in T2DM compared to the control (84). However, most recent clinical studies reported that serum Metrnl demonstrated a negative correlation with fasting insulin and HOMA-IR, as well as T2DM patients with lower Metrnl levels (51, 85–87).

Metrnl and polycystic ovarian syndrome

Polycystic ovarian syndrome (PCOS) is a women's endocrine condition with more susceptibility to insulin resistance and T2DM, of which one common treatment is insulin sensitizers (88). Considering Metrnl may play roles in insulin resistance and insulin resistance is a common finding in PCOS, two independent research teams analyzed the plasma level of Metrnl in PCOS. They both report that Metrnl level was decreased in PCOS and showed a negative correlation with insulin resistance, in contrast to changes in insulin resistance markers and FSH (54, 89, 90). Moreover, in

studies of patients with gestational diabetes mellitus in women of a similarly child-bearing period, Metrnl levels were significantly elevated between 24 and 28 weeks of pregnancy than normal gestation (91). Similar results were also confirmed in maternal and cord blood samples in the later stage of pregnancy; nevertheless, these increased Metrnl effects disappeared sharply after delivery (92). Taken together, a deeper understanding of the glucoregulatory mechanism of Metrnl may reveal novel strategies to treat insulin resistance and other metabolic disorders.

Metrnl and diabetes

In line with Metrnl ameliorating insulin resistance both at animal and cellular levels, many clinical studies have also reported correlations between Metrnl circulation levels and diabetes participants with contradictory results (Supplementary Table 1) and regarded Metrnl as an independent risk factor of T2DM. In newly diagnosed T2DM individuals, several studies reported that serum Metrnl showed lower levels than normal glucose tolerance (NGT). Besides, Metrnl was negatively correlated with a glycemic index (including HbA1c, HOMA-IR, FBG, fasting C-peptide) and positively correlated with HOMA-β (52, 85, 93–98). Another study reported this negative correlation in long-standing diagnosed T2DM patients (85). While after 12 weeks of metformin treatment, though Metrnl remained no changes, HbA1c and FBG reduced a lot (99). Interestingly, statins medicine therapy positively correlated with Metrnl level (94). It seems the duration of diabetes has little effect on Metrnl; thus, Metrnl may not directly reflect blood glucose fluctuations in T2DM. Besides, different drug therapy may influence Metrnl secretion.

However, Wang et al. (84) found Metrnl was elevated in prediabetes and was highest in T2DM compared to IGT and NGT. Similar findings were also reported by Chung et al. (100), Wang et al. (80), and Cherian et al. (101). Notably, part of these reports lacked indicator data concerning insulin resistance and insulin sensitivity, which was challenging to explain the negative correlation between blood Metrnl and FBG. Furthermore, a study on healthy Iranian adults also concerned with FBG showed a negative correlation with baseline plasma Metrnl (83). It is worth noting that Metrnl was found to be lower in COPD patients with comorbidities such as T2DM and CAD, instead, higher Metrnl level in protopathic exacerbations (56). Dadmanesh et al. (51) noticed conflicting data regarding Metrnl circulating levels in T2DM and put to serious evaluations concluding results that Metrnl was lower and showed an independent association with the risk of T2DM presence. More recently, Wu et al. (102) used a meta-analysis indicating no significant difference between T2DM and NGT individuals but found circulation Metrnl level was lower in subgroups with HOMA-IR ≥ four and age ≤ 50 years, while higher in subgroups with BMI < 25 kg/m^2. Collectively, this result may interfere with glucose-lowering drugs, duration of disease, sample size, age, BMI, and HOMA-IR; therefore, further longitudinal studies are required to clarify the relationship.

As diabetic nephropathy (DN) with impaired kidney function is the leading cause of end-stage renal disease, a study by Wang et al.

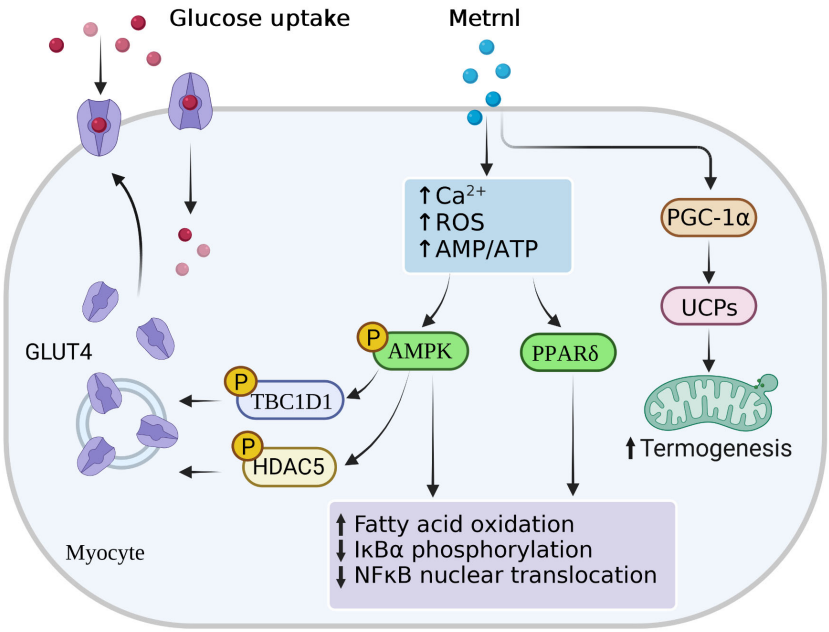

FIGURE 2
Main signal pathways of Metrnl in myocytes. Metrnl could activate AMP-activated protein kinase (AMPK) and peroxisome proliferator-activated receptor-δ (PPAR-γ) signaling by increasing intracellular calcium ion, reactive oxygen species (ROS), or AMP/ATP ratio levels in skeletal muscle cells. Activation of AMPK phosphorylation stimulated phosphorylation of HDAC5 and TBC1DI, both of which resulted in the GLUT4 transcription activation and translocation from the cytoplasm to the membrane. Highly PPAR-γ expressions and AMPK phosphorylation increased fatty acid oxidation, IκBα phosphorylation, and NFκB nuclear translocation. Besides, Metrnl also increased intramuscular PGC-1α and UCPs expressions, thus promoting mitochondria thermogenesis.

(103) compared serum Metrnl levels in healthy controls and T2DM patients with normoalbuminuria, microalbuminuria, or macroalbuminuria, showing that all T2DM subgroups were significantly decreased, with even lower levels in macroalbuminuria group. This study reported negative associations between circulating Metrnl and BUN, Cr, GFR, ACR, CCB treatment, and ACEI/ARB treatment. Similar negative correlations with Metrnl and indicators of renal function were also reported in diabetes by Chung et al. (100). These data suggested that circulation Metrnl levels may be involved in the progression of renal disease in T2DM; however, further studies are required to figure out such potential associations.

Metrnl regulations in lipid metabolism

Regulating the distribution of lipoprotein particles is crucial in maintaining body lipid metabolism, manifested by the liver producing and clearing lipids. Imbalances of lipoprotein would accelerate the accumulation of cholesterol in blood peripheral tissues, which leads to cardiometabolic disorders. In this part, we first concluded the direct effects of Metrnl on adipose tissue and adipocytes. Then we described the roles of Metrnl in lipoprotein homeostasis and lipid-associated diseases (Table 3). Finally, we introduced new findings of Metrnl therapeutical effect on cardiac diseases.

Direct effects on adipose tissue and adipocytes

Considering adipocytes represent the most crucial lipid-storing cell type, and Metrnl was expressed highly in subcutaneous adipose tissue (1); therefore, investigating Metrnl's direct effects on adipose tissue and adipocytes is essential. Metrnl can regulate adipocyte differentiation (59, 95, 104), and its expression could reduce during human adipogenesis (104). In mice of 3T3-L1 adipocytes and human SGBS cells model, overexpression of Metrnl inhibited pre-adipocytes in differentiation to mature adipocytes and promoted cell proliferation. In contrast, adipocyte-specific knockout of Metrnl upregulated adipocyte mature-specific markers and promoted lipid accumulation but had no significance on proliferation (59, 104). Notably, silencing adipocyte PPARγ or using PPARγ inhibitors demonstrated a decrease in Metrnl expression. This study suggested PPARγ was one of Metrnl signal pathways regulating adipocyte phenotypes, but the specific mechanism needed further exploration.

Although Metrnl was upregulated in pre-adipocytes and mature adipocytes with a transient decrease during adipocyte differentiation, active substances, including glucose, insulin, and fatty acids, stimulated adipocyte Metrnl expression with no effects, whereas omega-3 and omega-6 fatty acids inhibit Metrnl expression (95). In mice studies, overexpression of Metrnl increased the abundance of beige adipocytes and revealed a robust increase in thermogenic and β-oxidation gene programs (15). Similarly, the

TABLE 3 Key findings of preclinical studies on the metabolism of Metrnl.

Year	Ref.	Animal/Cell models	Key findings
			Glucose
2014	(15)	Normal	Promote white fat browning, increase thermogenic in adipose tissue, improve glucose tolerance
2015	(59)	HFD-induced obese	Antagonize insulin sensitivity at least *via* PPARγ pathway
2018	(58)	HFD-induced obese	Improve impaired insulin functions, rescue glucose intolerance, reduce weight gains
2020	(62)	Obese, diabetes	Improve glucose metabolism *via* calcium-dependent AMPKα2/GLUT4/HDAC5
2021	(22)	Non-obese diabetes	Delay the onset of diabetes, improve islet function
2021	(78)	Diabetes	Ameliorate pancreas islet β-cell functions *via* WNT/β-catenin pathway.
			Lipid
2017	(104)	Human adipocytes	Promote adipose tissue accumulation, inhibite adipocyte differentiation, decrease during adipogenesis
2018	(105)	HFD-induced obese	Decrease fat accumulation
2020	(20)	H9C2 cells	Decrease myocardial ischemia/reperfusion injury and endoplasmic stress *via* AMPK-PAK2
2020	(106)	Knockout mice	Adipose Metrnl regulate blood TG, liver Metrnl regulate HDL-C
2020	(107)	Cardiac injury	Attenuate oxidative damage, apoptosis, and cardiac dysfunction *via* cAMP/PKA/SIRT1 pathway
2021	(95)	3T3-L1 cells	A transient reduce during adipocyte differentiation, decreased by omega-3 and omega-6 fatty acids
2021	(108)	Cardiac hypertrophy	Prevent cardiomyocyte hypertrophy and dysfunction, autocrine actions, a biomarker of heart failure
2022	(48)	Cardial infarction	Promote angiogenesis and infarct repair, a high-affinity ligand of KIT receptor
			Bone and skeletal muscle
2020	(21)	Muscle injury	Promote muscle regeneration, regulate muscle satellite cells proliferation
2022	(109)	Bone fracture	Osteoinductive, promote bone fracture healing, strongest expression by osteoblasts

administration of recombinant Metrnl to HFD-induced mice model also stimulated the expression of broad beige thermogenic gene programs with accompanying weight loss (15, 40). Combining Metrnl-induced browning with these results indicated that Metrnl could be regarded as a classical adipokine to investigate its physiological mechanism further.

Metrnl and lipoprotein homeostasis

The distribution of lipoprotein particles is essential for maintaining human lipid homeostasis, whereas breaking this balance would lead to cholesterol imbalance and even a variety of diseases. Some clinical studies have reported that Metrnl was independently associated with adverse blood lipid parameters in metabolic diseases, including negatively correlating with triglyceride (TG), total cholesterol (TC), and low-density lipoprotein cholesterol (LDL-C) and positively correlating with high-density lipoprotein cholesterol (HDL-C) (55, 99, 100, 110, 111). In order to figure out the overall effects of Metrnl on clinical blood lipids, Qi et al. (106) generated global and tissue-specific knockout of Metrnl mice models. In this study, global-KO Metrnl didn't alter any lipid parameters under a normal chow diet but increased blood TG by 14%, TC by 16%, and HDL-C by 24% upon a high-fat diet. Consistent with these findings, Li et al. (59) have demonstrated adipose Metrnl could participate in TG metabolism as its deficiency deteriorated HFD-induced acute hypertriglyceridemia. In contrast, its overexpression in adipose tissue improved TG tolerance. Interestingly, liver-specific knockout of Metrnl reduced HDL and TC but didn't decrease VLDL release, similar to deficiency of total Metrnl (106). Moreover, intestine-specific knockout of Metrnl did not influence HDL or TC. These results imply that blood TG was at least partly modulated by adipose Metrnl rather than liver or intestine, as well tissue-specific Metrnl may control different blood lipid components.

Metrnl and atherosclerosis

Lipid metabolic abnormality is a significant risk factor for atherosclerosis (AS), closely associated with endothelial cell damage and dysfunction. In AS mice models, Metrnl mRNA was significantly decreased in the aorta while still highly expressed in healthy controls (112). Some studies found circulation Metrnl levels were reduced in AS and coronary artery disease (CAD) patients and negatively correlated with endothelial parameters, including baPWV, ICAM-1, VCAM-1, and E-selectin (51, 52, 94, 113). Moreover, circulating Metrnl was lower in elderly patients with chronic heart failure (CHF) and negatively correlated with cardiovascular mortality, CHF rehospitalization, and combined major adverse cardiac events (MACEs) (113). Of note, a previous study has demonstrated that Metrnl could ameliorate LPS-induced endothelial cells' inflammatory response (24). Consistent with these findings, based on a large-scale vascular adhesion molecules Genome-Wide Association Study (GWAS), Metrnl was identified as a candidate gene associated with carotid intima-media thickness (cIMT) in whole blood gene expression (114). cIMT is a new biomarker of subclinical AS and a predictor of impending cardiovascular events, where indicating Metrnl may also involve in AS development (115). It seemed endothelial impairment factors could facilitate Metrnl secretions by endothelial cells, and circulation Metrnl levels decreased significantly with the AS progression. Moreover, areas of aortic plaques, necrotic injuries, and lipid accumulations of aortic root were heavier in aorta plaque of endothelial Metrnl deficiency mice models than those in control, with more severe spontaneous atherosclerosis (112). These results suggested that the AS mechanism is related to Metrnl deficiency in endothelial cells.

Many studies have reported that Metrnl was a novel myokine with protective effects on cardiovascular diseases. Two previous studies have detected Metrnl abundantly expressed in cardiac muscle (15, 59), as well following Hu et al. (107) found it significantly decreased upon doxorubicin (DOX)-induced cardiotoxicity exposure. This study further found Metrnl could exert cardioprotective effects *via* activating the cAMP/PKA/SIRT1 pathway as cardiac-specific overexpression of Metrnl markedly improved mice cardiac dysfunction and survival status, while Metrnl deficiency aggravated cardiac injury. Of note, Metrnl could not affect the tumor-killing capacity of DOX (107). Rupérez et al. (108) also confirmed a similar conclusion: they constructed Metrnl-KO mice exhibiting asymmetrical cardiac hypertrophy, fibrosis, and aging. Conversely, overexpression of heart Metrnl could prevent cardiac remodeling. In addition, this study used cardiomyocytes *in vitro*, demonstrating that Metrnl could inhibit cardiac hypertrophy development, indicating a direct effect on cardiac cells.

Metrnl and heart regenerative

Although the human heart has limited regenerative capability after damage, stimulation of new blood vessel formation is an essential part of the reparative process and might be a potential approach to ameliorate heart function. When recognizing that cell-cell communications between cardiac myeloid cells and other nonmyocytes might participate in heart injury (116), Reboll et al. (48) found that Metrnl protein may serve as a potential mediator aspect of this cellular cross-talk. Notably, previous studies have noticed Metrnl expression was prominently increased in mouse infarcts and patients' tissue with acute myocardial infarction, but circulating Metrnl level was decreased (117). In mice with a cardiac attack, monocytes and macrophages migrated to the heart, producing Metrnl to stimulate the expansion of vascular endothelial cells, resulting in an angiogenic response that limited damage (118). Besides, delivering Metrnl protein with an infusion pump into the mouse could promote angiogenesis after acute myocardial infarction. More importantly, Metrnl was found as a ligand of KIT receptor tyrosine kinase and could respond to the

secreted protein stem cell factor (SCF) (119). The activation of KIT is necessary for the normal angiogenic response after cardiac infarction, and SCF is the function of maintaining KIT-expressing hematopoietic stem cells during development, both of which could stimulate the expansion of KIT-expressing mice endothelial cells (120). Accordingly, the role of METRNL-KIT signaling would open new avenues for developing therapies for cardiac disease.

Metrnl regulations in bone metabolism

Metrnl and osteoblasts

Many studies have reported that Metrnl was involved in skeletal development, remodeling, and some bone-related diseases. After constructing a human osteoblast full-length cDNA library, Gong et al. (121) screened unreported genes closely related AP-1 transcription complex and identified Metrnl as the only candidate gene. In multiple parts of mouse bones, RNA-seq demonstrated the strongest expression of Metrnl transcript by osteoblast. Meanwhile, Metrnl deficiency would decrease mice's osteogenic capacity in bone marrow stromal cells, suggesting that Metrnl is abundant in bone deposition areas where osteoblasts differentiate and activate (109). Besides, Huang et al. (109) found that Metrnl could increase osteoblast differentiation and mineralization *in vitro* and promote bone fracture healing. Notably, knockdown of the Metrnl gene did not affect overall skeletal development, fracture healing, or osteoblasts in the animals in this study. Nevertheless, it seemed overexpression of Metrnl would inhibit mineralized nodule formation (121). Recently, Cherian et al. (101) observed a strong positive association between serum Metrnl levels and various molecules with osteogenic properties in obesity and diabetes patients, suggesting Metrnl may potentially affect bone-related development complications.

Although Metrnl could affect osteoblasts both *in vitro* and vivo, considering the effects of Metrnl on inflammation, some studies regarded Metrnl play roles after skeletal injury precisely with the help of macrophages (17). Similar results were also observed in studies of skeletal muscle adjacent to skeletal anatomy, where Metrnl was highly expressed in the early stages after muscle damage while knocking out the Metrnl gene did not result in changes in various muscle properties either (21). Interestingly, many investigators noticed that numerous factors from local circulation were able to alter bone regeneration (122–124). Consequently, this academic team proposed a compensatory mechanism where Metrnl may be a compensating molecule lacking *in vitro* culture models. This would explain why Metrnl was dispensable for both bone and muscle development or healing *in vivo* but served as an osteoinductive molecule and an effector of skeletal muscle regeneration *in vitro* (63, 109). Taken together, supplementing Metrnl at cellular levels may potentially improve osteoblast function. Besides, further investigations are needed to understand specific mechanisms of Metrnl in osteogenic differentiation and how the body delivers Metrnl into sites of active bone formation.

Metrnl and skeletal-related diseases

Some studies have reported that Metrnl was expressed abnormally in the cartilage tissue and synovium of skeletal-related diseases. In patients with OA, serum Metrnl levels were significantly lower than normal healthy controls but elevated in synovial fluid (31). This confirmed a hypothesis that Metrnl in different tissues might have different environmental mechanisms. Similarly, in two gene expression profiles of cartilage tissue, compared with healthy cartilage from patients with traumatic femoral neck fractures alone, Metrnl was strongly downregulated in OA patients (ratio = 0.34) but upregulated in non-traumatic osteonecrosis of femoral head (NOFH) (ratio = 11.77) (125, 126). These revealed the Metrnl gene involved in pathogenetic differences in NOFH and OA cartilage damage, and it would be interesting to explore the mechanism further. Besides, as we mentioned in the previous section of Metrnl and autoimmune diseases, Metrnl was elevated in synovial fluid of PsA and RA compared to OA patients, and our team also found serum Metrnl levels were higher in RA with a positively correlated with disease activity indices (27, 36, 50). Collectively, the mechanism of Metrnl in skeletal-related diseases merits further research, especially bone-related autoimmune diseases, because immune function interacts with the homeostasis of the skeletal system's internal environment closely.

Metrnl regulations in obesity and exercise

Obesity is a worldwide health problem with an increased prevalence of metabolic-related disorders. Exercise is an effective strategy to prevent and treat obesity and its related metabolic syndromes. It is well-documented that changes in circulating cytokines could occur after exercise but with unclear mechanisms. Here we concluded circulation Metrnl levels in obese merged with or without metabolic diseases and discussed Metrnl involvements in bariatric surgery (Supplementary Table 1). We also discussed the roles of Metrnl after exercise and compared circulating Metrnl changes upon different exercises.

Metrnl and obesity

Obesity is an important promoter of chronic and low-grade inflammation states with lipid accumulation, which results in many metabolic syndromes (61, 127). Previously, Li et al. (1) discovered that Metrnl was upregulated in circulation and adipose tissue of HFD-induced obese mice. Similarly, Löffler et al. (104) reported that Metrnl was highly expressed in adipocytes of obese compared to lean children. These interactions with adipose tissue dynamics

indicated the association between Metrnl and obesity. However, correlations between serum Metrnl level and obesity indexes were contradictory. Some studies reported that simply obese individuals (29, 85, 103, 128) or obese patients with metabolic syndrome have been shown lower Metrnl levels and were negatively related to body mass index (BMI) (51, 54, 55, 85, 92, 94, 103, 129). Notably, this negative association was prone to arise in T2DM patients compared with other diseases. Actually, it seems more studies figured out that there is no relationship between Metrnl and BMI in healthy or metabolic syndrome (31, 52, 80, 83, 87, 89, 95, 99, 100). Apart from total height and body weight, the waist-to-hip ratio (WHR) was further measured but still no correlation (52). Considering visceral fat obesity (VFO) is close to obesity and insulin resistance, there were few studies on the correlations between Metrnl and VFO, as most obesity evaluations focused on measurements of waist circumference or BMI. Du et al. (111) used Dual Energy X-ray Absorptiometry (DXA) to quantify the visceral fat area and found that Metrnl level was independently inversely associated with visceral fat deposition. This finding was the first and only report demonstrating the association between Metrnl and VFO, which provided a possibility that Metrnl concentration may be a useful noninvasive, cost-effective marker for assessing VFO.

Moreover, some results also found a positive correlation between Metrnl levels and BMI. An Arab survey stratified T2DM and healthy controls based on obesity and found Metrnl plasma levels elevated more in obese T2DM (BMI > 30 kg/m^2) than in non-obese T2DM (20 kg/m^2 ≤ BMI ≤ 30 kg/m^2) (130). Wang et al. (84) and Cherian et al. (101) reported similar findings. This increase was probably one of the physiological regulation mechanisms to restore glucose tolerance or defense response to counteract metabolic stress. Of note, these studies have not excluded clinical confounding factors' effects, such as diabetes-related drugs, physical activity, sex, and age. Besides, obesity or overweight could accelerate the loss of muscle mass, as Metrnl was also secreted from muscle, where different Metrnl levels might result from adipose tissue dysfunction and sarcopenia. Collectively, larger sample sizes for clinical studies and more rigorous experimental designs are needed to identify the correlation between circulating Metrnl levels and obesity, thus determining whether Metrnl could be used as a biomarker of obesity.

Bariatric surgery (BS) has been currently the most effective therapy for morbid obesity and associated complications. A recent mice model study reported that Metrnl and UCPs were changed in favor of increased thermogenesis through fat browning to induce weight loss comparing laparoscopic sleeve gastrectomy (LSG) mice group with sham surgery and pair-fed groups (131, 132). They showed a positive correlation between Metrnl and weight loss after LSG-induced weight loss in adipose tissue, muscle, and plasma. Of note, this scholarly team recently reported the same results in the human interventional study (37). A similar clinical context study was also reported by Grander et al. (30), which found Metrnl expression was decreased in hepatic-and adipose tissues after BS in non-alcoholic fatty liver disease (NAFLD). Interestingly, Metrnl has been identified as a target protein with Iah1, a candidate gene for diet-induced NAFLD (133). Maybe Metrnl as one of the hepatokines play role in NAFLD progress but further investigations are needed to clarify the mechanism. However, another study by Pellitero et al. (128) showed the opposite result, which reported that Metrnl circulation levels were increased after LSG 6 and 12 months in obese patients, whereas at baseline patients with obesity showed lower. Schmid et al. (95) also observed serum Metrnl concentrations in patients undergoing BS and a low-calorie diet were increased after 3 months and back to baseline levels after 12 months, which also exerted no gender-specific effect. Taken together, these clinical studies showed contradicting results and this difference may attribute to co-morbidities, obesity, smaller sample size, or observation time as confounding factors. Further prospective studies with better design are required to better explain the relationship between Metrnl and weight loss or obesity.

Metrnl and exercise

Exercise-inducible soluble factors, such as adipokines, cytokines, myokines, and osteokines are regarded to play important roles in the body's response to exercise (134, 135). Metrnl was first described by Rao et al. (15) who investigated Metrnl's ability to moderate energy thermogenesis originally not in specific-METRNL transgenic mice but in PGC-1α4 transgenic mice. PGC-1α4 is an exercise-induced splice isoform of PPARγ coactivator 1a, where Metrnl was regarded as its downstream effector protein. A recent study reported by Amano et al. (136) supported this effector pathway of PGC-1α along with Metrnl. After they applied 4-week electrical stimulation to rats' legs, which aimed to simulate chronic resistance exercise, an apparent positive correlation was found between the expression of PGC-1α in brown adipose tissues and plasma Metrnl levels. Similar results have been confirmed by Bae et al. (137) who exerted an 8-week training on HFD-induced obese mice increasing muscle proteins including AMPK, PGC-1α, and plasma Metrnl. Further studies proved Metrnl can be significantly induced in various muscle depots and adipose tissue by exercise (15, 23, 62). Besides, up-regulation of intramuscular Metrnl induced by regular exercise would be a pathway to suppress obesity and metabolic syndromes (105, 138, 139). Jung et al. (58) reported that administration of Metrnl in obese mice could reduce body weight gain and rescue glucose intolerance, whereas not affect calorie intake. Moreover, results from Hafiz et al. (23) found that exercise exerted anti-inflammatory function by NLRP3 inflammasome activation of HFD-induced obese mice, and this program was associated with Metrnl anti-inflammatory effects in macrophages in muscle.

A number of clinical studies have reported higher circulation Metrnl levels in response to exercise (140–146). Interestingly, exercise with different intensity, type, or duration may also influence Metrnl activity. Some studies have investigated the effects of regular exercises on obese mice, such as undergoing treadmill training, with obtaining similar conclusion that Metrnl levels increases (137). Of note, a previous study didn't observe any changes in resting Metrnl level upon endurance training in mice (15). Given that recent research has reported beneficial effects of high-intensity interval training (HIIT) with metabolic diseases, they recently examined the impact of high-intensity interval training and

short-term interval training on the Metrnl mRNA of skeletal muscle biopsy samples in 9 healthy males (147). An increase in Metrnl expression at 3-hour recovery compared to rest was reported after a single bout of high-intensity interval exercise before training, yet no statistical significance of post-training increases. It would be interesting to determine whether increased muscle Metrnl expression was a common adaptive response to certain types of exercise.

However, a number of earlier studies were based on mRNA levels, while accompanied by different commercial ELISA coming into service (93) more results were prone to support that circulation Metrnl levels can be strongly induced by both acute and chronic exercise (148). More recently, a similar study on serum Metrnl levels to investigate the different types of exercise effect (including aerobic exercise, HIIT, and resistance exercise), all exercise groups significantly elevated Metrnl levels, whereas no assessment changes within the group (149) Additionally, Amano et al. (136) figured out the chronic resistance exercise training also up-regulated Mertnl levels in obese mice. As such, findings from Alizadeh et al. (150) suggested that human downhill running exercise, regarded as a muscle-damaging exercise protocol, significantly elevated Metrnl levels as well as positively correlated with eosinophils' number. Moreover, combined training (CT) for its metabolic benefits has been recommended by diabetes guidelines, Bonfante et al. (151) evaluated effects of 16-week-CT period on serum pro-thermogenic/anti-inflammatory inducers in overweight T2DM individuals and found Metrnl was positively correlated with brown adipose tissue (BAT) thermogenic activity. Interestingly, fed and fasting states in the pre-training or post-training also influence Metrnl secretion reported, with Metrnl was increased both in two states (152). Taken together, although some important questions remain unanswered, it would be interesting to evaluate Metrnl's roles in the beneficial effects of exercise with metabolic diseases.

Future perspectives and conclusions

Overall, well-documented evidence has suggested that this novel secreted protein exerts pleiotropic effects on inflammation, immunology, and metabolism. However, Metrnl is not secreted by the fixed model of cell types but depends on the concrete physiological and pathological context. Based on different tissue homeostasis, more preclinical studies are needed to clarify the molecular mechanisms that control the selective expression of Metrnl by different cell types. Meanwhile, contradictoriness in reported results highlights the necessity for more-accurate methods to measure Metrnl and for clinical studies to be better designed, revealing the role of Metrnl in different diseases. Whether Metrnl is used as a predictive biomarker or disease activity indicator for cardio-metabolic syndromes including morbid obesity, insulin resistance, T2DM, CAD, and PCOS, or other inflammatory immune diseases such as asthma, RA, OA, PsA, UC, CD, T1DM, and GD, depending on more rigorous prospective studies. Finally, based on current knowledge, trials to assess the application of Metrnl as a therapeutic agent in humans is premature but should be one of the research goals for the near future.

Author contributions

ZL conceived this article. ZL and ZG drafted the manuscript. TS and SZ drew the illustrations and tables. SY and MZ revised the article. ZL, ZG, TS, SZ, SY, and MZ checked and edited the article. HS supervised the article. All authors have read and agreed to the final version of the manuscript.

Funding

This review was supported by grants from the National Natural Science Foundation of China (No. 81373219) and the Liaoning Education Department (No. JC2019009).

Acknowledgments

We acknowledged that this article illustrations were created with BioRender Figures 1, 2.

Conflict of interest

The authors declare that the research was conducted in the absence of any commercial or financial relationships that could be construed as a potential conflict of interest.

Publisher's note

Supplementary material

The Supplementary Material for this article can be found online at: https://www.frontiersin.org/articles/10.3389/fimmu.2023.1098570/full#supplementary-material

References

1. Li ZY, Zheng SL, Wang P, Xu TY, Guan YF, Zhang YJ, et al. Subfatin is a novel adipokine and unlike meteorin in adipose and brain expression. *CNS Neurosci Ther* (2014) 20(4):344–54. doi: 10.1111/cns.12219

2. Zheng SL, Li ZY, Song J, Liu JM, Miao CY. Metrnl: A secreted protein with new emerging functions. *Acta Pharmacol Sin* (2016) 37(5):571–9. doi: 10.1038/aps.2016.9

3. Jørgensen JR, Fransson A, Fjord-Larsen L, Thompson LH, Houchins JP, Andrade N, et al. Cometin is a novel neurotrophic factor that promotes neurite outgrowth and neuroblast migration *in vitro* and supports survival of spiral ganglion neurons in vivo. *Exp Neurol* (2012) 233(1):172–81. doi: 10.1016/j.expneurol.2011.09.027

4. Surace C, Piazzolla S, Sirleto P, Digilio MC, Roberti MC, Lombardo A, et al. Mild ring 17 syndrome shares common phenotypic features irrespective of the chromosomal breakpoints location. *Clin Genet* (2009) 76(3):256–62. doi: 10.1111/j.1399-0004.2009.01203.x

5. Song Y, Choi JE, Kwon YJ, Chang HJ, Kim JO, Park DH, et al. Identification of susceptibility loci for cardiovascular disease in adults with hypertension, diabetes, and dyslipidemia. *J Transl Med* (2021) 19(1):85. doi: 10.1186/s12967-021-02751-3

6. Cookson WO, Ubhi B, Lawrence R, Abecasis GR, Walley AJ, Cox HE, et al. Genetic linkage of childhood atopic dermatitis to psoriasis susceptibility loci. *Nat Genet* (2001) 27(4):372–3. doi: 10.1038/86867

7. Morar N, Bowcock AM, Harper JI, Cookson WO, Moffatt MF. Investigation of the chromosome 17q25 PSORS2 locus in atopic dermatitis. *J Invest Dermatol* (2006) 126(3):603–6. doi: 10.1038/sj.jid.5700108

8. Wen D, Xiao Y, Vecchi MM, Gong BJ, Dolnikova J, Pepinsky RB. Determination of the disulfide structure of murine meteorin, a neurotrophic factor, by LC-MS and electron transfer dissociation-High-Energy collisional dissociation analysis of proteolytic fragments. *Anal Chem* (2017) 89(7):4021–30. doi: 10.1021/acs.analchem.6b04600

9. Ushach I, Burkhardt AM, Martinez C, Hevezi PA, Gerber PA, Buhren BA, et al. METEORIN-LIKE is a cytokine associated with barrier tissues and alternatively activated macrophages. *Clin Immunol* (2015) 156(2):119–27. doi: 10.1016/j.clim.2014.11.006

10. Ramialison M, Bajoghli B, Aghaallaei N, Ettwiller L, Gaudan S, Wittbrodt B, et al. Rapid identification of PAX2/5/8 direct downstream targets in the otic vesicle by combinatorial use of bioinformatics tools. *Genome Biol* (2008) 9(10):R145. doi: 10.1186/gb-2008-9-10-r145

11. Watanabe K, Akimoto Y, Yugi K, Uda S, Chung J, Nakamuta S, et al. Latent process genes for cell differentiation are common decoders of neurite extension length. *J Cell Sci* (2012) 125(Pt 9):2198–211. doi: 10.1242/jcs.097709

12. Berghoff M, Höpfinger A, Rajendran R, Karrasch T, Schmid A, Schäffler A. Evidence of a muscle-brain axis by quantification of the neurotrophic myokine METRNL (Meteorin-like protein) in human cerebrospinal fluid and serum. *J Clin Med* (2021) 10(15):3271. doi: 10.3390/jcm10153271

13. Jan V, Miš K, Nikolic N, Dolinar K, Petrič M, Bone A, et al. Effect of differentiation, *de novo* innervation, and electrical pulse stimulation on mRNA and protein expression of Na+,K+-ATPase, FXYD1, and FXYD5 in cultured human skeletal muscle cells. *PloS One* (2021) 16(2):e0247377. doi: 10.1371/journal.pone.0247377

14. Hong C, Wang Z, Zheng SL, Hu WJ, Wang SN, Zhao Y, et al. Metrnl regulates cognitive dysfunction and hippocampal BDNF levels in d-galactose-induced aging mice. *Acta Pharmacol Sin* (2022). doi: 10.1038/s41401-022-01009-y

15. Rao RR, Long JZ, White JP, Svensson KJ, Lou J, Lokurkar I, et al. Meteorin-like is a hormone that regulates immune-adipose interactions to increase beige fat thermogenesis. *Cell* (2014) 157(6):1279–91. doi: 10.1016/j.cell.2014.03.065

16. Li ZY, Fan MB, Zhang SL, Qu Y, Zheng SL, Song J, et al. Intestinal metrnl released into the gut lumen acts as a local regulator for gut antimicrobial peptides. *Acta Pharmacol Sin* (2016) 37(11):1458–66. doi: 10.1038/aps.2016.70

17. Ushach I, Arrevillaga-Boni G, Heller GN, Pone E, Hernandez-Ruiz M, Catalan-Dibene J, et al. Meteorin-like/Meteorin-β is a novel immunoregulatory cytokine associated with inflammation. *J Immunol* (2018) 201(12):3669–76. doi: 10.4049/jimmunol.1800435

18. Zuo L, Ge S, Ge Y, Li J, Zhu B, Zhang Z, et al. The adipokine metrnl ameliorates chronic colitis in il-10-/- mice by attenuating mesenteric adipose tissue lesions during spontaneous colitis. *J Crohns Colitis* (2019) 13(7):931–41. doi: 10.1093/ecco-jcc/jjz001

19. Zhang SL, Li ZY, Wang DS, Xu TY, Fan MB, Cheng MH, et al. Aggravated ulcerative colitis caused by intestinal metrnl deficiency is associated with reduced autophagy in epithelial cells. *Acta Pharmacol Sin* (2020) 41(6):763–70. doi: 10.1038/s41401-019-0343-4

20. Xu L, Cai Y, Wang Y, Xu C. Meteorin-like (METRNL) attenuates myocardial Ischemia/Reperfusion injury-induced cardiomyocytes apoptosis by alleviating endoplasmic reticulum stress *via* activation of AMPK-PAK2 signaling in H9C2 cells. *Med Sci Monit* (2020) 26:e924564. doi: 10.12659/MSM.924564

21. Baht GS, Bareja A, Lee DE, Rao RR, Huang R, Huebner JL, et al. Meteorin-like facilitates skeletal muscle repair through a Stat3/IGF-1 mechanism. *Nat Metab* (2020) 2(3):278–89. doi: 10.1038/s42255-020-0184-y

22. Yao Z, Lin P, Wang C, Wang K, Sun Y. Administration of metrnl delays the onset of diabetes in non-obese diabetic mice. *Endocr J* (2021) 68(2):179–88. doi: 10.1507/endocrj.EJ20-0351

23. Javaid HMA, Sahar NE, ZhuGe DL, Huh JY. Exercise inhibits NLRP3 inflammasome activation in obese mice *via* the anti-inflammatory effect of meteorin-like. *Cells* (2021) 10(12):3480. doi: 10.3390/cells10123480

24. Jung TW, Pyun DH, Kim TJ, Lee HJ, Park ES, Abd El-Aty AM, et al. Meteorin-like protein (METRNL)/IL-41 improves LPS-induced inflammatory responses *via* AMPK or PPARδ-mediated signaling pathways. *Adv Med Sci* (2021) 66(1):155–61. doi: 10.1016/j.advms.2021.01.007

25. Gao X, Leung TF, Wong GW, Ko WH, Cai M, He EJ, et al. Meteorin-β/Meteorin like/IL-41 attenuates airway inflammation in house dust mite-induced allergic asthma. *Cell Mol Immunol* (2022) 19(2):245–59. doi: 10.1038/s41423-021-00803-8

26. Wang J, Jia Z, Dang H, Zou J. Meteorin-like/Meteorin-β upregulates proinflammatory cytokines *via* NF-κB pathway in grass carp ctenopharyngodon idella. *Dev Comp Immunol* (2022) 127:104289. doi: 10.1016/j.dci.2021.104289

27. Bridgewood C, Russell T, Weedon H, Baboolal T, Watad A, Sharif K, et al. The novel cytokine Metrnl/IL-41 is elevated in psoriatic arthritis synovium and inducible from both entheseal and synovial fibroblasts. *Clin Immunol* (2019) 208:108253. doi: 10.1016/j.clim.2019.108253

28. Kocaman N, Artaş G. Can novel adipokines, asprosin and meteorin-like, be biomarkers for malignant mesothelioma? *Biotech Histochem* (2020) 95(3):171–5. doi: 10.1080/10520295.2019.1656344

29. Gholamrezayi A, Mohamadinarab M, Rahbarinejad P, Fallah S, Barez SR, Setayesh L, et al. Characterization of the serum levels of meteorin-like in patients with inflammatory bowel disease and its association with inflammatory cytokines. *Lipids Health Dis* (2020) 19(1):230. doi: 10.1186/s12944-020-01404-6

30. Grander C, Grabherr F, Enrich B, Meyer M, Mayr L, Schwärzler J, et al. Hepatic meteorin-like and krüppel-like factor 3 are associated with weight loss and liver injury. *Exp Clin Endocrinol Diabetes* (2021). doi: 10.1055/a-1537-8950

31. Sobieh BH, Kassem DH, Zakaria ZM, El-Mesallamy HO. Potential emerging roles of the novel adipokines adipolin/CTRP12 and meteorin-like/METRNL in obesity-osteoarthritis interplay. *Cytokine* (2021) 138:155368. doi: 10.1016/j.cyto.2020.155368

32. Akkus G, Koyuturk LC, Yilmaz M, Hancer S, Ozercan IH, Kuloglu T. Asprosin and meteorin-like protein immunoreactivity in invasive ductal breast carcinoma stages. *Tissue Cell* (2022) 77:101855. doi: 10.1016/j.tice.2022.101855

33. Kocaman N, Yuksel EI, Demir B, Calik I, Cicek D. Two novel biomarker candidates for differentiating basal cell carcinoma from trichoblastoma; asprosin and meteorine like peptide. *Tissue Cell* (2022) 76:101752. doi: 10.1016/j.tice.2022.101752

34. Mirzaoglu M, Yavuzkir S, Mirzaoglu C, Yurt N, Dagli AF, Ozcan Yildirim S, et al. Use of asprosin and subfatin for differential diagnosis of serous ovarian tumors. *Biotech Histochem* (2023) 98(2):140-146. doi: 10.1080/10520295.2022.2135763

35. Gong L, Huang G, Weng L, Xu J, Li Y, Cui W, et al. Decreased serum interleukin-41/Metrnl levels in patients with graves' disease. *J Clin Lab Anal* (2022) 36(10):e24676. doi: 10.1002/jcla.24676

36. Zhang S, Lei Y, Sun T, Gao Z, Li Z, Shen H. Elevated levels of metrnl in rheumatoid arthritis: Association with disease activity. *Cytokine* (2022) 159:156026. doi: 10.1016/j.cyto.2022.156026

37. Jamal MH, AlOtaibi F, Dsouza C, Al-Sabah S, Al-Khaledi G, Al-Ali W, et al. Changes in the expression of meteorin-like (METRNL), irisin (FNDC5), and uncoupling proteins (UCPs) after bariatric surgery. *Obes (Silver Spring)* (2022) 30(8):1629–38. doi: 10.1002/oby.23473

38. Lee J, Hever A, Willhite D, Zlotnik A, Hevezi P. Effects of RNA degradation on gene expression analysis of human postmortem tissues. *FASEB J* (2005) 19(10):1356–8. doi: 10.1096/fj.04-3552fje

39. Roth RB, Hevezi P, Lee J, Willhite D, Lechner SM, Foster AC, et al. Gene expression analyses reveal molecular relationships among 20 regions of the human CNS. *Neurogenetics* (2006) 7(2):67–80. doi: 10.1007/s10048-006-0032-6

40. Lee SD, Tontonoz P. Eosinophils in fat: Pink is the new brown. *Cell* (2014) 157(6):1249–50. doi: 10.1016/j.cell.2014.05.025

41. Legaki E, Arsenis C, Taka S, Papadopoulos NG. DNA Methylation biomarkers in asthma and rhinitis: Are we there yet? *Clin Transl Allergy* (2022) 12(3):e12131. doi: 10.1002/clt2.12131

42. Allen JE, Maizels RM. Diversity and dialogue in immunity to helminths. *Nat Rev Immunol* (2011) 11(6):375–88. doi: 10.1038/nri2992

43. Platts-Mills T, Vaughan J, Squillace S, Woodfolk J, Sporik R. Sensitisation, asthma, and a modified Th2 response in children exposed to cat allergen: A population-based cross-sectional study. *Lancet* (2001) 357(9258):752–6. doi: 10.1016/S0140-6736(00)04168-4

44. Knipper JA, Ivens A, Taylor MD. Helminth-induced Th2 cell dysfunction is distinct from exhaustion and is maintained in the absence of antigen. *PloS Negl Trop Dis* (2019) 13(12):e0007908. doi: 10.1371/journal.pntd.0007908

45. Manning AA, Zhao L, Zhu Z, Xiao H, Redington CG, Ding VA, et al. IL-39 acts as a friend to pancreatic cancer. *Med Oncol* (2018) 36(1):12. doi: 10.1007/s12032-018-1236-y

46. Manning AA, Zhao L, Zhu Z, Xiao H, Redington CG, Ding VA, et al. Correction to: IL-39 acts as a friend to pancreatic cancer. *Med Oncol* (2019) 36(2):22. doi: 10.1007/s12032-018-1244-y

47. Shivakumar M, Lee Y, Bang L, Garg T, Sohn KA, Kim D. Identification of epigenetic interactions between miRNA and DNA methylation associated with gene expression as potential prognostic markers in bladder cancer. *BMC Med Genomics* (2017) 10(Suppl 1):30. doi: 10.1186/s12920-017-0269-y

48. Reboll MR, Klede S, Taft MH, Cai CL, Field LJ, Lavine KJ, et al. Meteorin-like promotes heart repair through endothelial KIT receptor tyrosine kinase. *Science* (2022) 376(6599):1343–7. doi: 10.1126/science.abn3027

49. Soto H, Hevezi P, Roth RB, Pahuja A, Alleva D, Acosta HM, et al. Gene array analysis comparison between rat collagen-induced arthritis and human rheumatoid arthritis. *Scand J Immunol* (2008) 68(1):43–57. doi: 10.1111/j.1365-3083.2008.02117.x

50. Onuora S. Novel cytokine, IL-41, linked with PsA. *Nat Rev Rheumatol* (2019) 15 (11):636. doi: 10.1038/s41584-019-0314-7

51. Dadmanesh M, Aghajani H, Fadaei R, Ghorban K. Lower serum levels of meteorin-like/Subfatin in patients with coronary artery disease and type 2 diabetes mellitus are negatively associated with insulin resistance and inflammatory cytokines. *PloS One* (2018) 13(9):e0204180. doi: 10.1371/journal.pone.0204180

52. El-Ashmawy HM, Selim FO, Hosny TAM, Almassry HN. Association of low serum meteorin like (Metrnl) concentrations with worsening of glucose tolerance, impaired endothelial function and atherosclerosis. *Diabetes Res Clin Pract* (2019) 150:57–63. doi: 10.1016/j.diabres.2019.02.026

53. Sun H, Zhang Y, Wang J, Kong J. Correlation of serum meteorin-like concentration with the presence and severity of obstructive sleep apnoea syndrome. *Ann Clin Biochem* (2019) 56(5):593–7. doi: 10.1177/0004563219854115

54. Fouani FZ, Fadaei R, Moradi N, Zandieh Z, Ansaripour S, Yekaninejad MS, et al. Circulating levels of meteorin-like protein in polycystic ovary syndrome: A case-control study. *PloS One* (2020) 15(4):e0231943. doi: 10.1371/journal.pone.0231943

55. Liu ZX, Ji HH, Yao MP, Wang L, Wang Y, Zhou P, et al. Serum metrnl is associated with the presence and severity of coronary artery disease. *J Cell Mol Med* (2019) 23(1):271–80. doi: 10.1111/jcmm.13915

56. Kerget B, Afşin DE, Kerget F, Aşkın S, Akgün M. Is metrnl an adipokine İnvolved in the anti-inflammatory response to acute exacerbations of COPD? *Lung* (2020) 198(2):307–14. doi: 10.1007/s00408-020-00327-4

57. Brigger D, Riether C, van Brummelen R, Mosher KI, Shiu A, Ding Z, et al. Eosinophils regulate adipose tissue inflammation and sustain physical and immunological fitness in old age. *Nat Metab* (2020) 2(8):688–702. doi: 10.1038/s42255-020-0228-3

58. Jung TW, Lee SH, Kim HC, Bang JS, Abd El-Aty AM, Hacımüftüoğlu A, et al. METRNL attenuates lipid-induced inflammation and insulin resistance *via* AMPK or PPARδ-dependent pathways in skeletal muscle of mice. *Exp Mol Med* (2018) 50(9):1–11. doi: 10.1038/s12276-018-0147-5

59. Li ZY, Song J, Zheng SL, Fan MB, Guan YF, Qu Y, et al. Adipocyte metrnl antagonizes insulin resistance through PPARγ signaling. *Diabetes* (2015) 64(12):4011–22. doi: 10.2337/db15-0274

60. Varghese M, Song J, Singer K. Age and sex: Impact on adipose tissue metabolism and inflammation. *Mech Ageing Dev* (2021) 199:111563. doi: 10.1016/j.mad.2021.111563

61. Wu H, Ballantyne CM. Skeletal muscle inflammation and insulin resistance in obesity. *J Clin Invest* (2017) 127(1):43–54. doi: 10.1172/JCI88880

62. Lee JO, Byun WS, Kang MJ, Han JA, Moon J, Shin MJ, et al. The myokine meteorin-like (metrnl) improves glucose tolerance in both skeletal muscle cells and mice by targeting AMPKα2. *FEBS J* (2020) 287(10):2087–104. doi: 10.1111/febs.15301

63. Chazaud B. A macrophage-derived adipokine supports skeletal muscle regeneration. *Nat Metab* (2020) 2(3):213–4. doi: 10.1038/s42255-020-0186-9

64. Kajimura S, Spiegelman BM, Seale P. Brown and beige fat: Physiological roles beyond heat generation. *Cell Metab* (2015) 22(4):546–59. doi: 10.1016/j.cmet.2015.09.007

65. Chouchani ET, Kajimura S. Metabolic adaptation and maladaptation in adipose tissue. *Nat Metab* (2019) 1(2):189–200. doi: 10.1038/s42255-018-0021-8

66. Ruas JL, White JP, Rao RR, Kleiner S, Brannan KT, Harrison BC, et al. A PGC-1α isoform induced by resistance training regulates skeletal muscle hypertrophy. *Cell* (2012) 151(6):1319–31. doi: 10.1016/j.cell.2012.10.050

67. Townsend LK, Wright DC. Looking on the "brite" side exercise-induced browning of white adipose tissue. *Pflugers Arch* (2019) 471(3):455–65. doi: 10.1007/s00424-018-2177-1

68. Şekerci G, Erden Y, Tekin S. Effects of meteorin-like hormone on endocrine function of hypothalamo-hypophysial system and peripheral uncoupling proteins in rats. *Mol Biol Rep* (2022). doi: 10.1007/s11033-022-07374-5

69. Colaianni G, Cinti S, Colucci S, Grano M. Irisin and musculoskeletal health. *Ann N Y Acad Sci* (2017) 1402(1):5–9. doi: 10.1111/nyas.13345

70. Miao Y, Qin H, Zhong Y, Huang K, Rao C. Novel adipokine asprosin modulates browning and adipogenesis in white adipose tissue. *J Endocrinol* (2021) 249(2):83–93. doi: 10.1530/JOE-20-0503

71. BonDurant LD, Ameka M, Naber MC, Markan KR, Idiga SO, Acevedo MR, et al. FGF21 regulates metabolism through adipose-dependent and -independent mechanisms. *Cell Metab* (2017) 25(4):935–44.e4. doi: 10.1016/j.cmet.2017.03.005

72. Wu D, Molofsky AB, Liang HE, Ricardo-Gonzalez RR, Jouihan HA, Bando JK, et al. Eosinophils sustain adipose alternatively activated macrophages associated with glucose homeostasis. *Science* (2011) 332(6026):243–7. doi: 10.1126/science.1201475

73. Yan Q, Li W, Gong X, Hu R, Chen L. Transcriptomic and phenotypic analysis of CRISPR/Cas9-mediated gluk2 knockout in zebrafish. *Genes (Basel)* (2022) 13(8). doi: 10.3390/genes13081441

74. Coker RH, Weaver AN, Coker MS, Murphy CJ, Gunga HC, Steinach M. Metabolic responses to the Yukon Arctic ultra: Longest and coldest in the world. *Med Sci Sports Exerc.* (2017) 49(2):357–62. doi: 10.1249/MSS.0000000000001095

75. Saghebjoo M, Einaloo A, Mogharnasi M, Ahmadabadi F. The response of meteorin-like hormone and interleukin-4 in overweight women during exercise in temperate, warm and cold water. *Horm Mol Biol Clin Investig* (2018) 36(3). doi: 10.1515/hmbci-2018-0027

76. Sakers A, De Siqueira MK, Seale P, Villanueva CJ. Adipose-tissue plasticity in health and disease. *Cell* (2022) 185(3):419–46. doi: 10.1016/j.cell.2021.12.016

77. Petersen MC, Shulman GI. Mechanisms of insulin action and insulin resistance. *Physiol Rev* (2018) 98(4):2133–223. doi: 10.1152/physrev.00063.2017

78. Hu W, Wang R, Sun B. Meteorin-like ameliorates β cell function by inhibiting β cell apoptosis of and promoting β cell proliferation *via* activating the WNT/β-catenin pathway. *Front Pharmacol* (2021) 12:627147. doi: 10.3389/fphar.2021.627147

79. Yao DD, Yang L, Wang Y, Liu C, Wei YJ, Jia XB, et al. Geniposide promotes beta-cell regeneration and survival through regulating β-catenin/TCF7L2 pathway. *Cell Death Dis* (2015) 6(5):e1746. doi: 10.1038/cddis.2015.107

80. Wang C, Pan Y, Song J, Sun Y, Li H, Chen L, et al. Serum metrnl level is correlated with insulin resistance, but not with β-cell function in type 2 diabetics. *Med Sci Monit* (2019) 25:8968–74. doi: 10.12659/MSM.920222

81. Matthews DR, Hosker JP, Rudenski AS, Naylor BA, Treacher DF, Turner RC. Homeostasis model assessment: Insulin resistance and beta-cell function from fasting plasma glucose and insulin concentrations in man. *Diabetologia* (1985) 28(7):412–9. doi: 10.1007/BF00280883

82. Sinaiko AR, Caprio S. Insulin resistance. *J Pediatr* (2012) 161(1):11–5. doi: 10.1016/j.jpeds.2012.01.012

83. Alizadeh H, Alizadeh A. Association of meteorin-like hormone with insulin resistance and body composition in healthy Iranian adults. *Diabetes Metab Syndr* (2020) 14(5):881–5. doi: 10.1016/j.dsx.2020.05.031

84. Wang K, Li F, Wang C, Deng Y, Cao Z, Cui Y, et al. Serum levels of meteorin-like (Metrnl) are increased in patients with newly diagnosed type 2 diabetes mellitus and are associated with insulin resistance. *Med Sci Monit* (2019) 25:2337–43. doi: 10.12659/MSM.915331

85. Onalan E, Cavlı C, Dogan Y, Onalan E, Gozel N, Buran I, et al. Low serum levels of meteorin-like/subfatin: An indicator of diabetes mellitus and insulin resistance? *Endokrynol Pol* (2020) 71(5):397–403. doi: 10.5603/EP.a2020.0038

86. Timurkaan M, Timurkaan ES. Two important players for type 2 diabetes mellitus: Metrnl and asprosin. *Clin Lab* (2022) 68(9). doi: 10.7754/Clin.Lab.2021.211015

87. Ugur K, Erman F, Turkoglu S, Aydin Y, Aksoy A, Lale A, et al. Asprosin, visfatin and subfatin as new biomarkers of obesity and metabolic syndrome. *Eur Rev Med Pharmacol Sci* (2022) 26(6):2124–33. doi: 10.26355/eurrev_202203_28360

88. Diamanti-Kandarakis E, Dunaif A. Insulin resistance and the polycystic ovary syndrome revisited: an update on mechanisms and implications. *Endocr Rev* (2012) 33 (6):981–1030. doi: 10.1210/er.2011-1034

89. Deniz R, Yavuzkir S, Ugur K, Ustebay DU, Baykus Y, Ustebay S, et al. Subfatin and asprosin, two new metabolic players of polycystic ovary syndrome. *J Obstetrics Gynaecol* (2021) 41(2):279–84. doi: 10.1080/01443615.2020.1758926

90. Chen P, Jia R, Liu Y, Cao M, Zhou L, Zhao Z. Progress of adipokines in the female reproductive system: A focus on polycystic ovary syndrome. *Front Endocrinol (Lausanne)* (2022) 13:881684. doi: 10.3389/fendo.2022.881684

91. Yavuzkir S, Ugur K, Deniz R, Ustebay DU, Mirzaoglu M, Yardim M, et al. Maternal and umbilical cord blood subfatin and spexin levels in patients with gestational diabetes mellitus. *Peptides* (2020) 126:170277. doi: 10.1016/j.peptides.2020.170277

92. Lappas M. Maternal obesity and gestational diabetes decrease metrnl concentrations in cord plasma. *J Matern Fetal Neonatal Med* (2021) 34(18):2991–5. doi: 10.1080/14767058.2019.1676713

93. Zheng SL, Li ZY, Zhang Z, Wang DS, Xu J, Miao CY. Evaluation of two commercial enzyme-linked immunosorbent assay kits for the detection of human circulating metrnl. *Chem Pharm Bull (Tokyo)* (2018) 66(4):391–8. doi: 10.1248/cpb.c17-00846

94. Fadaei R, Dadmanesh M, Moradi N, Ahmadi R, Shokoohi Nahrkhalaji A, Aghajani H, et al. Serum levels of subfatin in patients with type 2 diabetes mellitus and its association with vascular adhesion molecules. *Arch Physiol Biochem* (2020) 126 (4):335–40. doi: 10.1080/13813455.2018.1538248

95. Schmid A, Karrasch T, Schäffler A. Meteorin-like protein (Metrnl) in obesity, during weight loss and in adipocyte differentiation. *J Clin Med* (2021) 10(19):4338. doi: 10.3390/jcm10194338

96. Khajebishak Y, Faghfouri AH, Soleimani A, Madani S, Payahoo L. Exploration of meteorin-like peptide (metrnl) predictors in type 2 diabetic patients: The potential role of irisin, and other biochemical parameters. *Horm Mol Biol Clin Investig* (2022). doi: 10.1515/hmbci-2022-0037

97. Cheng JX, Yu K. New discovered adipokines associated with the pathogenesis of obesity and type 2 diabetes. *Diabetes Metab Syndr Obes* (2022) 15:2381–9. doi: 10.2147/DMSO.S376163

98. Tuncer Kara K, Kizil M, Çakmak E, Yildirim TT, Kilinc F, Kuloğlu T, et al. Comparison of plasma and salivary meteorin-like protein levels in patients with newly diagnosed type-2 diabetes and treated with metformin. *Eur Rev Med Pharmacol Sci* (2022) 26(19):7145–50. doi: 10.26355/eurrev_202210_29900

99. Lee JH, Kang YE, Kim JM, Choung S, Joung KH, Kim HJ, et al. Serum meteorin-like protein levels decreased in patients newly diagnosed with type 2 diabetes. *Diabetes Res Clin Pract* (2018) 135:7–10. doi: 10.1016/j.diabres.2017.10.005

100. Chung HS, Hwang SY, Choi JH, Lee HJ, Kim NH, Yoo HJ, et al. Implications of circulating meteorin-like (Metrnl) level in human subjects with type 2 diabetes. *Diabetes Res Clin Pract* (2018) 136:100–7. doi: 10.1016/j.diabres.2017.11.031

101. Cherian P, Al-Khairi I, Jamal M, Al-Sabah S, Ali H, Dsouza C, et al. Association between factors involved in bone remodeling (Osteoactivin and OPG) with plasma levels of irisin and meteorin-like protein in people with T2D and obesity. *Front Endocrinol (Lausanne)* (2021) 12:752892. doi: 10.3389/fendo.2021.752892

102. Wu Q, Dan YL, He YS, Xiang K, Hu YQ, Zhao CN, et al. Circulating meteorin-like levels in patients with type 2 diabetes mellitus: A meta-analysis. *Curr Pharm Des* (2020) 26(44):5732–8. doi: 10.2174/1381612826666201007163930

103. Wang R, Hu D, Zhao X, Hu W. Correlation of serum meteorin-like concentrations with diabetic nephropathy. *Diabetes Res Clin Pract* (2020) 169:108443. doi: 10.1016/j.diabres.2020.108443

104. Löffler D, Landgraf K, Rockstroh D, Schwartze JT, Dunzendorfer H, Kiess W, et al. METRNL decreases during adipogenesis and inhibits adipocyte differentiation leading to adipocyte hypertrophy in humans. *Int J Obes (Lond)* (2017) 41(1):112–9. doi: 10.1038/ijo.2016.180

105. Bae JY. Aerobic exercise increases meteorin-like protein in muscle and adipose tissue of chronic high-fat diet-induced obese mice. *BioMed Res Int* (2018) 2018:6283932. doi: 10.1155/2018/6283932

106. Qi Q, Hu WJ, Zheng SL, Zhang SL, Le YY, Li ZY, et al. Metrnl deficiency decreases blood HDL cholesterol and increases blood triglyceride. *Acta Pharmacol Sin* (2020) 41(12):1568–75. doi: 10.1038/s41401-020-0368-8

107. Hu C, Zhang X, Song P, Yuan YP, Kong CY, Wu HM, et al. Meteorin-like protein attenuates doxorubicin-induced cardiotoxicity *via* activating cAMP/PKA/SIRT1 pathway. *Redox Biol* (2020) 37:101747. doi: 10.1016/j.redox.2020.101747

108. Rupérez C, Ferrer-Curriu G, Cervera-Barea A, Florit L, Guitart-Mampel M, Garrabou G, et al. Meteorin-like/Meteorin-β protects heart against cardiac dysfunction. *J Exp Med* (2021) 218(5):e20201206. doi: 10.1084/jem.20201206

109. Huang R, Balu AR, Molitoris KH, White JP, Robling AG, Ayturk UM, et al. The role of meteorin-like in skeletal development and bone fracture healing. *J Orthop Res* (2022) 40(11):2510–21. doi: 10.1002/jor.25286

110. Ding X, Chang X, Wang J, Bian N, An Y, Wang G, et al. Serum metrnl levels are decreased in subjects with overweight or obesity and are independently associated with adverse lipid profile. *Front Endocrinol (Lausanne)* (2022) 13:938341. doi: 10.3389/fendo.2022.938341

111. Du Y, Ye X, Lu A, Zhao D, Liu J, Cheng J, et al. Inverse relationship between serum metrnl levels and visceral fat obesity (VFO) in patients with type 2 diabetes. *Diabetes Res Clin Pract* (2020) 161:108068. doi: 10.1016/j.diabres.2020.108068

112. Kong YY, Li GQ, Zhang WJ, Hua X, Zhou CC, Xu TY, et al. Nicotinamide phosphoribosyltransferase aggravates inflammation and promotes atherosclerosis in ApoE knockout mice. *Acta Pharmacol Sin* (2019) 40(9):1184–92. doi: 10.1038/s41401-018-0207-3

113. Cai J, Wang QM, Li JW, Xu F, Bu YL, Wang M, et al. Serum meteorin-like is associated with weight loss in the elderly patients with chronic heart failure. *J Cachexia Sarcopenia Muscle* (2022) 13(1):409–17. doi: 10.1002/jcsm.12865

114. Castaneda AB, Petty LE, Scholz M, Jansen R, Weiss S, Zhang X, et al. Associations of carotid intima media thickness with gene expression in whole blood and genetically predicted gene expression across 48 tissues. *Hum Mol Genet* (2021) 31(7):1171–82. doi: 10.1093/hmg/ddab236

115. Naqvi TZ, Lee MS. Carotid intima-media thickness and plaque in cardiovascular risk assessment. *JACC Cardiovasc Imaging* (2014) 7(10):1025–38. doi: 10.1016/j.jcmg.2013.11.014

116. Swirski FK, Nahrendorf M. Cardioimmunology: The immune system in cardiac homeostasis and disease. *Nat Rev Immunol* (2018) 18(12):733–44. doi: 10.1038/s41577-018-0065-8

117. Yilmaz M, Cagri Goktekin M, Ilhan N. Subfatin concentration decreases in acute coronary syndrome. *Biochem Med (Zagreb)* (2022) 32(2):020704. doi: 10.11613/BM.2022.020704

118. Srivastava D. Cellular cross-talk in heart repair. *Science* (2022) 376(6599):1271–2. doi: 10.1126/science.adc8698

119. Huynh K. Meteorin-like protein repairs the ischaemic heart *via* receptor KIT in endothelial cells. *Nat Rev Cardiol* (2022) 19(9):575. doi: 10.1038/s41569-022-00752-3

120. Majithia A, Bhatt DL. Novel antiplatelet therapies for atherothrombotic diseases. *Arterioscler Thromb Vasc Biol* (2019) 39(4):546–57. doi: 10.1161/ATVBAHA.118.310955

121. Gong W, Liu Y, Wu Z, Wang S, Qiu G, Lin S. Meteorin-like shows unique expression pattern in bone and its overexpression inhibits osteoblast differentiation. *PloS One* (2016) 11(10):e0164446. doi: 10.1371/journal.pone.0164446

122. Vi L, Baht GS, Whetstone H, Ng A, Wei Q, Poon R, et al. Macrophages promote osteoblastic differentiation *in-vivo*: Implications in fracture repair and bone homeostasis. *J Bone Miner Res* (2015) 30(6):1090–102. doi: 10.1002/jbmr.2422

123. Zeng Y, Shih YV, Baht GS, Varghese S. *In vivo* sequestration of innate small molecules to promote bone healing. *Adv Mater* (2020) 32(8):e1906022. doi: 10.1002/adma.201906022

124. Baht GS, Silkstone D, Vi L, Nadesan P, Amani Y, Whetstone H, et al. Exposure to a youthful circulaton rejuvenates bone repair through modulation of β-catenin. *Nat Commun* (2015) 6:7131. doi: 10.1038/ncomms8131

125. Xu Y, Barter MJ, Swan DC, Rankin KS, Rowan AD, Santibanez-Koref M, et al. Identification of the pathogenic pathways in osteoarthritic hip cartilage: commonality and discord between hip and knee OA. *Osteoarthritis Cartilage* (2012) 20(9):1029–38. doi: 10.1016/j.joca.2012.05.006

126. Wang W, Liu Y, Hao J, Zheng S, Wen Y, Xiao X, et al. Comparative analysis of gene expression profiles of hip articular cartilage between non-traumatic necrosis and osteoarthritis. *Gene* (2016) 591(1):43–7. doi: 10.1016/j.gene.2016.06.058

127. Wu H, Ballantyne CM. Metabolic inflammation and insulin resistance in obesity. *Circ Res* (2020) 126(11):1549–64. doi: 10.1161/CIRCRESAHA.119.315896

128. Pellitero S, Piquer-Garcia I, Ferrer-Curriu G, Puig R, Martínez E, Moreno P, et al. Opposite changes in meteorin-like and oncostatin m levels are associated with metabolic improvements after bariatric surgery. *Int J Obes (Lond)* (2018) 42(4):919–22. doi: 10.1038/ijo.2017.268

129. Ferns GA, Fekri K, Shahini Shams Abadi M, Banitalebi Dehkordi M, Arjmand MH. A meta-analysis of the relationship between serums metrnl-like protein/subfatin and risk of type 2 diabetes mellitus and coronary artery disease. *Arch Physiol Biochem* (2021), 1–7. doi: 10.1080/13813455.2021.1899239

130. AlKhairi I, Cherian P, Abu-Farha M, Madhoun AA, Nizam R, Melhem M, et al. Increased expression of meteorin-like hormone in type 2 diabetes and obesity and its association with irisin. *Cells* (2019) 8(10). doi: 10.3390/cells8101283

131. Jamal MH, Abu-Farha M, Al-Khaledi G, Al-Sabah S, Ali H, Cherian P, et al. Effect of sleeve gastrectomy on the expression of meteorin-like (METRNL) and irisin (FNDC5) in muscle and brown adipose tissue and its impact on uncoupling proteins in diet-induced obesity rats. *Surg Obes Relat Dis* (2020) 16(12):1910–8. doi: 10.1016/j.soard.2020.07.022

132. Aleassa EM. Comment on: Effect of sleeve gastrectomy on the expression of meteorin-like (METRNL) and irisin (FNDC5) in muscle and brown adipose tissue and its impact on (UCPs) in diet-induced obesity rats. *Surg Obes Relat Dis* (2020) 16(12):1918–9. doi: 10.1016/j.soard.2020.08.027

133. Masuya T, Suzuki M, Tsujimura J, Kanamori S, Miyasaka Y, Ohno T, et al. Ablation of Iah1, a candidate gene for diet-induced fatty liver, does not affect liver lipid accumulation in mice. *PloS One* (2020) 15(5):e0233087. doi: 10.1371/journal.pone.0233087

134. Ost M, Coleman V, Kasch J, Klaus S. Regulation of myokine expression: Role of exercise and cellular stress. *Free Radic Biol Med* (2016) 98:78–89. doi: 10.1016/j.freeradbiomed.2016.02.018

135. Szabó MR, Pipicz M, Csont T, Csonka C. Modulatory effect of myokines on reactive oxygen species in Ischemia/Reperfusion. *Int J Mol Sci* (2020) 21(24):9382. doi: 10.3390/ijms21249382

136. Amano Y, Nonaka Y, Takeda R, Kano Y, Hoshino D. Effects of electrical stimulation-induced resistance exercise training on white and brown adipose tissues and plasma meteorin-like concentration in rats. *Physiol Rep* (2020) 8(16):e14540. doi: 10.14814/phy2.14540

137. Bae JY, Woo J, Kang S, Shin KO. Effects of detraining and retraining on muscle energy-sensing network and meteorin-like levels in obese mice. *Lipids Health Dis* (2018) 17(1):97. doi: 10.1186/s12944-018-0751-3

138. Saeidi A, Tayebi SM, Khosravi A, Malekian F, Khodamoradi A, Sellami M, et al. Effects of exercise training on type 2-diabetes: The role of meteorin-like protein. *Health Promot Perspect* (2019) 9(2):89–91. doi: 10.15171/hpp.2019.12

139. Martínez-Gayo A, Félix-Soriano E, Sáinz N, González-Muniesa P, Moreno-Aliaga MJ. Changes induced by aging and long-term exercise and/or DHA supplementation in muscle of obese female mice. *Nutrients* (2022) 14(20):4240. doi: 10.3390/nu14204240

140. Huang S, Cao L, Cheng H, Li D, Li Y, Wu Z. The blooming intersection of subfatin and metabolic syndrome. *Rev Cardiovasc Med* (2021) 22(3):799–805. doi: 10.31083/j.rcm2203086

141. Alizadeh H. Meteorin-like protein (Metrnl): A metabolic syndrome biomarker and an exercise mediator. *Cytokine* (2022) 157:155952. doi: 10.1016/j.cyto.2022.155952

142. Miao ZW, Hu WJ, Li ZY, Miao CY. Involvement of the secreted protein metrnl in human diseases. *Acta Pharmacol Sin* (2020) 41(12):1525–30. doi: 10.1038/s41401-020-00529-9

143. Alizadeh H. Myokine-mediated exercise effects: The role of myokine meteorin-like hormone (Metrnl). *Growth Factors* (2021) 39(1-6):71-78. doi: 10.1080/08977194.2022.2032689

144. Gonzalez-Gil AM, Elizondo-Montemayor L. The role of exercise in the interplay between myokines, hepatokines, osteokines, adipokines, and modulation of inflammation for energy substrate redistribution and fat mass loss: A review. *Nutrients* (2020) 12(6):1899. doi: 10.3390/nu12061899

145. Gries KJ, Zysik VS, Jobe TK, Griffin N, Leeds BP, Lowery JW. Muscle-derived factors influencing bone metabolism. *Semin Cell Dev Biol* (2022) 123:57–63. doi: 10.1016/j.semcdb.2021.10.009

146. Huh JY. The role of exercise-induced myokines in regulating metabolism. *Arch Pharm Res* (2018) 41(1):14–29. doi: 10.1007/s12272-017-0994-y

147. Eaton M, Granata C, Barry J, Safdar A, Bishop D, Little JP. Impact of a single bout of high-intensity interval exercise and short-term interval training on interleukin-6, FNDC5, and METRNL mRNA expression in human skeletal muscle. *J Sport Health Sci* (2018) 7(2):191–6. doi: 10.1016/j.jshs.2017.01.003

148. Tok Ö, Kişioğlu SV, Ersöz H, Kahveci B, Göktaş Z. Effects of increased physical activity and/or weight loss diet on serum myokine and adipokine levels in overweight adults with impaired glucose metabolism. *J Diabetes Complications* (2021) 35 (5):107892. doi: 10.1016/j.jdiacomp.2021.107892

149. Akbulut T, Cinar V, Ugur K, Yardim M, Karagoz ZK, Aydin S. Effect of regular exercise on the levels of subfatin and asprosin: A trial with different types of exercise. *Eur Rev Med Pharmacol Sci* (2022) 26(8):2683–91. doi: 10.26355/eurrev_202204_28598

150. Alizadeh A, Alizadeh H. Downhill running exercise increases circulating level of myokine meteorin-like hormone in humans. *J Sports Med Phys Fitness* (2021) 62 (5):700–4. doi: 10.23736/S0022-4707.21.12246-7

151. Bonfante ILP, Monfort-Pires M, Duft RG, da Silva Mateus KC, de Lima Júnior JC, Dos Santos Trombeta JC, et al. Combined training increases thermogenic fat activity in patients with overweight and type 2 diabetes. *Int J Obes (Lond)* (2022) 46 (6):1145–54. doi: 10.1038/s41366-022-01086-3

152. Bonfante ILP, Duft RG, Mateus K, Trombeta J, Finardi EAR, Ramkrapes APB, et al. Acute/Chronic responses of combined training on serum pro-thermogenic/Anti-inflammatory inducers and its relation with fed and fasting state in overweight type 2 diabetic individuals. *Front Physiol* (2021) 12:736244. doi: 10.3389/fphys.2021.736244

frontiers | Frontiers in Immunology

TYPE Original Research
PUBLISHED 24 March 2023
DOI 10.3389/fimmu.2023.1104550

OPEN ACCESS

EDITED BY
Dariusz Jan Skarzynski,
Wrocław University of Environmental and Live Sciences, Poland

REVIEWED BY
Kang Chao,
The Sixth Affiliated Hospital of Sun Yat-sen University, China
Sławomir Wołczyński,
Medical University of Bialystok, Poland

*CORRESPONDENCE
Benjamin K. Tsang
btsang@ohri.ca

SPECIALTY SECTION
This article was submitted to Cytokines and Soluble Mediators in Immunity, a section of the journal Frontiers in Immunology

RECEIVED 21 November 2022
ACCEPTED 13 March 2023
PUBLISHED 24 March 2023

CITATION
Salehi R, Asare-Werehene M, Wyse BA, Abedini A, Pan B, Gutsol A, Jahangiri S, Szaraz P, Burns KD, Vanderhyden B, Li J, Burger D, Librach CL and Tsang BK (2023) Granulosa cell-derived miR-379-5p regulates macrophage polarization in polycystic ovarian syndrome. *Front. Immunol.* 14:1104550. doi: 10.3389/fimmu.2023.1104550

Granulosa cell-derived miR-379-5p regulates macrophage polarization in polycystic ovarian syndrome

Reza Salehi[1,2,3,4], Meshach Asare-Werehene[1,2,3], Brandon A. Wyse[4], Atefeh Abedini[5], Bo Pan[6], Alex Gutsol[7], Sahar Jahangiri[4], Peter Szaraz[4], Kevin D. Burns[7], Barbara Vanderhyden[2,3,5], Julang Li[6], Dylan Burger[1,3,7], Clifford L. Librach[4,8,9,10] and Benjamin K. Tsang[1,2,3]*

[1]Chronic Disease Program, Ottawa Hospital Research Institute, Ottawa, ON, Canada, [2]Department of Obstetrics and Gynecology, University of Ottawa, Ottawa, ON, Canada, [3]Department of Cellular and Molecular Medicine and Center for Infection, Immunity and Inflammation, University of Ottawa, Ottawa, ON, Canada, [4]CReATe Fertility Centre, Toronto, ON, Canada, [5]Cancer Therapeutics Program, Ottawa Hospital Research Institute, Ottawa, ON, Canada, [6]Department of Animal BioScience, University of Guelph, Guelph, ON, Canada, [7]Division of Nephrology, Department of Medicine, Kidney Research Centre, University of Ottawa, Ottawa, ON, Canada, [8]Department of Obstetrics & Gynaecology, University of Toronto, Toronto, ON, Canada, [9]Department of Physiology, University of Toronto, Toronto, ON, Canada, [10]Institute of Medical Sciences, University of Toronto, Toronto, ON, Canada

Polycystic ovarian syndrome (PCOS) is associated with hyperandrogenemia and ovarian antral follicle growth arrest. We have previously demonstrated that androgen-induced exosomal release of miR-379-5p (miR379) from preantral follicle granulosa cells increases the proliferation of target cells *via* phosphoinositide-dependent kinase 1 (PDK1) upregulation. Androgen also increases inflammatory M1 macrophage abundance, but reduces anti-inflammatory M2 polarization in rat antral and preovulatory follicles. However, the role of small extracellular vesicles (sEVs; also known as exosomes) secretion in determining the cellular content and function of miRNAs in exosome-receiving cells is largely unknown. Our objectives were to determine: 1) the regulatory role of granulosa cells (GC)-derived exosomal miR379 on macrophage polarization and ovarian inflammation; 2) whether miR379-induced M1 polarization regulates GC proliferation; and 3) if this regulated process is follicular stage-specific. Compared with non-PCOS subjects, PCOS subjects had a higher M1/M2 ratio, supporting the concept that PCOS is an inflammatory condition. Ovarian overexpression of miR379 increased the number of M1 macrophages and the M1/M2 ratio in preantral follicles specifically. Transfection of macrophages with a miR379 mimic reduced the cellular content of PDK1 and induced M0→M1 polarization; whereas its inhibitor polarized M0→M2. Conditioned media from macrophages transfected with miR379 mimic and follicular fluid from PCOS subjects had higher galectin-3

content, a pro-inflammatory cytokine which specifically suppresses human antral follicle GC proliferation. These results indicate that miR379 inhibits M2 macrophage polarization, a condition which suppresses GC proliferation in a follicle stage-dependent manner, as exhibited in PCOS.

KEYWORDS

miR-379-5p, PCOS (polycystic ovarian syndrome), macrophage, PDK1, granulosa cells, extracellular vesicle, exosomes

Introduction

Polycystic ovarian syndrome (PCOS) is a multi-factorial heterogeneous syndrome with complex pathologies. PCOS is associated with androgen excess, increased ovarian preantral follicular growth, antral follicle growth arrest and chronic anovulation (1). In PCOS subjects, the peripheral level of chronic inflammatory markers (e.g. galectin-3) is positively correlated with hyperandrogenemia (2–5). We have shown that DHT increases inflammatory M1 macrophages and the M1/M2 ratio, but reduces anti-inflammatory M2 macrophages in rat antral and preovulatory follicles (6); supporting the concept that PCOS is an inflammatory response. However, it is not known how hyperandrogenism regulates macrophage polarization in the ovaries, and if microRNAs (miRNAs) are involved in this response.

miRNAs are small non-coding RNAs which play important roles in the regulation of macrophage polarization by post-transcriptionally down-regulating target gene expression (7–9). Exosomes (also known as small extracellular vesicles) are nano-sized vesicles which measure between 30 – 200 nm, and are involved in cell-cell communication (10–12) by selectively packaging and transferring bioactive materials (e.g. miRNAs (13, 14)). We have demonstrated that 89 miRNAs, including miR-379-5p (miR379), are differentially expressed in an androgenized rat PCOS model (15). miR379 is a member of the cluster delta-like homolog 1 gene and the type III iodothyronine deiodinase gene (DLK1-DIO3) (16). Our recent findings using an androgenized rat PCOS model exhibited lower granulosa cell (GC) miR379 but higher phosphoinositide-dependent kinase-1 (PDK1; a miR379 target) content and increased proliferation (17). Androgen reduces GC miR379 content by increasing its exosome release in preantral follicles, but not in antral follicles *in vitro*. These findings suggest that increased exosomal miR379 release in GCs is a proliferative response to androgenic stimulation, specific to the preantral stage of follicle development, and that dysregulation of this response at the antral stage is associated with follicular growth arrest, as observed in human PCOS (17).

The PI3K/AKT pathway is involved in M2 macrophage polarization and inhibition of phosphatase and tensin homolog (PTEN; an inhibitor of the AKT pathway) increases the levels of Arginase 1 and M2 polarization (18, 19). Moreover, inhibition of AKT phosphorylation through knockdown of PDK1 increases M1 polarization and the susceptibility of mice to endotoxin shock (20). However, further studies are required to determine if and how the uptake GC-derived exosomal miR379 by macrophages would alter their polarization.

In this current study, our specific objectives were to examine whether: 1) miR379 regulates macrophage polarization; 2) suppressed M2-macrophage polarization inhibits GC proliferation and steroidogenesis; and 3) the above responses are follicular stage-dependent. Our overall hypothesis was that the uptake of GC-derived exosomal miR379 induces macrophage polarization to inflammatory (M1) and increases inflammatory cytokine secretion, a response which inhibits GC proliferation in the antral, but not preantral follicles.

Materials and methods

Reagents and antibodies

Cell culture media (M199), DMEM/F12, fetal bovine serum (FBS), penicillin and streptomycin, L-glutamine, sodium pyruvate, and trypsin were purchased from Invitrogen (Burlington, Canada). Diethylstilbestrol (DES), equine chorionic gonadotropin (eCG), HEPES and bovine serum albumin (BSA) were from Sigma (St. Louis, MO). 5α-dihydrotestosterone (DHT) was obtained from Steraloids (Newport, RI). Anti-rabbit and -mouse IgG conjugated with horseradish peroxidase and reagents for SDS-PAGE were purchased from Bio-Rad Laboratories (Mississauga, Ontario, Canada). Enhanced chemiluminescent reagent was from Thermo Fisher Scientific (Rockford, IL).

Animals, DHT implant, bone marrow derived macrophages, macrophage polarization, GCs and miRNA transfection

All animal procedures were carried out in accordance with the Guidelines for the Care and Use of Laboratory Animals, Canadian Council on Animal Care, and were approved by the University of Ottawa Animal Care Committee. Female Sprague Dawley rats (Charles River, Montreal, Canada) were maintained on 12 h cycle (light and dark) and given food and water ad libitum. Immature female rats at 21 day of age were implanted subcutaneously with silicone capsules without (control, sham control) or with DHT

(DHT, Steraloids Inc., Newport, USA), as previously described (6, 21) to continuously release 83 µg DHT/day for 28 days. Sham control animals received identical pellets lacking the steroid. Bone marrow cells were collected from the femur and tibia of 21 days old rats and were cultured and differentiated into macrophages in DMEM/F12 containing recombinant rat macrophage colony-stimulating factor (50 ng/mL; PeproTech, 400-28) for 7 days *in vitro*. Half of the culture media was replaced with fresh media on Day 3. On day 7, macrophages (1.0×10^6 cells) were collected and polarized to M1 and M2, using LPS (10 ρg/mL) + IFN-γ (20 ng/mL; 36 h) and IL-4 (20 ng/ml; 36 h), respectively. In some experiments, macrophages were transfected with miR-379-5p mimic (100 nM) or inhibitor (100 nM; mirVana Life Technologies, Inc.) or scrambled (100 nM) sequence, using Lipofectamine RNAiMAX (Life Technologies, Inc.) for 18 h before treatment *in vitro* (22).

Granulosa cells from preantral follicles (DES-primed 21-day old rats; 1 mg/d, s.c. for 3 consecutive days) and antral follicles (eCG–injected 22-day old rats; 10 IU i.p., animals sacrificed 2 days post-injection) were isolated by follicular puncture (21). Granulosa cells were plated (1×10^6 per well in a 6 well plate) overnight in M199 with 10% FBS under a humidified atmosphere of 95% air and 5% CO2. After culture overnight in serum-free medium, granulosa cells were treated with or without DHT (1 µM; 36 h). DMSO and alcohol were added to the control group (final concentration of 0.001% and 0.005%, respectively) as a vehicle for DHT. Our laboratory has previously examined different concentrations of DHT on various ovarian parameters *in vitro* (23), including follicular growth, granulosa cell proliferation, apoptosis, steroidogenesis and androgen receptor content. We found that 1 µM DHT is the optimal concentration, and hence was used in the current study.

In granulosa cell-macrophage co-culture experiments, granulosa cell-derived exosomal miR-379-5p was tracked by transfecting granulosa cells with alexa-647-labelled miR-379-5p mimic (100 nM; mirVana Life Technologies, Inc.) and GFP-tagged CD63 (System Bioscience; CYTO120-PA-1). Macrophages were imaged by Zeiss LSM880 with AiryScan FAST at the Cell Biology and Image Acquisition at the University of Ottawa.

Conditioned media from rat BMDMs transfected with miR-379-5p mimic (CM-mimic; mirVana mimics, MC10316, ThermoFisher) or inhibitor (CM-inhibitor; mirVana inhibitor, MH10316; 18h) were collected and added (1:10 ratio) to preantral and antral follicle granulosa cells, and cultured further for 36 h.

Immunofluorescence, protein extraction and western blotting

At the time of animal euthanization, the ovaries were fixed in 4% formalin, dehydrated, embedded in paraffin, and cut into 4-µm sections. Sections were de-paraffinized in xylene and rehydrated through a 100-70% ethanol gradient. Antigen retrieval was achieved by boiling the slides in TRIS/EDTA (pH 9.0) or citrate (pH 6.0) buffer in a microwave for 15 min. Sections were blocked with 10% donkey serum in 1% bovine serum albumin in phosphate-buffered saline for 40 min, followed by overnight incubation at 4°C with primary antibodies. Primary antibodies, including mouse anti-CD68 (1:100; Abcam) and rabbit anti-CD163 (1:100; Abcam) were diluted in 1% BSA/PBS. Secondary donkey- anti-mouse and donkey-anti-rabbit fluorescent antibodies conjugated with Cy3 and Alexa488 (1:100; Jackson Immunoresearch) incubated for 1 h at room temperature were used to localize or co-localize primary antibodies. The fluorescent dye Hoechst 33342 (1:10,000; Molecular Probes) was used to stain the nuclei. Sections were protected with VectaShield mounting medium (Vector Labs), scanned by Axio Scan.Z1 (Carl Zeiss, Gottingen, Germany) and recorded with the Axion Vision program (Axion Vision software, Zeiss). The macro (FIJI software) was used to apply colour threshold-based selection for the respective signals/channels which then counted the selected particles.

At the end of the culture period, granulosa cells were harvested by trypsin treatment and lysed using Cell Lysis Buffer (Cat#: 9803; Cell Signaling Technology, Inc; Beverly, Massachusetts). Protein extraction and western blotting were performed as described previously (21). Antibodies and their dilutions are summarized in Supplementary Table 1. Proteome Profiler Rat XL Cytokine Array (R&D Systems; ARY030) was conducted, as per the manufacturer's instructions, to compare the content of 79 different cytokines in macrophage culture media. Protein extraction and western blotting were performed as described previously (21).

Production of recombinant lentiviral particles and injection

The lentiviral gene transfer plasmids pLV-[hsa-miR-379-5p] (Cat.no. miR-p209m) and pLV-[miR-control] (Cat.no. mir-p000) were purchased from the BioSettia Company (San Diego, California, USA); production of recombinant lentiviral particles was performed as per manufacturer's protocol. Briefly, HEK 293T cells were co-transfected with the transfer vector and the helper plasmids pMD2.G (Addgene) and psPAX2 (Addgene), using the calcium phosphate co-precipitation method. Prior to transfection, $6x10^6$ 293T cells were seeded in 10 cm plates for 24 h in modified Dulbecco's culture medium containing FBS (10%), penicillin (100 IU/ml), and streptomycin (100 mg/ml) in 5% CO_2. The culture medium was changed one hour prior to transfection and a total of 18 µg of plasmid DNA was added per dish: [envelope plasmid pMD2.G (3µg), packaging plasmid psPAX2 (6 µg) and transfer vector plasmid (9 µg)]. The precipitate, formed from adding the plasmids to a final volume of 540 µl and 60 µl of 2.5 M $CaCl_2$ and then 600 ml of 2x HEPES-buffered saline, was added dropwise immediately to the cultures. The medium was then replaced every 24 h with fresh medium for high-concentration virus production. A high-titered virus was achieved through serial ultracentrifugation, as previously described (24). Briefly, the viral supernatant was collected and filtered through a 0.45 µm filter and transferred into sterilized Ultra-Clear centrifuge tubes (Beckman cat. no. 344058). The viral supernatant was centrifuged (16,500 x g, 90 min, 4°C), pooled, and stored in aliquots at -80°C.

Animals were randomly divided into 2 groups (control and DHT implants) and left and right ovaries in each animal were injected with RFP virus particles and miR-379-5p mimic, respectively, sacrificed 28 days post-injection, and the number and type of macrophages (M1 and M2) at each follicle stage were

compared. Viral particles containing RFP or miR-379-5p were injected (2 µl) using a syringe with a glass micro-injection needle (50 µm diameter), as described previously (25).

Human samples

All human FF and granulosa cell specimens were obtained from the CReATe Biobank, CReATe Fertility Centre with written informed consent. The CReATe Biobank (banking protocols approved by Veritas IRB (Approval#16518), collects biological materials from consenting patients, according to the best practice-based standards of biobanking [7]. Patients undergoing IVF-ICSI have been treated by a routine antagonist protocol, with gonadotropin starting dosing and adjustments based on response to stimulation by the treating physician. Follicles have been collected 35-36hrs following trigger injection. The cumulus-oocyte complex was collected from the aspirate for denudation. The resulting aspirate, containing granulosa cells and follicular fluid, was collected by CReATe BioBank personnel and processed. All samples from the Biobank were approved for use in this study by the Veritas IRB (Approval#16487) and The Ottawa Hospital REB (Protocol #20170453-01H)]. Human ovarian follicular cells and fluids (FF; Supplementary Table 2) were collected from lean PCOS (based on Rotterdam criteria; BMI<30) and non-PCOS subjects (premenopausal, 18-40 years) with normal thyroid function and prolactin levels, undergoing assisted reproduction treatment at the CReATe Fertility Centre, Toronto, Canada. Exclusion criteria include (1): known causes of oligomenorrhea other than PCOS; and (2) use of hormone treatment, birth control pill, insulin sensitizers, lipid lowering agents, or medications known to influence insulin sensitivity or serum androgens, within 3 months of the study onset. All FF (PCOS, n = 17 & non-PCOS, n = 20) and follicular cells (PCOS, n = 19 & non-PCOS, n = 19) specimens were obtained from the CReATe Biobank, CReATe Fertility Centre (26–28). Regarding human granulosa cell cultures, each replicate experiment was conducted using the pool of three non-PCOS antral follicle granulosa cell samples (1×10^6 cells per well; Supplementary Table 3). The same follicular fluids used in Figure 3B were added to non-PCOS granulosa cells. In this experiment, 200 µl of follicular fluid was added to 2 mL of culture media and a pool of two follicular fluids were used in each experimental replicate. To neutralize galectin-3, neutralizing antibody (Miltenyi Biotec; 130-112-969; 20 µl) was added to follicular fluid (200 µl), incubated 30 min in room temperature and then added to granulosa cell cultures. Isotype control antibody, rat IgG2a (Miltenyi Biotec; 130-102-652) was added to PCOS and non-PCOS experimental groups. Human recombinant galectin-3 (R & D systems; n = 3; 0.03 ng/mL) was added to non-PCOS granulosa cell cultures.

Flow cytometry, multiplex magnetic bead immunoassay and ELISA assays

Cleared follicular fluid samples (n=17 PCOS, n=20 non-PCOS) were diluted (1:2) with Calibrator Diluent and distributed into a 96 well plate. Samples were assayed utilizing immunoassay, according to the manufacturer's instructions (Luminex Assay, R&D Systems, Oakville, ON). All samples were assayed in technical duplicates. The following analytes were assessed using a Luminex Assay: Cystatin C, Galectin-1, Galectin-3, IL6, and Osteoprotegerin. Briefly, the analytes were captured using specific immunoglobulin-coated magnetic beads, while a biotin-conjugated antibody was added to provide analyte-specific quantitative readout, and a fluorophore-conjugated (PE) detection antibody was added to amplify the signal to detection range. Washes were conducted between additions to remove any unbound molecules. Finally, the beads were resuspended in wash buffer and analyzed using the MACSQuant Analyzer flow cytometer (Miltenyi Biotec, Germany). Events corresponding to beads were selected based on forward scatter (FSC) and side scatter (SSC). Specific single analyte bead populations were identified and selected using APC and PE-Vio770 filters (Classification Fluorescence). Each individual population was then assessed using the PE filter to determine the median fluorescence intensity (MFI) of the population. The MFI of the standards were plotted against the known concentration of the standards and a standard curve was constructed. Utilizing linear regression, concentrations were determined for each analyte.

Rat and human granulosa cells were fixed, permeabilized and stained for Ki67. Regarding macrophage polarization assessment, human follicular cells were fixed, permeabilized and stained for macrophage pan marker (CD68) and polarization markers (human M1: CD68+HLA-DR+ and M2: CD68+CD206+). Rat BMDMs were also fixed and stained for the macrophage polarization markers, M1: CD86+ and M2: CD163+. Flow cytometric acquisition was performed and analyzed as described previously (6).

Concentration of TNF-α was measured by a rat TNF-α ELISA kit (Abcam, ab100785) in 100 µl of CM-mimic and CM-inhibitor. All ELISA measurements were carried out according to the manufacturer's instructions. Optical densities (OD) were determined at 450 nm and compared to a standard curve, using a microtiter plate reader. The blank was subtracted from the triplicate readings for each standard and test sample.

Statistics

T-tests, and one-, two-, or three-way analyses of variance (ANOVA) were used to assess the effects of, and interactions between variables. This was followed by multiple comparison analysis with Tukey post hoc test, using Prism v.7 (GraphPad, San Diego, CA) and Sigma plot v.12 (Systat Software, San Jose, CA). $P < 0.05$ was considered statistically significant.

SPSS (v 25) was used to assess the sensitivity and specificity of FF galectin-1 and -3 content alone or in combination with anti-Müllerian hormone (AMH) in prediction of PCOS. Significant variables were entered into a forward logistic regression predicting PCOS status. Forward regression was used to preserve power with multiple predictors, avoid multicollinearity, and develop the most parsimonious model possible (29). Final models were then used to develop ROC curves comparing the final logisitc regressions models to PCOS status. ROC curves were compared

using Medcalc (v. 19.5.6). Outlier analysis was undertaken visually and through the use of standardized z scores, and normality was examined visually as well as through skew and kurtosis analysis (29). Multicollinearity was examined in all models.

Results

Macrophages uptake GC-derived exosomal miR379. To confirm whether macrophages take up GC-derived exosomes, GCs were co-cultured with macrophages using Transwell^{TM} dishes. To track GC-derived exosomes and miR379 in co-culture system, GCs were transfected with CD63 (exosome marker)-GFP (green) and Alexa-647 labelled miR379 (red) (Supplementary Figure S1). Tracking GC-derived exosomes and miR379 signals indicated that macrophages engulf GC-derived exosomal labeled miR379 (orange) (Figure 1A).

MiR379 polarizes macrophages to M1 by targeting PDK1. To determine if PDK1 is involved in macrophage polarization, M0 macrophages were polarized to M1 and M2 by culturing with LPS +IFNγ and IL4, respectively, and PDK1 content was assessed (Figure 1B). Our results indicate that IL-4-induced M2 had greater PDK1 content compared to LPS+IFN-γ-induced M1, implicating PDK1 in macrophage polarization. To further investigate the role of miR379 in macrophage polarization, BMDMs were pretreated with miR379 mimic and cellular PDK1 content was assessed. Pretreatment of BMDMs with miR379 mimic alone or in combination with IL-4-induced M2 reduced PDK1 to a similar level of LPS+IFN-γ-M1 (Figure 1B). MiR379 targets PDK1 and inhibits the AKT pathway, a signaling cascade which plays a significant role in M2 polarization. Therefore, to further investigate the role of miR379 in macrophage polarization, BMDMs (M0) and M2 macrophages were transfected with miR379 mimic or inhibitor and macrophage polarization was assessed. Our flow cytometry results showed that transfection of macrophages with miR379 mimic polarized M0 to M1 (as evidenced by an increase in CD86 positivity), whereas its inhibitor polarized M0 to M2 (as evidenced by an increase in CD163 staining), suggesting that miR379 induces M1 polarization, possibly through targeting PDK1 (Figure 1C).

MiR379 increases M1/M2 ratio in preantral follicle stage. To determine the role of miR379 in macrophage polarization *in vivo* and whether miR379 overexpression could have a synergic effect with androgens in androgenized rats, lentiviral miR379 mimic was introduced under the ovarian bursa and ovarian macrophage population and polarization were compared in the following treatments: lentivirus-RFP (control), lentivirus-RFP-miR379, DHT+lentivirus-RFP, DHT+lentivirus-RFP-miR379 (Supplementary Figure S2, Figure 1D). Our results indicated that ovarian miR379 overexpression reduced the M2 population in preantral, early antral and preovulatory follicles of control rats and increased M1 macrophages in preantral follicles of control and DHT rats. This resulted in an increased M1/M2 ratio in the preantral follicles of control rats only. On the other hand, androgen excess increased the M1 population in both antral and preovulatory follicles, but reduced the M2 population in all follicular stages. These results suggest that miR379 exerts its immune-modulatory effect mainly at the preantral follicle stage (Figure 1C).

MiR379-induced M1 polarization regulates GC proliferation, and aromatase content and is follicular stage-dependent. To determine if miR379-induced M1 polarization alters GC proliferation and aromatase content, and if this is follicular stage-dependent, conditioned media from BMDM transfected with miR379 mimic (CM-mimic), miR379 inhibitor (CM-inhibitor) or DHT were added to GC cultures of preantral and antral follicles (Figure 2A); and MCM2 (proliferation) and aromatase contents were assessed. CM-mimic increased aromatase protein content ($p<0.05$) without significantly affecting proliferation in preantral follicle GCs (Figure 2A), while it reduced aromatase levels and proliferation of GCs from antral follicles (Figure 2A). The aromatase and proliferative responses were not significantly influenced by the presence of the CM-inhibitor compared to control in both follicle stages. Taken together, these results suggest that miR379-induced M1 polarization suppresses GC proliferation and aromatase content specifically at the antral follicle stage.

MiR379-induced M1 polarization increases the levels of inflammatory cytokines in conditioned media. To investigate the role of cytokines in GC proliferation and aromatase content, CM-mimic and CM-inhibitor cytokines were first profiled by the Proteome Profiler Cytokine Array. Our results indicate that CM-mimic mainly contained inflammatory cytokines, including Cystatin C, galectin-1, galectin-3, TNFRS11B, PAI-1 and Osteopontin, compared to CM-inhibitor (Figure 2B). These are shared cytokines between CM-mimic and CM-inhibitor with > 3-fold changes in their signal intensity ratio. We further validated the Proteome Profiler Cytokine Array results by assessing TNF-α in CM-mimic and CM-inhibitor using an ELISA. Our results confirmed that TNF-α is a specific cytokine in CM-mimic (Supplementary Figure S3).

Increased M1/M2 ratio and inflammatory cytokines (galectin-1 and 3) indicate a pro-inflammatory condition in ovaries of PCOS subjects. Follicular macrophage population and polarization were assessed to examine their association with human antral follicle GCs from PCOS and non-PCOS subjects (Figure 3). PCOS subjects had a significantly lower M2 population ($p<0.01$), resulting in a higher M1/M2 ratio ($p<0.001$), compared to non-PCOS subjects (Figure 3A).

To further investigate if an increased M1/M2 ratio in PCOS subjects is associated with higher inflammatory cytokines in follicular fluid (FF), the concentration of galectin-1, galectin-3, Osteoprotegerin, IL6 and Cystatin C were compared between FF from PCOS and non-PCOS subjects. Our results indicated that FF content of galectin-1 and -3 were significantly higher in PCOS subjects compared to the non-PCOS subjects; however, there was no difference in other cytokines (Figure 3B, Supplementary Table 2).

Galectin-3 suppresses GC proliferation in antral, but not preantral follicles. To determine if reduced antral follicle GC

10.3389/fimmu.2023.1104550

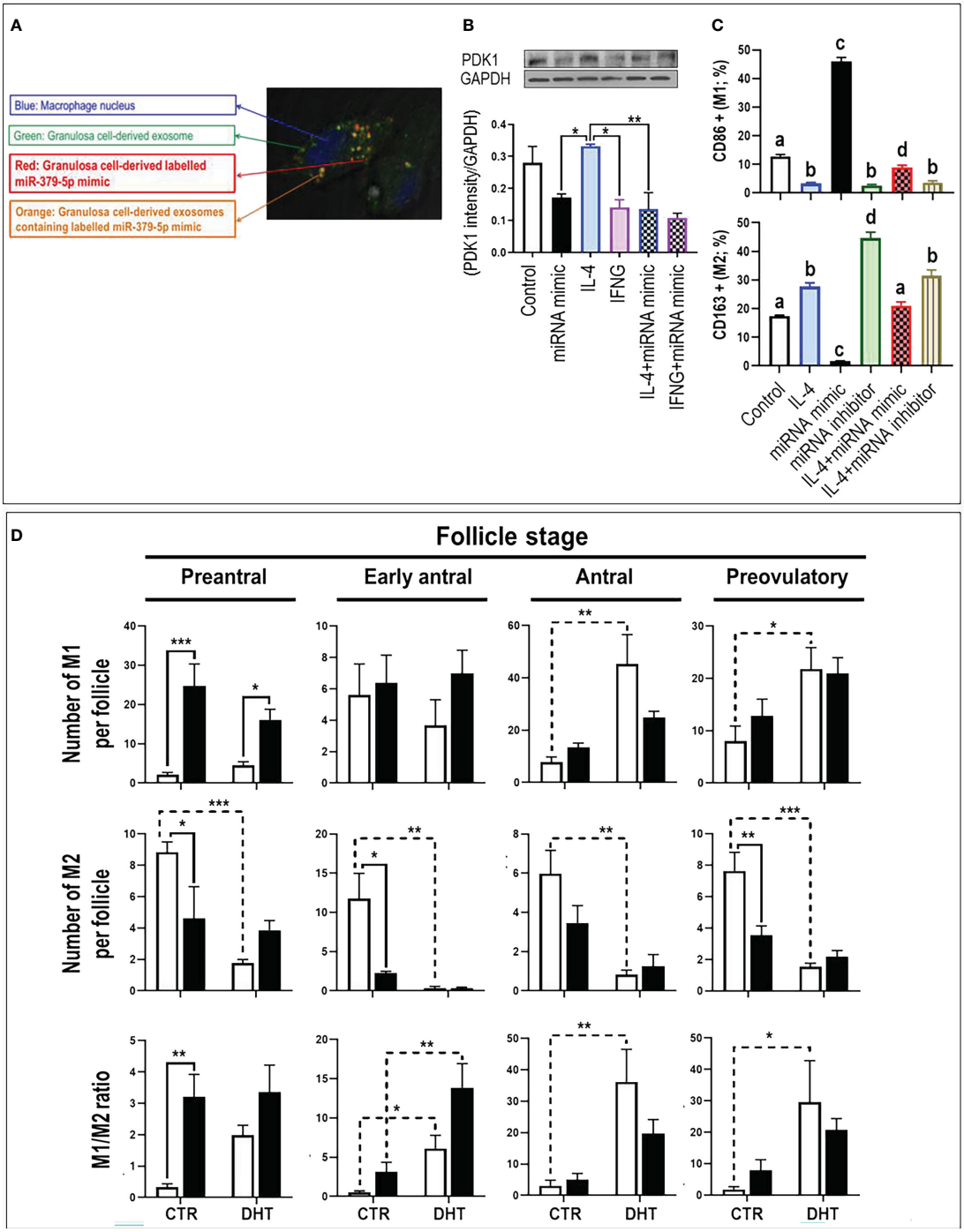

FIGURE 1
MiR-379-5p (miR379) increases M1/M2 ratio in preantral follicle stage by targeting PDK1. **(A)** Granulosa cells were transfected with CD63-GFP (green) and Alexa-647 labelled miR-379-5p (red), allowing the tracking of exosome and miR-379-5p in co-culture system. Tracking granulosa cell derived exosomes (green; GFP) and miR-379-5p (red; alexa-647) signals indicate that macrophages engulfs granulosa cell derived exosomes containing labeled miR-379-5p (orange). **(B)** IL4-induced M2 had greater PDK1 content compared to IFNγ-induced M1. Pre-treatment of bone marrow derived macrophages with miR379 mimic alone or in combination with IL4 reduced PDK1 to a similar level of IFNγ-M1. **(C)** miR379 polarizes macrophages towards M1. Transfection of macrophages with miR379 mimic polarized M0 to M1, a mechanism which was reversed by its inhibitor. **(D)** The ovarian miR379 overexpression increased M1 population in preantral follicles of both control and DHT rats. MiR379 overexpression significantly reduced M2 population in preantral, early antral and preovulatory follicles, increasing the M1/M2 ratio in control preantral follicles. Androgen excess increased M1 population in antral and preovulatory follicles, but reduced M2 population in all stages. The ratio of M1/M2 increased in early antral, antral and preovulatory follicles in response to androgen; Results are expressed as mean±SEM (n=3 replicates each with 2 rats/group). Data were analyzed by one-way ANOVA & tukey post hoc. *P<0.05; **P<0.01; ***P<0.001; **(C)** Different letters indicate significant differences between groups (P<0.05). To produce bone marrow derived macrophage, bone marrow cells were isolated from rat femur and tibia and differentiated to macrophages with M-CSF for 7 days in vitro. Granulosa cells were isolated from preantral follicles (diethylstilbestrol-primed immature rats; day 21, 1 mg/d, subcutaneously, for 3 consecutive days) and transfected with miR-379-5p mimic (mirVana mimics, MC10316, Thermo-Fisher; 18h) and were further cultured for 36h. Macrophages were polarized to M1 and M2 by LPS (10 pg/mL) + IFN-γ (20 ng/mL) and IL-4 (20ng/mL) treatment for 36h, respectively.

10.3389/fimmu.2023.1104550

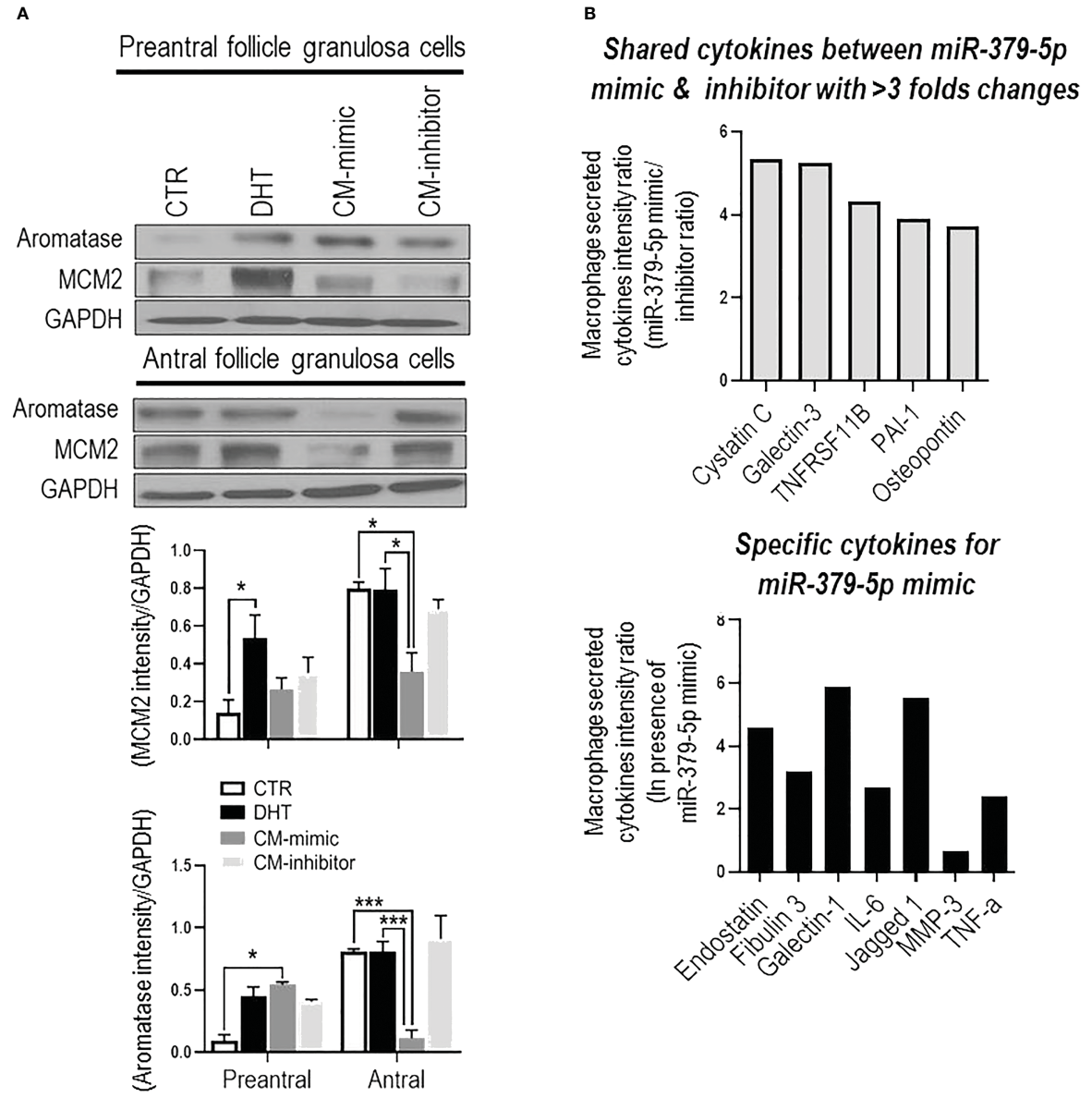

FIGURE 2
MiR-379-5p-induced M1 polarization regulates granulosa cell proliferation in a follicular stage-specific manner by increasing pro-inflammatory cytokine level. **(A)** Conditioned media from macrophages transfected by miR379 mimic (CM-mimic) increases aromatase content without affecting proliferation in preantral follicle GC, while it reduces aromatase and proliferation in that of antral follicles. The aromatase and proliferative responses were not significantly influenced by the presence of the CM-inhibitor compared to control in both follicle stages; **(B)** Profile of cytokines (Proteome Profiler Rat XL Cytokine Array; R&D Systems) in macrophage condition medium indicates that CM-mimic had higher content of inflammatory cytokines, including Cystatin C (5.4 fold), Galectin-3 (5.3 fold), TNFRS11B (4.3 fold), PAI-1 (3.9 fold) and Osteopontin (3.7 fold). In addition, Endostatin, Fibulin 3, TNF-α, Galectin-1, IL-6, Jagged 1 and MMP3 were specific cytokines to CM-mimic. Results are expressed as mean±SEM (n=3 replicates each with 2 rats/group). Data were analyzed by two-way ANOVA and tukey post hoc. *P<0.05, ***P<0.001.

proliferation in response to CM-mimic is as a result of galectin-1 or galectin-3 action; and whether this response is follicular stage-dependent, rat preantral and antral GC were cultured with galectin-1 (0, 0.6, 6 and 60 ng/mL) and galectin-3 (0, 0.03, 0.3 and 3 ng/mL), and their proliferation were assessed based on the changes in Ki67-positive cells (flow cytometry). The concentrations of galectin-1 and galectin-3 for *in vitro* studies were selected based on their average FF concentration in human PCOS subjects; i.e. 6 and 0.3 ng/mL, respectively. Our results demonstrated that while galectin-1 did not affect GC proliferation in both preantral and antral follicles, galectin-3 significantly reduced GC proliferation in antral, but not preantral follicles (Figure 3C).

Our previous studies indicate that antral follicle GC from PCOS subjects exhibit lower proliferation compared to those of non-PCOS (17). Here, to further investigate if reduced antral follicle GC in human PCOS subjects could be a result of higher galectin-3, non-

10.3389/fimmu.2023.1104550

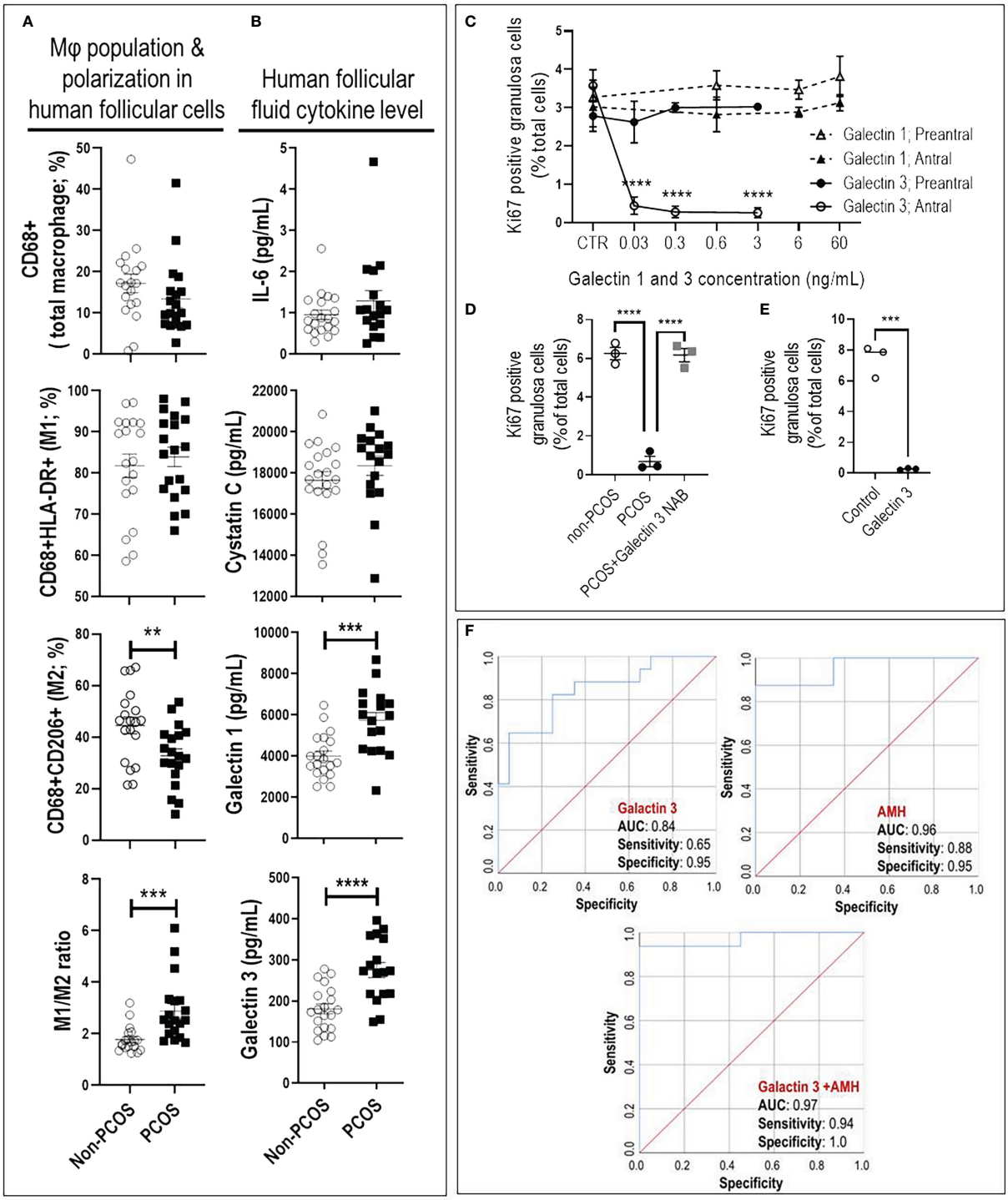

FIGURE 3
Increased M1/M2 ratio and galectin-3 suppresses granulosa cell proliferation in antral, but not preantral follicle stage, as evident in PCOS. **(A)** PCOS subjects had lower M2 population and higher M1/M2 ratio compared to non-PCOS; **(B)** PCOS subjects had higher FF content of galectin-1 and -3 compared to non-PCOS; **(C)** Galectin-1 did not affect rat GC proliferation in preantral and antral follicles, galectin-3 significantly reduced GC proliferation in antral but not preantral follicles; **(D)** Adding PCOS FF to non-PCOS GCs significantly reduced cell proliferation compared to those treated with non-PCOS FF. However, the effect of PCOS FF on GC proliferation was blocked using galectin-3 neutralizing antibody; **(E)** Adding human recombinant galectin-3 to non-PCOS GCs significantly suppress proliferation; **(F)** The combination of galectin-3 and Anti-Müllerian hormone (AMH) improve sensitivity and specificity of PCOS prediction compared to AMH. AMH: AUC=0.96 with sensitivity=0.88 and specificity=0.95 ($p<0.0001$); Galectin-3: AUC=0.84 with sensitivity=0.65 and specificity=0.95 ($p<0.001$); Galectin-3+AMH: AUC=0.977 with sensitivity=0.94 and specificity=1 ($p<0.0001$). Results are expressed as mean±SEM (n=3 replicates each with 2 rats/group). Data were analyzed by two-way ANOVA and tukey post hoc. $^{**}P<0.01$, $^{***}P<0.001$, $^{****}P<0.0001$.

PCOS GCs (Supplementary Table 3) were treated with FF of non-PCOS and PCOS subjects (1:10 dilution) and cell proliferation was assessed by Ki67 staining. Treatment of GC with PCOS FF significantly suppressed proliferation compared to that of non-PCOS, a response reversible by neutralization of galectin-3 in PCOS FF (Figure 3D). To demonstrate if human GC proliferation could be down-regulated by galectin-3, antral follicles GCs from non-PCOS subjects were treated with recombinant galectin-3 protein. Flow cytometry results indicate that galectin-3 significantly reduced antral follicle GC proliferation, as evident by a marked decrease in Ki67-positive cells (Figure 3E).

The combination of galectin-3 and AMH improves sensitivity and specificity of PCOS prediction. To determine if galectin-1 and galectin-3 can be used as predictors for PCOS, we first compared potential predictors using univariate analysis between PCOS and non-PCOS subjects, including Age, BMI, LH, Trigger E2, AMH, galectin-1, galectin-3, Cystatin C, Osteoprotegerin and IL6. Our results indicated that AMH, galectin-1 and galectin-3 were significantly increased in PCOS compared to non-PCOS subjects; therefore, they could play as potential predictors for PCOS status (Figure 3B, Supplementary Table 2). To identify the most precise explanatory model, AMH, galectin-1 and galectin-3 were entered into a forward entry binary logistic regression model. In the final model, AMH was identified (P= 0.04) as the only predictor for PCOS status, explaining 65% of the variance in PCOS diagnosis. There was a significant correlation found between AMH and both galectin-1 (R=0.33; P=0.04) and galectin-3 levels (R=0.48; P=0.003), indicating that AMH may mitigate the importance of galectin-1 and galectin-3 as a predictor of PCOS. To further explore the predictive power of galectin-1 and galectin-3, AMH was excluded from the model, and galectin-1 and -3 were retained. In this model, galectin-3 remained in model (P=0.003) and explained 36% of the variance in PCOS diagnosis. As the final step, to investigate the test performance of galectin-3 vs AMH (Figure 3F), three ROC curves were constructed: AMH, galectin-3, and galectin-3+AMH. The AMH model was significant ($P < 0.0001$), with an area under the curve (AUC) of 0.96, and it also outperformed the galectin-3 only model ($P < 0.001$, AUC=0.84). Although the combination of galectin-3+AMH did not change the AUC (0.97), it improved the model sensitivity and specificity, 0.94 and 1.00, respectively (Figure 3F).

Discussion

Exosomes play important roles in intercellular communication by serving as vehicles for transferring cellular constituents such as proteins, lipids and nucleic acids. However, very little is known about the role of exosome release in determining the cellular miRNA content and function in exosome-receiving cells. We have recently found that exosome release serves as a proliferative mechanism to regulate the cellular miR-379-5p (miR379) content in preantral follicle development in response to androgen stimulation (17). More specifically, androgen induces exosomal miR379 release in GC from preantral, but not antral follicles. Reduced preantral follicle GC miR379 content increases PDK1 content and enhances their proliferation (17). In this study, we have demonstrated that uptake of GC-derived exosomes containing miR379 by macrophages inhibits PDK1 and shifts macrophage polarization to M1. Similarly, deletion of PTEN increased the levels of Arg1 and M2 polarization, indicating a major role of the AKT pathway in anti-inflammatory macrophage polarization (18, 19). Moreover, inhibition of AKT phosphorylation through knockdown of PDK1 increased M1 polarization and increased the susceptibility of mice to endotoxin shock (20). These results suggest that the regulation of PDK1-AKT signaling is a central node for controlling M2 polarization and increased macrophage miR379 content through uptake of GC-derived exosomal miR379 inhibits PDK1-mediated M2 polarization.

Macrophage polarization is very important in GC proliferation, ovarian follicular development and ovulation (6). Studies with androgenized rats and human PCOS subjects have demonstrated that androgen suppresses ovarian M2 polarization and significantly increases the M1/M2 ratio in antral follicles (6). Similarly, in this study androgen significantly increased the M1/M2 ratio in early antral, antral and preovulatory follicles. On the other hand, ovarian overexpression of miR379 inhibited M2, increased M1 and the M1/M2 ratio in preantral follicles sepcifically. These results support our previous findings where androgen induced specific exosome packaging and release of miR379 from preantral follicle GCs; as well as promoting uptake of miR379 enriched exosomes. This suppressed androgen-induced proliferation by increasing miR379 cellular content in preantral follicle GCs (17). These results suggest that uptake of GC derived miR379 enriched exosomes inhibits PDK1 in macrophages; a process that polarizes them to M1.

Galectins are a family of evolutionarily conserved carbohydrate-binding proteins (30, 31) involved in cell activation, differentiation, proliferation, migration and apoptosis (32–35). Culture media from macrophages treated with miR379 mimic and FF from PCOS subjects exhibited a significantly higher galectin-1 and galectin-3 content. Further investigation on the influence of galectins on GC proliferation indicates that galectin-3, but not galectin-1, suppressed antral follicle GC proliferation. This response appeared to be follicle stage specific as no significant reduction in preantral follicle GC proliferation was observed under the same conditions. Histological assessment of ovarian sections demonstrates that macrophages and apoptotic GCs are the main source of galectin-3 (36–38). Galectin-3 is pro-inflammatory cytokine and deletion of galectin-3 in mice reduced inflammation, number of macrophages and IL1β production (39). Galectin-3 has both anti- and pro-apoptotic effects (40). Studies on human thymocytes and T cells demonstrate that, in contrast to the anti-apoptotic function of intracellular galectin-3, extracellular galectin-3 directly induces apoptosis in human thymocytes and T cells through CD71 (40). Therefore, our results demonstrate, for first time, that macrophage-derived galectin-3 suppresses GC proliferation in follicle stage-dependent manner. Further studies are required to determine the precise cellular mechanisms involved.

AMH is produced by GCs from follicles that are < 8 mm (41, 42) and regulates early follicular recruitment (43). PCOS subjects have a higher serum concentration of AMH (44, 45) and AMH correlates with oligoamenorrhea and hyperandrogenism (46–50), AMH has been proposed as a biomarker for PCOS (51). Serum level of galectin-3 is significantly higher in PCOS subjects (52, 53), is associated with insulin resistance (52, 54) and has been proposed as a biomarker for detecting prediabetes, diabetes (55) and inflammation (56). In the present study we found that FF from PCOS subjects had higher galectin-3 content and in combination with AMH improves the sensitivity and specificity of PCOS prediction compared to AMH alone. However, further studies are needed to determine how galectin-3 regulates follicular growth and ovarian function.

In conclusion, our findings suggest that miR379 inhibits M2 macrophage polarization, increases the M1/M2 ratio, as well as macrophage secretion of galectin-3. These responses inhibit GC proliferation in antral, but not preantral follicles. This phenomenon is likely initiated through the release of granulosa cell-derived exosomal miR379 in a follicular-stage dependent manner. Therefore, we propose a hypothetical model to facilitate future investigation into the role of GC-derived exosomal miR379 in the androgenic control of macrophage polarization and subsequently GC proliferation (Figure 4). Androgen induces GC exosomal miR379 release from preantral but not antral follicles. The uptake of GC derived exosomal miR379 suppresses PDK1 in macrophages, shifting them to M1. M1 macrophage secretes higher levels of galectin-3 in FF; an inflammatory cytokine that specifically suppresses GC proliferation in antral, but not preantral follicles (Figure 4). In this study, we demonstrated that androgen-induced miR379 regulates GC proliferation by macrophage-derived galectin-3 in a follicle stage-dependent manner. However, further studies are required to determine 1) how galectin-3 regulates follicular growth and ovarian function; 2) if, and how, obesity alters galectin-3 in PCOS subjects; and 3) whether and how metformin could reduce the galectin-3 levels in PCOS subjects.

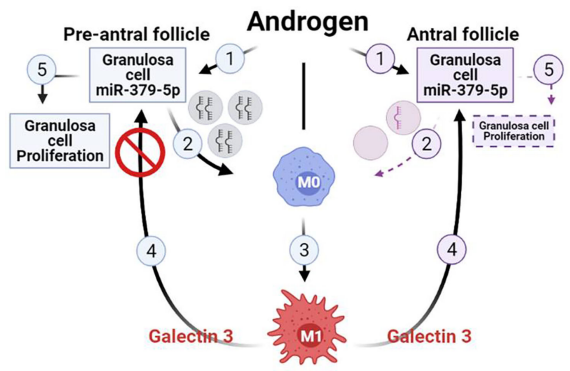

FIGURE 4
Hypothetical model illustrating that uptake of GC-derived exosomal miR-379-5p by macrophages increases M1 and macrophage release of galectin-3, a response which inhibits GC proliferation in antral but not preantral follicles. Androgen induces GC exosomal miR379 release from preantral but not antral follicles. The uptake of GC-derived exosomal miR379 suppresses PDK1 in macrophages, a cellular mechanism shifting macrophage polarization towards M1. M1 macrophage secretes higher level of galectin-3 in FF, a inflammatory cytokine that specifically suppressed GC proliferation in antral but not preantral follicles. (Created in BioRender.com).

Data availability statement

The raw data supporting the conclusions of this article will be made available by the authors, without undue reservation.

Ethics statement

All human FF and granulosa cell specimens were obtained from the CReATe Biobank, CReATe Fertility Centre with written informed consent. The CReATe Biobank [banking protocols approved by Veritas IRB (Approval#16518), collects biological materials from consenting patients, according to the best practice-based standards of biobanking. All samples from the Biobank were approved for use in this study by the Veritas IRB (Approval#16487) and The Ottawa Hospital REB (Protocol #20170453-01H)]. The patients/participants provided their written informed consent to participate in this study. All animal procedures were carried out in accordance with the Guidelines for the Care and Use of Laboratory Animals, Canadian Council on Animal Care, and were approved by the University of Ottawa Animal Care Committee.

Author contributions

RS and BT designed the experiments. RS, AA, BW, MA-W, BP and AG performed the experiments. PS, SJ and CL provided human samples. KB, DB, BV, JL contributed analytic tools. RS analyzed experimental data. RS prepared the manuscript with input from BT, BV, DB, KB, JL, and CL. All authors contributed to the article and approved the submitted version. BT and CL provided financial support for the project.

Funding

This work was supported by grant MOP-119381 from the Canadian Institutes of Health Research (to BKT); postdoctoral fellowships from the Lalor Foundation, Mathematics of Information Technology and Complex Systems (Mitacs, FR35174; to RS) and CReATe Fertility Centre's funding contribution to MITACS fellowship (to RS). MA-W received research fellowship support from MITACS (globalink award), Ovarian Cancer Canada (OCC) and Taggart-Parkes Foundation.

Conflict of interest

The authors declare that the research was conducted in the absence of any commercial or financial relationships that could be construed as a potential conflict of interest.

Publisher's note

All claims expressed in this article are solely those of the authors and do not necessarily represent those of their affiliated organizations, or those of the publisher, the editors and the reviewers. Any product that may be evaluated in this article, or claim that may be made by its manufacturer, is not guaranteed or endorsed by the publisher.

Supplementary material

The Supplementary Material for this article can be found online at: https://www.frontiersin.org/articles/10.3389/fimmu.2023.1104550/full#supplementary-material

References

1. Dunaif A. Insulin resistance and the polycystic ovary syndrome: mechanism and implications for pathogenesis. *Endocr Rev* (1997) 18(6):774–800. doi: 10.1210/edrv.18.6.0318

2. Xiong YL, Liang XY, Yang X, Li Y, Wei LN. Low-grade chronic inflammation in the peripheral blood and ovaries of women with polycystic ovarian syndrome. *Eur J obstetr gynecol Reprod Biol* (2011) 159(1):148–50. doi: 10.1016/j.ejogrb.2011.07.012

3. Amato G, Conte M, Mazziotti G, Lalli E, Vitolo G, Tucker AT, et al. Serum and follicular fluid cytokines in polycystic ovary syndrome during stimulated cycles. *Obstetr gynecol* (2003) 101(6):1177–82. doi: 10.1016/s0029-7844(03)00233-3

4. Kelly CC, Lyall H, Petrie JR, Gould GW, Connell JM, Sattar N. Low grade chronic inflammation in women with polycystic ovarian syndrome. *J Clin Endocrinol Metab* (2001) 86(6):2453–5. doi: 10.1210/jcem.86.6.7580

5. Diamanti-Kandarakis E, Paterakis T, Alexandraki K, Piperi C, Aessopos A, Katsikis I, et al. Indices of low-grade chronic inflammation in polycystic ovary syndrome and the beneficial effect of metformin. *Hum Reproduction* (2006) 21 (6):1426–31. doi: 10.1093/humrep/del003

6. Lima PDA, Nivet AL, Wang Q, Chen YA, Leader A, Cheung A, et al. Polycystic ovary syndrome: possible involvement of androgen-induced, chemerin-mediated ovarian recruitment of monocytes/macrophages. *Biol reproduction* (2018) 99(4):838–52. doi: 10.1093/biolre/ioy096

7. Graff JW, Dickson AM, Clay G, McCaffrey AP, Wilson ME. Identifying functional microRNAs in macrophages with polarized phenotypes. *J Biol Chem* (2012) 287(26):21816–25. doi: 10.1074/jbc.M111.327031

8. Curtale G, Rubino M, Locati M. MicroRNAs as molecular switches in macrophage activation. *Front Immunol* (2019) 10:799. doi: 10.3389/fimmu.2019.00799

9. Essandoh K, Li Y, Huo J, Fan GC. MiRNA-mediated macrophage polarization and its potential role in the regulation of inflammatory response. *Shock* (2016) 46 (2):122–31. doi: 10.1097/SHK.0000000000000604

10. Burns GW, Brooks KE, Spencer TE. Extracellular vesicles originate from the conceptus and uterus during early pregnancy in sheep. *Biol Reproduction* (2016) 94 (3):56. doi: 10.1095/biolreprod.115.134973

11. O'Neil EV, Burns GW, Ferreira CR, Spencer TE. Characterization and regulation of extracellular vesicles in the lumen of the ovine uterusdagger. *Biol reproduction* (2020) 102(5):1020–32. doi: 10.1093/biolre/ioaa019

12. O'Neil EV, Burns GW, Spencer TE. Extracellular vesicles: Novel regulators of conceptus-uterine interactions? *Theriogenology* (2020) 150:106–12. doi: 10.1016/j.theriogenology.2020.01.083

13. Navakanitworakul R, Hung WT, Gunewardena S, Davis JS, Chotigeat W, Christenson LK. Characterization and small RNA content of extracellular vesicles in follicular fluid of developing bovine antral follicles. *Sci Rep* (2016) 6:25486. doi: 10.1038/srep25486

14. Hu J, Tang T, Zeng Z, Wu J, Tan X, Yan J. The expression of small RNAs in exosomes of follicular fluid altered in human polycystic ovarian syndrome. *PeerJ* (2020) 8:e8640. doi: 10.7717/peerj.8640

15. Hossain MM, Cao M, Wang Q, Kim JY, Schellander K, Tesfaye D, et al. Altered expression of miRNAs in a dihydrotestosterone-induced rat PCOS model. *J Ovarian Res* (2013) 6(1):36. doi: 10.1186/1757-2215-6-36

16. Han Z, He H, Zhang F, Huang Z, Liu Z, Jiang H, et al. Spatiotemporal expression pattern of mirg, an imprinted non-coding gene, during mouse embryogenesis. *J Mol histol* (2012) 43(1):1–8. doi: 10.1007/s10735-011-9367-x

17. Salehi R, Wyse BA, Abedini A, Pan B, Hasegawa T, Xue Y, et al. Androgen-induced exosomal miR-379-5p release determines granulosa cell fate: The cellular mechanism of anovulatory polycystic ovaries. *Pre-print (Research Square)* (2020). doi: 10.21203/rs.3.rs-2599745/v1

18. Sahin E, Haubenwallner S, Kuttke M, Kollmann I, Halfmann A, Dohnal AM, et al. Macrophage PTEN regulates expression and secretion of arginase I modulating innate and adaptive immune responses. *J Immunol* (2014) 193(4):1717–27. doi: 10.4049/jimmunol.1302167

19. Kral JB, Kuttke M, Schrottmaier WC, Birnecker B, Warszawska J, Wernig C, et al. Sustained PI3K activation exacerbates BLM-induced lung fibrosis *via* activation of pro-inflammatory and pro-fibrotic pathways. *Sci Rep* (2016) 6:23034. doi: 10.1038/srep23034

20. Chaurasia B, Mauer J, Koch L, Goldau J, Kock AS, Bruning JC. Phosphoinositide-dependent kinase 1 provides negative feedback inhibition to toll-like receptor-mediated NF-kappaB activation in macrophages. *Mol Cell Biol* (2010) 30 (17):4354–66. doi: 10.1128/MCB.00069-10

21. Wang Q, Kim JY, Xue K, Liu JY, Leader A, Tsang BK. Chemerin, a novel regulator of follicular steroidogenesis and its potential involvement in polycystic ovarian syndrome. *Endocrinology* (2012) 153(11):5600–11. doi: 10.1210/en.2012-1424

22. Vinas JL, Burger D, Zimpelmann J, Haneef R, Knoll W, Campbell P, et al. Transfer of microRNA-486-5p from human endothelial colony forming cell-derived exosomes reduces ischemic kidney injury. *Kidney Int* (2016) 90(6):1238–50. doi: 10.1016/j.kint.2016.07.015

23. Kim JY, Xue K, Cao M, Wang Q, Liu JY, Leader A, et al. Chemerin suppresses ovarian follicular development and its potential involvement in follicular arrest in rats treated chronically with dihydrotestosterone. *Endocrinology* (2013) 154(8):2912–23. doi: 10.1210/en.2013-1001

24. Pan B, Toms D, Shen W, Li J. MicroRNA-378 regulates oocyte maturation *via* the suppression of aromatase in porcine cumulus cells. *Am J Physiol Endocrinol Metab* (2015) 308(6):E525–34. doi: 10.1152/ajpendo.00480.2014

25. Sun XF, Li YP, Pan B, Wang YF, Li J, Shen W. Molecular regulation of miR-378 on the development of mouse follicle and the maturation of oocyte in vivo. *Cell Cycle* (2018) 17(18):2230–42. doi: 10.1080/15384101.2018.1520557

26. Campbell LD, Betsou F, Garcia DL, Giri JG, Pitt KE, Pugh RS, et al. Development of the ISBER best practices for repositories: Collection, storage, retrieval and distribution of biological materials for research. *Biopreservation biobanking* (2012) 10(2):232–3. doi: 10.1089/bio.2012.1025

27. Fuchs Weizman N, Wyse BA, Szaraz P, Defer M, Jahangiri S, Librach CL. Cannabis alters epigenetic integrity and endocannabinoid signalling in the human follicular niche. *Hum Reprod (Oxford England)* (2021) 36(7):1922–31. doi: 10.1093/humrep/deab104

28. Kenigsberg S, Wyse BA, Librach CL, da Silveira JC. Protocol for exosome isolation from small volume of ovarian follicular fluid: Evaluation of ultracentrifugation and commercial kits. *Methods Mol Biol (Clifton NJ)* (2017) 1660:321–41. doi: 10.1007/978-1-4939-7253-1_26

29. Cookingham LM, Goossen RP, Sparks AET, Van Voorhis BJ, Duran EH. Successful treatment algorithm for evaluation of early pregnancy after *in vitro* fertilization. *Fertil steril* (2015) 104(4):932–7 e1. doi: 10.1016/j.fertnstert.2015.07.1133

30. Kasai K, Hirabayashi J. Galectins: a family of animal lectins that decipher glycocodes. *J Biochem* (1996) 119(1):1–8. doi: 10.1093/oxfordjournals.jbchem.a021192

31. Barondes SH, Castronovo V, Cooper DN, Cummings RD, Drickamer K, Feizi T, et al. Galectins: a family of animal beta-galactoside-binding lectins. *Cell* (1994) 76 (4):597–8. doi: 10.1016/0092-8674(94)90498-7

32. Perillo NL, Pace KE, Seilhamer JJ, Baum LG. Apoptosis of T cells mediated by galectin-1. *Nature* (1995) 378(6558):736–9. doi: 10.1038/378736a0

33. Yang RY, Hsu DK, Liu FT. Expression of galectin-3 modulates T-cell growth and apoptosis. *Proc Natl Acad Sci USA* (1996) 93(13):6737–42. doi: 10.1073/pnas.93.13.6737

34. Perillo NL, Marcus ME, Baum LG. Galectins: versatile modulators of cell adhesion, cell proliferation, and cell death. *J Mol Med* (1998) 76(6):402–12. doi: 10.1007/s001090050232

35. Goldring K, Jones GE, Thiagarajah R, Watt DJ. The effect of galectin-1 on the differentiation of fibroblasts and myoblasts in vitro. *J Cell sci* (2002) 115(Pt 2):355–66. doi: 10.1242/jcs.115.2.355

36. Devouassoux-Shisheboran M, Deschildre C, Mauduit C, Berger G, Mejean-Lebreton F, Bouvier R, et al. Expression of galectin-3 in gonads and gonadal sex cord stromal and germ cell tumors. *Oncol Rep* (2006) 16(2):335–40. doi: 10.3892/or.16.2.335

37. Heo SD, Park C, Kim J, Ahn M, Shin T. Unilaminar follicular cells transiently express galectin-3 during ovarian folliculogenesis in pigs. *Tissue Cell* (2017) 49(1):106–11. doi: 10.1016/j.tice.2016.11.003

38. Lohr M, Kaltner H, Lensch M, Andre S, Sinowatz F, Gabius HJ. Cell-type-specific expression of murine multifunctional galectin-3 and its association with follicular atresia/luteolysis in contrast to pro-apoptotic galectins-1 and -7. *Histochem Cell Biol* (2008) 130(3):567–81. doi: 10.1007/s00418-008-0465-0

39. Simovic Markovic B, Nikolic A, Gazdic M, Bojic S, Vucicevic L, Kosic M, et al. Galectin-3 plays an important pro-inflammatory role in the induction phase of acute colitis by promoting activation of NLRP3 inflammasome and production of IL-1beta in macrophages. *J Crohn's colitis* (2016) 10(5):593–606. doi: 10.1093/ecco-jcc/jjw013

40. Stillman BN, Hsu DK, Pang M, Brewer CF, Johnson P, Liu FT, et al. Galectin-3 and galectin-1 bind distinct cell surface glycoprotein receptors to induce T cell death. *J Immunol* (2006) 176(2):778–89. doi: 10.4049/jimmunol.176.2.778

41. Jeppesen JV, Anderson RA, Kelsey TW, Christiansen SL, Kristensen SG, Jayaprakasan K, et al. Which follicles make the most anti-mullerian hormone in humans? evidence for an abrupt decline in AMH production at the time of follicle selection. *Mol Hum reproduction* (2013) 19(8):519–27. doi: 10.1093/molehr/gat024

42. Weenen C, Laven JS, Von Bergh AR, Cranfield M, Groome NP, Visser JA, et al. Anti-mullerian hormone expression pattern in the human ovary: potential implications for initial and cyclic follicle recruitment. *Mol Hum reproduction* (2004) 10(2):77–83. doi: 10.1093/molehr/gah015

43. Knight PG, Glister C. TGF-beta superfamily members and ovarian follicle development. *Reproduction* (2006) 132(2):191–206. doi: 10.1530/rep.1.01074

44. Li L, Chen X, Mo Y, Chen Y, Wenig M, Yang D. Elevated serum anti-mullerian hormone in adolescent and young adult Chinese patients with polycystic ovary syndrome. *Wiener klinische Wochenschrift* (2010) 122(17-18):519–24. doi: 10.1007/s00508-010-1426-x

45. Pigny P, Merlen E, Robert Y, Cortet-Rudelli C, Decanter C, Jonard S, et al. Elevated serum level of anti-mullerian hormone in patients with polycystic ovary syndrome: relationship to the ovarian follicle excess and to the follicular arrest. *J Clin Endocrinol Metab* (2003) 88(12):5957–62. doi: 10.1210/jc.2003-030727

46. Nardo LG, Yates AP, Roberts SA, Pemberton P, Laing I. The relationships between AMH, androgens, insulin resistance and basal ovarian follicular status in non-obese subfertile women with and without polycystic ovary syndrome. *Hum reproduction* (2009) 24(11):2917–23. doi: 10.1093/humrep/dep225

47. Eldar-Geva T, Margalioth EJ, Gal M, Ben-Chetrit A, Algur N, Zylber-Haran E, et al. Serum anti-mullerian hormone levels during controlled ovarian hyperstimulation in women with polycystic ovaries with and without hyperandrogenism. *Hum reproduction* (2005) 20(7):1814–9. doi: 10.1093/humrep/deh873

48. Piltonen T, Morin-Papunen L, Koivunen R, Perheentupa A, Ruokonen A, Tapanainen JS. Serum anti-mullerian hormone levels remain high until late reproductive age and decrease during metformin therapy in women with polycystic ovary syndrome. *Hum reproduction* (2005) 20(7):1820–6. doi: 10.1093/humrep/deh850

49. van Rooij IA, Broekmans FJ, te Velde ER, Fauser BC, Bancsi LF, de Jong FH, et al. Serum anti-mullerian hormone levels: a novel measure of ovarian reserve. *Hum reproduction* (2002) 17(12):3065–71. doi: 10.1093/humrep/17.12.3065

50. Laven JS, Mulders AG, Visser JA, Themmen AP, De Jong FH, Fauser BC. Anti-mullerian hormone serum concentrations in normoovulatory and anovulatory women of reproductive age. *J Clin Endocrinol Metab* (2004) 89(1):318–23. doi: 10.1210/jc.2003-030932

51. Iliodromiti S, Kelsey TW, Anderson RA, Nelson SM. Can anti-mullerian hormone predict the diagnosis of polycystic ovary syndrome? a systematic review and meta-analysis of extracted data. *J Clin Endocrinol Metab* (2013) 98(8):3332–40. doi: 10.1210/jc.2013-1393

52. Yilmaz H, Celik HT, Ozdemir O, Kalkan D, Namuslu M, Abusoglu S, et al. Serum galectin-3 levels in women with PCOS. *J endocrinol Invest* (2014) 37(2):181–7. doi: 10.1007/s40618-013-0032-y

53. Anik Ilhan G, Kanlioglu C, Arslan G, Yildizhan B, Pekin T. Galectin-3 as a novel biomarker in women with PCOS. *Arch gynecol obstetr* (2018) 298(4):821–5. doi: 10.1007/s00404-018-4862-x

54. Alves MT, de Souza IDP, Ferreira CN, Candido AL, Bizzi MF, Oliveira FR, et al. Galectin-3 is a potential biomarker to insulin resistance and obesity in women with polycystic ovary syndrome. *Gynecol Endocrinol* (2020) 36(9):760–3. doi: 10.1080/09513590.2020.1739267

55. Yilmaz H, Cakmak M, Inan O, Darcin T, Akcay A. Increased levels of galectin-3 were associated with prediabetes and diabetes: new risk factor? *J Endocrinol Invest* (2015) 38(5):527–33. doi: 10.1007/s40618-014-0222-2

56. Pang J, Nguyen VT, Rhodes DH, Sullivan ME, Braunschweig C, Fantuzzi G. Relationship of galectin-3 with obesity, IL-6, and CRP in women. *J Endocrinol Invest* (2016) 39(12):1435–43. doi: 10.1007/s40618-016-0515-8

frontiers | Frontiers in Immunology

TYPE Original Research
PUBLISHED 20 June 2023
DOI 10.3389/fimmu.2023.1098602

OPEN ACCESS

EDITED BY
Yujing Zhang,
Nanjing University, China

REVIEWED BY
Ya-fei Qin,
Tianjin Medical University General Hospital, China
Yongbo Huang,
Guangzhou Medical University, China

*CORRESPONDENCE
Rongli Lu
lurongli@csu.edu.cn
Pinhua Pan
pinhuapan668@csu.edu.cn

RECEIVED 15 November 2022
ACCEPTED 24 May 2023
PUBLISHED 20 June 2023

CITATION
Zhou A, Tang H, Peng W, Wang Y, Tang X, Yang H, Lu R and Pan P (2023) KL-6 levels in the connective tissue disease population: typical values and potential confounders–a retrospective, real-world study. *Front. Immunol.* 14:1098602. doi: 10.3389/fimmu.2023.1098602

KL-6 levels in the connective tissue disease population: typical values and potential confounders–a retrospective, real-world study

Aiyuan Zhou[1,2,3,4,5], Haiyun Tang[6], Wenzhong Peng[1,2,3,4,5], Yanan Wang[1,2,3,4,5], Xiaoping Tang[1,2,3,4,5], Hang Yang[1,2,3,4,5], Rongli Lu[1,2,3,4,5]* and Pinhua Pan[1,2,3,4,5]*

[1]Department of Respiratory Medicine, National Key Clinical Specialty, Branch of National Clinical Research Center for Respiratory Disease, Xiangya Hospital, Central South University, Changsha, Hunan, China, [2]Center of Respiratory Medicine, Xiangya Hospital, Central South University, Changsha, Hunan, China, [3]Department of Respiratory Medicine, Clinical Research Center for Respiratory Diseases in Hunan Province, Changsha, Hunan, China, [4]Department of Respiratory Medicine, Hunan Engineering Research Center for Intelligent Diagnosis and Treatment of Respiratory Disease, Changsha, Hunan, China, [5]National Clinical Research Center for Geriatric Disorders, Xiangya Hospital, Changsha, Hunan, China, [6]Department of Radiology, Xiangya Hospital, Central South University, Changsha, Hunan, China

Background: Krebs von den Lungen 6 (KL-6) is a potential biomarker for determining the severity of interstitial lung disease (ILD) in patients with connective tissue disease (CTD). Whether KL-6 levels can be affected by potential confounders such as underlying CTD patterns, patient-associated demographics, and comorbidities needs further investigation.

Methods: From the database created by Xiangya Hospital, 524 patients with CTD, with or without ILD, were recruited for this retrospective analysis. Recorded data included demographic information, comorbidities, inflammatory biomarkers, autoimmune antibodies, and the KL-6 level at admission. Results of CT and pulmonary function tests were collected one week before or after KL-6 measurements. The percent of predicted diffusing capacity of the lung for carbon monoxide (DLCO%) and computed tomography (CT) scans were used to determine the severity of ILD.

Results: Univariate linear regression analysis showed that BMI, lung cancer, TB, lung infections, underlying CTD type, white blood cell (WBC) counts, neutrophil (Neu) counts, and hemoglobin (Hb) were related to KL-6 levels. Multiple linear regression confirmed that Hb and lung infections could affect KL-6 levels independently; the β were 9.64 and 315.93, and the P values were 0.015 and 0.039, respectively. CTD-ILD patients had higher levels of KL-6 (864.9 vs 463.9, $P < 0.001$) than those without ILD. KL-6 levels were closely correlated to the severity of ILD assessed both by CT and DLCO%. Additionally, we found that KL-6 level was an independent predictive factor for the presence of ILD and further constructed a decision tree model to rapidly determine the risk of developing ILD among CTD patients.

Conclusion: KL-6 is a potential biomarker for gauging the incidence and severity of ILD in CTD patients. To use this typical value of KL-6, however, doctors should take Hb and the presence of lung infections into account.

KEYWORDS

CTD, ILD, KL-6, CTD-ILD, CTD-NILD

1 Introduction

Connective tissue diseases (CTDs), including systemic lupus erythematosus (SLE), rheumatoid arthritis (RA), systemic sclerosis (SSc), inflammatory myositis (IM), Sjogren's syndrome (SS), and mixed connective tissue disease (MCTD), are commonly complicated by the involvement of many organ systems, such as the lung and the kidney (1, 2). CTD-related pulmonary lesions are mainly manifested as interstitial changes, which are named CTD-interstitial lung disease (CTD-ILD). CTD-ILD is one of the main causes of high morbidity and even mortality among CTD patients. High-resolution computed tomography (HRCT) is an important means of differentiating early ILD. However, it is challenging to perform routine screening due to the limitations of cost, radiation, and other considerations; as such, the identification of biomarkers able to recognize ILD could decrease economic costs and increase the timeliness of therapy to improve patient outcomes.

It is generally accepted that alveolar epithelial cell (AEC) injury is the key event for the occurrence of ILD. The published studies have shown that damaged AEC can secrete a large number of pro-fibrotic factors, provoking the migration, proliferation, activation, and myofibroblast differentiation of fibroblasts and causing the accumulation of extracellular matrix, leading to irreversible lung fibrosis (3–5). Therefore, measuring the level of molecules secreted by damaged epithelial cells is a potential means to assess the severity of the injury and to predict the incidence of ILD.

Krebs von den Lungen-6 (KL-6) is a circulating high-molecular-weight mucin-like glycoprotein, also categorized as MUC1, that is expressed primarily on alveolar type II pneumocytes and bronchial epithelial cells. Accumulation of KL-6 can further disrupt alveolar capillaries and the regeneration of AEC2 (6, 7). Meanwhile, patients with ILD often also have systemic inflammatory response syndrome, leading to more severe AEC2 damage and more KL-6 release (8). Additionally, KL-6 is reported to be one of the key molecules involved in epithelial-mesenchymal interactions by regulating myofibroblast differentiation (9). Because there are no epitopes in animals other than apes, there have been few animal studies on KL-6. However, KL-6 has been reported to be detectable in mice expressing human MUC1(hMUC1-exp) mice and can reflect the severity of bleomycin-induced lung fibrosis (10). All of the above factors may be the underlying pathological mechanisms of KL-6 to predict the incidence of ILD and to predict its prognosis.

The available studies have shown that elevated serum levels of KL6 are related to disease severity (11–14). However, there are drawbacks to these previous studies: the greatest issue is the exclusion of patients with comorbidities. Patients with CTD were more likely to also have cancer (15, 16), lung infections (17), and tuberculosis(TB) (18, 19). These comorbidities may also result in abnormal KL-6 levels, which may cause some confusion for clinicians attempting to judge the presence or severity of ILD. Additionally, the conclusions are not convincing enough because the sample size is typically low-less than 100 cases. Moreover, KL-6 levels at baseline may vary depending on the different underlying types of CTD. In addition, whether patient-related demographic characteristics such as age, gender, and BMI, among others, can affect KL-6 levels also needs further investigation, and these potential confounders may have an influence on the real value of KL-6 in assessing the presence or severity of ILD among patients with CTD.

As such, we performed this retrospective study to determine the potential confounding factors related to KL-6 levels and to re-identify the role of KL-6 among patients with CTD-ILD after adjusting for confounders. Most importantly, we constructed a decision tree model to predict the incidence of ILD.

2 Methods

This research was approved by the local Ethics Committee of the Xiangya Hospital of Central South University and was conducted in accordance with the Declaration of Helsinki and its

Abbreviations: AEC, alveolar epithelial cell; AFP, alpha fetoprotein; ANOVA, analysis of variance; AUC, the area under the curve; BMI, body mass index; CA125,Carbohydrate antigen 125; CA242, Carbohydrate antigen 242; CA199, Carbohydrate antigen 199; CEA, carcinoembryonic antigen; CRP, C-reaction protein; CTD, connective tissue diseases; CTD-ILD, connective tissue diseases associated interstitial lung disease; C3, complement C3; C4, complement C4; HRCT, high resolution computed tomography; COPD, chronic obstructive pulmonary disease; DLCO, diffusing capacity of the lungs for carbon monoxide; Eos, eosinophil; ESR, erythrocyte sedimentation rate; FEV_1, forced expired volume in one second; FVC, forced vital capacity; Hb, hemoglobulin; KL-6, Krebs Von den Lungen-6; LDL, Low-density lipoprotein; Lym, lymphocyte; CTD, mixed connective tissue disease; Neu, neutrophil; NSE, neuron-specific enolase; PM/DM, polymyositis/dermatomyositis; RA, rheumatoid arthritis; SLE, systemic lupus erythematosus, SjS, Sjögren's syndrome; SSc, systemic sclerosis; ROC: receiver operating characteristic curve; TB, tuberculosis; TC, total cholesterol; TGF-β, transforming growth factor beta; UCTD, unspecified connective tissue disease; WBC, white blood cell.

amendments. The Ethics number is 202104005, and it is approved on May 6th, 2021". The detail information was shown on (https://ethics.tonoinfo.com/#/home/zndxxyyy). Informed consent was waived because of the retrospective nature of the study, and the analysis used anonymous clinical data.

2.1 Study design and subjects

This was a retrospective study. Data were collected from the database setup by the Xiangya Hospital of Central South University (Hunan, China). This database recruited patients diagnosed with ILD, COPD, or lung cancer in both the outpatient and inpatient departments of Xiangya Hospital for 20 years. We screened the inpatients with KL-6 measurements in the entire database. For patients with multiple KL-6 tests, we collected the first test on admission. Then, we searched for the discharge diagnosis in the medical records with the following keywords: 'RA', 'SLE', 'SSc', 'polymyositis (PM)', 'dermatomyositis (DM)', 'anti-synthetase antibody syndrome', 'inflammatory myopathy', 'SS', 'undetermined CTD', and 'mixed CTD'. Then, two pulmonologists and radiologists double checked the CT images of these recruited patients. We excluded patients without CT data. Finally, we divided the recruited patients into a CTD-NILD group and a CTD-ILD group based on the presence of ILD. Professional radiologists and pulmonologists double checked the diagnosis of ILD. The recorded data comprised basic demographic information, including age, gender, BMI, blood type, occupation, smoking history, dust exposure, and atopy history. In addition, regular blood biochemical tests, KL-6 levels, CT scans, and lung function parameters were also collected. All the data were collected at admission. CT and pulmonary function results were collected within 1 week of the KL-6 data.

2.2 Pulmonary function data

The pulmonary function test was performed by professional technicians with a spirometer (MasterScreen-Body/Diff, CareFusion, Germany) according to the American Thoracic Society guidelines. The severity of diffusion impairment was assessed by DLCO%, (grade 1, DLCO% ≥80%; grade 2, 60 ≤DLCO% <80%; grade 3, 40 ≤DLCO% <60%, grade 4, DLCO% <40%).

2.3 Severity assessment of ILD by CT scan

One professional radiologist, who was blinded to the clinical information, graded the ILD severity of CT scans semi-quantitatively (grade 1, 0–25%; grade 2, 26%–50%; grade 3, 51%–75%; grade 4, 76%–100%) (11).

2.4 KL-6 measurements

Serum KL-6 concentrations (μg/mL) were measured through the KL-6 assay using the latex-enhanced immunoturbidimetric assay method by qualified laboratory physicians. 500μg/ml was the cutoff point for differentiating normal and abnormal.

2.5 Statistical analysis

Continuous variables are presented as the mean and standard deviation (if the data were normally distributed) and the median and interquartile range (IQR) values (if the data were not normally distributed). Categorical variables are described as frequency rates and percentages. We compared the means for continuous variables with the t-test or analysis of variance (ANOVA) if the data were normally distributed. We used a non-parametric test for non-normally distributed data. We analysed proportions of categorical variables with a χ^2 test. We used Pearson's and Spearman's rank correlation coefficients to analyse the relationship between KL-6 and other parameters. We used a receiver operating characteristic (ROC) curve to determine the cut-off point of KL-6 for predicting the incidence of CTD-ILD. We calculated the results shown in this paper according to the censoring method. We used R Statistical Software (http://www.R-project.org, The R Foundation) and the Free Statistics analysis platform for the statistical analyses. We considered $P < 0.05$ to be statistically significant.

3 Results

3.1 Clinical characteristics of the study population

We retrospectively reviewed 965 inpatients with KL-6 measurements in the database. Overall, 534 patients had a diagnosis of CTD, but we excluded 10 patients due to a lack of CT data. Finally, 524 patients were recruited. Among these patients, 455 were diagnosed with CTD-ILD (Supplementary Figure 1). The mean age (55.1 vs 50.9 years, $P = 0.008$) was significantly higher in the ILD group. Other variables, including sex, blood type, the underlying CTD group, and comorbidities, were similar between these two groups. In the CTD-ILD group, there were 31 cases of RA, 13 cases of SLE, 99 cases of SSc, 20 cases of primary SjS, 174 cases of DM, and 65 patients with MCTD and 53 with UCTD (Table 1). The lung diffuse function including DLCO (5.0 vs 4.1, $P = 0.043$) and DLCO% (63.4 vs 52.9, $P = 0.050$) were much higher in patients with CTD but without ILD than in patients with CTD-ILD (Table 2). Patients with CTD-ILD had lower CRP (7.2 vs 16.1 mg/L, $P = 0.038$), NSE (6.9 vs 8.4 ng/ml, $P = 0.043$) and C4 levels (204.0 vs 241.9 mg/L, $P = 0.03$) than CTD patients without ILD (n = 69). While CTD-ILD patients had higher levels of KL-6 (864.9 vs 463.9 μg/ml, $P < 0.001$) (Table 2). When we stratified the data by the type of underlying CTD, we found that PM had the highest KL-6 level (995.7 μg/ml) of all types of CTD (Figure 1A). Then, we further analyzed the KL-6 level between CTD and CTD-ILD based on underlying CTD subgroups. We observed that serum KL-6 values were significantly higher in patients with specific CTD-ILD, including PM (1097.0 vs 454.7 μg/ml, $P < 0.001$), SSc (823.7 vs 485.2 μg/ml, $P = 0.0028$), and UCTD (690.6 vs 330.5 μg/ml, $P = 0.038$) (Figure 1B). In addition, we found that patients with PM

10.3389/fimmu.2023.1098602

TABLE 1 Demographic data of all the subjects.

Variables	Total (N=524)	CTD-NILD (N=69)	CTD-ILD (N=455)	*P*
Age(year)	54.5±12.0	50.9±13.1	55.1±11.7	0.008
sex, n (%)				
Female	159 (30.3)	26 (37.7)	133 (29.2)	0.155
Male	365 (69.7)	43 (62.3)	322 (70.8)	
Occupation, n (%)				0.549
Farmers	142 (27.1)	17 (24.6)	125 (27.5)	
Employees	82 (15.6)	12 (17.4)	70 (15.4)	
Freelancer	101 (19.3)	16 (23.2)	85 (18.7)	
Retired	61 (11.6)	7 (10.1)	54 (11.9)	
Unemployed	132 (25.2)	15 (21.7)	117 (25.7)	
Students	6 (1.1)	2 (2.9)	4 (0.9)	
Blood type				0.216
A	51 (9.7)	6 (8.7)	45 (9.9)	
B	35 (6.7)	5 (7.2)	30 (6.6)	
O	63 (12.0)	3 (4.3)	60 (13.2)	
AB	13 (2.5)	1 (1.4)	12 (2.6)	
Unknown	362 (69.1)	54 (78.3)	308 (67.7)	
BMI(kg/m^2)	22.0 ± 3.2	21.3 ± 3.9	22.1 ± 3.2	0.431
Smoking history, n (%)				< 0.001
No	312 (59.5)	54 (78.3)	258 (56.7)	
Yes	212 (40.5)	15 (21.7)	197 (43.3)	
Occupation exposure, n (%)				0.552
No	473 (97.5)	30 (96.8)	443 (97.6)	
Yes	12 (2.5)	1 (3.2)	11 (2.4)	
Specific CTDs				0.289
PM/DM	198 (37.8)	24 (34.8)	174 (38.2)	
SjS	25 (4.8)	5 (7.2)	20 (4.4)	
SLE	18 (3.4)	5 (7.2)	13 (2.9)	
RA	36 (6.9)	5 (7.2)	31 (6.8)	
SSc	116 (22.1)	17 (24.6)	99 (21.8)	
MCTD	70 (13.4)	5 (7.2)	65 (14.3)	
UCTD	61 (11.6)	8 (11.6)	53 (11.6)	
Comorbidities				
Lung cancer	106 (20.2)	11 (15.9)	95 (20.9)	0.341
TB	34 (6.5)	8 (11.6)	26 (5.7)	0.109
COPD	46 (8.8)	3 (4.3)	43 (9.5)	0.163
Severe infections	34 (6.5)	4 (5.8)	30 (6.6)	1

(Continued)

TABLE 1 Continued

Variables	Total (N=524)	CTD-NILD (N=69)	CTD-ILD (N=455)	*P*
Hospital expense(w)	1.3 (0.9-2.2)	1.3 (0.9-2.2)	1.2 (0.8-2.2)	0.381
Hospital stays	8.0 (7.0-12.0)	8.0 (7.0-11.0)	8.0 (7.0-12.0)	0.868

CTD, connective tissue diseases; CTD-ILD, connective tissue diseases associated interstitial lung disease. BMI, body mass index; RA, rheumatoid arthritis; SLE, systemic lupus erythematosus, SjS, Sjögren's syndrome; SSc, systemic sclerosis; PM/DM, polymyositis/dermatomyositis; MCTD, mixed connective tissue disease; UCTD, unspecified connective tissue disease.

showed the highest KL-6 relative to other CTD patterns in the CTD-ILD group ($P < 0.001$) but presented no difference in the CTD group ($P = 0.246$) (Figure 1C).

3.2 Factors associated with KL-6 levels

Univariate linear regression analysis showed that BMI, lung cancer, TB, pulmonary infections, white blood cell (WBC) counts, hemoglobin (Hb), neutrophil counts and underlying CTD type were related to the KL-6 level. Age, gender, smoking index, atopy history, dust exposure, and combination with COPD had no effect on the KL-6 level. Patients with high Hb were more likely to present higher KL-6 levels ($\beta = 6.03$, $P = 0.017$). Subjects diagnosed with pulmonary infections had higher KL-6 levels than those with only CTD-ILD but no infections. Multiple linear regression confirmed that Hb and pulmonary infections could affect the KL-6 level independently; the β were 9.64 and 315.93, and the *P* values were

TABLE 2 Clinical characteristics of the subject population.

Variables	Total	CTD-NILD	CTD-ILD	*P*
Blood routine test				
Hb	116.7 ± 19.9	119.2 ± 24.6	116.4 ± 19.1	0.272
Neu	4.4 (2.9, 6.9)	4.2 (2.9, 7.0)	4.4 (2.9, 6.9)	0.856
Eos	0.1 (0.0, 0.1)	0.1 (0.0, 0.2)	0.1 (0.0, 0.1)	0.866
Lym	1.0 (0.7, 1.4)	1.1 (0.7, 1.6)	1.0 (0.7, 1.4)	0.204
WBC	6.3 (4.4, 9.2)	6.3 (4.4, 9.2)	6.3 (4.4, 9.2)	0.439
Inflammatory marker				
CRP	8.0 (3.3, 22.9)	16.1 (7.4, 25.3)	7.2 (3.2, 22.4)	0.038
ESR	47.0 (18.0, 81.0)	50.0 (0.0, 94.0)	47.0 (21.0, 79.5)	0.678
Autoimmune antibody				
C3	821.0±201.4	846.0 ± 191.4	819.5 ± 202.2	0.558
C4	206.2±77.6	241.9 ± 93.4	204.0 ± 76.2	0.030
dsDNA(+)	17	0	17	1
ANA(+)	228	9	219	0.343
Ro52	126	3	123	0.088
Jo.1	24	0	24	0.610
Scl.70	46	2	44	1
SSB	16	1	15	0.540
SSA	59	2	57	1
KL-6	780.5 (470.4, 1373.0)	463.9 (322.9, 753.9)	864.9 (547.6, 1518.0)	<0.001
Tumor markers				
CEA	1.6 (0.8, 3.1)	1.0(0.8-1.5)	1.7 (0.9, 3.2)	0.073
NSE	7.0 (5.3, 9.0)	8.4 (7.6, 10.7)	6.9 (5.2, 9.0)	0.043
AFP	1.8 (1.4, 2.6)	1.7 (1.4, 3.1)	1.8 (1.4, 2.6)	0.986

(Continued)

TABLE 2 Continued

Variables	Total	CTD-NILD	CTD-ILD	*P*
CA125	12.6 (7.6, 25.1)	11.1 (9.7, 22.7)	12.6 (7.5, 25.1)	0.785
CA242	4.5 (3.3, 5.4)	5.4 (5.4, 5.4)	4.5 (3.3, 5.4)	0.527
CA199	8.4 (4.6, 17.1)	8.9 (6.1, 11.9)	8.3 (4.6, 17.6)	0.791
Lung function				
FEV_1	1.9 ± 0.4	2.0 ± 0.3	1.9 ± 0.5	0.082
FEV_1%	80.9 ± 14.7	83.5 ± 10.2	80.6 ± 15.1	0.186
FVC%	81.9 ± 15.1	84.9 ± 11.6	81.6 ± 15.4	0.132
FVC	2.4 ± 0.6	2.5 ± 0.3	2.4 ± 0.6	0.080
DLCO	4.1 ± 1.4	5.0 ± 2.4	4.1 ± 1.4	0.043
DLCO%	53.4 ± 16.5	63.4 ± 26.7	52.9 ± 15.9	0.050

CTD, connective tissue diseases; CTD-ILD, connective tissue diseases associated interstitial lung disease; Hb, hemoglobulin; Neu, neutrophil; Eos, eosinophil; Lym, lymphocyte; WBC, white blood cell; CRP, C-reaction protein; C3, complement C3; C4, complement C4; ESR, erythrocyte sedimentation rate; KL-6, Krebs Von den Lungen-6; CEA, carcinoembryonic antigen; NSE, neuron-specific enolase; AFP, alpha fetoprotein; CA125,Carbohydrate antigen 125; CA242, Carbohydrate antigen 242; CA199, Carbohydrate antigen 199; FEV_1, forced expired volume in one second; FVC, forced vital capacity; DLCO, diffusing capacity of the lungs for carbon monoxide.

0.015 and 0.039, respectively (Table 3). The formula for correcting KL6 is Y=-422.24+315.93*1 (when lung infection exists) +9.64 *Hb.

3.3 The role of KL-6 in assessing the severity of CTD-ILD

Patients with severe (grade 4) diffusion function impairment presented the highest KL-6 level of all three grades; the mean values of KL-6 in different diffusion impairment grades were 1054.7, 780.7, 614.2, and 542.6(μg/ml), respectively (Figure 2A). Additionally, semiquantitative grades of ILD on the CT scan were significantly correlated to the KL-6 level (Rho = 0.426, $P < 0.001$). Serum KL-6 levels successfully differentiated grades 1 and 2 ($P < 0.001$), as well as grades 2 and 3 ($P < 0.001$) in patients with CTD-ILD (Figure 2B). Grade 3 and grade 4 showed similar KL-6 levels. Therefore, serum KL-6 can be used to reflect the current status of CTD-ILD defined by CT scans. To utilize the serum KL-6 level in clinical practice, the

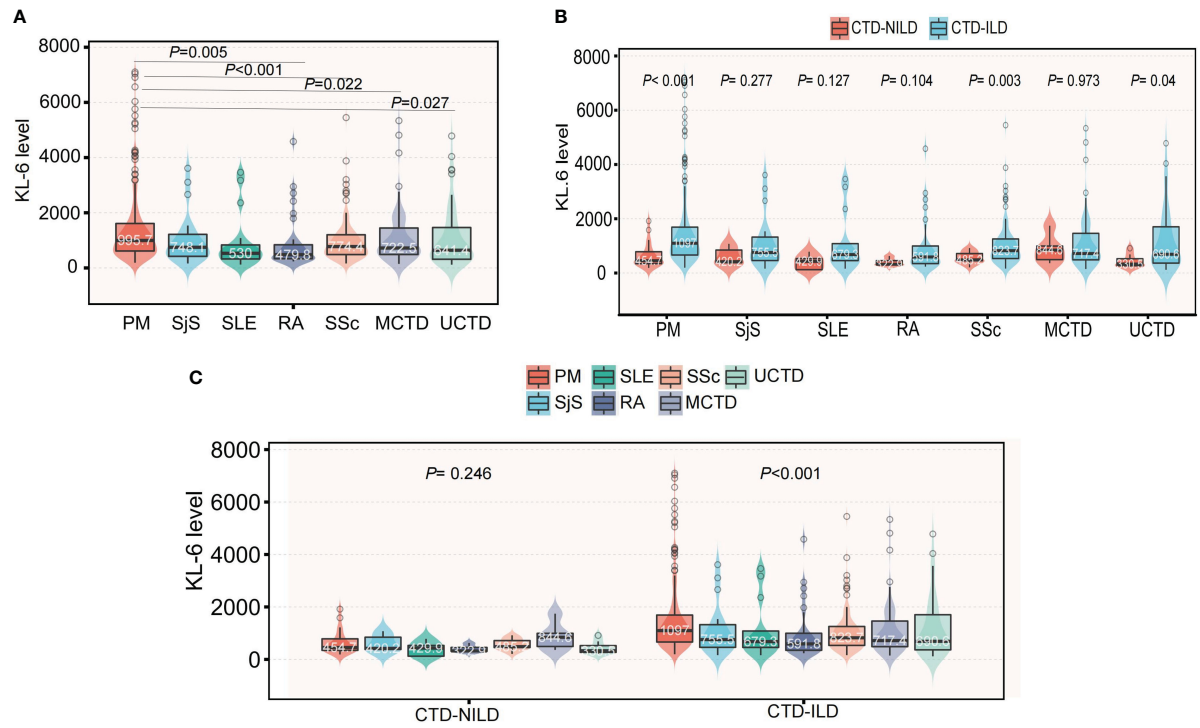

FIGURE 1
The differences of KL-6 level among specific CTD patterns. **(A)** The differences of KL-6 levels among specific CTD patterns in the whole population. **(B)** Subgroup analysis of the differences of KL-6 level between CTD-NILD and CTD-ILD groups based on underlying CTD pattern. **(C)** Subgroup analysis of the differences of KL-6 level among different CTD patterns based on the presence of ILD.

10.3389/fimmu.2023.1098602

TABLE 3 Factors associated with KL-6 level.

Variables	β	95%CI	*P*	*Adjusted* β	*Adjusted P*
Age	5.13	-3.09~13.35	0.221		
Gender(male)	58.18	-156.44~272.79	0.595		
BMI	39.63	2.67~76.6	0.036	28.61	0.158
Smoking history (No)	104.1	-96.79~304.98	0.309		
Atopy history	53.98	-273.71~381.66	0.746		
Dust exposure	-132.46	-809.16~544.23	0.701		
Comorbidities					
Lung cancer	-335.95	-579.93~-91.97	0.007	-182.91	0.199
TB	-454.06	-852.82~-55.3	0.026	-383.57	0.102
COPD	-150.77	-499.29~197.75	0.396		
Lung infections	331.95	110.73~ 553.16	0.003	315.93	0.039
CTD(ref:PM)					
SjS	-446.85	-918.57~24.86	0.064	-125.39	0.683
SLE	-540.4	-1087.53~6.73	0.053	-209.14	0.589
RA	-576.24	-978.91~-173.56	0.005	-164.11	0.514
SSc	-467.32	-727.18~-207.46	<0.001	-91.15	0.581
MCTD	-362.76	-671.8~-53.72	0.022	-101.93	0.589
UCTD	-369.02	-694.47~-43.57	0.027	0.97	0.996
Blood routine test					
WBC	31.60	6.47~ 56.74	0.014	-124.62	0.165
Eos	-132.68	-803.61~538.24	0.698		
Hb	6.03	1.1~10.97	0.017	9.64	0.015
Neu	39.26	12.43~66.10	0.004	140.32	0.143
Inflammatory marker					
CRP	0.98	-1.49~3.45	0.436		
ESR	1.05	-1.72,3.81	0.457		

BMI, body mass index; TB, tuberculosis; COPD, chronic obstructive pulmonary disease; CTD, connective tissue diseases; RA, rheumatoid arthritis; SLE, systemic lupus erythematosus, SjS, Sjögren's syndrome; SSc, systemic sclerosis; PM/DM, polymyositis/dermatomyositis; MCTD, mixed connective tissue disease; UCTD, unspecified connective tissue disease; Hb, hemoglobulin; Neu, neutrophil; Eos, eosinophil; WBC, white blood cell; CRP, C-reaction protein; ESR, erythrocyte sedimentation rate; KL-6, Krebs Von den Lungen-6.

cut-off points of KL-6 values to predict the presence of ILD in CTD patients were analyzed by ROC. The analysis showed that the KL-6 level at 532.75 U/mL was the best cut-off point for differentiating ILD among CTD patients. The AUC value was 0.736, with a 95% CI of 0.680–0.792. The sensitivity and specificity were 75.4% and 65.2%, respectively (Figure 3A). Then, we further explored the cut-off point of KL-6 to assess the severity of ILD among patients with CTD-ILD quantified by semiquantitative grades on CT scans and lung function stratified by DLCO%. The cut-off point for KL-6 was 643.15 μg/ml, the AUC values of KL-6 levels to differentiate grade 3 and 4 defined by DLCO% was 0.625, and the sensitivity and specificity were 69.4% and 58.5%, respectively. In addition, the positive and negative predictive values were 79.1% and 46.8%, respectively (Figure 3B). Furthermore, the AUC values of KL-6 levels to differentiate grade 3 and 4 defined by CT scan were 0.762 (95% CI: 0.706–0.818), the negative predictive value was 92.0%, and the cut-off point of KL-6 was 1060.75 μg/ml (Figure 3C).

3.4 The relationship between KL-6 and lung function, CT scan hints

The KL-6 level showed a mild, negative relationship with FEV_1%, FVC%, DLCO, and DLCO%. The R values were –0.18, –

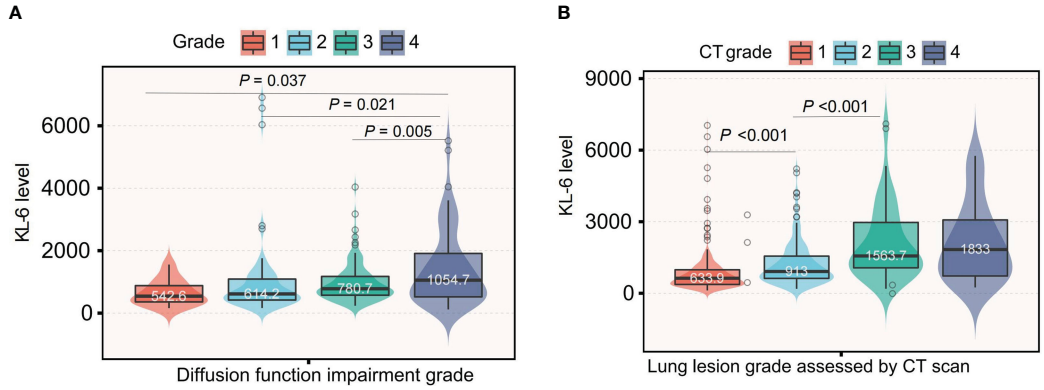

FIGURE 2
Comparison of KL-6 level based on the severity of ILD assessed by both CT scan and DLCO%; **(A)** Comparison of KL-6 level based on the severity of ILD assessed by DLCO%; **(B)** Comparison of KL-6 level based on the severity of ILD assessed by CT scan.

0.21, –0.20, and –0.24, respectively (Supplementary Figure 2).Then, we compared the predictive value of KL6 combined with DLCO and KL6 combined with FVC with that of KL-6 alone to diagnose ILD. We found that KL6, whether combined with DLCO or FVC, had a similar predictive value to ILD as KL-6 alone to diagnose ILD (Supplementary Figure 3).

We analysed the association between different CT signs with KL-6 levels and found that patients with CT signs related to ILD, – including ground-glass opacity, honeycomb, and reticular shadow – presented higher levels of KL-6 than patients without these corresponding signs (918.3 vs 703.3μg/ml, P=0.003). Other signs, such as emphysema, consolidation, nodules, or tumous, had no relation to the KL-6 level. After adjustment for significant signs, we found that only ILD-related signs had an effect on the KL-6 level β = 415.26, P = 0.001 (Supplementary Figure 4 and Supplementary Table 1).

3.5 Serum KL-6 levels are associated with the presence of ILD

We performed a logistic regression analysis of factors related to ILD and found that age, cough, dyspnoea, complement C4, smoking status and KL-6 may be related to ILD. Multivariable regression analysis revealed that KL-6 levels were independently associated with ILD (Table 4). The likelihood of ILD incidence increased 10.51 times in patients with abnormal levels compared with patients with normal KL-6 levels (OR 10.51, 95%CI 3.7~29.84, P <0.001; Table 4).To further analyse the stability of the adjusted model, we stratified patients by gender, age, smoking status, cough, dyspnoea, and complement C4. The forest plot revealed that there were no significant interactions between the aforementioned subgroups (P >0.05, Figure 4).

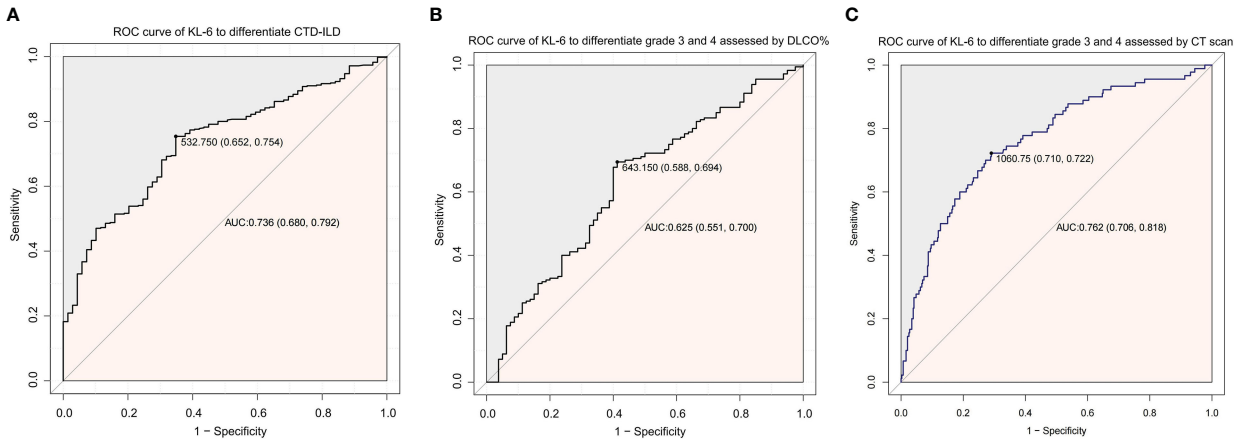

FIGURE 3
ROC curve analysis to utilize the role of KL-6 in CTD patients. **(A)** ROC curve of KL-6 levels to differentiate the presence of ILD among CTD patients. **(B)** ROC curve of KL-6 levels to differentiate Grade 3 and Grade 4 assessed by DLCO%. **(C)** ROC curve of KL-6 levels to differentiate Grade 3 and Grade 4 assessed by CT scan.

10.3389/fimmu.2023.1098602

TABLE 4 Factors associated with ILD.

Variables	OR (95%CI)	*P*	*Adjusted* OR (95%CI)	*P*
Age	2.17 (1.28~3.68)	0.004	0.73 (0.28~1.93)	0.528
Gender(male)	0.68 (0.4~1.16)	0.157		
Occupation	0.79 (0.36~1.76)	0.568		
Smoking Status	2.75 (1.51~5.02)	0.001	3.81 (1.22~11.85)	0.021
Atopy history	0.47 (0.18~1.22)	0.12		
Dust exposure	0.74 (0.09~5.96)	0.781		
Comorbidities				
Lung cancer	1.39 (0.7~2.75)	0.343		
TB	0.46 (0.2~1.07)	0.071		
COPD	2.3 (0.69~7.62)	0.174		
Lung infections	1.65 (0.87~3.12)	0.124		
CTD (ref:PM)				
SjS	0.55 (0.19~1.61)	0.275		
SLE	0.36 (0.12~1.09)	0.072		
RA	0.86 (0.3~2.41)	0.767		
SSc	0.8 (0.41~1.57)	0.521		
MCTD	1.79 (0.66~4.9)	0.255		
UCTD	0.91 (0.39~2.15)	0.837		
Cough	1.74 (1.05~2.9)	0.033	0.66 (0.22~1.99)	0.458
Dyspnea	2.51 (1.49~4.25)	0.001	0.83 (0.28~2.52)	0.748
Blood test				
WBC	0.98 (0.92~1.04)	0.557		
Eos	0.43 (0.09~1.99)	0.279		
Hb	0.99 (0.98~1.01)	0.272		
Neu	1 (0.93~1.07)	0.954		
CRP	1 (0.99~1)	0.448		
ESR	1 (0.99~1.01)	0.944		
C3	0.94 (0.75~1.17)	0.557		
C4	0.57 (0.34~0.95)	0.032	0.53 (0.3~0.93)	0.027
TC	1.28 (0.88~1.87)	0.193		
LDL	1.34 (0.79~2.3)	0.282		
KL-6	5.06 (2.98~8.59)	<0.001	10.51 (3.7~29.84)	<0.001

ILD, interstitial lung disease; COPD, chronic obstructive pulmonary disease; PM/DM, polymyositis/dermatomyositis; SLE, systemic lupus erythematosus; RA, rheumatoid arthritis; SjS, Sjögren's syndrome; SSc, systemic sclerosis; MCTD, mixed connective tissue disease; UCTD, unspecified connective tissue disease; WBC, white blood cell; Eos, eosinophil; Hb, hemoglobulin; Neu, neutrophil; CRP, C-reaction protein; ESR, erythrocyte sedimentation rate; C3, complement C3; C4, complement C4; TC, total cholesterol; LDL, Low-density lipoprotein; KL-6, Krebs Von den Lungen-6.

3.6 A decision tree based on KL-6 levels to assess ILD

Based on the above factors obtained by logistic regression analysis, we constructed decision tree models (Figure 5). When the KL-6 level is > 533 μg/ml, the probability of the patient having ILD is 70%. If the KL-6 level is < 233 μg/ml and there is no smoking history, then the probability of patients having ILD is only 2%. Based on the decision tree, KL-6 is an important factor for evaluating ILD. In the crude model, the weight of KL-6 is 61.9%.

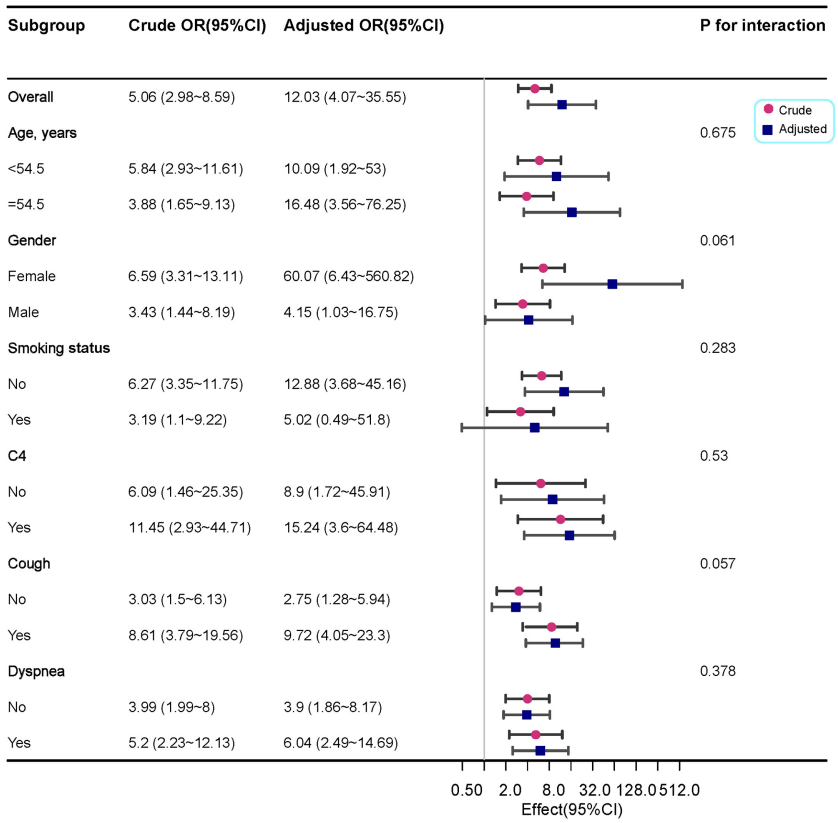

FIGURE 4
Forest plot for the subgroup analysis of the presence of ILD according to KL-6 levels. For each group of interest, the gray horizontal lines represent the 95% confidence interval (CI).

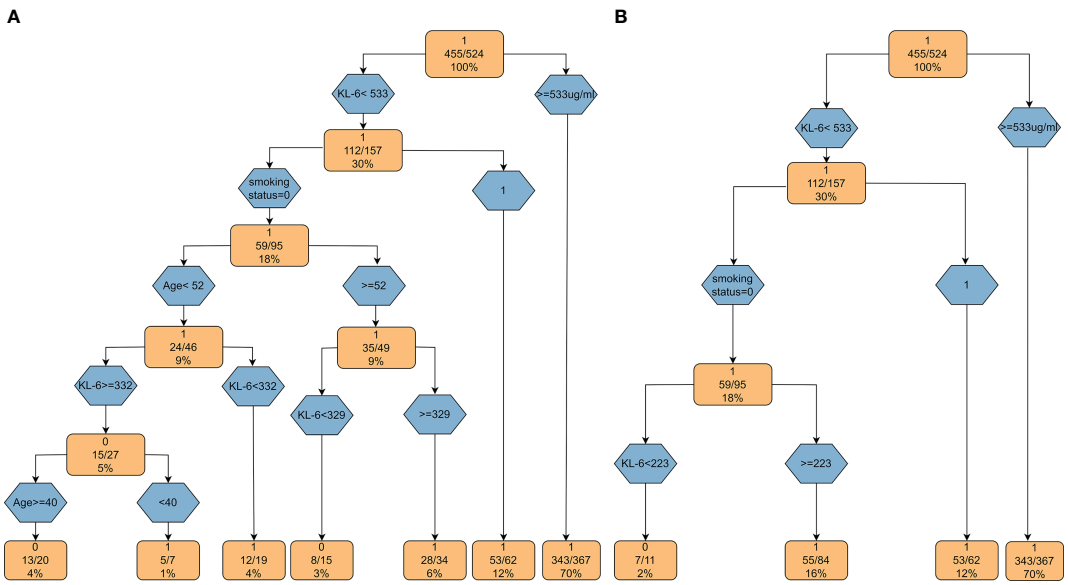

FIGURE 5
Decision tree models based on KL-6. **(A)** The decision tree model based on the factors obtained by univariate regression analysis; **(B)** The decision tree model based on the variables from multiple regression analysis.

After matching various confounding factors, the weight of KL-6 is 75.4%, as shown in Supplementary Table 2.

4 Discussion

In this study, we comprehensively analysed the factors affecting KL-6 and investigated its clinical significance among patients with CTD. We found that Hb and lung infections could affect the KL-6 level independently. KL-6 presented a significant correlation with the severity of CTD-ILD not only measured with CT scan but also stratified by DLCO%. More importantly, we constructed a decision tree model to determine the presence of ILD, which would be beneficial for future clinical work. To our knowledge, this is the first study to systematically investigate the factors affecting KL-6 levels; additionally, we developed a decision tree model to determine the presence of ILD among patients with CTD in the real world without the exclusion of patients with comorbidities.

KL-6 as a biomarker of lung epithelial cell injury has been widely used among ILD patients. However, whether patients' self-reported characteristics, including age, BMI, and gender, would have an effect on KL-6 levels remains seldom investigated. In addition, some of the patients have more than one pulmonary disease; as ILD is likely to be combined with lung cancer, COPD, and TB, patients with these diseases would have abnormal levels of KL-6, and most of them were excluded in clinical trials (15, 18, 20), the clinical use of KL-6 levels among these overlap patients should be comprehensively assessed. In this study, we found that Hb and lung infections could affect KL-6 levels independently, suggesting that KL-6 should be better adjusted by Hb and further corrected if patients were complicated by lung infections. The relationship between KL-6 and Hb is seldom reported; a recent study showed that KL-6 and Hb can both be used to assess bone marrow fibrosis (21), but the interaction between KL-6 and Hb is still unknown, and the mechanism through which Hb is correlated to KL-6 needs further investigation. Several studies have shown that lung infections could elevate the expression of KL-6 (22–24). In this study, we confirmed that lung infections could increase the serum KL-6 level after adjusting for other confounders, indicating that clinicians should check CTD patients for anemia or accompanying lung infections once they receive the results of KL-6 levels.

KL-6 has been reported to have a role in evaluating ILD severity among CTD patients. We found that SSc or IM had a relatively high prevalence of ILD compared with RA, SLE, and SjS, which was in close agreement with another study (11), indicating that patients who tend to have SSc, IM, or PM should be screened for ILD more frequently. Patients with PM showed the highest KL-6 relative to other CTD patterns in the CTD-ILD group but presented no difference in the CTD group, suggesting that the underlying CTD type had no effect on the KL-6 level, but patients with PM were more likely to have worse lung conditions.

In previous studies, researchers have reported significant inverse correlations between serum KL-6 levels and DLCO% in patients with polymyositis and dermatomyositis (25, 26). We also found that KL-6 presented a significant correlation with the severity of CTD-ILD not only measured with CT, but also stratified by DLCO%. We further analysed the relationship between CT signs and the KL-6 level and found that the KL-6 level was correlated with ILD signs, including ground-glass opacity, honeycomb, and reticular shadow, but was not related to COPD signs. Doishita et al. (27) also reported positive correlations between KL-6 levels and both the presence and activity of ILD. KL-6, a mucin-associated glycoprotein, may be a trigger for transforming growth factor beta(TGF-β) signalling and fibrosis (28, 29), giving it the potential to be a biomarker not only of the presence of ILD but also of disease activity. A higher KL-6 level indicates greater ground-glass opacity, honeycomb, or reticular shadow lesions, suggesting that KL-6 should be an alternative method to screen ILD among patients with CTD without the radiology-associated risk. More importantly, it may also have the potential to predict the prognosis of patients with CTD-ILD. Multiple logistic regression analysis revealed that KL-6 is an independent predictive factor for the presence of ILD among patients with CTD. Based on this result, we constructed a decision tree model to predict the possibility of ILD based on a set of decision rules.

There are some limitations to the current study. First, we collected the data from our database, patients who had KL6 measurements were more likely to have ILD. Therefore, the sample size of patients with CTD-NILD was much smaller than that of patients with CTD-ILD, but this did not affect our main findings that KL-6 levels should be corrected for Hb and lung infections. Second, not all the patients underwent high-resolution CT. However, in our hospital the scanning thickness is 1.0 mm for conventional CT and 0.6 mm for high-resolution CT, both of which can identify interstitial lesions. Hence, the absence of high-resolution CT would not affect the identification of ILD lesions. Additionally, a small number of patients in CTD-NILD group do not have lung fuction data, but the correlation analysis between KL-6 and the severity of ILD were from the CTD-ILD group, the absence of lung function in the CTD-NILD group had no effect on the main findings. Finally, due to the small sample size, we could not verify the accuracy of the decision tree. Thus, longitudinal cohort studies will be essential in the future.

5 Conclusion

Hb and lung infections are independent factors affecting KL-6 levels among CTD-ILD patients. KL-6 is a potential biomarker to predict ILD and assess the ILD severity in the real world.

Data availability statement

The raw data supporting the conclusions of this article will be made available by the authors, without undue reservation.

Ethics statement

The studies involving human participants were reviewed and approved by the ethics committee of Xiangya Hospital, Central South University (No. 202104005). Written informed consent for participation was not required for this study in accordance with the national legislation and the institutional requirements.

Author contributions

AZ, RL, and PP designed the study. All authors contributed toward recruiting subjects, statistical analysis and drafting the paper, and each of the authors agreed to be accountable for all aspects of the work. All authors contributed to the article and approved the submitted version.

Funding

This study was supported by grants from The Youth Science Foundation of Xiangya Hospital (2022Q06 to AZ), the Natural Science Foundation of Hunan Province, China (No. 2023JJ41025 to AZ), the Scientific Research Project of Hunan Health Commission (Grant No.D202303029041), Project Program of National Clinical Research Center for Geriatric Disorders (Xiangya Hospital, Grant No. 2020LNJJ05), The National Key Clinical Specialist Construction Program of China (Grant Number z047-02), and Key R & D Program of Hunan Province (No.2022SK2038).

Acknowledgments

We wish to thank Dr. David R Price (Division of Pulmonary and Critical Care Medicine, Weill Cornell Medical College) for proofreading the manuscript.

Conflict of interest

The authors declare that the research was conducted in the absence of any commercial or financial relationships that could be construed as a potential conflict of interest.

Publisher's note

Supplementary material

The Supplementary Material for this article can be found online at: https://www.frontiersin.org/articles/10.3389/fimmu.2023.1098602/full#supplementary-material

References

1. Yu H, Nagafuchi Y, Fujio K. Clinical and immunological biomarkers for systemic lupus erythematosus. *Biomolecules* (2021) 11(7):928. doi: 10.3390/biom11070928

2. Khanna D, Tashkin DP, Denton CP, Renzoni EA, Desai SR, Varga J. Etiology, risk factors, and biomarkers in systemic sclerosis with interstitial lung disease. *Am J Respir Crit Care Med* (2020) 201(6):650–60. doi: 10.1164/rccm.201903-0563CI

3. Yao C, Guan X, Carraro G, Parimon T, Liu X, Huang G, et al. Senescence of alveolar type 2 cells drives progressive pulmonary fibrosis. *Am J Respir Crit Care Med* (2021) 203(6):707–17. doi: 10.1164/rccm.202004-1274OC

4. Olajuyin AM, Zhang X, Ji HL. Alveolar type 2 progenitor cells for lung injury repair. *Cell Death Discovery* (2019) 5:63. doi: 10.1038/s41420-019-0147-9

5. Lopez-Rodriguez E, Gay-Jordi G, Knudsen L, Ochs M, Serrano-Mollar A. Improved alveolar dynamics and structure after alveolar epithelial type II cell transplantation in bleomycin induced lung fibrosis. *Front Med (Lausanne)* (2021) 8:640020. doi: 10.3389/fmed.2021.640020

6. Hant FN, Ludwicka-Bradley A, Wang HJ, Li N, Elashoff R, Tashkin DP, et al. Scleroderma lung study research G surfactant protein d and KL-6 as serum biomarkers of interstitial lung disease in patients with scleroderma. *J Rheumatol* (2009) 36(4):773–80. doi: 10.3899/jrheum.080633

7. Zhang T, Shen P, Duan C, Gao L. KL-6 as an immunological biomarker predicts the severity, progression, acute exacerbation, and poor outcomes of interstitial lung disease: a systematic review and meta-analysis. *Front Immunol* (2021) 12:745233. doi: 10.3389/fimmu.2021.745233

8. Elhai M, Hoffmann-Vold AM, Avouac J, Pezet S, Cauvet A, Leblond A, et al. Performance of candidate serum biomarkers for systemic sclerosis-associated interstitial lung disease. *Arthritis Rheumatol* (2019) 71(6):972–82. doi: 10.1002/art.40815

9. Xu L, Yan DR, Zhu SL, Gu J, Bian W, Rong ZH, et al. KL-6 regulated the expression of HGF, collagen and myofibroblast differentiation. *Eur Rev Med Pharmacol Sci* (2013) 17(22):3073–7.

10. Sakai M, Kubota T, Ohnishi H, Yokoyama A. A novel lung injury animal model using KL-6-measurable human MUC1-expressing mice. *Biochem Biophys Res Commun* (2013) 432(3):460–5. doi: 10.1016/j.bbrc.2013.01.123

11. Lee JS, Lee EY, Ha YJ, Kang EH, Lee YJ, Song YW. Serum KL-6 levels reflect the severity of interstitial lung disease associated with connective tissue disease. *Arthritis Res Ther* (2019) 21(1):58. doi: 10.1186/s13075-019-1835-9

12. Zheng M, Lou A, Zhang H, Zhu S, Yang M, Lai W. Serum KL-6, CA19-9, CA125 and CEA are diagnostic biomarkers for rheumatoid arthritis-associated interstitial lung disease in the Chinese population. *Rheumatol Ther* (2021) 8(1):517–27. doi: 10.1007/s40744-021-00288-x

13. Wu X, Wu LJ, Luo CN, Shi YM, Zou JM, Meng XY. The diagnostic value of serum KL-6 in connective tissue disease associated interstitial lung disease. *Zhonghua Yi Xue Za Zhi* (2019) 99(40):3172–5. doi: 10.1136/annrheumdis-2019-eular.7673

14. He Q, Tang Y, Huang J, Rao Y, Lu Y. The value of KL-6 in the diagnosis and assessment of interstitial lung disease. *Am J Transl Res* (2021) 13(8):9216–23.

15. Watanabe S, Saeki K, Waseda Y, Murata A, Takato H, Ichikawa Y, et al. Lung cancer in connective tissue disease-associated interstitial lung disease: clinical features and impact on outcomes. *J Thorac Dis* (2018) 10(2):799–807. doi: 10.21037/jtd.2017.12.134

16. D'alessandro M, Bergantini L, Cameli P, Pieroni M, Refini RM, Sestini P, et al. Serum concentrations of KL-6 in patients with IPF and lung cancer and serial measurements of KL-6 in IPF patients treated with antifibrotic therapy. *Cancers (Basel)* (2021) 13(4):689. doi: 10.3390/cancers13040689

17. Simon TA, Boers M, Hochberg M, Baker N, Skovron ML, Ray N, et al. Comparative risk of malignancies and infections in patients with rheumatoid arthritis initiating abatacept versus other biologics: a multi-database real-world study. *Arthritis Res Ther* (2019) 21(1):228. doi: 10.1186/s13075-019-1992-x

18. Zafari P, Golpour M, Hafezi N, Bashash D, Esmaeili SA, Tavakolinia N, et al. Tuberculosis comorbidity with rheumatoid arthritis: gene signatures, associated biomarkers, and screening. *IUBMB Life* (2021) 73(1):26–39. doi: 10.1002/iub.2413

19. Miwa S, Suzuki Y, Shirai M, Ohba H, Kanai M, Eifuku T, et al. Assessment of serum KL-6 as a prognostic marker in pulmonary tuberculosis patients. *Int J Tuberc Lung Dis* (2013) 17(2):240–2. doi: 10.5588/ijtld.12.0498

20. Ishikawa N, Hattori N, Tanaka S, Horimasu Y, Haruta Y, Yokoyama A, et al. Levels of surfactant proteins a and d and KL-6 are elevated in the induced sputum of chronic obstructive pulmonary disease patients: a sequential sputum analysis. *Respiration* (2011) 82(1):10–8. doi: 10.1159/000324539

21. Nam M, Hur M, Park M, Kim H. Novel usefulness of Krebs von den lungen 6 (KL-6) with hemoglobin and lactate dehydrogenase for assessing bone marrow fibrosis. *Diagnostics (Basel)* (2022) 12(3):628. doi: 10.3390/diagnostics12030628

22. Frix AN, Schoneveld L, Ladang A, Henket M, Duysinx B, Vaillant F, et al. And guiot J could KL-6 levels in COVID-19 help to predict lung disease? *Respir Res* (2020) 21(1):309. doi: 10.1186/s12931-020-01560-4

23. D'alessandro M, Bergantini L, Cameli P, Curatola G, Remediani L, Bennett D, et al. Serial KL-6 measurements in COVID-19 patients. *Intern Emerg Med* (2021) 16 (6):1541–5. doi: 10.1007/s11739-020-02614-7

24. Kubota M, Haruta T. The role of serum KL-6 measurement in common pediatric respiratory infections. *J Infect Chemother* (2006) 12(1):22–4. doi: 10.1007/s10156-005-0416-9

25. Hu C, Wu C, Yang E, Huang H, Xu D, Hou Y, et al. Serum KL-6 is associated with the severity of interstitial lung disease in Chinese patients with polymyositis and dermatomyositis. *Clin Rheumatol* (2019) 38(8):2181–7. doi: 10.1007/s10067-019-04501-9

26. Wang Y, Chen S, Lin J, Xie X, Hu S, Lin Q, et al. Lung ultrasound b-lines and serum KL-6 correlate with the severity of idiopathic inflammatory myositis-associated interstitial lung disease. *Rheumatol (Oxford)* (2020) 59(8):2024–9. doi: 10.1093/rheumatology/kez571

27. Doishita S, Inokuma S, Asashima H, Nakachi S, Matsuo Y, Rokutanda R, et al. Serum KL-6 level as an indicator of active or inactive interstitial pneumonitis associated with connective tissue diseases. *Intern Med* (2011) 50(23):2889–92. doi: 10.2169/internalmedicine.50.5866

28. Majewski S, Szewczyk K, Zal A, Bialas AJ, Milkowska-Dymanowska J, Piotrowski WJ. Serial measurements of circulating KL-6, SP-d, MMP-7, CA19-9, CA-125, CCL18, and periostin in patients with idiopathic pulmonary fibrosis receiving antifibrotic therapy: an exploratory study. *J Clin Med* (2021) 10(17):3864. doi: 10.3390/jcm10173864

29. Aloisio E, Braga F, Puricelli C, Panteghini M. Prognostic role of Krebs von den lungen-6 (KL-6) measurement in idiopathic pulmonary fibrosis: a systematic review and meta-analysis. *Clin Chem Lab Med* (2021) 59(8):1400–8. doi: 10.1515/cclm-2021-0199

Frontiers in Immunology

Explores novel approaches and diagnoses to treat immune disorders.

The official journal of the International Union of Immunological Societies (IUIS) and the most cited in its field, leading the way for research across basic, translational and clinical immunology.

Discover the latest Research Topics

See more →

Frontiers

Avenue du Tribunal-Fédéral 34
1005 Lausanne, Switzerland
frontiersin.org

Contact us

+41 (0)21 510 17 00
frontiersin.org/about/contact